

# **DEVELOPMENT OF HYBRID ELECTRICAL DISCHARGE MACHINING**

**THESIS**

*Submitted in fulfillment of the requirement of degree of*

***DOCTOR OF PHILOSOPHY***

*to*

***J C BOSE UNIVERSITY OF SCIENCE & TECHNOLOGY***

***YMCA FARIDABAD***

*by*

**SANJAY KUMAR**

(Registration No - YMCAUST/Ph43/2012)

*Under the supervision of*

**Dr. SANDEEP GROVER**  
Supervisor  
Professor  
Deptt.of Mechanical Engineering  
JCB UST YMCA, Faridabad

**Dr. R. S. WALIA**  
Supervisor  
Professor  
Deptt. of Mechanical Engineering  
DTU, Delhi



**Department of Mechanical Engineering  
Faculty of Engineering and Technology  
J C Bose University of Science & Technology, YMCA  
Sec-6, Mathura Road, Faridabad, Haryana, India**

**FEBRUARY, 2019**

## Undertaking from the candidate

This is to certify that the PhD thesis entitled “**DEVELOPMENT OF HYBRID ELECTRICAL DISCHARGE MACHINING**” is submitted in fulfilment of the requirement for the Degree of Doctor of Philosophy in Mechanical Engineering Department, Faculty of Engineering & Technology, J C Bose University of Science & Technology, YMCA Faridabad, during the academic year 2018-19 is a bonafide record work. The thesis is based on the individual, original work carried out by me, which is previously unpublished research work.



25/02/2019

Sanjay Kumar

Reg. No. - YMCAUST/Ph43/2012

## CERTIFICATE

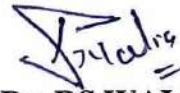
This is to certify that the PhD thesis entitled “**DEVELOPMENT OF HYBRID ELECTRICAL DISCHARGE MACHINING**” by Mr Sanjay Kumar submitted in fulfilment of the requirement for the Degree of Doctor of Philosophy in Mechanical Engineering Department, Faculty of Engineering & Technology, J C Bose University of Science & Technology, YMCA Faridabad, during the academic year 2018-19 is a bonafide record work carried out under our guidance and supervision.

We further declare that to the best of our knowledge, the thesis does not contain any part of any work which has been submitted for the award of any degree either in this university or in any other university.

It is further testified that the entire text of the PhD thesis has been read thoroughly and it is as per guidelines.



**Dr. SANDEEP GROVER**  
Supervisor  
Professor  
Deptt. of Mechanical Engineering  
JCB UST YMCA Faridabad



**Dr. RS WALIA**  
Supervisor  
Professor  
Deptt. of Mechanical Engineering  
DTU, Delhi

Dated: 25/2/19

## ABSTRACT

A conventional EDM process would hardly be a complete solution for present industrial metal cutting requirement. Lots of research work is going on throughout the world to ameliorate its productivity and process stability. The perception of ultrasonic vibration (UV) in conventional EDM is a novelty of this process and has the potential of metal cutting with high accuracy, surface quality and productivity. The necessity of hybrid process has become even more significant because of the futuristic materials with their high potency, high creep, and fatigue resistance properties. Heat affected zone, residual stresses and poor metal removal rate (MRR) are the major drawbacks of normal EDM. The conventional methods of flushing by infusion, suction, side flushing were insufficient to meet the new technological challenges of EDM. Fresh dielectric is a vital condition to release spark by ionization within the gap. In a UV assisted Hybrid-EDM process, stationary machining gap is supplanted with an element responding movement of conventional EDMs framework components (i.e. Tool, workpiece and dielectric). The hypothesis is flushing of contaminated dielectric, to stabilize discharge conditions and avoid abnormal discharges. UV perception is accomplished by traversing mechanical vibration to any of the sub-system of EDM either tool, work piece or dielectric medium with the help of UV generating devices. In EDM process, oxides (or debris) are created and accumulated in the sparkling gap between an electrode and a work-piece. It required dedicated experimental investigation to analysis the impacts of work piece vibration at the machining characteristics are contemplated at various amplitudes. The focus should be given to develop a mathematical model for Ultrasonic vibration assisted Wire-EDM including important parameters and their interactions with multi-performance characteristics of Hybrid-WEDM. Almost all previous studies focused mainly on the effects of single or a small range of vibration amplitude with continuous vibrations only. It may also be considered as discontinuous vibration is one of the most suitable parameters for the implementation of ultrasonic vibration in Wire-EDM for machining of material of exceptional hardness, wear resistance and high mechanical strength. Surface finish and residual stresses are the most sort-out output parameters in field of precision die manufacturing. These are the machining characteristic that plays a very critical role in determining the quality of engineering components. Good quality surfaces improve

the fatigue strength, corrosion and wear resistance of the workpiece. Vital conditions for accomplishing productive in Hybrid-EDM comprise in understanding the present and forthcoming objective and attribute of the Hybrid-EDM. Thither is a requirement for basic, orderly and logical scientific approach for analyzing of different perceptions considering in EDM. An effort has been made to identify qualitative and quantitative parameters and their interactions to provide useful information for the implementation of ultrasonic vibration in EDM. The prevalence this analytical study is both controllable parameters and objectives functions considered on the same platform.

This research work deals with design, development, application and comparison of ultrasonic vibration assisted in Hybrid-WEDM process. In this research work, discontinuous ultrasonic vibrations assisting Wire-EDM process with more range of amplitude of vibration are introduced for machining of high carbon high chromium D2 and D3 steel. Experiments are conduct to investigate Metal removal rate, Surface roughness, and Residual stresses under a wide range of machining conditions. An orthogonal array based on the Taguchi experimental design along with Response Surface Methodology (RSM) are used to plan the experiments and data and assessed with the Analysis of Variance (ANOVA) to determine the significant machining parameters for various machining characteristics.

The optimal machining parameters of the ultrasonic assisted EDM are established to achieve a sophisticated process with higher efficiency of the Hybrid-WEDM applications for modern industrial requirements. The entire set of experiments was carried out in a phased manner. The experiments in each phase were repeated three times. The different phases of experiments and the techniques used for the experimentation are as follows:

#### **Phase -I**

➤ Development of experimental set up, providing varying range of input parameters in continuous and discontinuous ultrasonic vibrations assisting wire-EDM process with more range of amplitude of vibration for measuring the selected responses.

#### **Phase -II**

- Investigation of the effects of Continuous/discontinuous vibrations assisting Wire EDM process parameters on quality characteristics viz. erosion rate, surface roughness and residual stresses.
- Optimization of quality characteristics of machined parts.
- Prediction of optimal sets of Ultrasonic vibrations assisting Wire-EDM process parameters.
- Prediction of optimal values of quality characteristics
- Prediction of confidence interval (95%CI)
- Experimental verification of optimized individual quality characteristics

The Taguchi's OA used for experimentation on Continuous/Discontinue vibration vibrations assisting Wire-EDM process under parameter design approach has been used to obtain the above objectives.

#### **Phase –III**

- Development of mathematical models and response surfaces of cutting rate, surface roughness using response surface methodology

The half fractional second order central composite rotatable design is to be used to plan the experiments and the input parameters like amplitude of vibration, pulse on time, pulse off time, peak current, Wire Feed rate under continuous and no-vibration to ascertain their effects on the MRR and SR.

#### **Phase –IV**

- Development of single response optimization model using desirability function
- Development of multi objective optimization models using desirability function
- Determination of optimal sets of process parameters for desired combinations of quality characteristics
- Experimental verification of quality characteristics optimized in different combinations

#### **Phase –V**

- Development of multi objective optimization models using Taguchi technique and utility concept
- Determination of optimal sets of ultrasonic vibrations assisting Wire-EDM process parameters for desired combined quality characteristics
- Experimental verification of quality characteristics optimized in different combinations.

### **Chapter wise breakup of the present thesis is given below:**

**Chapter 1** will comprise of introduction to convention EDM and Hybrid-EDM system for this research work. The developments in the field of Hybrid-EDM will be discussed. The Hybrid system chosen for the present research is ultrasonic vibration assisted EDM, which finds widespread application in advanced metal cutting industry. The advantages and application of conventional EDM along the limitations will to be discussed in this.

**Chapter 2** the retrospective literature review will be given under different conditions, optimization of process parameters, multi-objective optimization of machining parameters used in respect to the ultrasonic vibration assisted Hybrid-EDM. Depending upon literature review the gaps are identified for the present research work. The problem will be defined to enhance the performance of Hybrid-EDM to improve the machining stability and surface morphology. Then objectives of present work will be decided for this present research. The research objectives and different Phases of Experimentation discussed will be presented.

**Chapter 3** will discuss the Graph theory approach used to know the relative interdependency and legacy of various dependent and driver variables, which in past have been speculatively analyzed with likelihood instead of assurance without considering Hybrid-EDM as whole system. The chapter will include identification and categorization of the various decisive factors and sub-factors affecting the performance Hybrid-EDM. The range of Hybrid-EDM process performance index that has been achieved and intensity of factors affecting will be calculated quantitatively in this chapter.

**Chapter 4** will include the Interpretive Structural Modelling(ISM) & MICMAC analysis methodologies for effective and economical execution of ultrasonic vibration assistance in Hybrid-EDM technological reforms. To come up to such labyrinthine difficulties of UV implementation in EDM framework, ISM approach is necessary to recognize fitting determination characteristics, and to acquire the most suitable blend of parameters in conjunction with the genuine metal cutting requirement for execution of such innovative technological reforms.

**Chapters 5** will include the details of Taguchi experimental design technique and Response Surface Methodology. Also, the data analysis procedure will be described in this chapter.

**Chapter 6** will deal with design and fabrication of experimental set-up. The various components of Hybrid-WEDM process and their function will be discussed in this chapter.

**Chapter 7** will deal with selection of process parameters and their range selection. An Ishikawa cause-effect diagram has been proposed for this purpose and will be elaborate in this. The levels of process parameters and material which are finalized and selected will be discussed. The experimentation and measurement of response parameters will also be discussed. The scheme of experiment will also be included in this chapter.

**Chapter 8** will include the experimental results and analysis on the Taguchi method (Phase-II). The results are discussed for the response parameters viz. erosion rate, residual stresses and surface morphology. This chapter also deals with the development of mathematical models and 3-D graphs through Response Surface Methodology (Phase-III). The results will be discussed for the response parameters viz. MRR and SR including Residual stresses and surface morphology.

**Chapter 9** will deal with the development of multi-objective optimization models using utility function and Taguchi technique. The responses will be simultaneously optimized and the optimal levels of the process parameters will be discussed.

**Chapter 10** will comprise of the future scope of the present work which will show its importance with future prospects. Afterwards the limitations of this work will be discussed. Suggestions for future work on the related topics have been enumerated.



## ACKNOWLEDGEMENT

I take the opportunity to express my heartfelt adulation and gratitude to my supervisor, Dr. Sandeep Grover, Professor, Mechanical Engineering Department, J C Bose University of Science & Technology, YMCA Faridabad and Dr. Ravinderjit Singh Walia, Professor, Mechanical and Production Engineering Department, Delhi Technological University, Delhi for their unreserved guidance, constructive suggestions, thought provoking discussions and unabashed inspiration in nurturing this research work. It has been a benediction for me to spend many opportune moments under the guidance of the perfectionists at the acme of professionalism. The present work is a testimony to their alacrity, inspiration and ardent personal interest, taken by them during the course of this thesis work in its present form.

I am grateful to Dr. Tilak Raj, Professor and Head, Mechanical Engineering Department, J C Bose University of Science & Technology, YMCA Faridabad for providing facilities to carry out the investigations. Thanks are also due to Dr. M. L. Aggarwal, Professor and former Head, Mechanical Engineering Department, J C Bose University of Science & Technology, YMCA Faridabad to facilitate my experimental work. I would like to thank Department of Mechanical and Production, DTU Delhi, India, for providing surface roughness and stresses analyzer facility.

I would like to thank Mr. Lalit Mohan HOS (Electronic), Mr. Udai Narain Singh Kushwaha (Instructor) for extending their help during this work. It is a pleasure to acknowledge the support and help extended by all my colleagues.

I cannot close these prefatory remarks without expressing my deep sense of gratitude and reverence to my dear father and my mother for their blessings and endeavour to keep my moral high throughout the period of my work. I feel extremely happy to express my sincere appreciation to my wife Geeta my son Shreyash and daughter Bhawna for their understanding, care, support and encouragement.

I want to express my sincere thanks to all those who directly or indirectly helped me at various stages of this work.

Above all, I express my indebtedness to the "ALMIGHTY" for all His blessing and kindness.

(SANJAY KUMAR)

# CONTENTS

Certificate  
Acknowledgement  
Abstract

List of tables  
List of figures  
Nomenclature  
List of appendices

Page No.

## Chapter 1 INTRODUCTION

1		
1.1	Background of Electric Discharge Machining (EDM) Process	1
1.2	Basic Principle of EDM	2
1.3	Material Removal Mechanism	4
1.4	Hybrid Electrical Discharge Machining Processes	5
1.4.1	Electro-Chemical Discharge Machining (ECDM)	7
1.4.2	Powder mixed Electrical Discharge Machining (PMEDM)	8
1.4.3	Abrasive Jet Electrical Discharge Machining (AJEDM)	8
1.4.4	Magnetic Field Assisted Electrical discharge Machining (MFEDM)	9
1.4.5	Laser Beam assisted Electrical Discharge Machining (LBEDM)	9
1.4.6	Ultrasonic vibration Assisted EDM (US-EDM)	11
1.4.7	Ultrasonic Vibration Assisted Wire-EDM (US-WEDM)	11
1.4.7.1	Ultrasonic wire vibration Assisted Wire-EDM	11
1.4.7.2	Ultrasonic work-piece vibration assisted Wire-EDM	11
1.5	Advantages of EDM	12
1.6	Applications of EDM	13
1.7	Limitation of Traditional EDM process	16

## Chapter 2 LITERATURE SURVEY AND PROBLEM FORMULATION 17

2.1	Review of Literature	17
2.2	Identified gaps in the literature	23
2.3	Statement of the problem	24
2.4	Objective of present investigation	25
2.5	Different Phases of achieving objective	26

## Chapter 3 ANALYSZING AND COMPARITIVE STUDY OF HYBRID EDM

	<b>USING GTA APPROACH</b>	29
3.1	Identification and categorization of factors	30
3.1.1	Flushing (H1)	31
3.1.2	Cavitation (H2)	32
3.1.3	Abnormal Discharge (H3)	33
3.1.4	Dimensional Accuracy (H4)	34
3.1.5	Surface Morphology (H5)	35
3.2	Methodology	37
3.3	Digraph representation for Hybrid-EDM process performance	38
3.3.1	Digraph generation at System Level for Hybrid-EDM factors	38
3.3.2	Digraph generation at Sub-system Level for Hybrid-EDM Sub-factors	39

3.4	Process performance Matrix representation [Hybrid-EDM]	40
3.4.1	Process performance characteristic matrix [CM- Hybrid-EDM]	41
3.4.2	Process performance variable characteristic matrix [VCM- Hybrid-EDM]	41
3.4.3	Process performance variable permanent matrix [VPM- Hybrid-EDM]	42
3.5	Permanent representation for Hybrid-EDM performance function	43
3.6	Quantification of ' $H_i$ 's and ' $h_{ij}$ 's	45
3.7	Illustration of Hybrid-EDM performance Index	47
3.7.1	Matrix permanent function generation at system Level	47
3.7.2	Matrix and variable permanent function generation at sub-system Level	47
3.7.3	Quantification of ' $H_i$ 's and ' $h_{ij}$ 's for Hybrid-EDM sub-system level	48
3.8	Calculation of Permanent function for Hybrid-EDM system and subsystem Level	50
3.9	Coefficient of variation of Hybrid-EDM performance Index for system and sub-system level	51
3.10	A Comparative study of the performance Ultrasonic Vibration Assisted Hybrid-EDM under three modes of vibration	52
3.10.1.	Identification of Hybrid EDM performance Index Factors	53
3.10.2.	Digraph representation for process performance factors	54
3.10.3.	Matrix representation process performance	55
3.10.4.	Quantification of $K_i$ 's and $K_{ij}$ 's	57
3.10.5.	Range of Hybrid EDM performance Index under three mode	57
3.11.	Interim conclusion	59
<b>Chapter 4</b>	<b>ISM ANALYSIS FOR HYBRID EDM</b>	<b>63</b>
4.1	Introduction	64
4.2	Application of Interpretive Structural Modelling(ISM)	64
4.2.1	Identification of the various drivers	64
4.2.2	Development of Structural Self-Interaction Matrix (SSIM)	66
4.2.3	Reachability Matrix	67
4.2.4	Atomization of Level	68
4.3	Formation of ISM model	70
4.4	MICMAC analysis for affecting and reliance coefficient	71
4.5	Interim conclusion	73
<b>Chapter 5</b>	<b>EXPERIMENTAL DESIGN METHODOLOGY</b>	<b>76</b>
5.1	Taguchi Experimental and analysis	76
5.1.1	Taguchi philosophy	76
5.1.2	Experimental Design strategy	77
5.1.3	Loss Function	79
5.1.3.1	Average loss-function for product population	80
5.1.3.2	Other loss functions	81
5.1.4	Signal to Noise ratio	82
5.1.5	Relation between S/N Ratio and Loss Function	84
5.2	Response Surface Methodology	89
5.2.1	Central composite second order Rotatable Design	93
5.2.2	Estimation of the coefficients	94
5.2.3	Analysis of Variance	99
5.2.4	Significance testing of the coefficient	99
5.2.5	Adequacy of the model	101

<b>Chapter 6 DESIGN AND FABRICATION OF EXPERIMENTAL SET-UP</b>	104
6.1 Basic Principle	104
6.2 Ultrasonic System	105
6.2.1 Ultrasonic generator and Piezo-electric Transducer	106
6.2.2 Continuous and discontinuous Control system	107
6.2.3 Cantilever plate with holding fixture	108
6.2.4 Wire Electric Discharge Machine Tool	109
<b>Chapter 7 PROCESS PARAMETER SELECTION AND EXPERIMENTATION</b>	114
7.1 Selection of process parameters and their ranges	114
7.1.1 Type of vibration	116
7.1.2 Amplitude of vibration and Peak Current for cutting rate	117
7.1.3 Amplitude of vibration and Peak Current for Surface Morphology	118
7.2 Work-piece Material	122
7.3 Response Characteristics	123
7.3.1 Cutting Speed(CS)/ Material Removal Rate (MRR)	124
7.3.2 Surface Roughness	125
7.3.3 Residual stresses	126
7.4 Scheme of Experiments	130
7.4.1 Scheme of Experiments (Phase-II)	130
7.4.1.1 Selection of Orthogonal Array (OA) and Parameter Assignment	131
7.4.1.2 Experimentation (Phase-II)	132
7.4.2 Scheme of Experiments (Phase-III)	133
7.4.2.1 Coding of Variables	134
7.4.2.2 Experimentation precaution	135
<b>Chapter 8 EXPERIMENTAL RESULTS AND ANALYSIS</b>	137
8.1 Analysis and discussion of results (Phase-II)	137
8.1.1 Effect of type of vibration (Ultrasonic vibration Parameter)	138
8.1.2 Effect amplitude of vibration (Ultrasonic vibration Parameter)	141
8.1.3 Effect of workpiece thickness parameters (Material Parameter)	144
8.1.4 Effect of Duty cycle and Peak Current (Electrical parameters)	146
8.1.5 Effect of wire feed rate (Non electrical parameter)	150
8.1.6 Selection of optimal levels for cutting rate(CR)	152
8.1.6.1 Estimation of optimum cutting rate response	154
8.1.6.2 Confirmation experiment	155
8.1.7 Selection of optimal level for Residual stresses (RS)	156
8.1.7.1 Estimation of optimal Residual stress response	157
8.1.7.2 Confirmation experiment	158
8.1.8 Selection of optimal level for surface roughness (RS)	159
8.1.8.1 Estimation of optimum for surface roughness response	160
8.1.8.2 Confirmation experiment	161
8.2 Analysis and discussion of results (Phase-III)	162
8.2.1 ANOVA for MRR of Hybrid-WEDM	162
8.2.2 ANOVA for Surface Roughness of Hybrid-WEDM	167
8.3 Multi Response optimization using desirability function (Phase-IV)	171
<b>Chapter 9 MULTI CHARACTERISTICS OPTIMIZATION USING UTILITY FUNCTION</b>	174
9.1 Introduction	174
9.2 Multi-response optimization through Utility Concept (Phase-V)	175
9.2.1 The utility concept	175

9.2.2	Determination of utility value	176
9.2.3	The algorithm	178
9.2.4	Utility for the Model for CR, RS and SR (Phase-V)	178
	9.2.4.1 Construction of preference scales	179
	9.2.4.2 Calculation of Utility Value	179
	9.2.4.3 Analysis of Utility data for optimal setting of process parameters	181
	9.2.4.4 Optimal value of quality characteristics (Predicted means)	183
<b>Chapter 10 CONCLUSION AND SCOPE FOR FUTURE WORK</b>		188
10.1	Experimental Details	188
10.2	Conclusion	190
10.3	Limitation and scope for future work	193
<b>REFERENCES</b>		194
<b>LIST OF PUBLICATIONS</b>		202

## List of Figures

No	Title	Page No
Figure 1.1	A Schematic diagram of Die-sink Electric Discharge machining (EDM) machine tool.	3
Figure 1.2	Basic components of EDM	3
Figure 1.3	Detail of WEDM Cutting process	4
Figure 1.4	Research and development areas in Hybrid EDM.	5
Figure 1.5	The basic elements traditional EDM System.	9
Figure 1.6	Piezoelectric ultrasonic vibration generating device.	10
Figure 1.7	Precision fast hole and micro-hole EDM drilling (AA EDM Corporation)	14
Figure 1.8	Holes, slots and shaped holes for larger aerospace blades, vanes, rings, burner, etc. (AA EDM Corporation)	15
Figure 2.1	Recent developments in Hybrid -EDM with various input process parameters, Performance indexes and the Hypothesis Tested.	23
Figure 3.1	Contribution of various factors in Hybrid -EDM performance considered by researchers	31
Figure 3.2	Modified Framework for Hybrid -EDM performance Index Evaluation.	36
Figure 3.3	Hybrid -EDM process performance evaluation digraph. Nodes: 1. Flushing (H1); 2. Cavitation (H2); 3. Abnormal Discharge (H3); 4. (H4); 5. Surface Morphology (H5);	38
Figure 3.4	The digraph representation for Flushing	39
Figure 3.5	The digraph representation for Cavitation	39
Figure 3.6	The digraph representation for abnormal discharge	39
Figure 3.7	The digraph representation for Dimensional accuracy	40
Figure 3.8	The digraph representation for Surface morphology	40
Figure 3.9	Contribution of various attributes for different mode of vibration in Hybrid -EDM	53
Figure 3.10	Hybrid EDM performance Index factors digraph for Attributes; (1) Flushing (K <sub>1</sub> ); (2) Cavitation (K <sub>2</sub> ); (3) Abnormal discharge (K <sub>3</sub> ); (4) Dimensional accuracy (K <sub>4</sub> ); (5) Surface Morphology (K <sub>5</sub> ); and (6) Ergonomic & Chemical effect (K <sub>6</sub> )	54
Figure 3.11	Strake diagram for the frequency of factors considered in literature for mode of vibration 1) Tool; 2) Workpiece; 3) Dielectric medium;	58
Figure 4.1	Flow chart for the ISM Methodology	65
Figure 4.2	ISM hierarchy model for the perceptual drivers affecting the Hybrid EDM	71
Figure 4.3	Affecting coefficient and Reliance coefficient diagram.	73
Figure 5.1	(a, b): The Taguchi Loss-Function and the Traditional Approach (Ross, 1988)	81
Figure 5.2	(a,b): The Taguchi Loss-Function for LB and HB Characteristics (Barker, 1990)	82
Figure 5.3	Taguchi Experimental Design and Analysis Flow Diagram	86
Figure 5.4	Central Composite Rotatable Design in 3X-Variables	94

Figure 6.1	The developed set up design for Ultrasonic vibration assisted Wire-EDM	104
Figure 6.2	Model for debris and cavitation bubbles removal through gap for Hybrid-WEDM :(a) workpiece upward motion due to cantilever motion and (b) workpiece downward motion due to cantilever motion	105
Figure 6.3	Schematic diagram of experimental setup for ultrasonic vibration of work piece in Wire-EDM.	105
Figure 6.4	a) 21.5 kHz frequency transducer and; b) 120W Ultrasonic PCB	107
Figure 6.5	Continuous and discontinuous vibration mode On/Off	107
Figure 6.6	Circuit diagram for Continuous and discontinuous vibration mode	108
Figure 6.7	Cutting edge of ultrasonic vibration actuator as a cantilever beam.	108
Figure 6.8	Varying amplitude with Cutting Edge Ultrasonic vibration as a cantilever beam	109
Figure 6.9	Pictorial Views of Wire Cut EDM used for experimentation.	111
Figure 6.10	(a) Wire Feed Spool; (b) Display Screen and Emergency Power off Button.	111
Figure 7.1	Ishikawa cause and effect diagram for Hybrid Wire-EDM	115
Figure 7.2	Comparison of cutting rate (mm/min) in Normal Wire-EDM, continuous and discontinuous vibration assisted EDM for high Carbon high Chromium Steel (Peak current 120A, Servo voltage 1150, pulse-on time 120 $\mu$ s and duty cycle 62 %)	116
Figure 7.3	Graphical presentation of Cutting rate variation vs. peak current	117
Figure 7.4.	Graphical presentation of residual stresses variation vs peak current	119
Figure 7.5	Full 2D and 3D debey ring and its residual stresses profile with peak current 160 amp and pulse on time 100, Pulse off time 50, Servo Voltage 1150 units at No-Vibration; Residual stress= 176MPa	120
Figure 7.6	Full 2D and 3D debey ring and its residual stresses profile with peak current 160 amp and pulse on time 100, Pulse off time 50, Servo Voltage 1150 units at 10 $\mu$ m amplitude of vibration; Residual stress= 170MPa	121
Figure 7.7	Full 2D and 3D debey ring and its residual stresses profile with peak current 160 amp and pulse on time 100, Pulse off time 50, Servo Voltage 1150 units at 15 $\mu$ m amplitude of vibration; Residual stress=139MPa	121
Figure 7.8	Full 2D and 3D debey ring and its residual stresses profile with peak current 160 amp and pulse on time 100, Pulse off time 50, Servo Voltage 1150 units at 20 $\mu$ m amplitude of vibration; Residual stress=149MPa	122
Figure 7.9	AISI D3 steel Materials Cut for Phase-II experimentation	122
Figure 7.10	AISI D2 tool steel Materials Cut for Phase-III experimentation	124
Figure 7.11	Surface Roughness Tester (Taylor Hobson Surtronic 3+ profilometer)	126

Figure 7.12	Portable X-ray Residual Stress Analyzer ( $\mu$ -X360FULL 2D X-ray detection)	126
Figure 7.13	Geometric representation of the $\cos(\alpha)$ geometry using a 2D Single position of detector.	129
Figure 8.1	Main Effect and S/N ratio of type of Vibration on cutting rate	138
Figure 8.2	Main Effect and S/N ratio of type of Vibration on residual stress	138
Figure 8.3	Main Effect and S/N ratio of type of Vibration on surface roughness	138
Figure 8.4	Residual stress graphs for continuous vibration	140
Figure 8.5	Residual stress graphs for discontinuous vibration	141
Figure 8.6	Residual stress graphs for No-vibration	142
Figure 8.7	Main Effect and S/N ratio of amplitude of Vibration on cutting rate	142
Figure 8.8	Main Effect and S/N ratio of amplitude of Vibration on residual stress	143
Figure 8.9	Main Effect and S/N ratio of amplitude of Vibration on surface roughness	143
Figure 8.10	FWHM graph at 10 $\mu$ m amplitude of vibration	144
Figure 8.11	FWHM graph at 14 $\mu$ m amplitude of vibration	145
Figure 8.12	FWHM graph at 18 $\mu$ m amplitude of vibration	145
Figure 8.13	Main Effect and S/N ratio of workpiece thickness on cutting rate	145
Figure 8.14	Main Effect and S/N ratio of workpiece thickness on residual stress	146
Figure 8.15	Main Effect and S/N ratio of workpiece thickness on surface roughness	146
Figure 8.16	Main effect and S/N peak current of vibration on cutting rate	147
Figure 8.17	Main effect and S/N peak current of vibration on residual stresses	147
Figure 8.18	Main effect and S/N peak current of vibration on surface roughness	147
Figure 8.19	Main effect and S/N duty cycle of vibration on cutting rate	148
Figure 8.20	Main effect and S/N duty cycle of vibration on residual stresses	149
Figure 8.21	Main effect and S/N duty cycle of vibration on surface roughness	150
Figure 8.22	Main effect and S/N wire feed rate on cutting rate	151
Figure 8.23	Main effect and S/N wire feed rate on residual stresses	151
Figure 8.24	Main effect and S/N wire feed rate on surface roughness	152
Figure 8.25	Effect of peak current and pulse on time on MRR	164
Figure 8.26	Effect of peak current and pulse off time on MRR	164
Figure 8.27	Effect of wire feed rate and pulse off time on MRR	165
Figure 8.28	Normal Plots of Residuals for MRR	165
Figure 8.29	Predicted vs. Actual for MRR	168
Figure 8.30	Effect of peak current and pulse off time on SR	169
Figure 8.31	Effect of pulse on time and peak current on SR	169
Figure 8.32	Effect of pulse on time and amplitude of vibration	169
Figure 8.33	Effect of pulse off time and amplitude of vibration	169
Figure 8.34	Normal Plots of Residuals for SR	170



Figure 8.35	Predicted vs. Actual for SR	170
Figure 8.36	Overall desirability variations with Amplitude of vibration vs. pulse on time	172
Figure 8.37	Overall desirability variations with Amplitude of vibration vs. peak current	172
Figure 8.38	Bar Graph of combined Desirability for MRR and SR	173
Figure 9.1	Effect of Type of Vibration on S/N ratio and Utility	185
Figure 9.2	Effect of Amplitude of Vibration on S/N ratio and Utility	185
Figure 9.3	Effect of Peak current on S/N ratio and Utility	186
Figure 9.4	Effect of Duty cycle on S/N ratio and Utility	186
Figure 9.5	Effect of Wire feed rate on S/N ratio and Utility	186
Figure 9.6	Effect of Workpiece thickness on S/N ratio and Utility	187

## List of Tables

S. No.	Title	Page No.
Table 3.1	Factors and sub-factors affecting the Hybrid -EDM process performance	29
Table 3.2	Value of Hybrid -EDM performance factors ( $H_i$ )	46
Table 3.3	Quantification measure of interdependency of diagonal elements 'hij'	47
Table 3.4	Quantification of flushing sub-factors	49
Table 3.5	Quantification of Cavitation sub-factors	49
Table 3.6	Quantification of Abnormal discharge sub-factors	49
Table 3.7	Quantification of Dimensional accuracy sub-factors	49
Table 3.8	Quantification of Surface morphology sub-factors	50
Table 3.9	The Coefficient of variation of index values of the permanent function	51
Table 3.10	Relative importance diagonal value ( $K_i$ ) for tool, workpiece and dielectric	59
Table 3.11	The performance Index values for three modes of vibrations	61
Table 4.1	Drivers of Ultrasonic vibration assisted Hybrid-EDM	66
Table 4.2	Structural self-interaction matrix for the Hybrid-EDM drivers.	66
Table 4.3	Rudimentary reachability matrix for the variables	67
Table 4.4	Ultimate reachability matrix for the variables.	67
Table 4.5	Cycle Repetition -1; atomization of level for drivers	68
Table 4.6	CycleRepetition-2; atomization of level for drivers	69
Table 4.7	CycleRepetition-3; atomization of level for drivers	69
Table 4.8	CycleRepetition-4; atomization of level for drivers.	69
Table 4.9	CycleRepetition-5; atomization of level for drivers.	69
Table 4.10	CycleRepetition-6; atomization of level for drivers.	69
Table 4.11	CycleRepetition-7; atomization of level for drivers.	70
Table 4.12	CycleRepetition-8; atomization of level for drivers.	70
Table 5.1	Components of Central Composite Second Order Rotatable Design	95
Table 5.2	Analysis of Variance for Central Composite Second Order Rotatable Design	100
Table 5.3	Central Composite Second Order Rotatable Design Matrix for 5 Variables (Kumar, 1994)	102
Table 6.1	Wire- EDM machine tool specifications.	110
Table 7.1	Chemical composition of workpiece material phase-II (AISI D3 steel).	123
Table 7.2	Properties at room Temperature for AISI D3	123

Table 7.3	Chemical composition of workpiece material (AISI D2).	123
Table 7.4	Properties at room Temperature for AISI D2	124
Table 7.5	Measurement Condition	126
Table 7.6	The controlled parameters and their Levels of experimental design (Phase-II)	130
Table 7.7	The L18 (21 * 37) OA (Parameters assigned) with Response (Phase I)	131
Table 7.8	Experimental plan and Results of performance characteristics	133
Table 7.9	Design Summary for statistical software used	134
Table 7.10	Process Parameters range and their Levels	134
Table 7.11	Coded Values and Real Values of the Variables (Phase III)	135
Table 7.12	Experimental trail conditions and results of response characteristics (MRR and SR)	136
Table 8.1	Experimental results of Map of 3D debey ring and its residual stresses profile with peak current varies from 100-180 Amp: i) No vibration; ii) Continuous vibrations; iii) Discontinuous vibration; other parameters constant.	149
Table 8.2	Experimental results of residual Stress profile by controlling XY axis stage with duty cycle varies from 66-78 % using; i) No vibration; ii) Continuous vibrations; iii) Discontinuous vibration; other parameters constant.	150
Table 8.3	Main effects of Cutting rate (mm/min) (Raw Data) at various levels Larger is better	153
Table 8.4	Main effects of Cutting rate (S/N Ratio) at various levels Larger is better	153
Table 8.5	Analysis of variance of Raw data for Cutting rate	153
Table 8.6	Analysis of variance of S/N ratio for Cutting rate	153
Table: 8.7	Confirmation experiments results values observed for quality characteristics	155
Table: 8.8	Main Effects of Residual stresses (MPa) (Raw Data) at various levels smaller is better	156
Table 8.9	Main Effects of Residual stresses (MPa) (S/N Ratio) at various levels smaller is better	156
Table 8.10	Analysis of variance of raw data for Residual stresses (MPa)	156
Table 8.11	Analysis of variance of S/N ratio for Residual stresses (MPa)	156
Table 8.12	Main Effects of surface roughness ( $\mu\text{m}$ ) (Raw Data) at various levels smaller is better	159
Table 8.13	Main Effects of surface roughness ( $\mu\text{m}$ ) (S/N Ratio) at various levels smaller is better	159
Table 8.14	Analysis of variance of Raw data for surface roughness ( $\mu\text{m}$ )	160
Table 8.15	Analysis of variance of S/N ratio for surface roughness ( $\mu\text{m}$ )	163
Table 8.16	Pooled analysis of variance for MRR	167
Table	Pooled analysis of variance for Surface roughness	168

8.17		
Table 9.1	Experimental results of various response characteristics	177
Table 9.2	Optimal setting and values of process parameters (individual quality characteristics optimization)	179
Table 9.3	Calculated Utility data based on responses	181
Table 9.4	Main Effects of Utility Raw Data (: CR, RS and SR)	182
Table 9.5	Main Effects of Utility S/N Data (: CR, RS and SR)	182
Table 9.6	ANOVA for Utility raw data (CR, RS and SR)	182
Table 9.7	ANOVA Utility S/N Data: (CR, RS and SR)	182
Table	Taguchi Methodology (Phase-II)	188
10.1		
Table	Response Surface Methodology (Phase-III)	189
10.2		

# CHAPTER 1

## INTRODUCTION

---

### 1.1. Background of Electric Discharge Machining (EDM) Process:

Electrical discharge machining (EDM) is a spark machining process, and also known as sparks eroding, burning, die sinking, wire burning or wire erosion process. It is an advanced manufacturing process whereby the replica of preferred profile is obtained by using regular electrical discharges or sparks. This manufacturing process can be classified into two groups based on the commonly uses in today's metal cutting world:

- Sinker EDM
- Wire-cut EDM

The types of electrical discharge machines introduced were the Die-sink in 1943 and the Wire-cut machine in 1960s. These electrical discharge machine tools follows the same basic principle in order to shape the surfaces of metal using a dielectric liquid and a tool that releases a high intensity electric spark. Material is detached from the workpiece by a sequence of high rate of recurrence current discharges amid two electrodes, alienated by a dielectric liquid and conditional on an electric voltage. One of the electrodes is called the tool-electrode, or basically the "tool" or "electrode," while the other is called the workpiece-electrode, or "work piece". There is no tangible material contact occurred amid the tool electrode and workpiece. The discharges produced by electrical phenomena, namely spark has been closely related to the development of heating energy sources. Joseph Priestley (1733-1804), an English Theologian and Chemist was the first to find out in 1766 erosion craters appeared by electric discharges on the cathode face: Priestley also inspected the affect of the electrode material and of the discharge current on the craters size. The history of EDM itself begins in 1943, with the development of its principle by Russian scientists Boris and Natalya Lazarenko in Moscow. The Soviet government assigned them to examine the erosion caused by discharge between tungsten electrical contacts, a dilemma which was principally critical for upholding of automotive engines during the Second World War. Putting the electrodes in oil, they found that the sparks were

more uniform and predictable than in air. They had then the idea to reverse the phenomenon, and to use controlled sparking as an erosion method (Lazarenko B.R., 1943). It is also during this period that industries produced the first EDM machines. Swiss industries were involved very early in this market, and still remain leaders nowadays. Agie was founded in 1954, and les Ateliers des Charmilles produced their first machine in 1955. Due to the poor quality of electronic components, the performances of the machines were limited at that time. In the 1960's, the progress of the semi-conductor industry permitted significantly improvements in EDM machines. Die-sinking machines became reliable and produced surfaces with controlled quality, whereas wire-cutting machines were still at their very beginning. Wire EDM (WEDM) was initiated in the late 1960s', and has revolutionized the tool and die, mold, and metalworking manufacturing. WEDM was considered as an exceptional selection of the traditional EDM process, which utilizes an electrode to instate the eroding procedure. Be that as it may, WEDM uses a ceaselessly voyaging wire electrode equipped of lean copper or tungsten of breadth 0.05-0.30 mm, which is fit for accomplishing little corner radii. The wire is kept in strain utilizing a mechanical tensioning hardware decreasing the propensity of creating incorrect parts. Amid the WEDM cutting, the material is dissolved in front of the wire and there is no immediate contact amid the work piece and the wire and reduces the unwanted residual stresses. This advanced cutting tool is probably the most exciting and diversified machine tool developed for this industry in the last fifty years, and has numerous advantages to offer. It can machine anything that is electrically conductive paying little mind to the hardness from moderately usual materials, for instance, tool steel, aluminum, copper, and graphite, to outlandish space-age compounds as well as hastaloy, waspaloy, inconel, titanium, carbide.

## **1.2. Basic principle of EDM:**

EDM is a practice of material removal from a work piece surface by a swift series of short time electric sparks. The tool used for die-sink EDM spark eroding is an electrode whose form is a negative reproduction of the shape to be formed on the surface of the component. The schematic of a Die-Sink EDM machine tool is shown in Figure 1.1. The tool and the work piece figure the two conductive electrodes in the electric circuit. Pulsed electrical power is abounding to the electrodes from a divided power supply unit. The suitable feed action of the tool towards the work piece is

endowed with for sustaining a constant gap sandwiched between the tool and the work piece through machining.

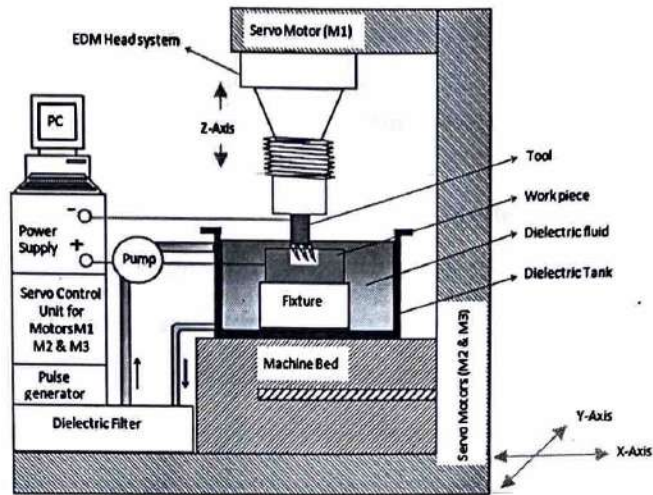


Figure 1.1: A Schematic diagram of Die-sink Electric Discharge machining (EDM) machine tool (S. Kumar et al., 2016)

This is accomplished by either a servo motor control or stepper motor control of the tool holder. As material gets eroded from the machining surface of the work piece, the tool is stimulated downward towards the workpiece to uphold a stable inter-electrode space. The tool and the work piece are sunked in a dielectric tank and flushing arrangements are obtained for the appropriate stream of dielectric in the inter-electrode space. Usually in oil die-sinking EDM, pulsed DC power supply is preferred wherever the tool is connected to the negative terminal and the work piece is connected to the positive terminal. The pulse occurrence may vary from a few kHz to several MHz.

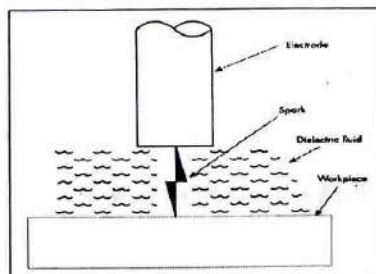


Figure 1.2: Basic components of EDM (Jameson, 2001)

The inter-electrode gap is in the range of a few tens of micro meters to a few hundred micro meters. Material removal rates upto  $300 \text{ mm}^3/\text{min}$  can be achieved during EDM. The surface finish (Ra value) can be as high as  $50 \mu\text{m}$  during rough

machining and even less than 1  $\mu\text{m}$  during finish machining. Figure 1.2 illustrates the basic components of the EDM process.

### 1.3. Material Removal Mechanism:

Material removal mechanism of sinker-EDM and wire-EDM occupied an electric erosion effect i.e. the collapse of electrode material accompanying any form of electric discharge (The discharge is usually through a gas, liquid or in some cases solids). A necessary situation for generating a discharge is the ionization of the dielectric that is, separation of its molecules into ions and electrons. As soon as appropriate voltage is apply across the electrodes, the potential strength of the electric field between them loudening, until at some predetermined importance, the individual electrons ruptured from the surface of the cathode and are prompted towards the anode under the persuade of field forces. In the movement of inter-electrode gap, the electrons smash together with the neutral molecules of the dielectric, coming off electrons from them and originate ionization.

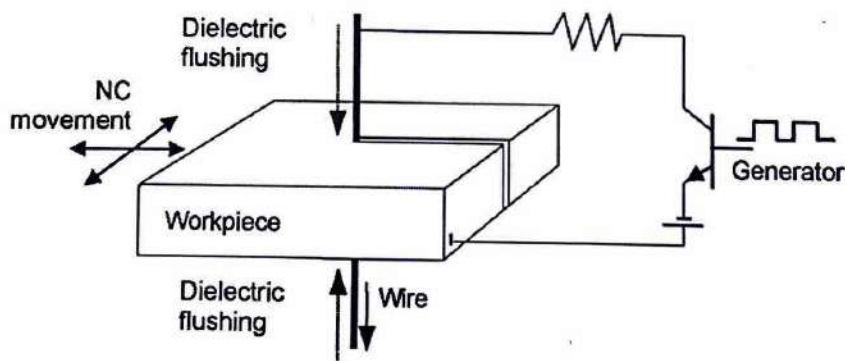


Figure 1.3: Detail of WEDM Cutting process(Sanchez et al., 2007)

At a particular time, the ionization turned out to be such that a slight guide of uninterrupted conductivity is formed. When this takes place, there is a extensive flow of electrons beside the channel to the anode, consequential in a momentary current impulse or spark. The release of energy associating the discharge pilots to the generation of exceptionally high temperature, between  $8,000^{\circ}$  and  $12,000^{\circ}\text{C}$ , sourcing fusion or unfinished vaporization of the metal and the dielectric fluid at the point of discharge. The metal as fluid fall is scattered into the space encircling the tool electrode by the volatile pressure of the vaporous items in the discharge response



(Pandey and Shan, 1983). This contributes in the formation of a modest pit at the purpose of discharge in the work piece. The measure of clasping pressure required to hold little, thin and delicate parts is insignificant, averting harm or contortion to the workpiece. The EDM leaves no leftover burrs on the workpiece, which diminishes or dispenses with the requirement for resulting finishing activities.

In Wire-EDM, wire electrode is negative charged and consistently moving whereas the work piece is positive anode. The flashes will produce between two firmly divided anodes affected by dielectric fluid. The low viscosity and fast cooling rate property of distilled water is utilized as dielectric in Wire-EDM, as a result of its low thickness and (Lok and Lee, 1997). No indisputable hypothesis has been built up for this complex machining process. Nonetheless, experimental proof recommends that the connected voltage makes an ionized channel between the closest purposes of the work piece and the wire terminals in the underlying stage. In the following stage the real discharge happens with overwhelming stream of current and the obstruction of the ionized channel slowly diminishes. The high intensity of current keeps on assisting ionizes the channel and an intense attractive field is created. This attractive field packs the ionized divert and results in restricted heating. Indeed, even with flashes of brief length, the temperature of wire can locally ascend to high esteem which is more than the liquefying purpose of the work material because of change of the dynamic vitality of electrons into heat. The high energy dissolves a piece of material from both the wire and work piece by locally softening and vaporizing the surface material and along these lines it is the overwhelming heat disintegration process.

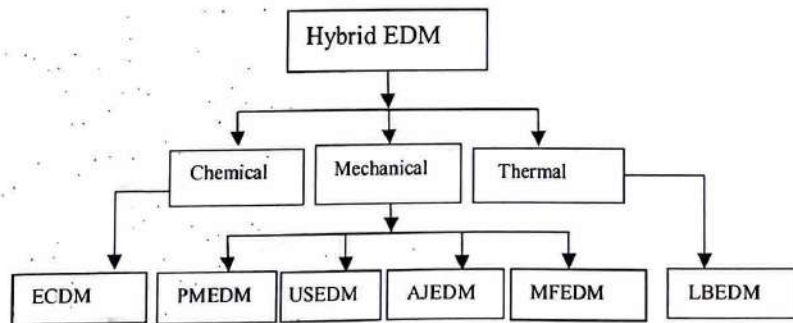


Figure 1.4: Research and development areas in Hybrid EDM (S. Kumar et al., 2016).

#### 1.4. Hybrid Electrical Discharge Machining processes:

Hybrid Electrical Discharge Machining is an advanced empirical approach ignites the researchers and boosts them up to meet the limitations of normal EDM. The

researchers have explored various non-conventional methods along traditional EDM, such as electrochemical machining, ultrasonic machining and abrasive jet machining etc. In literature, several descriptions of the term hybrid machining were found. Kozak, Rajurkar, (2001) define hybrid machining as a combination of two or more processes to improve productivity. These hybrid processes were introduced to take advantages of individual processes profitably and to minimize potential disadvantages of two's. A Hybrid EDM can be classified on the basis of utility of secondary non-conventional method used as discussed below:

- The method which facilitate control of necessary EDM process condition such as flushing, normal electric discharge condition and gap etc.
- The method which improve machining characteristics for EDM process such as MRR, Surface finish, Dimensional accuracy or reduce Tool wear etc.

The various Non-conventional methods combined with traditional EDM process in literature are shown in Figure 1.4. These are grouped into six major categories as mentioned below here for performance and efficiency enhancement of normal EDM process.

- Electro-Chemical Discharge Machining (ECDM) (Basak and Ghosh, 1997)
- Powder mixed Electrical Discharge Machining (PMEDM)(Kansal et al., 2007)
- Ultrasonic vibration Assisted EDM (HYBRID EDM)[(Abdullah and Shabgard, 2008)
- Abrasive Jet Electrical Discharge Machining (AJEDM)[(Lin et al., 2012)
- Magnetic Field Assisted Electrical discharge Machining (MFEDM)[(Lin et al., 2009)
- Laser Beam assisted Electrical Discharge Machining (LBEDM)(Rasheed, 2013)

This Hybrid EDM not only improves the machining rate but also make machining of advance materials possible which cannot be machined previously (B. Bhattacharyya, B.N. Doloi, 1999).

Hybrid EDM process for increasing the performance index comprise some of the combined simple shearing and erosion action of high kinetic energy posed by particles (mechanical) , melting & evaporation (thermal) and oxidation & precipitation (chemical), on workpiece surface for cutting . The involvement of these erosive actions changes both physical and chemical conditions of parent processes

under the influence of other controllable parameters. The combined erosive action of powder addition, laser beam localized heat and ion beam give better results with spark erosion. The performance of Hybrid technology may be considerably different from those that are characteristic of the component processes (Ji et al., 2013). Productivity of electro discharge/electrochemical (EDCM) hybrid machining, which consists in making use of electrical discharges in electrolyte to metal removal is  $5\pm 50$  times greater than productivity of ECM or EDM processes (Mediliyegedara et al., 2005).

#### **1.4.1. Electrochemical Discharge Machining (ECDM):**

Electrochemical discharge machining (ECDM) process is an electrically controlled thermo-chemical hybrid machining process. In this process, the metal is removed as a resultant of combined effects, heating by electric spark and chemical decomposition of metal schematic (Basak and Ghosh, 1997). In other word a simultaneous action of electrical spark discharges (ESD) and electrochemical (EC) reaction. A substantial experimental works has been investigated by Kulkarni, (2007) for micro machining of holes with high aspect ratio. Synchronized and transient measurements revealed the discrete nature of the process; it also helped in formulating the basic mechanism for the discharge formation and the material removal. Kulkarni et al., (2002) took advantage of the similarity of ECM and EDM processes simple replaced dielectric fluid to mixture of HCl with distilled Water to induce chemical machining mechanism. Jawalkar et al., (2012) highlighted processing condition and materials being investigated by the researchers with this hybrid process. Most of the researchers worked on glass as work material under different machining parameters subsequently varying results. According to them a generalized metal remove mechanism theory for ECDM process is yet to be reveal.

#### **1.4.2. Powder mixed Electrical Discharge Machining (PMEDM):**

The applied hypothesis for powder mixed hybrid process is addition of metallic powder and abrasives in EDM dielectric medium improve the machining efficiency (Kansal et al., 2007). The process instability of traditional EDM in pure kerosene results the arcing and short-circuit effect (Yan et al., 2012). Some also observed that excessive powder concentration cause unstable machining process due to the short-circuiting because of decrease in dielectric resistivity. Most researchers focused on

optimization of the process parameters, but still areas such as effect of pulse interval, polarity and powders of some alloys such as vanadium chromium and magnesium are to be explored referring to work surface characteristic.

#### **1.4.3. Abrasive Jet Electrical Discharge Machining (AJEDM):**

The hybrid process comprises Abrasive Jet Machining and electrical sparks that can increase the machining drastically. The stream of fine grains mixed with dielectric affecting with high kinetic energy cause erosive action not only increase MRR but also helps to generate fine surface integrities (Lin et al., 2012). Machining is accomplished by directing mixture in the machining gap at high speed possessed by abrasives and thermal energy of electrical discharge. The jet action also improves the flushing of contaminated dielectric medium. Lin et al., (2012) incorporated the AJM with EDM process to permute the machining performance. They used  $\text{Al}_2\text{O}_3$  and SiC abrasive grains directed on to the machining surface. The experimental results show this combined process is superior to the dry EDM both in MRR and Surface Roughness. The author claimed increase in MRR between 32-46% at peak current 9-6 A individually. They observed a relationship between SR and peak currents only up to a certain limit, which increases with peak current. Beside, the SR increased with the pulse duration first, and then it reduce with the further extended the pulse duration.

#### **1.4.4. Magnetic Field Assisted Electrical discharge Machining (MFAEDM):**

In this hybrid process the magnetic forces are combined with the normal EDM process by a specially designed device that expels debris for the machining gap to maintain the normal EDM process condition. As discussed previously the accumulation of debris in machining gap contaminate the dielectric medium due to which abnormal discharging occurred that affect the surface quality of the workpiece and process stability. The hypothesis for combining magnetic force in EDM device is reduction of probability of abnormal electrical discharge, so the machining efficiency could be improved significantly (Lin et al., 2009). Cao et al., (2009) worked on to main disadvantage of EDM that are low MRR and poor surface finish. They combined the a constant magnetic field on both side of discharge channel the discharge current and pulse duration were chosen as the variable to investigate the effect on MRR and surface roughness.

#### 1.4.5. Laser Beam assisted Electrical Discharge Machining (LBAEDM):

Li et al., (2006) proposed hybrid machining processes consisting laser beam machining (LBM) and EDM for drilling micro-holes of next generation fuel injection nozzles. The conditions of LBM and EDM were examined by them to meet the desired alignment of nozzle hole. Kuo and Huang, (2003) used LBM in EDM to produce micro holes and compared the results with Micro-EDM process for dimensional accuracy regarding over cut and tapered angle. From experimentation, they concluded that performing micro-EDM and LBM such as MRR and dimensional accuracy is mainly depends upon the laser power, wavelength, pulse duration, frequency discharge energy, and thermal properties of the material. The heat affected zone around the micro-hole machined by LBM is higher as compared to the micro-hole machined by the micro-EDM. Rasheed, (2013) performed exclusive work on comparison of Micro-hole produced by laser beam assisted EDM and traditional EDM process. He observed that although the MRR was high in Micro-EDM but the surface morphology of the hole was poor.

#### 1.4.6. Ultrasonic vibration Assisted EDM (HYBRID EDM):

Ultrasonic vibration assisted Electrical Discharge Machining (HYBRID EDM) process is a promising hybrid process and an active area of research. Researchers have investigated this hybrid process for normalizing the EDM's necessary process conditions and performance characteristics enhancement for advanced materials. HYBRID EDM can be consider as a system itself as shown in Figure 1.5 comprises four main elements Tool vibrating electrode, Workpiece vibration, Dielectric medium vibration with Control mechanism system

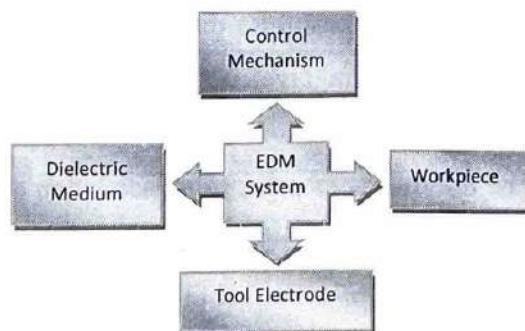


Figure 1.5 The basic elements of traditional EDM System.

Ultrasonic vibration (UV) is accomplished by traversing vibration to any of the sub-system except control sub-system as mentioned above in a traditional EDM system with the help of UV generating devices.

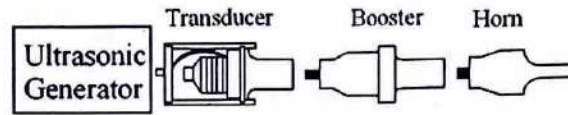


Figure 1.6 Piezoelectric ultrasonic vibration generating device.

An Integrated UV generating device comprises generator, transducer, booster and horn/sonotrode is easily available in market in Figure 1.6. Simply by redesigning the horn and/or sonotrode longitudinal ultrasonic vibration can transferred to any of sub-system of traditional EDM system.

This hybrid process has been proposed to machine high strength materials i.e. composites and super alloys with complex geometries successfully. In Hybrid EDM the relative stationary machining gap is replaced by relative reciprocating motion of sub-system (Tool, Workpiece and Dielectric) with intention to better circulation of dielectric fluid to attain normal necessary discharge conditions and improved performance index. The objective of introducing high frequency longitudinal vibration to EDM tool is to provide better control over process conditions (Masuzawa and Heuvelman, 1983). The effective enhancement by imparting UV action to tool electrode is primarily ascribed to the better transmission of dielectric and debris elimination from work piece surface (Praneetpongung et al., 2010). Singh et al., (2011) concluded from their experiments and analytical studies that discontinuous ultrasonic workpiece vibrations improve the MRR by improving the dielectric flushing to a greater extent. The reason for different machining performance is due to the difference in pumping action created by different ultrasonic vibrations. The regular duration, breadth and number of micro-cracks amplify with the peak current and pulse interval. The micro-cracks seem to reduce when the peak current and pulse duration are set at low levels with discontinuous vibration. The alternating ultrasonic vibrations leave less volume of re-solidified bits and pieces in each crater which gets extinguished with adjacent dielectric parting a rougher surface with minute micro cracks.

#### **1.4.7. Ultrasonic vibration Assisted Wire-EDM (US-WEDM):**

US-WEDM process is considered as the most prominent and successful technique among the strategies for enhancing the flushing condition and machining effectiveness. This hybrid process is viable methods for enhancing the flushing condition in ultrasonic wave assisted EDM. Utilizations of ultrasonic vibration to Wire-EDM was introduced and developed by Guo et al., (1997) and Lee et al., (1998). The surface morphology was additionally moved forward through this method. They demonstrated that the vibrating wire made various nodes and antinodes. The quantity of nodes and antinodes would increment if the frequency of vibration incremented. The relocation of antinodes expanded the fluid pressure variety and dissemination of dielectric stream and subsequently enhances the flushing of molten materials

##### **1.4.7.1. Ultrasonic wire vibration Assisted Wire-EDM (Wire-USWEDM):**

Ultrasonic wire vibration Assisted Wire-EDM (Wire-USWEDM) process is a promising hybrid process and an active area of research. Kavtaradze et al., (1989) reported about superposition of ultrasonic vibrations in wire electrode. Moreover, Lipchanskii, (1991) experimentally investigated the ultrasonic vibration-assisted WEDM and found improvement in process performance. Guo et al., (1995) developed a mechanism consisting of a transducer, a wire holder and an ultrasonic generator mounted on a WEDM to study the vibration of the wire. The wire was vibrated to 12mm amplitude on 35 kHz frequency to investigate the machining mechanism of WEDM assisted by ultrasonic vibration of the wire. It has been observed that ultrasonic vibration increases the cutting efficiency of WEDM by 30% and reduce the roughness of the machined surface remarkably. The results show that the cutting rate increases whether or not the displacement of vibration is coincided with the cutting direction. The overall machined surface tolerance is found to be dependent on the modes of vibration of the wire under the conditions of ultrasonic assistance. The surface residual tensile stress is also reduced with ultrasonic vibration.

##### **1.4.7.2. Ultrasonic work-piece vibration assisted Wire-EDM :**

In the past investigations, vibration was conferred to the wire while exceptionally a couple of analysts have ever uncovered about vibrating the workpiece. The limitation

originates from the weight and the irregular state of workpiece, which make it hard to vibrate at the resonating frequency. The principle issue related with this improvement was to contemplate the fundamental consistency of applying workpiece vibration to the WEDM procedure by thinking up an extraordinary methodology and apparatus. In the USWEDM tests proposed by Han et al., (2013), the unpleasant cutting procedure was tried and the vibration of Ti6/4 workpiece was utilized parallel to the cutting heading by a level plane set transducer. The workpiece (horn itself) and transducer together was not submerged in the dielectric water keeping in mind the end goal to keep the entrance of water inside the transducer, rather deionised water was flushed to the machining zone at a pressure of 1.5Pa from best and base sides of the workpiece. The outcome of tests demonstrated that the machining rate expanded with an expansion of vibration frequency up to 14μm and somewhat diminished from that point, which enhanced most extreme more than 10% contrasted and the machining rate without vibration. It was additionally watched that the machining rate was higher for the more slender workpiece (5mm) than that for the thicker one (10mm) as the machining region was more prominent in the last case. Contrasting to the vibration of wire, the flat vibration of workpiece changed the start hole of entire start region in the meantime, not simply changing some start purposes of wire vibrating (Hoang and Yang, 2013). So it could quicken the slurry course between the wire and workpiece all the more viciously and increment the cutting rate. Additionally, with the upsides of workpiece-energized strategy the use of small scale WEDM in tools and passed on machining industry could be all the more generally extended.

### **1.5. Advantages of EDM process:**

Traditional EDM machines can be programmed for vertical machining, orbital, vectorial, directional, helical, conical, rotational, spin and indexing machining cycles. This adaptability provides EDM process much compensation over traditional manufacturing technology.

- **Flexibility to Metals:**

The method can be adapted to all electrically conducting metals and alloys and does not matters of their melting points, mechanical properties. This process is suitable to various advanced material.



- **Profiles and contours :**

Any complicated profiles and contours that can be developed on the tool can be reproduced on the work piece. Highly complex profiles and contours shapes can be made by shaping the tool with divide sectioned profiles, by welding, brazing or by pertaining swiftly setting conductive epoxy adhesives.

- **Machining of hard metals:**

This EDM process can be used for particularly hardened material. Hence, the deformation of the work piece produced out of the heat treatment process can be eradicated. Time of machining for hard metals is less than conventional machining processes.

- **Residual stress:**

This processes developed minimum residual stresses on the machined surface as compare to other traditional machine tools. It is attributable to the verity that the bodily contact between the tool and the work piece is purged. Thus, delicate and lean workplaces can be machined without deformation and stresses.

- **Surface quality:**

Perforated type of exterior surface finish by design generates space for lubricants causing the die life to develop. Hard and corrosion resistant surfaces, fundamentally desirable for die making, can be generated.

#### **1.6. Application of EDM:**

The EDM is utilized for the fabrication of tool and dies having muddled profiles and various different segments. The EDM gives financial focal points to making stamping tool and dies, wire drawing and expulsion tool and dies, forging dies, multifaceted shape mould cavities and so forth.

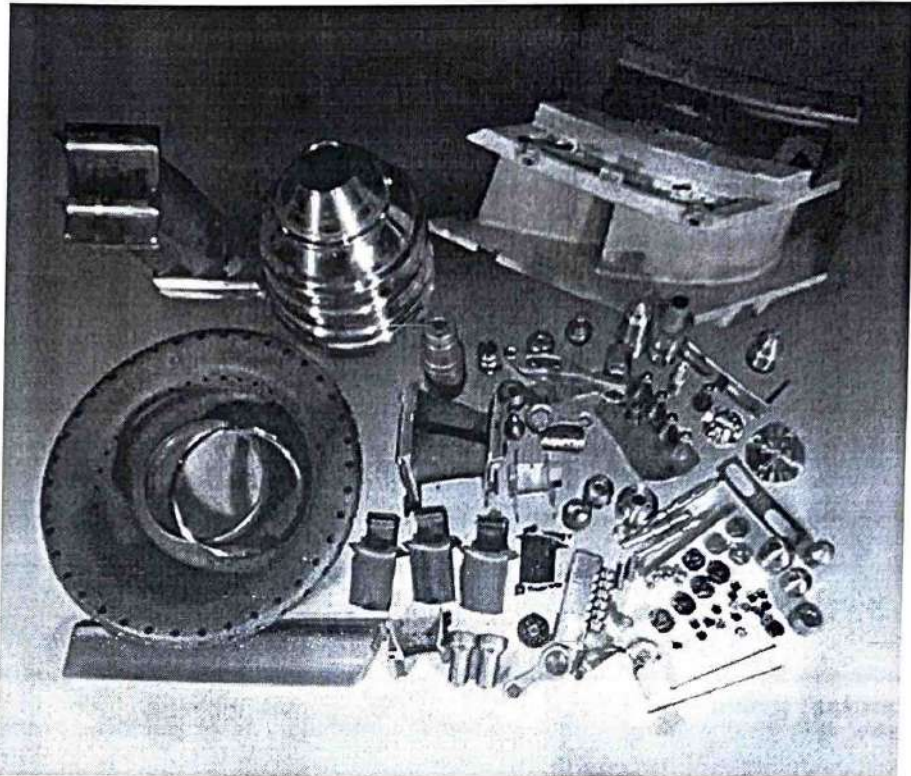


Figure 1.7 Precision fasthole and micohole EDM drilling (AA EDM Corporation)

It has been to a great degree utilized for machining of intriguing materials utilized as a part of aviation ventures, obstinate metals, hard carbides and heat treated capable steels. Typical EDM application includes fine cutting with tread shaped electrodes (wire-cutting EDM), drilling of micro-holes, tread cuttings, helical profile milling, rotary forming, curved hole drilling. Manufacturers also produce EDM machines for the specific purpose of removing broken tools (drill bits or taps) from work pieces. In this application, the process is termed "metal disintegration machining". Delicate work piece like copper parts for fitting into the vacuum tubes can be produced by this method. The work piece in this case is fragile to withstand the cutting tool load during conventional machining. Fig 1.7 and 1.8 show some of the components produced by EDM techniques.

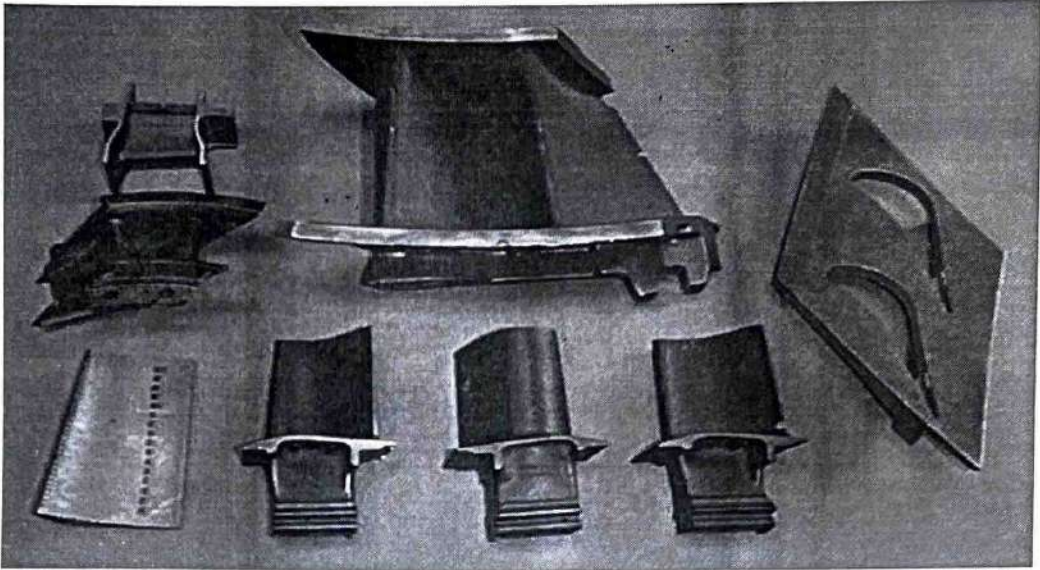


Figure 1.8 Holes, slots and shaped holes for larger aerospace blades, vanes, rings, burner, etc. (AA EDM Corporation)

The present application of WEDM process includes automotive, aviation, mould, tool and die manufacturer. WEDM applications can also be found in the medical, optical, dental, jeweler industries, and in the automotive and aerospace R & D areas (Ho et al., 2004).

The machine's capacity to work unattended for quite a long time or even days additionally expands the allure of the procedure. Machining thick segments of material, as thick as 200 mm, notwithstanding utilizing PC to precisely scale the extent of the part, make this procedure particularly important for the manufacture of tools and dies of different kinds. The machining of press stamping dies the tools is improved in light of the fact that the punch, pass on, punch plate and stripper, all can be machined from a typical CNC program. Without WEDM, the manufacture procedure requires numerous long stretches of terminals creation for the ordinary EDM system, and additionally numerous long periods of manual granulating and cleaning. With WEDM the general manufacture time is lessened by 37%, notwithstanding, the handling time is diminished by 66%.

### 1.7. Limitation of Traditional EDM Process:


The advanced materials (Nimonic, Titanium, Inconel, Composite Materials, TiNi SMA, Niobium, Tungsten and Aluminum Alloys) ignite the necessity to develop further this traditional EDM processes. Researchers have been consistently working on traditional EDM with an aim to accomplish better dissemination of dielectric liquid and stable discharge conditions that resulted in enhanced MRR, thin recast layer, better process stability, high aspect ratio, and vitality productive arcing and short-circuit (A. Kumar et al., 2016). But traditional EDM alone unable to meet the today's industrial metal cutting challenges. There is a need of innovative brain storming to providing better control over EDM machining conditions. Some other limitations associated with this process are discussed below;

- Poor flushing away of machined debris.
- Frequent adhesion of the tool electrode to the workpiece.
- Higher fraction of unwanted discharge states for manufacturing of high aspect ratio micro geometries holes.
- Stagnation of debris.
- Extensive tool wear.
- Low material removal rate.
- Unwanted gases generate during machining pollute the environment.
- Residual stresses and micro-cracks deteriorated strength of material.
- Thick recast layer and heat effect zone of machined surface.

The unpredictability of gap dimensions especially with intricate work piece geometry reduces the desired achievable accuracy. Hybrid Electrical Discharge Machining is a splendid concept gaining attentions of researchers to meet these limitations

## LITERATURE SURVEY AND PROBLEM FORMULATION

## 2.1. Literature Review



Electrical discharge machining (EDM) is a fascinating advance manufacturing technology, exclusively for machining of aerospace, automotive industry and surgical components (Pandey and Shan, 1983). But machining of advance materials (Nimonic, Titanium, Inconel, Composite Materials, TiNi SMA, Niobium, Tungsten and Aluminium Alloys) for high accuracy and high surface quality deteriorate its performance. A normal EDM process would hardly be a complete solution for present industrial metal cutting requirement. The institution of advanced materials ignites the necessity to develop further this traditional EDM processes. Some of the common limitations with normal EDM are discussed in section 1.7 of Chapter 1. The problem magnifies especially with intricate work piece geometry reduces the desired achievable accuracy and precision. The Hybrid Electrical Discharge Machining is a splendid concept gaining attentions of researchers to meet these limitations.

Lots of research work is going on throughout the world to ameliorate its productivity and process stability. The perception of ultrasonic vibration (UV) in conventional EDM is a novelty to this process, with the potential of improved metal cutting with high accuracy, surface quality and productivity. It is because of unique characteristics of longitudinal ultrasonic mechanical vibration that can propagate through solids with a frequency of above 15 kHz (Kuo, 2009). A basic EDM system comprises three main elements i.e. Tool electrode, Work piece, Dielectric medium along with a control mechanism system as show in Figure 1.6 (Chapter 1).

In this Hybrid EDM process, stationary machining gap is supplanted with an element responding movement of conventional EDMs framework components (i.e. Tool, workpiece and dielectric) in die-sink EDM. The hypothesis is flushing of contaminated dielectric and to stabilize discharge conditions to avoid abnormal discharges. UV perception is accomplished by traversing mechanical vibration to any of the sub-system of EDM either tool, work piece or dielectric medium with the help of UV generating devices. The stationary machining gap is replaced by dynamic

reciprocating motion of sub-elements (Tool, Workpiece or Dielectric medium) with intention to enhance flushing of dielectric fluid and necessary discharge conditions.

Murti and Philip, (1987) discussed cavitation effect of UV in EDM. According to them, Cavitation is nucleation, development, and burst of vaporous air pockets that was caused by acoustic pressure. The ultrasonic field's force caused by acoustic pressure was the major components having huge impacts in UV assisted EDM. Cavitation bubbles rare occurrence was firmly correlated as the role of acoustic pressure, motions recurrence, dielectric liquid density and sound speed in dielectric medium. This backward and forth spatial variation prompts expanded hydrostatic pressure gradient to flush the contaminated dielectric. Only a few researchers have examined ultrasonic vibration aided wire-EDM in the accessible available literature domain.

Some very early experimental investigations were undertaken by Kavtaradze et al., (1989) and Lipchanskii, (1991). Most of these work focused on transfer of ultrasonic vibration to wire electrode. The main hypothesis for that concept was flushing of sullied dielectric fluid, regular successful discharge condition and surface morphology under different controllable parameters to assess the likelihood instead of the assurance of quality characteristics.

Zhixin et al., (1995) elucidated that the ultrasonic waves spread as a flexible wave from tool electrode and results in elective pressure and rarefaction of dielectric medium to workpiece. The mechanical vibration of workpiece caused the molten metal and gas gone up to evacuate effortlessly and come about less short circuits.

Guo et al., (1995) endeavoured the wire vibration along and normal to the cutting direction and vindicated 30% increment in cutting rate as well as diminishment in surface roughness. They also proposed the mechanism of metal cutting for ultrasonic vibration of the wire and concluded that ultrasonic vibration of wire prompted less stress in the wire that reduced frequent wire breakage. They specified that the high-frequency ultrasonic vibration of wire move the discharge focuses and influenced the discharge wave dispersion more uniform in whole discharge channels.

According to Lee et al., (1998), the high frequency directing activity of the tooltip, drained the debris from discharge gap and sucked new dielectric into cutting region.

The action of tooltip enhanced discharge frequency and thereby increased metal removal rate (MRR).

Lin et al., (2000) analysed the machining characteristic of titanium alloy using UV of tool electrode. They claimed that UV improved discharge wave form and thereby diminish spark delay, which encouraged the typical normal discharge condition. Contrasted with the instance of "without ultrasonic vibrations", the spark recurrence was higher. The chronic discharge wave profile appeared to have prompted an expansion in the machining effectiveness.

According to Ghoreishi and Atkinson,(2002), acoustic pressure made more molten metal to expelled from the crater, that caused gas bubbles and debris a solid float. These cavitation air pockets progressed toward surface becoming non-round and drive rapid planes of fluid into the machining surfaces, and make shock waves. They also described that the inbuilt control system of EDM diminished the current and reduced gap between tool and workpiece. The inbuilt control system of EDM influenced the discharge gap, and coagulation of debris prompted arcing and short/open circuit.

Ghoreishi and Atkinson,(2002) also implemented various innovative flushing method in normal EDM, as they observed that the conventional methods of flushing by infusion, suction, side flushing were insufficient to meet the new technological challenges of EDM. Fresh dielectric was a vital condition required to release spark through ionization of the dielectric within gap.

Wansheng et al., (2002) proposed UV in EDM for machining of deep holes and explained that the sensitive servo and pulse system tried to keep up the fundamental consistent state for EDM machining for proficient release. Ultrasonic vibration at high discharge energy setting encourages the penetration of atoms and ion onto the machined surface that are escaped from tool electrode evaporation and dielectric medium ionization. The acoustic forces so raised results in apparent increment in micro-hardness of machined surface.

Huang et al., (2003) described that ultrasonic vibration of workpiece developed solid stirring impact and brought about amazing evacuation in small micro-EDM process that enhanced more than 60 times of the machining effectiveness.

Nishiwaki et al., (2008) illustrated that at the point when a large mess of debris and bubble existed at the discharge gap, the electrical discharge ended up noticeably

anomalous. The debris coagulation within the discharge gap contributed to condition of abnormal discharge.

Yu et al., (2009) transacted ultrasonic vibration to enhance the aspect ratio. They pointed out that presence of debris and bubble in discharge gap provoked the secondary sparks between the tool and the debris. They also observed that the machining speed slow down when the hole was drilled deeply in normal micro-hole drilling by EDM. The planetary movement of an electrode provided an uneven gap through which the bubbles and debris escaped from the working area easily to avoid blocking of dielectric flow into working area in normal micro-hole drilling. Where as in ultrasonic tool vibration, the tool electrode feed rate increased significantly. The UV action of tool enhanced the wetting effect in discharge gap.

Abdullah et al., (2009) described the effect of ultrasonic vibration on surface integrity. They concluded that ultrasonic wave in dielectric medium could create an extensive variety of pits and exposed fresh profoundly warmed uncut workpiece surfaces that might be in charge of the disintegration of the tool and workpiece materials. They also imparted ultrasonic vibration and found slight increment in the tool wear and decrease in recast layer thickness.

Marinescu et al., (2009) proposed solution for the performance of ultrasonic vibration assisted EDM. They discussed that the collapse of cumulative micro jets and all bubbles rose from the discharge region; produced shock waves parallel to machined surface, these were accountable of poor surface finish.

Kuo, (2009) analyzed the application of vibration in EDM. They observed that, execution of vibration in EDM process relied upon the discharge energy, whereas higher discharge energy stimulated surface roughness. The application of ultrasonic vibration decrease span of arcing and vast numbers of arcing per pulse duration and hence significant reduce the machining time.

Peng and Liao, (2004) explained that the cyclic pressure apply a positive pressure to cavitation bubbles and push the dielectric elements together, while extension cycles triggered a critical size of bubble until it rough crumple in the gap.

Singh et al., (2011) accomplished finite element analysis followed by experimental investigation and acclimated that the pumping action caused by workpiece ultrasonic vibration in Die-sink EDM. Dielectric medium directed out while workpiece upward



movement was like the beating action of the reciprocating pumps, amid the falling motion of the workpiece sucked dielectric inside the discharge gap.

Shabgard et al., (2013) perceived the fuzzy logic algorithm for optimization and modeling of multiple objective problems in UV assisted EDM. A fuzzy model for the prediction of tool wear ratio (TWR), MRR, and surface roughness for tungsten carbide (WC-10%Co), machining were developed and validated with experimental results. They suggested that the MRR and surface roughness increase with the pulse on time and peak current.

Iwai et al., (2013) used UV of tool electrode in EDM to machine polycrystalline composite diamond. They claimed that the pounding action of the tool electrode creates alternative suction of fresh and exhaust of contaminated dielectric and facilitate the most appropriate condition for dielectric ionization in the gap.

Schubert et al., (2013) discussed the enhancement of micro EDM, they claimed the Ultrasonic vibration of tool tip activity, forces the frontal discharge region. The two noteworthy aftermath of UV of the tool is dielectric medium vibration and intermittent bolster withdrawal developments of ionization region width through the vibrating parts.

Hoang and Yang, (2013) transferred ultrasonic vibration to work piece. They recognized that the ultrasonic vibration of workpiece brought some 1.5 times higher machining rate compared to that of wire vibration in Wire-EDM. They acquired cutting rate 2.5 times to that of the normal wire-EDM process and at the same time increase the wire cutting accuracy with minimum kerf width.

Han et al., (2013) studied the effect of workpiece as a horn ultrasonic vibration in wire EDM, and discussed the effect of workpiece vibration on kerf width, machining rate and surface finish. They observed 10% improvement in machining rate, but ironically surface roughness also increased with that.

Shabgard and Alenabi, (2015) evaluated the surface morphology under Ultrasonic vibration of tool. They concluded that ultrasonic vibration of tool reduced abnormal discharge and open circuit pulses and increases normal discharges that stabilize the machining process. They also explained that low pulse energy generate low heat effected zone, whereas thick heat effected zone and high crack density was obtained at high pulse energy in both UV assisted EDM and normal EDM process. They also

explained with the help of SEM cross-section micrographs of machined surface that a thin lamina of condensed molten metal with varying thickness and typically very hard beneath this. This entrapped lamina of condensed molten metal causes residual stress concentration, micro-holes and cracks; this ultimately leads to poor surface morphology of workpiece.

The pulse on time increase the discharge energy that caused high dissipation of molten metal and large crater size left behind. The surface roughness results were not consistent with low frequency of vibration (Chugh et al., 2015). The unpredictable and stochastic nature of the factors associated with this process limits its maximum capacity utilization. Ultrasonic vibration was introduced to widen Die-sink EDM's machining adequacy with confounded geometry at high accuracy. (Kumar et al., 2016)

Kumar et al., (2017) identified the 21 sub-factors affecting the overall performance of Hybrid EDM and they further grouped these factors into five major factors. They concluded that flushing and dimensional accuracy obtained through these waves, were the main contributors to the Hybrid EDM performance.

Khosrozadeh and Shabgard, (2017) studied the effect of UV in Die-sink EDM. They concluded that the Residual stresses generated due to UV of the tool are of compressive in nature and smaller than that of conventional EDM.

In an exclusive work carried out by Nani, (2017), concluded that wire vibration increase the intensity of dielectric liquid breakdown. The hammering action caused by an ultrasonic field to that debris helped in improving the surface finish.

Muttamara et al., (2018) applied ultrasonic vibration in EDM using Tin powder combined with dielectric medium and observed that the combined effect can diminish the cracks on machined.

Liu et al., (2018) applied a simulation study to demonstrate the mechanism of debris remove UV assisted Hybrid EDM process. They observed that the high frequency and amplitude of vibration enhance the dielectric fluid circulation between the tool and electrode. This ultrasonic vibration of tool facilitate in process stability.

## 2.2. Identified Gaps in Literature:

Form literature survey, It has been found that the ultrasonic vibration in EDM process is a convoluted undertaking. Recent developments in ultrasonic vibration assisted Hybrid-EDM with various input process parameters, performance indexes and the hypothesis tested are shown in Figure 2.2.

The researchers have formulated and tested these hypotheses experimentally to evaluate the probability rather than certainty of hypothesis. It was found that hypotheses such as MRR, SR and residual stresses had been less explored for normal Wire-EDM, whereas flushing of contaminated dielectric fluid and dimensional accuracy hypotheses had been considered more frequently and significantly contributes the performance of Hybrid-EDM process. In literature review, some qualitative parametric challenges such as flushing (Evacuation of debris, pumping effect and stirring effect) and abnormal discharge (arcing and short circuit, discharge wave distribution) were observed. The concept of ultrasonic vibration in EDM is still under developing stage.

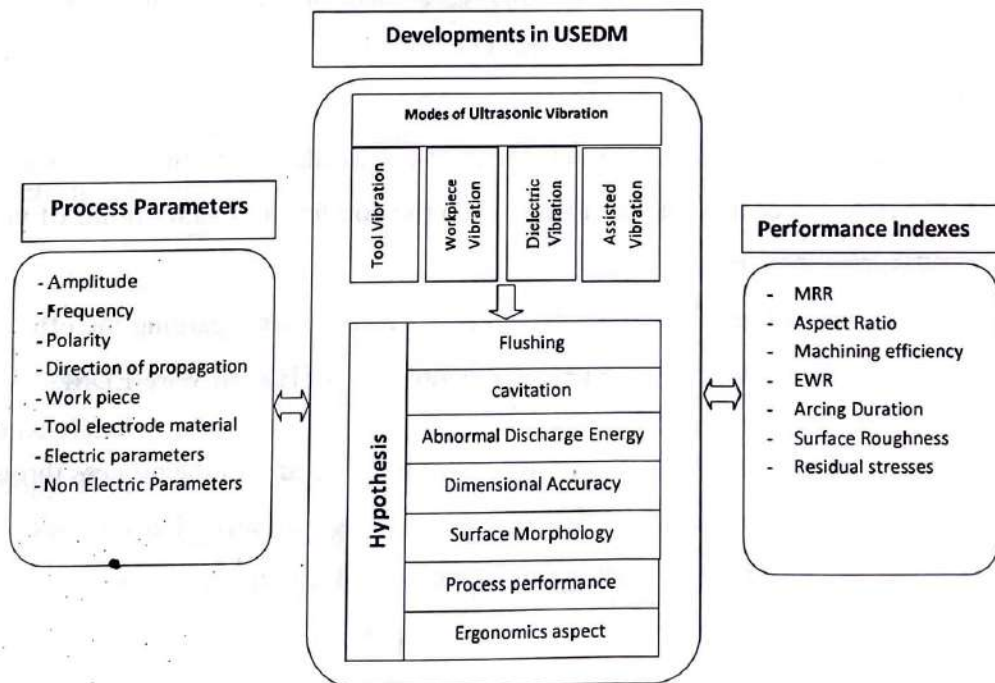


Fig. 2.1 Recent developments in Hybrid EDM with various input process parameters, Performance indexes and the Hypothesis Tested.

There are different technical difficulties associated with execution of this process. The measures and attributes of Hybrid-EDM process contrast each other, and generate uncertainty conditions and yield lots of space for further growth. After a comprehensive study of the existing literature, the gaps have been observed in ultrasonic vibration assisted Hybrid EDM process.

- A few efforts have been made in recognizing and ranking of qualitative and quantitative factors affecting the implementation of Ultrasonic Vibration in EDM process.
- Almost negligible efforts have been made to establish relative importance and correlation among these qualitative/quantitative factors by quantitatively analyzing their inheriting strength in implementing Ultrasonic vibration in EDM.
- Almost all studies investigated the influence of continuous tool and wire vibrations only. Study on work piece vibration is limited and only with narrow range of amplitude of vibrations. Also discontinuous work piece vibration remains untouched.
- Literature review reveals that limited researchers have carried out the work on Ultrasonic vibration in Wire-EDM which includes developments, monitoring and control of the process.
- There is no or very limited information available in the direction of optimization of process parameters from the component quality point of view of Hybrid Wire-EDM.
- There are conflicting opinions from various researchers regarding the effect of some of the variables on the response parameters of Hybrid Wire-EDM.

Although some efforts have been reported towards the control of the process through analytical modeling to suggest the process mechanisms, yet several key issues (e.g. Mechanism of dielectric fluid flushing in normal EDM and hybrid EDM process to enhance productivity etc.) remained mostly untouched.

### **2.3. Statement of the problem:**

The outcomes built up in literature convey that better machining yield for ultrasonic vibration can be obtained in normal EDM. In EDM process, oxides (or debris) are

created and accumulated in the sparkling gap between an electrode and a work-piece. It required dedicated experimental investigation to analysis the impacts of work piece vibration at the machining characteristics are contemplated at various amplitudes. The focus should be given to develop a mathematical model for Ultrasonic vibration assisted Wire-EDM including important parameters and their interactions with multi-performance characteristics of Hybrid Wire-EDM. Almost all previous studies focused mainly on the effects of single or a small range of vibration amplitude with continuous vibrations only. It may also be considered as discontinuous vibration is one of the most suitable parameters for the implementation of ultrasonic vibration in Wire-EDM for machining of material of exceptional hardness, wear resistance and high mechanical strength. Surface finish and residual stresses are the most sort-out output parameters in field of precision die manufacturing. These are the machining characteristic that plays a very critical role in determining the quality of engineering components. Good quality surfaces improve the fatigue strength, corrosion and wear resistance of the workpiece. Vital conditions for accomplishing productive in Hybrid-EDM comprise in understanding the present and forthcoming objective and attribute of the Hybrid-EDM. There is a requirement of basic, orderly and logical scientific approach for analyzing different perceptions considering in EDM. An effort is required to identify qualitative and quantitative parameters and their interactions to provide useful information for the implementation of ultrasonic vibration in EDM. The prevalence this analytical study is both controllable parameters and objectives functions considered on the same platform.

#### **2.4. Objective of present investigation:**

This research work deals with design, development, application and comparison of ultrasonic vibration assisted in Wire-EDM process in selected advanced manufacturing technology. However the previous studies focused mainly on the effects of single or a small range of vibration amplitude with continuous vibrations only. In this research work, synchronized discontinuous ultrasonic vibrations assisting Wire-EDM process with more range of amplitude of vibration are introduced for machining of high carbon high chromium D2 and D3 steel. . Experiments are conduct to investigate metal removal rate, surface roughness, and residual stresses under a wide range of machining conditions.

- Enlistment and categorization the decisive factors in the path of adoption and implementation of Ultrasonic vibration assisted EDM under different mode of vibration.
- Established relative importance among these qualitative/quantitative factors by quantitatively analyzing their inheriting strength.
- Compared the performance under three modes of ultrasonic vibration imparted to Hybrid EDM process through logical and structural graph theoretical methodology.
- Development of Set up for Hybrid Wire-EDM process.
- Optimization of quality characteristics for High carbon High Chromium D2 and D3 steel material.
- Prediction of optimal sets of proposed hybrid EDM process parameters.
- Prediction of optimal values of quality characteristics.
- Experimental verification of optimized individual quality characteristics.

An orthogonal array based on the Taguchi experimental design along with Response Surface Methodology (RSM) are used to plan the experiments and data and assessed with the Analysis of Variance (ANOVA) to determine the significant machining parameters for higher MRR and wire feed rate.

The optimal machining parameters of the ultrasonic assisted EDM are established to achieve a sophisticated process with higher efficiency of the Hybrid wire-EDM applications for modern industrial requirements.

## **2.5. Different Phases of Achieving Objective:**

### **Phase -I**

➤ Development of experimental set up, providing varying range of input parameters in continuous and discontinuous ultrasonic vibrations assisting wire-EDM process with more range of amplitude of vibration for measuring the selected responses.

## **Phase –II**

- Investigation of the effects of Continuous/discontinuous vibrations assisting Wire EDM process parameters on quality characteristics viz. erosion rate, surface roughness and residual stresses.
- Optimization of quality characteristics of machined parts.
- Prediction of optimal sets of Ultrasonic vibrations assisting Wire-EDM process parameters.
- Prediction of optimal values of quality characteristics
- Prediction of confidence interval (95%CI)
- Experimental verification of optimized individual quality characteristics

The Taguchi's OA used for experimentation on Continuous/Discontinue vibration vibrations assisting Wire-EDM process under parameter design approach has been used to obtain the above objectives.

## **Phase –III**

- Development of mathematical models and response surfaces of cutting rate, surface roughness using response surface methodology

The half fractional second order central composite rotatable design is to be used to plan the experiments and the input parameters like amplitude of vibration, pulse on time, pulse off time, peak current, wire feed rate under continuous and no-vibration to ascertain their effects on the MRR and SR.

## **Phase –IV**

- Development of single response optimization model using desirability function
- Development of multi objective optimization models using desirability function
- Determination of optimal sets of process parameters for desired combinations of quality characteristics
- Experimental verification of quality characteristics optimized in different combinations

## **Phase –V**

- Development of multi objective optimization models using Taguchi technique and utility concept
- Determination of optimal sets of ultrasonic vibrations assisting Wire-EDM process parameters for desired combined quality characteristics
- Experimental verification of quality characteristics optimized in different combinations.



### ANALYSZING AND COMPARITIVE STUDY OF HYBRID EDM USING GTA APPROACH

---

In this study, some qualitative as well as quantitative parameters have been identified through literature that affecting Hybrid-EDM performance. The parameters under considering were flushing (Evacuation of debris, pumping effect and stirring effect) and abnormal discharge (arcing and short circuit, discharge wave distribution). On the premise of literature surveys, the main factors and sub-factors affecting Hybrid-EDM process execution were recognized and gathered in Table 3.1. There was a requirement of simple, systematic and logical methods or mathematical tools to guide for considering and selection of attributes/objectives and their interrelations for the proposed process. To meet the various technological challenges, an interactive Graph theory approach was selected with pre-defined objective to compare attributes, and likewise obtain the most appropriate combination of attributes. This methodology allowed for interactive enhancement and test of knowledge of ultrasonic vibration assisted EDM. A Graph theory approach is a logical and systematical approach useful for modeling and analyzing various science and technological problems (Rao and Gandhi, 2002). An endeavor has been made through this present work to know the nature and therefore assessed the relative interdependency and legacy of various dependent and driver variables, which in past have been speculatively analyzed with likelihood instead of assurance without considering Hybrid -EDM as whole system. The principle objectives of this study are:

- To identify and categorize the various decisive factors and sub-factors affecting the performance Hybrid-EDM under process.
- To establish interdependency among these qualitative/quantitative factors by quantitatively analyzing their inheriting strength using the Graph-Theoretic Approach (GTA).
- To achieve a range and coefficient of variation of performance index value through a structural GTA methodology.

Graph theory approach allowed monitoring of the simultaneous effect of all the factors. This interactive methodology provided approximate solution in a reasonable time frame and cost with reasonable effort.

### 3.1. Identification and categorization of factors:

Form literature survey, It has been found that the ultrasonic vibration in traditional EDM process is a convoluted undertaking. There were sure attributes which contribute for Hybrid -EDM process performance index grouped here in this study and discussed in next paragraphs.

Table 3.1 Factors and sub-factors affecting the Hybrid -EDM process performance

Factors	Sub-Factors	Reference
1. Flushing	1. Suction & Exhaust of Dielectric due to Pumping Action	(J Singh et al., 2011) (Kremer et al., 1991)(Schubert et al., 2013)(Zhixin et al., 1995a) (Ghiculescu et al., 2014)
	2. Debris and gas bubble debris evacuation	(Kremer et al., 1991)(Kremer et al., 1989) (Kim et al., 2006) (Ghiculescu et al., 2014)
	3. Frequency of pumping action	(Lee et al., 1998)
	4. Stirring effect	(Liew et al., 2014) (Huang et al., 2003)
2. Cavitation	1. Ultrasonic field force	(Murti and Philip, 1987)(Ghiculescu et al., 2012)
	2. Acoustic pressure	(Murti and Philip, 1987)(Kremer et al., 1991) (Ghiculescu et al., 2014)
	3. Dielectric fluid density	(Liew et al., 2014) (Shabgard and Alenabi, 2015)
	4. Sound velocity in dielectric	(Liew et al., 2014)
	5. Vibration amplitude	(Liew et al., 2014) (Ogawa et al., 2012)
3. Abnormal Discharge	Arcing & short circuit	(Ghoreishi and Atkinson, 2002)(Mahardika et al., 2012)
	Debris concentration	(Nishiwaki et al., 2008) (Yu et al., 2009)
	Discharge wave Distribution	(Guo et al., 1997) (Lin et al., 2000)
4. Dimensional Accuracy	Aspect ratio	(Prihandana et al., 2009) (Ho et al., 2004) (Wansheng et al., 2002)
	Tool Wear	(Narasimhan et al., 2005) (Mohri et al., 1991)
	Wetting effect	(Yu et al., 2009) (Kwan, K. M., Benatar, 2001)
	Traverse direction of UV	(Nishiwaki et al., 2008) (Iwai et al., 2013)
	Tool geometry	(Narasimhan et al., 2005)
5. Surface Morphology	Thickness of recast and heat effect layer	(Kremer et al., 1989) (Meseet et al., 2014) (Abdullah et al., 2009)
	Size of micro holes & cracks	(Shabgard et al., 2013)
	Residual stress	(Kremer et al., 1991)
	Micro-Hardness	(Shabgard et al., 2013) (Lin et al., 2001)

It was found that researchers have less explored the influence of factors such as cavitation, abnormal discharge, where as flushing of contaminated dielectric fluid, dimensional accuracy and surface morphology were the most frequently considered factors significantly affecting the performance of Hybrid-EDM process as shown in Figure 3.1.

**3.1.1. Flushing(H<sub>1</sub>):**

Flushing is characterized as the right flow of dielectric liquid between the tool and the work piece (Pandey and Shan, 1983). Generally the flushing was accomplished by infusion, suction, side flushing and pumping activity (Ghoreishi and Atkinson, 2002). The hammering action of tool electrode splashes contaminated dielectric fluid and allowed the fresh to move into the gap (Kremer et al., 1989). The high frequency pumping action of the tool tip, pumped the debris away and sucked fresh dielectric into machining region, increased discharge efficiency and metal removing rate (MRR)(Lee et al., 1998). The mechanical vibration influenced the frontal discharge gap due to two major effects. One of which was vibration of dielectric medium and other was working gap width through periodic feed-retraction-movements of the vibrating parts (Schubert et al., 2013).

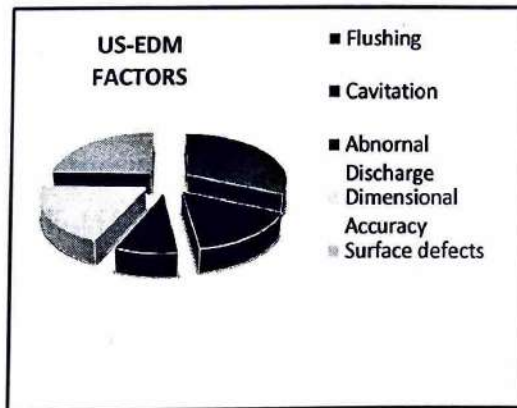


Figure 3.1 Contribution of various factors in Hybrid -EDM performance considered by researchers

The strong stirring effect caused by UV action, which resulted in excellent flushing in micro EDM process that increased the machining efficiency more than 60 times (Huang et al., 2003). Stirring effect was helpful to uniformly distribute the carbon nano-fibers in the dielectric fluid (Liew et al., 2014). The ultrasonic waves propagated as elastic wave through tool electrode and resulted in alternative

compression and rarefaction of dielectric medium to workpiece (Zhixin et al., 1995a). The mechanical vibration caused relative motion of tool to the workpiece imparted the kinetic energy to the discharged debris. This caused the debris and gas bubbles to remove easily and resulted fewer short circuits occurred in discharging (Kim et al., 2006). Singh et al. (2012) developed FEA model using ANSYS 5.4 software for the analysis pressure variation. The pumping action was taken for the analysis. For the FLOTRAN CFD elements, the velocity were obtained from the conservation of momentum principle and the pressure was obtained from the conservation of mass principle. They demonstrated that dielectric fluid was pumped out while work-piece upward motion and that was similar to the pumping action of the reciprocating pumps. And during the downward motion of the workpiece dielectric was sucked inside.

### 3.1.2. Cavitation (H<sub>2</sub>):

Murthi and Philip (1987) identified cavitation (nucleation, growth, and burst of gaseous bubbles), ultrasonic field forces (radiation force, Stoke's force, Bernoulli's attraction), and acoustic streaming as the factors having significant effects in ultrasonic assisted EDM. This phenomenon was strongly related to acoustic pressure, oscillations frequency, dielectric fluid density, sound velocity in dielectric and vibration amplitude (Marinescu et al., 2009)**Error! Reference source not found.** Those alternating pressure variations lead to increased hydrostatic pressure variation (Kremer et al., 1991). Compression cycles exerted a positive pressure and push the liquid molecules together, while expansion cycles increased a critical size of bubble until it violent collapse in the liquid (Pang et al., 2011). The violent collapse of bubbles in the gap, generated shock waves parallel to machined surface, was responsible of roughness decrease. Pressure variation caused more molten metal to be removed from the carter, causing debris a strong drift (Ghoreishi and Atkinson, 2002). Ghiculescu et al. (2012) proposed FEM model of metal removing mechanism of ultrasonic tool vibration assisted Micro EDM. They considered thermal and cavitation effects of UV using cosmol metaphysics and time dependent heat transfer in solids. The Ultrasonic oscillation period consists of semi period of dielectric compression from the gap and a stretching semi period. That could generate a wide range of pits and produce newly exposed highly heated surfaces that may be responsible for the erosion of the tool and workpiece materials (Abdullah et al., 2009). The cavitation

occurred more easily when the homogeneity of the liquid was disturbed by external particles. The debris within the discharge gap created during the EDM enhanced the cavitation effect.

### 3.1.3. Abnormal Discharge (H<sub>3</sub>):

In EDM metal removing is due to thermal phenomenon caused by local temperature in the region of 8000-12000 °C (Hassan Abdel Gawad El-Hofy, 2005). A layer of metal melted and ejected due to electric discharge as a result of ionization of dielectric medium, and tiny particles from the workpiece surface evacuated called debris. However, when debris remained between the electrode and the workpiece surface, the electric discharge occurred not between the electrode and the workpiece surface but between the debris and the electrode (Yu et al., 2009).

The accumulation of debris in discharge gap that restricted the further machining is called a state of abnormal discharge. The performance of EDM process depended on the discharge energy, where as higher discharge energy lead to poor surface finish. The control system reduced the current or energy and smaller the gap. That made control task more complex and accumulation debris might build a bridge between the electrode and workpiece, allowing arcing to occur that lead to short and open circuit (Abdullah and Shabgard, 2008).

Nishiwaki et al. (2008) measured the discharge gap and depth of hole by using the pulse echo technique during EDM process. Elastic waves generated during electrical discharge in gap, these waves passed through workpiece and variations of the received elastic waves were detected by ultrasonic transducer. Elastic waves were caused at electric discharge points could not be detected because the elastic waves become a noise. When debris concentration becomes high an abnormal electric discharge state occurred. Then, the work piece could not be machined further. In order to control the abnormal discharge state flushing of these highly concentrated debris discharge gap is must. The total duration of arcing was reduced by the application vibration and decreased with increasing frequency. The numbers of arc discharge increased with frequency and resulted in significant reduction of machining time (Garn et al., 2011). Adhesion occurred when the molten metal of the workpiece become attached to the tool electrode, caused the abnormal discharge as a result of

short-circuiting between the workpiece and tool electrode, and inhibiting recovery of EDM machining. Ultrasonic vibration was used to remove adhesion and hence arcing and short circuit that increased metal removing rate (Mahardika et al., 2012).

Yu et al. (2009) observed that the machining speed slowed down when the hole was drilled deeply in normal micro-hole drilling by EDM. The planetary movement of an electrode provided an uneven gap through which the bubbles and debris escaped from the working area easily to avoid blocking the dielectric flow into working area occurred in normal micro-hole drilling. In ultrasonic vibration assistance, the tool electrode feed rate increased significantly because the Ultrasonic vibration enhanced the wetting effect in discharge gap. The high-frequency ultrasonic vibration shifted the discharge points and made the discharge wave distribution more uniform and form discharge channels (Guo et al., 1997). The debris produced from the melted metal could accumulate in the discharge gap and cluster with carbon element and tar produced from the pyrolysis of kerosene, thus making the discharge condition abnormal and leading to arcing. The ignition delay reduced due to discharge wave form that improved the bridging effect to facilitate the normal discharge (Lin et al., 2000). A higher discharge frequency and regular discharge wave profile obtained by ultrasonic vibration increase machining efficiency compared to without vibration (Prihandana et al., 2009).

#### **3.1.4. Dimensional Accuracy (H<sub>4</sub>):**

The machining of holes with high aspect ratio and depth faced dimensional inaccurate, the inaccuracy increases with complex geometry. The tapered hole and overcut were resultant of critical frontal tool wears (Ho et al., 2004). Dimensional accuracy was a function of tool geometry (shape and size) and its path (Narasimhan et al., 2005). Tool wear was affected by the precipitation of carbon from the hydrocarbon dielectric onto the electrode surface during sparking. The rapid wear on the electrode edge was due to the failure of carbon to precipitate at difficult-to-reach regions of the electrode (Mohri et al., 1991). In addition, the worn electrode reduced the machining accuracy because the generated feature was the result of a combination of the tool electrode shape and its tool path (Narasimhan et al., 2005). Ultrasonic vibration assistance of workpiece slightly decreases the tool wear ratio (TWR) on finishing regime, the exception is found at pulse-on time 50 $\mu$ s (Shabgard et al., 2011).

When the debris traversed longer distance before to be expelled completely, these could generate more sparks between tool and the workpiece walls and resulted higher overcut (Teimouri and Baseri, 2013). The adhesion of the oil-decomposed carbon to the electrode surface caused by electrode wear rate and it was higher when complex direction of prorogation of vibration imparted(Iwai et al., 2013). High aspect ratio restricted the debris evacuation because of the turned over edges of the craters, secondary discharge occurred easily at hole internal surface that caused taper dimensional inaccuracy (Wansheng et al., 2002). Wetting effect of ultrasonic vibration weakened the boundary between bubble and dielectric that cause reduction of viscous resistance and the bubbles were broken easily and consequently higher aspect ratio can be achieved (Yu et al., 2009). Srivastava and Pandey, (2012) and Abdullah et al (2009) applied the ultrasonic vibration causes slight increase in the tool wear as the amount of recast layer deposited on the tool reduced.

### 3.1.5. Surface Morphology ( $H_s$ ):

A typical cross-section of work surface after traditional EDM process exhibits a thin layer of molten metal and has no fixed thickness usually very hard below this. The molten metal region of workpiece layer in extremely hot region vaporized and expelled away by high pressure wave generate due to dielectric turbulence from the electric discharge, while material underneath remain solid. This caused stress concentration, pinholes and micro-cracks and eventually led to poor strength of the workpiece (Guu, Y. H., Hocheng, 2001). According to Lin et al. (2000), the possible reason for thin recast layer in the combination EDM/USM process was the completely remove of molten metal for the gap.

In Hybrid-EDM process the recast layer was more regular and continuous, it was sometime slightly thicker. The residual stresses set up to a certain depth only, no significant effect was observed at the surface, residual stresses having the same value without or with vibrations(Kremer et al., 1989). Lin et al. (2001) find that softening layer adjoining hardness layer improved the hardness of machined surface significantly. Singh et al. (2012) conducted experimentation with continues and discontinues UV action of workpiece and found that ultrasonic vibration decreased the size and numbers of micro-cracks on work surface.

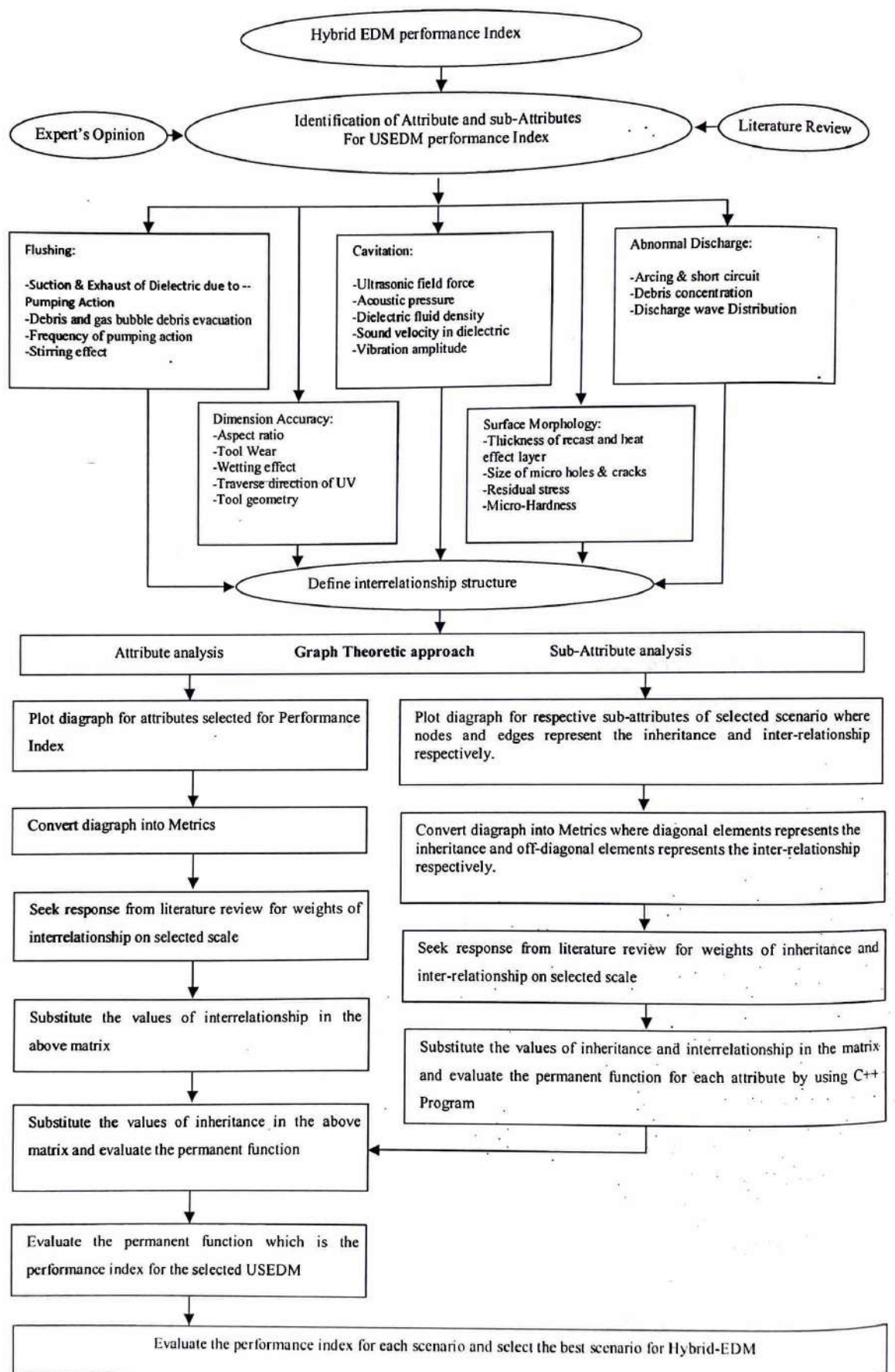




Figure 3.2 Modified Framework for Hybrid-EDM performance Index Evaluation (Agrawal et al., 2016).

### 3.2. Methodology:

A definitive objective of GTA is to demonstrating and analyzing target factors through scientifically substances to assess dependency or independency and communications exist among qualitative/quantitative variables of a framework (Wani, M.F., Gandhi, 1999). In this study, a modified framework is developed shown in Figure 3.2. The step by step approach is explained in next paragraphs. Various researchers have used GTA methodology to evaluate the performance in manufacturing technology. Rao and Gandhi, (2002) proposed digraph and matrix strategy to assess machinability of work piece and failure cause examination of machine tool. Gandhi and Agrawal, (1994) exhibited GTA strategy for framework wear investigation. The Hybrid-EDM performance index elements distinguished and gathered in this paper with likelihood rather than assurance.

The GTA approach gives a precise normal for the Hybrid-EDM performance, albeit new for advance manufacturing technology, to abstain from speculating and instinct in touching base at conclusions. A network showing factors and their interactions has been proposed to model the Hybrid-EDM process through graph representation.

If interactions are not direction dependent, the environment is represented by an undirected graph; if direction dependent, it is called a digraph representation (Grover et al., 2004). The five major factors and their corresponding sub-factors are utilized to assess the degree of the performance index as indicated in equation 3.1.

$$\text{Hybrid -EDM Performance index} = f \{ (H_1)^a, (H_2)^b, (H_3)^c, (H_4)^d \& (H_5)^e \} \dots\dots\dots(3.1)$$

Where  $H_1, H_2, H_3, H_4$  &  $H_5$  represent the inheritance value of factors affecting the Hybrid-EDM performance Index; and intensity of dependency value a, b, c, d and e are the extend of individual factors affecting the objective function.

The endeavor here is to co-relate these five critical elements, their quantification of inheritance value based on sub-elements and interdependencies of these critical

elements, dependency value of individual factors obtained through digraph correlation representation (Grover et al., 2006).

### 3.3. Digraph representation for Hybrid-EDM process performance:

A digraph is utilized to speak to the restrictive variables of Hybrid-EDM process index and their interdependency as far as hubs and edges. In an undirected diagram, no bearing is allocated to the edges in the graph, while coordinated diagrams or digraphs have directional edges (Deo, 2017). A Hybrid-EDM process performance digraph speaks to the procedure steadiness measure of attributes or elements ( $H_i$ 's) through its hubs and the edges compare to the reliance of components ( $h_{ij}$ 's). " $h_{ij}$ " demonstrates the level of reliance of the  $i^{th}$  component on the  $j^{th}$  variable. In the digraph " $h_{ij}$ " is spoken to as a guided edge from hub  $i$  to hub  $j$ . The digraph licenses us to imagine the Hybrid-EDM elements and gives sentiment complex associations among components.

#### 3.3.1. Digraph generation at System Level for Hybrid-EDM factors:

The five broad factors identified in the previous section from literature review i.e flushing ( $H_1$ ), cavitation ( $H_2$ ), abnormal discharge ( $H_3$ ), dimensional accuracy ( $H_4$ ) and surface morphology ( $H_5$ ) are directed edges in the performance digraph represent the dependence of one factor on another shown in Figure 3.3.

The Cavitation ( $H_2$ ) is shown affecting all other factors. Flushing ( $H_1$ ) affects other three factors, i.e. a directed edge from ( $H_1$ ) to abnormal discharge  $H_3$ , Dimensional Accuracy ( $H_4$ ) and Surface Morphology ( $H_5$ ); researchers have attempted some innovative ideas to achieve this by injection, suction, side flushing and pumping action and through addition assistances (Pandey and Singh, 2010).

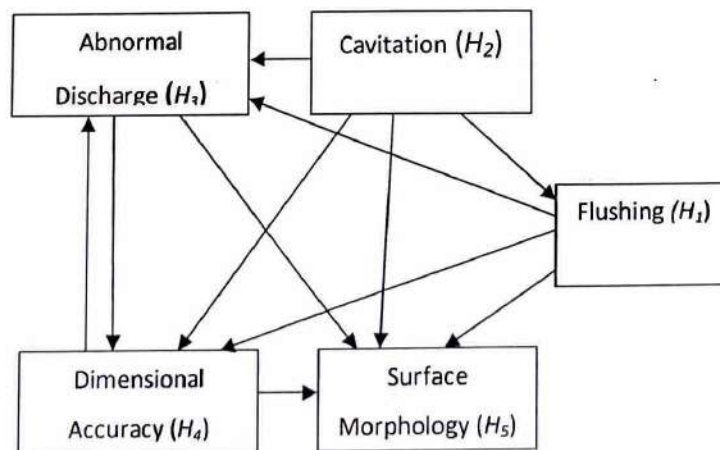
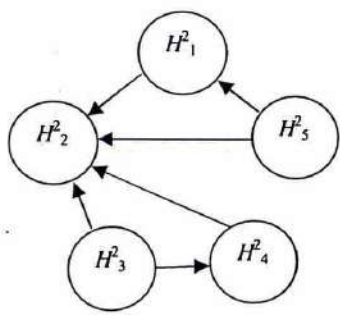


Figure 3.3. Hybrid-EDM process performance evaluation digraph. Nodes: 1. Flushing ( $H_1$ ); 2. Cavitation ( $H_2$ ); 3. Abnormal Discharge ( $H_3$ ); 4. ( $H_4$ ); 5. Surface Morphology ( $H_5$ );

Abnormal discharge factors ( $H_3$ ) affects  $H_4$  and  $H_5$ . Surface Morphology ( $H_5$ ) is affected by all the factors. It may be noted that the Surface Morphology cannot affect flushing, cavitations and other factors (thus no directed edge from  $H_5$  to other factors).

**3.3.2. Digraph generation at Sub-system Level for Hybrid-EDM Sub-factors:**

The interdependency of sub-factor at sub-system levels are visualized through digraphs as shown in Figure 3.4. to 3.8. Superscript denotes the subsystem and subscript indicate the sub-factor affecting the subsystem.



Flushing

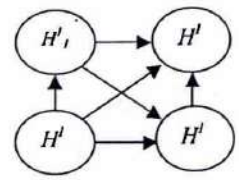


Figure 3.4. The digraph representation for

Figure 3.5. The digraph representation for Cavitation

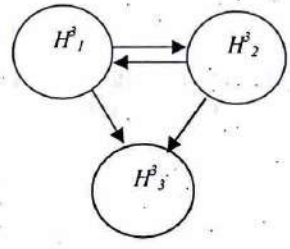


Fig. 3.6. The digraph representation for abnormal discharge

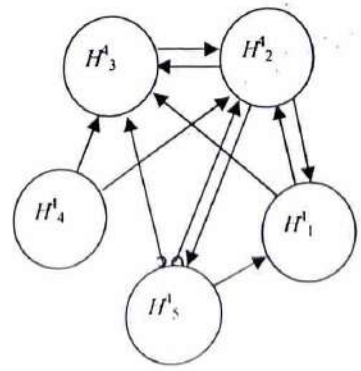


Figure 3.7. The digraph representation for Dimensional accuracy

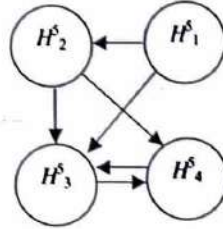


Figure 3.8. The digraph representation for Surface morphology

### 3.4. Process performance Matrix representation [Hybrid-EDM]:

Since a digraph is a visual representation, it helps in analysis to a limited extent only (Grover et al., 2006). To establish an expression for Hybrid-EDM performance index, the digraph is represented in matrix form, which is convenient in computer processing also. A digraph of five factors leading to a 5<sup>th</sup> order symmetric (0, 1) matrix  $[A] = [h_{ij}]$ . The rows and columns in the matrix represent interactions among factors, i.e.  $h_{ij}$  represents the interaction of the ' $i^{th}$ ' factor with the ' $j^{th}$ ' factor;

$$h_{ij} = 1; \text{ if factor 'i' is connected to factor 'j'}$$

$$= 0, \text{ otherwise:}$$

Generally  $h_{ij} \neq h_{ji}$  as Hybrid-EDM performance factors are directional and  $h_{ii} = 0$ , as a factor is not interacting with itself. The Hybrid-EDM process performance matrix is square and non-symmetric and is analogous to the adjacency matrix in graph theory. The Hybrid-EDM matrix ' $[A]$ ' representing the digraph shown in Figure 16 is written as Equation 3.2;

$$\begin{array}{l}
 \text{Factors} \\
 H_1 \\
 H_2 \\
 H_3 \\
 H_4 \\
 H_5 \\
 \dots\dots\dots(3.2)
 \end{array}
 [A] =
 \begin{array}{c}
 H_1 \quad H_2 \quad H_3 \quad H_4 \quad H_5 \\
 \begin{bmatrix}
 1 & 0 & 0 & 0 & 0 \\
 0 & 1 & 0 & 0 & 0 \\
 0 & 0 & 1 & 0 & 0 \\
 0 & 0 & 0 & 1 & 0 \\
 0 & 0 & 0 & 0 & 1
 \end{bmatrix}
 \end{array}$$

Off-diagonal elements with value 0 or 1 represent the interdependency of Hybrid-EDM performance factors. The diagonal elements are 0 since the effect/inheritance of Hybrid-EDM performance factors is not taken into consideration. To consider this, another Hybrid-EDM characteristic matrix is defined.

### 3.4.1. Process performance characteristic matrix [CM- Hybrid-EDM]:

Let 'H' as the variable representing Hybrid-EDM process performance factors. The characteristic matrix already used to characterize Hybrid-EDM process performance elements. The Hybrid-EDM characteristic matrix '[B]' as shown in Equation 3.3, for the digraph shown in Fig 3.7, may be expressed as  $[H I-A]$ , where '[A]' is the matrix represented in Equation 3.2 and consider '[I]', an identity matrix.

$$[B] = \begin{matrix} & \text{Factors} & H_1 & H_2 & H_3 & H_4 & H_5 \\ \begin{matrix} H_1 \\ H_2 \\ H_3 \\ H_4 \\ H_5 \end{matrix} & & \begin{bmatrix} H & 0 & -1 & -1 & -1 \\ -1 & H & -1 & -1 & -1 \\ 0 & 0 & H & -1 & -1 \\ 0 & 0 & -1 & H & -1 \\ 0 & 0 & 0 & 0 & H \end{bmatrix} & & & & \end{matrix} \quad \dots\dots(3.3)$$

In the [B] matrix the value of all diagonal elements is the same, i.e. all Hybrid-EDM performance factors have been assigned the same value which is not true in practice, since all Hybrid-EDM process performance factors have different values depending on various sub-factors affecting them. Moreover interdependencies have been assigned values of 0 and 1 depending on whether it is there or not. To consider this, another matrix, the Hybrid-EDM process performance variable characteristic matrix is considered.

### 3.4.2. Process performance characteristic matrix [VCM- Hybrid-EDM]:

The Hybrid-EDM process performance variable characteristic matrix takes into consideration the effect of different factors and their interactions. The digraph in Fig 3.7 is considered for defining [VCM- Hybrid-EDM]. As stated earlier the 'H<sub>i</sub>'s and 'h<sub>ij</sub>'s represent nodes and edges, respectively, in the digraph. Consider a matrix '[C]' with off-diagonal elements 'h<sub>ij</sub>' representing interactions between Hybrid-EDM factors, i.e. instead of 1 (as in Equation 3.3).

Another matrix '[D]' is taken with diagonal elements ' $H_i$ ',  $i = 1, 2, 3, 4, 5$  where the ' $H_i$ ' represent the effect of various factors, i.e. instead of ' $H$ ' only (as in Equation 3.3). Considering matrices '[C]' and '[D]', VCM- Hybrid-EDM is expressed as:  $[E] = [D-C]$

$$[E] = \begin{matrix} \text{Factors} & H_1 & H_2 & H_3 & H_4 & H_5 \\ H_1 & \left[ \begin{array}{cccccc} H_1 & 0 & -h_{13} & -h_{14} & -h_{15} \\ -h_{21} & H_2 & -h_{23} & -h_{24} & -h_{25} \\ 0 & 0 & H_3 & -h_{34} & -h_{35} \\ 0 & 0 & -h_{43} & H_4 & -h_{45} \\ 0 & 0 & 0 & 0 & H_5 \end{array} \right] \\ H_2 & \\ H_3 & \\ H_4 & \\ H_5 & \end{matrix}$$

.....(3.4)

The matrix provides a powerful tool through its determinant, called the variable characteristic Hybrid-EDM performance multinomial [VC-Hybrid-EDM]. This is a characteristic of the Hybrid-EDM process and represents the Hybrid-EDM performance of the process, considering the effect of Hybrid-EDM process elements and their interactions. Due to consideration of selective interaction of Hybrid-EDM process performance factors (as per Fig 3.7), some of the diagonal elements in the matrix in Equation 3.4 are zero. The determinant of the matrix in Equation 3.4, i.e. the variable characteristic Hybrid-EDM multinomial, carries positive and negative signs with some of its coefficients. Hence complete information in the Hybrid-EDM performance will not be obtained as some will be lost due to addition and subtraction of numerical values of diagonal and off diagonal elements (i.e. ' $H_i$ 's and ' $h_{ij}$ 's). Thus the determinant of the variable characteristic matrix, i.e. the matrix in Equation 3.4, does not provide complete information concerning the Hybrid-EDM process performance. For this, another Hybrid-EDM process performance variable permanent matrix, [VPM- Hybrid-EDM], is introduced.

### 3.4.3. Process performance variable permanent matrix [VPM- Hybrid-EDM]:

The performance in Hybrid-EDM process enabled when the effect of all the factors is maximum. Since total quantitative value is not obtained in [VCM- Hybrid-EDM], the Hybrid-EDM process performance variable permanent matrix is defined for the

process in general (assuming interactions among all factors) as  $[H] = [D + C]$ , where  $[D]$  and  $[C]$  have the same meaning as stated earlier.

$$[H] = \begin{matrix} & \begin{matrix} \text{Factors} & H_1 & H_2 & H_3 & H_4 & H_5 \end{matrix} \\ \begin{matrix} H_1 \\ H_2 \\ H_3 \\ H_4 \\ H_5 \end{matrix} & \begin{bmatrix} H_1 & h_{12} & h_{13} & h_{14} & h_{15} \\ h_{21} & H_2 & h_{23} & h_{24} & h_{25} \\ h_{31} & h_{32} & H_3 & h_{34} & h_{35} \\ h_{41} & h_{42} & h_{43} & H_4 & h_{45} \\ h_{51} & h_{52} & h_{53} & h_{54} & H_5 \end{bmatrix} \end{matrix}$$

.....(3.5)

Thus, the variable permanent process performance matrix [VPM- Hybrid-EDM] corresponding to the five-critical factors of this process performance digraph (Figure 3.3) is given by

$$\text{VPM - Hybrid - EDM} = [H^*] = \begin{matrix} & \begin{matrix} \text{Factors} & H_1 & H_2 & H_3 & H_4 & H_5 \end{matrix} \\ \begin{matrix} H_1 \\ H_2 \\ H_3 \\ H_4 \\ H_5 \end{matrix} & \begin{bmatrix} H_1 & 0 & h_{13} & h_{14} & h_{15} \\ h_{21} & H_2 & h_{23} & h_{24} & h_{25} \\ 0 & 0 & H_3 & h_{34} & h_{35} \\ 0 & 0 & h_{43} & H_4 & h_{45} \\ 0 & 0 & 0 & 0 & H_5 \end{bmatrix} \end{matrix}$$

.....(3.6)

The diagonal elements  $H_1, H_2, H_3, H_4$  and  $H_5$  represent the contribution of the five critical factors in creating the process performance and the off-diagonal elements represent interdependencies of each element in the matrix. The contribution can be expressed quantitatively and is explained later in this paper.

### 3.5. Permanent representation for Hybrid-EDM performance function:

Both digraph and matrix representations are not unique as these change by changing the labeling of nodes. To develop a unique representation, independent of labeling, a permanent function of the matrix VPM-HYBRID-EDM (Variable Permanent Matrix-HYBRID-EDM) is proposed for this purpose. Permanent is a standard matrix function and is used in combinatorial mathematics (Jurkat and Ryser, 1966). The permanent function is obtained in a similar manner as its determinant. A negative sign appears in the calculation of determinant while in the permanent, i.e. the variable permanent function, positive signs reduce these negative signs. These computation processes result in a multinomial (Equation 3.6) that's every term has a physical significance

related to the environment. This multinomial representation includes all the information regarding critical elements including human aspects and strategic policies and interactions amongst them. Quantitative Hybrid-EDM evaluation of an organization is obtained from VPF-HYBRID-EDM by substituting numerical values of the 'H<sub>i</sub>'s and 'h<sub>ij</sub>'s which are obtained analytically or by comparing to ideal cases. This single numerical index is the representation of a typical Hybrid-EDM environment in quantitative terms. The variable permanent Hybrid-EDM function (VPF-HYBRID-EDM), being the characteristic of the Hybrid-EDM environment of an organization is a powerful tool for its analysis. The VPF-HYBRID-EDM expression corresponds to the five-factor digraph/VPM-HYBRIDUS-EDM and is given by;

$$\begin{aligned}
 & [\text{VPF - HYBRID-EDM}] = \text{per} [H^*] \\
 & \text{per} [H^*] = \left[ \prod_{i=1}^m H_i \right] + \left[ \sum_i \sum_j \sum_k \sum_l \sum_m \sum_n (h_{ij} h_{ji}) H_k H_l H_m \right] \\
 & + \left[ \sum_i \sum_j \sum_k \sum_l \sum_m (h_{ij} h_{jk} h_{ki} + h_{ik} h_{kj} h_{ji}) H_l H_m \right] \\
 & + \left[ \sum_i \sum_j \sum_k \sum_l \sum_m (h_{ij} h_{ji}) (h_{kl} h_{lk}) H_m \right. \\
 & \left. + \sum_i \sum_j \sum_k \sum_l \sum_m (h_{ij} h_{jk} h_{kl} h_{li} + h_{il} h_{lk} h_{kj} h_{ji}) H_m \right] \\
 & + \left[ \sum_i \sum_j \sum_k \sum_l \sum_m (h_{ij} h_{ji}) (h_{kl} h_{lm} h_{mk} + h_{km} h_{ml} h_{lk}) \right. \\
 & \left. + \sum_i \sum_j \sum_k \sum_l \sum_m (h_{ij} h_{jk} h_{kl} h_{lm} h_{mi} + h_{im} h_{ml} h_{lk} h_{kj} h_{ji}) \right] \dots\dots\dots(3.8)
 \end{aligned}$$

Equation 3.6 is the complete expression for the considered proposed process, as it considers the presence of all factors and all of the possible interdependency and inheritance between the various factors. The terms are the sets of distinct diagonal elements (i.e., 'H<sub>i</sub>'s) and loops of off-diagonal elements of different sizes (i.e., h<sub>ij</sub> h<sub>ji</sub>, h<sub>ij</sub> h<sub>jk</sub> h<sub>ki</sub>, etc.).

The permanent of the matrix (i.e. Equation 3.7) is a mathematical expression in symbolic form. It ensures an estimate of the theprocess performance. Equation 3.8



contains  $M!$  terms. Each term is useful for Hybrid-EDM experts as each term serves as a test for the interdependency. Equation 3.8 contains terms arranged in  $M+ 1$  group, where  $M$  is the number of factors, which in this case is 5. The physical significance of various grouping is explained as follows.

- The first term (grouping) represents a set of  $M$  unconnected Hybrid-EDM performance factors, i.e.  $H_1 H_2 H_3 \dots H_m$
- The second grouping is absent in the absence of self-loops.
- Each term of the third grouping represents a set of two-element Hybrid-EDM loops (i.e.  $h_{ij} h_{ji}$ ) and is the resultant process interdependency and inheritance of characteristics 'i' and 'j' and the process measure of the remaining  $M-2$  unconnected elements.
- Each term of the fourth grouping represents a set of three-element Hybrid-EDM loops ( $h_{ij} h_{jk} h_{ki}$  or its pair  $h_{ik} h_{kj} h_{ji}$ ) and the Hybrid-EDM performance measure of the remaining  $M-3$  unconnected elements.
- The fifth grouping contains two subgroups. The terms of the first sub grouping consist of two-element Hybrid-EDM loops (i.e.  $h_{ij}h_{ji}$  and  $h_{kl}h_{lk}$ ) and Hybrid-EDM component ( $H_m$ ). The terms of the second grouping are a product of four-element Hybrid-EDM loops (i.e.  $h_{ij} h_{jk} h_{kl} h_{li}$ ) or its pair (i.e.  $h_{il} h_{lk} h_{kj} h_{ji}$ ) and Hybrid-EDM performance components (i.e.  $H_m$ ).
- The terms of the sixth grouping are also arranged in two sub-groupings. The terms of the first sub-grouping are a product of a two-element process performance loop (i.e.  $h_{ij} h_{ji}$ ) and a three-element proposed process loop (i.e.  $h_{kl} h_{lm} h_{mk}$ ) or its pair (i.e.  $h_{km} h_{ml} h_{lk}$ ). The second sub-grouping consists of a five-component processloop (i.e.  $h_{ij} h_{jk} h_{kl} h_{lm} h_{mi}$ ) or its pair ( $h_{im} h_{ml} h_{lk} h_{kj} h_{ji}$ ).

Similarly other terms of the expression are defined. Thus, the Hybrid-EDM performance Index function characterizes a mode of vibration for the considered machining operation as it contains all possible structural components of the factors and their interdependency and inheritance.

### 3.6. Quantification of ' $H_i$ 's and ' $h_{ij}$ 's:

Quantification of the ' $H_i$ 's and ' $h_{ij}$ 's (i.e. the diagonal and off-diagonal elements of permanent matrix of Hybrid-EDM performance Index) is required for evaluation of

Hybrid-EDM performance. The qualitative measure of the factors (i.e. the ' $H_i$ 's) is evaluated considering each ' $H_i$ 's as a subsystem and the graph theoretic approach is applied in each system. The Hybrid-EDM performance index is a measure of the ease with which a material can satisfactorily be machined in a given machining operation. The Hybrid-EDM performance function defined above i.e., Equation 3.8 is used for evaluation of the performance index as it contains the presence of factors and their inherent interdependency. The numerical value of the Hybrid-EDM performance function is called the performance index. As the Hybrid-EDM performance function contains only positive terms, therefore higher values of ' $H_i$ 's and ' $h_{ij}$ 's will result in an increased value of the Hybrid-EDM performance index. To calculate this index, the required information from literature review and expert opinion are the values of ' $H_i$ 's and ' $h_{ij}$ 's. The value of ' $H_i$ ' is obtained from a standard or specified test. If a quantitative value is not available, then a ranked value judgement on a scale, e.g., from 0 to 10, is adopted.

The value of  $H_i$  and  $h_{ij}$  are evaluated with the Table 3.2 is suggested, which represents the performance attributes on a qualitative scale.

Table 3.2. Value of Hybrid EDM performance factors ( $H_i$ )

Qualitative measure of Factors	Assigned value of importance of factors ( $H_i$ )
Extremely low	1
Very low	2
Low	3
+Below average	4
Average	5
Above average	6
High	7
Very high	8
Extremely High	9

It is workable for a given process some of the  $H_i$  qualities will be subjective and the rest quantitative. Also, these quantitative qualities will have diverse units. It is in this way attractive to change over or standardize the quantitative estimation of the  $H_i$  on the same scale as the subjective quality, i.e., 0 to 10.

The interdependency between two characteristics (i.e.,  $h_{ij}$ ) for a given Hybrid-EDM operation is likewise appointed a quality on the scale 0 to 5 from Table 3.3 and is masterminded into six classes. The relative interdependency suggests that a property

"i" is contrasted and another trait "j" as far as its interdependency for the given Hybrid-EDM process.

Table 3.3 Quantification measure of interdependency of diagonal elements ' $h_{ij}$ '

S. NO	Class description	Qualitative measure of interdependencies of ' $h_{ij}$ 's
1	Very Strongly dependent	5
2	Strongly dependent	4
3	Medium dependent	3
4	Weakly dependent	2
5	Very weakly dependent	1

### 3.7. Illustration of Hybrid-EDM Performance Index:

As discussed, the Hybrid-EDM performance is a function of five elements and their interdependence. Although it is very difficult (and not common) to talk about Hybrid-EDM performance in quantitative terms, the variable permanent function Hybrid-EDM performance (i.e. Equation 3.6) is a useful tool and estimate of the this process.

#### 3.7.1. Matrix permanent function generation at system Level:

It is a function of various Hybrid-EDM elements, their interdependencies and complexities. Hence the proposed process performance index Hybrid-EDM process is given as:

Hybrid-EDM performance index =  $\text{per}[H^*]$  = Permanent value of [VPM-Hybrid-EDM];

$$VPM - Hybrid - EDM = \text{per}[H^*] = \begin{matrix} \text{Factors} & H_1 & H_2 & H_3 & H_4 & H_5 \\ \begin{matrix} H_1 \\ H_2 \\ H_3 \\ H_4 \\ H_5 \end{matrix} & \begin{bmatrix} H_1 & 0 & 5 & 5 & 4 \\ 4 & H_2 & 3 & 3 & 4 \\ 0 & 0 & H_3 & 4 & 3 \\ 0 & 0 & 3 & H_4 & 2 \\ 0 & 0 & 0 & 0 & H_5 \end{bmatrix} \end{matrix}$$

.....(3.9)

#### 3.7.2. Matrix and variable permanent function generation at sub-system Level:

Using generalized equation the variable permanent matrix (VPM) for each sub-system digraph (Figure 3.4-3.8) is written in equations (3.10, 3.11, 3.12, 3.13 and 3.14). The interdependency between sub-factors are assigned using table below, while the inheritance is assigned in next step.

$$\begin{array}{l}
 \text{sub factors} \quad H_1^1 \quad H_2^1 \quad H_3^1 \quad H_4^1 \\
 \text{VPM for Flushing} = \text{per}[H^1] = \begin{array}{l} H_1^1 \\ H_2^1 \\ H_3^1 \\ H_4^1 \end{array} \begin{bmatrix} H_1^1 & 5 & 0 & 3 \\ 0 & H_2^1 & 0 & 0 \\ 5 & 4 & H_3^1 & 4 \\ 0 & 4 & 0 & H_4^1 \end{bmatrix} \\
 \dots\dots(3.10)
 \end{array}$$

$$\begin{array}{l}
 \text{sub factors} \quad H_1^2 \quad H_2^2 \quad H_3^2 \quad H_4^2 \quad H_5^2 \\
 \text{VPM for Cavitation} = \text{per}[H^2] = \begin{array}{l} H_1^2 \\ H_2^2 \\ H_3^2 \\ H_4^2 \\ H_5^2 \end{array} \begin{bmatrix} H_1^2 & 4 & 0 & 0 & 0 \\ 0 & H_2^2 & 0 & 0 & 0 \\ 0 & 4 & H_3^2 & 4 & 0 \\ 0 & 5 & 0 & H_4^2 & 0 \\ 3 & 5 & 0 & 0 & H_5^2 \end{bmatrix} \\
 \dots\dots(3.11)
 \end{array}$$

$$\begin{array}{l}
 \text{sub factors} \quad H_1^3 \quad H_2^3 \quad H_3^3 \\
 \text{VPM for Abnormal Discharge} = \text{per}[H^3] = \begin{array}{l} H_1^3 \\ H_2^3 \\ H_3^3 \end{array} \begin{bmatrix} H_1^3 & 2 & 2 \\ 5 & H_2^3 & 5 \\ 3 & 0 & H_3^3 \end{bmatrix} \dots\dots \\
 (3.12)
 \end{array}$$

$$\begin{array}{l}
 \text{VPM for Dim. Accuracy} = \text{per}[H^4] = \\
 \text{sub factors} \quad H_1^4 \quad H_2^4 \quad H_3^4 \quad H_4^4 \quad H_5^4 \\
 \begin{array}{l} H_1^4 \\ H_2^4 \\ H_3^4 \\ H_4^4 \\ H_5^4 \end{array} \begin{bmatrix} H_1^4 & 4 & 3 & 0 & 0 \\ 4 & H_2^4 & 3 & 0 & 5 \\ 4 & 0 & H_3^4 & 0 & 0 \\ 0 & 3 & 3 & H_4^4 & 0 \\ 4 & 4 & 4 & 0 & H_5^4 \end{bmatrix} \dots\dots (3.13)
 \end{array}$$

$$\begin{array}{l}
 \text{VPM for Surface Morphology} = \text{per}[H^5] = \\
 \text{sub factors} \quad H_1^5 \quad H_2^5 \quad H_3^5 \quad H_4^5 \\
 \begin{array}{l} H_1^5 \\ H_2^5 \\ H_3^5 \\ H_4^5 \end{array} \begin{bmatrix} H_1^5 & 3 & 4 & 3 \\ 0 & H_2^5 & 2 & 2 \\ 0 & 0 & H_3^5 & 4 \\ 0 & 0 & 3 & H_4^5 \end{bmatrix} \dots\dots (3.14)
 \end{array}$$

### 3.7.3. Quantification of 'H<sub>i</sub>'s and 'h<sub>ij</sub>'s for Hybrid-EDM sub-system level:

The values of these factors and their interdependence for diagonal elements are found on the basis of the data available in the literature and the experience of manufacturing personnel. If a quantitative value is not available, then a ranked value

judgment on a scale (e.g., from 1 to 10) is adopted from Table 3.2, suggested for this purpose. To assign numerical values to the interdependence of barrier ' $h_{ij}$ ' off diagonal elements the opinions of manufacturing experts can be recorded. But this interdependence of factors cannot be measured directly and, hence, qualitative values may be adopted. These qualitative values of the interdependence of enablers are also assigned from Table 3.3 on a scale (e.g., 1 to 5), as suggested in Table (3.4, 3.5, 3.6, 3.7 & 3.8).

Table 3.4. Quantification of Flushing sub-factors

Factors	Flushing(H1)			
Sub-Factors	H11	H12	H13	H14
Quantitative value	8	9	7	6

Table 3.5. Quantification of Cavitation sub-factors

Factors	Cavitation(H2)				
Sub-Factors	H21	H22	H23	H24	H25
Quantitative value	2	9	8	7	7

Table 3.6. Quantification of Abnormal discharge sub-factors

Factors	Abnormal discharge (H3)		
Sub-Factors	H31	H32	H33
Quantitative value	9	8	7

Table 3.7. Quantification of Dimensional accuracy sub-factors

Factors	Dimensional accuracy (H4)				
Sub-Factors	H41	H42	H43	H44	H45
Quantitative value	7	9	7	6	8

Table 3.8. Quantification of Surface morphology sub-factors

Factors	Surface morphology (H5)			
Sub-Factors	H51	H52	H53	H54
Quantitative value	8	8	7	7

**3.8.Calculation of Permanent function for Hybrid-EDM system and subsystem Level:**

The value of permanent function of each system and sub-system is evaluated by generalized equation 8. A computer program in MATLAB has been developed for it. Values of diagonal elements to sub-system have been provided in Table (3.4, 3.5, 3.6, 3.7 and 3.8) using Table 3.4. These values are selected based on the previously published research, pervious experiments and FEA analysis carried by authors. Permanent function or index values of each sub-system are obtained under different conditions of sub-factors.

$$\begin{array}{l}
 \text{sub factors } H_1^1 \ H_2^1 \ H_3^1 \ H_4^1 \\
 VPM \ H_1 = per[H^1] = \begin{array}{l} H_1^1 \\ H_2^1 \\ H_3^1 \\ H_4^1 \end{array} \begin{bmatrix} 8 & 5 & 0 & 3 \\ 0 & 9 & 0 & 0 \\ 5 & 4 & 7 & 4 \\ 0 & 4 & 0 & 6 \end{bmatrix} = 3024
 \end{array}$$

$$\begin{array}{l}
 \text{sub factors } H_1^2 \ H_2^2 \ H_3^2 \ H_4^2 \ H_5^2 \\
 VPM \ H_2 = per[H^2] = \begin{array}{l} H_1^2 \\ H_2^2 \\ H_3^2 \\ H_4^2 \\ H_5^2 \end{array} \begin{bmatrix} 2 & 4 & 0 & 0 & 0 \\ 0 & 9 & 0 & 0 & 0 \\ 0 & 4 & 8 & 4 & 0 \\ 0 & 5 & 0 & 7 & 0 \\ 3 & 5 & 0 & 0 & 7 \end{bmatrix} = 7056
 \end{array}$$

$$\begin{array}{l}
 \text{sub factors } H_1^3 \ H_2^3 \ H_3^3 \\
 VPM \ H_3 = per[H^3] = \begin{array}{l} H_1^3 \\ H_2^3 \\ H_3^3 \end{array} \begin{bmatrix} 9 & 2 & 2 \\ 5 & 8 & 5 \\ 3 & 0 & 7 \end{bmatrix} = 652
 \end{array}$$

$$\begin{array}{l}
 \text{sub factors } H_1^4 \ H_2^4 \ H_3^4 \ H_4^4 \ H_5^4 \\
 VPM \ H_4 = per[H^4] = \begin{array}{l} H_1^4 \\ H_2^4 \\ H_3^4 \\ H_4^4 \\ H_5^4 \end{array} \begin{bmatrix} 7 & 4 & 3 & 0 & 0 \\ 4 & 9 & 3 & 0 & 5 \\ 4 & 0 & 7 & 0 & 0 \\ 0 & 3 & 3 & 6 & 0 \\ 4 & 4 & 4 & 0 & 8 \end{bmatrix} = 46632
 \end{array}$$

$$VPM H_5 = per[H^5] = \begin{matrix} \text{sub factors} & H_1^5 & H_2^5 & H_3^5 & H_4^5 \\ H_1^5 & 8 & 3 & 4 & 3 \\ H_2^5 & 0 & 8 & 2 & 2 \\ H_3^5 & 0 & 0 & 7 & 4 \\ H_4^5 & 0 & 0 & 3 & 7 \end{matrix} = 3904$$

$$VPM HYBRID - EDM = per[H^*] =$$

$$\begin{matrix} \text{Factors} & H_1 & H_2 & H_3 & H_4 & H_5 \\ H_1 & 3024 & 0 & 5 & 5 & 4 \\ H_2 & 4 & 7056 & 3 & 3 & 4 \\ H_3 & 0 & 0 & 652 & 4 & 3 \\ H_4 & 0 & 0 & 3 & 46632 & 2 \\ H_5 & 0 & 0 & 0 & 0 & 3904 \end{matrix} = 3.28647 \times 10^{18}$$

### 3.9. Coefficient of variation of Hybrid-EDM performance Index for system and sub-system level:

The coefficient of variation for Hybrid-EDM performance index can be evaluated by assuming the hypothetical extreme values of the Hybrid-EDM sub-factors matrix diagonal elements. The index value is maximum or minimum when all the factors are affecting extremely high (9) or extremely low (1) as in Table 3.2, to the diagonal elements of the permanent function matrix correspondingly from Table 3.5. Hence, the Hybrid-EDM performance index value can be calculated at these extreme values of sub-factors index.

Table 3.9. The Coefficient of variation of index values of the permanent function

Permanent function	Performance Index value	Maximum performance Index	Minimum performance Index	Coefficient of variation of index
Per(H1)	3024	6561	6	7.90
Per(H2)	7056	59049	1	76.10
Per(H3)	652	903	47	37.26
Per(H4)	46632	109449	737	15.36
Per(H5)	3904	7533	13	3.47
Per(H*)	3.28647X1018	2.88436X1020	2.70278X106	99.84

### **3.10. A Comparative study of the performance Ultrasonic Vibration Assisted Hybrid-EDM under three modes of vibration:**

In literature, UV action in traditional EDM system is imparted with Magneto or Piezo-electric actuator. A Piezo-electric actuator is basically an assembly of generator and convertor (transducer and sonotrode) as shown in Figure 1.6, to produce mechanical vibration with optimum amplitude at fixed frequency called resonance frequency (Kei-Lin, 2009). The horn designed for this should have slightly lower own frequency than that resonance frequency of the actuator to get maximum amplitude of vibration. The maximum amplitude is obtained for titanium horn that is very costly (Nanu et al., 2011). These limitations resist the applicability of UV action for tool and workpiece in EDM system.

Ultrasonic dielectric medium vibration might provide a good solution for this problem. Ultrasonic vibration to dielectric fluid had significant effect on machining time and tool wear but had not significant effects on machining characteristics (Ichikawa and Natsu, 2013). Dielectric medium vibration improved maximum machining depth, hole geometry, MRR and surface topography (Liew et al., 2014). Cavitation helped to achieve high aspect ratio and improve surface topology as ultrasound decrease the diameters of microspheres. There was a significant improvement in micro structure, micro cracks, surface finish and machining time (Prihandana et al., 2011).

Cavitation occurred more easily when the homogeneity of the liquid was being disturbed by particles. Within the discharge gap, tiny particles debris formed during the EDM process stuck to cavitation bubbles facilitate flushing (Liew et al., 2014). The gas bubbles of the cavitation phenomenon can become stable gas bubbles.



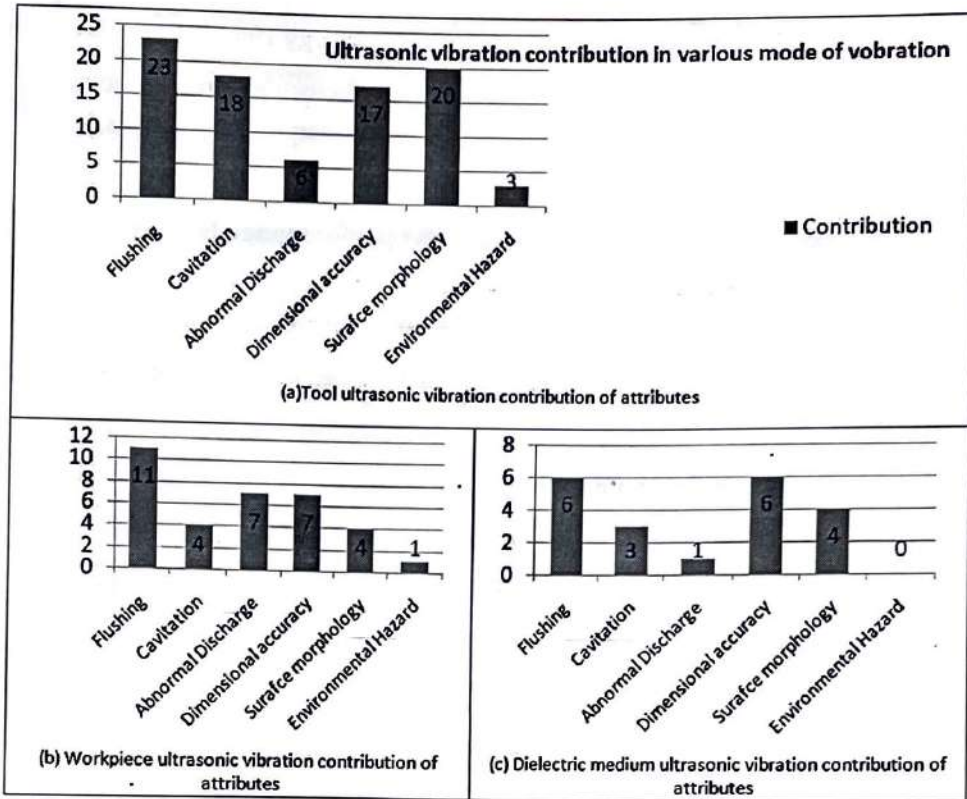


Figure 3.9 Contribution of various attributes for different mode of vibration in Hybrid -EDM

It rises and creates a stream transporting these tiny particles out of the discharge gap and contributes to homogenization of dielectric medium (Schubert et al., 2013). A Schematic model for debris and cavitation bubble removal through the UV action of dielectric medium is shown in Figure 3.9.

### 3.10.1. Identification of Hybrid EDM performance Index Factors:

Form literature survey, It was found that the ultrasonic vibration in traditional EDM process is a convoluted undertaking. There are sure factors which contribute for this process performance index, that were grouped here in Figure 3.9. These factors significantly contribute the performance index. The researchers had formulated and tested these factors using scientific and interactive design approaches to evaluate the probability rather than certainty of factor (Kumar et al., 2017). It was found that factors attributes such as cavitation, abnormal discharge have been less explored, whereas flushing of contaminated dielectric fluid; dimensional accuracy and surface morphology have been considered more frequently. Researchers have considered the less influencing factors such as abnormal discharge (23.7%) and environment hazard & chemical reactions (6.8%). Whereas flushing of contaminated dielectric fluid

(84.7%), dimensional accuracy (50.8%), surface morphology (64.4%) and cavitation (42.4%) are the most significantly contributing factors found affecting the performance of this process.

### 3.10.2. Digraph representation for process performance factors:

The effectiveness of the UV action depends upon the relative importance of the factors identified through literature review. A specific scientific approach cannot be used to analyze this system, as of complex interrelation and relative importance among factors. The concept of introducing three modes of ultrasonic vibration to EDM system could be successfully implemented without proper selection of these factors i.e. Flushing, cavitation, abnormal discharge, dimensional inaccuracy, surface morphology, environment hazard & chemical effects.

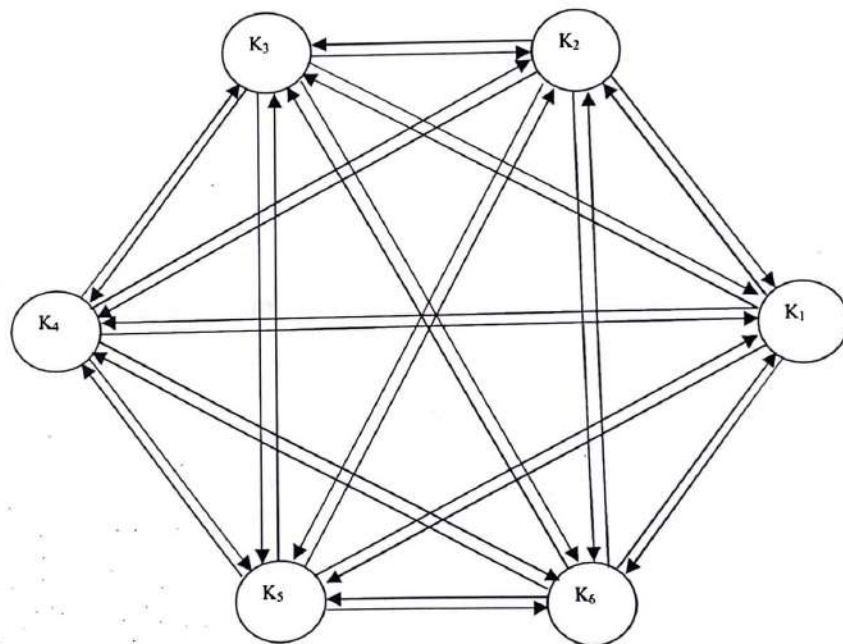


Figure 3.10 Hybrid EDM performance Index factors digraph for Attributes; (1) Flushing (K<sub>1</sub>); (2) Cavitation (K<sub>2</sub>); (3) Abnormal discharge (K<sub>3</sub>); (4) Dimensional accuracy (K<sub>4</sub>); (5) Surface Morphology (K<sub>5</sub>); and (6) Ergonomic & Chemical effect (K<sub>6</sub>)

A schematically interaction representation among six factors that corresponding to performance are shown in Figure 3.10. The digraph permits us to visualize the performance factors and gives a feeling of relative importance between the factors.

This digraph is basically used to represent the conditional factors of the proposed process and relative importance among each other in terms of nodes and edges. This digraph characterizes the process performance quantify of characteristics or factors ( $K_i$ 's) through its nodes and the edges match to the importance of factors ( $K_{ij}$ 's). " $K_{ij}$ " indicates relative importance of the  $j^{\text{th}}$  factor over the  $i^{\text{th}}$  factor. In the digraph  $K_{ij}$  is represented as a directed edge from node  $i$  to node  $j$ .

### 3.10.3. Matrix representation process performance:

A digraph of  $M$  factors leading to an  $M^{\text{th}}$  order matrix  $A = [K_{ij}]$ . This is an  $M \times M$  matrix and considers all factors (i.e.,  $K_i$ ) and their relative importance (i.e.,  $K_{ij}$ ). This matrix  $[A]$ , for the performance index digraph in Equation (3.15) for the this process as;

$$\begin{array}{c} \text{Factors} \\ K_1 \\ K_2 \\ K_3 \\ K_4 \\ K_5 \\ \vdots \\ K_m \end{array} \begin{array}{c} K_1 \\ K_2 \\ K_3 \\ K_4 \\ K_5 \dots \\ K_m \end{array} \begin{bmatrix} K_{11} & K_{12} & K_{13} & K_{14} & K_{15} \dots & K_{1m} \\ K_{21} & K_{22} & K_{23} & K_{24} & K_{25} \dots & K_{2m} \\ K_{31} & K_{32} & K_{33} & K_{34} & K_{35} \dots & K_{3m} \\ K_{41} & K_{42} & K_{43} & K_{44} & K_{45} \dots & K_{4m} \\ K_{51} & K_{52} & K_{53} & K_{54} & K_{55} \dots & K_{5m} \\ \vdots & \vdots & \vdots & \vdots & \vdots & \vdots \\ K_{m1} & K_{m2} & K_{m3} & K_{m4} & K_{m5} \dots & K_{m6} \end{bmatrix} \dots (3.15)$$

The rows and columns in the matrix represent relative importance among factors, i.e.  $K_{ij}$  represents the relative importance of the  $i^{\text{th}}$  factor with the  $j^{\text{th}}$  factor: where  $K_i$  is the value of the  $i^{\text{th}}$  attribute represented by node,  $K_{ij}$  is the relative importance of the  $i^{\text{th}}$  attribute over the  $j^{\text{th}}$  represented by the edge  $K_{ij}$ . The permanent of this matrix  $A$ , i.e.,  $\text{per}[A]$ , is clear as the performance index functions with six factors along relative importance are expressed in Equation (3.16).

$$\begin{array}{c} \text{Factors} \\ K_1 \\ K_2 \\ K_3 \\ K_4 \\ K_5 \\ K_6 \end{array} \begin{array}{c} K_1 \\ K_2 \\ K_3 \\ K_4 \\ K_5 \\ K_6 \end{array} \begin{bmatrix} K_{11} & K_{12} & K_{13} & K_{14} & K_{15} & K_{16} \\ K_{21} & K_{22} & K_{23} & K_{24} & K_{25} & K_{26} \\ K_{31} & K_{32} & K_{33} & K_{34} & K_{35} & K_{36} \\ K_{41} & K_{42} & K_{43} & K_{44} & K_{45} & K_{46} \\ K_{51} & K_{52} & K_{53} & K_{54} & K_{55} & K_{56} \\ K_{61} & K_{62} & K_{63} & K_{64} & K_{65} & K_{66} \end{bmatrix} \dots (3.16)$$

The permanent is a standard matrix function and is used in combinatorial mathematics (Jurkat and Ryser, 1966). Application of this permanent concept will lead to a better appreciation of performance index factors of the proposed process. By

using this, no negative sign will appear in the expression (unlike the determinant of a matrix in which a negative sign can appear) and hence no information will be lost. The performance index permanent function for matrix can be expressed as Equation (3.17);

$$\begin{aligned}
 per[A] = & \left[ \prod_{i=1}^m K_i \right] + \left[ \sum_i \sum_j \sum_k \sum_l \sum_m \sum_n (K_{ij}K_{ji})K_k K_l K_m \right] \\
 & + \left[ \sum_i \sum_j \sum_k \sum_l \sum_m (K_{ij}K_{jk}K_{kl} + K_{ik}K_{kj}K_{ji})K_l K_m \right] \\
 & + \left[ \sum_i \sum_j \sum_k \sum_l \sum_m (K_{ij}K_{ji})(K_{kl}K_{lk})K_m \right. \\
 & \left. + \sum_i \sum_j \sum_k \sum_l \sum_m (K_{ij}K_{jk}K_{kl}K_{li} + K_{il}K_{lk}K_{kj}K_{ji})K_m \right] \dots\dots\dots(3.17) \\
 & + \left[ \sum_i \sum_j \sum_k \sum_l \sum_m (K_{ij}K_{ji})(K_{kl}K_{lm}K_{mk} + K_{km}K_{ml}K_{lk}) \right. \\
 & \left. + \sum_i \sum_j \sum_k \sum_l \sum_m (K_{ij}K_{jk}K_{kl}K_{lm}K_{mi} + K_{im}K_{ml}K_{lk}K_{kj}K_{ji}) \right]
 \end{aligned}$$

Equation (3.17) is the complete expression for this process, as it considers all elements and all of the possible relative importance between the factors.

$$\begin{aligned}
per(A) = & \left[ \prod_{i=1}^6 K_i \right] + \left[ \sum_i \sum_j \sum_k \sum_l \sum_m \sum_n (K_{ij}K_{ji})K_kK_lK_mK_n \right] \\
& + \left[ \sum_i \sum_j \sum_k \sum_l \sum_m \sum_n (K_{ij}K_{jk}K_{kl} + K_{lk}K_{kj}K_{ji})K_lK_mK_n \right] \\
& + \left[ \sum_i \sum_j \sum_k \sum_l \sum_m \sum_n (K_{ij}K_{ji})(K_{kl}K_{lk})K_mK_n \right. \\
& \left. + \sum_i \sum_j \sum_k \sum_l \sum_m \sum_n (K_{ij}K_{jk}K_{kl}K_{li} + K_{il}K_{kl}K_{kj}K_{ji})K_mK_n \right] \\
& + \left[ \sum_i \sum_j \sum_k \sum_l \sum_m \sum_n (K_{ij}K_{ji})(K_{kl}K_{lm}K_{mk} + K_{km}K_{ml}K_{lk})K_m \right. \\
& \left. + \sum_i \sum_j \sum_k \sum_l \sum_m \sum_n (K_{ij}K_{jk}K_{kl}K_{lm}K_{mi} + K_{in}K_{mi}K_{lk}K_{kj}K_{ji})K_n \right] \\
& + \left[ \sum_i \sum_j \sum_k \sum_l \sum_m \sum_n (K_{ij}K_{ji})(K_{kl}K_{lk}K_{mn}K_{nk} + K_{kn}K_{mn}K_{lk}K_{lk}) \right. \\
& + \sum_i \sum_j \sum_k \sum_l \sum_m \sum_n (K_{ij}K_{jk}K_{ki})(K_{lm}K_{mn}K_{mk}) \\
& + \sum_i \sum_j \sum_k \sum_l \sum_m \sum_n (K_{ij}K_{ji})(K_{kl}K_{lk})(K_{nm}K_{mn}) \\
& \left. + \sum_i \sum_j \sum_k \sum_l \sum_m \sum_n (K_{ij}K_{jk}K_{kl}K_{lm}K_{mn}K_{ni} + K_{in}K_{nm}K_{ml}K_{lk}K_{kj}K_{ji}) \right] \dots\dots(3.18)
\end{aligned}$$

The terms are  $K_i$  sets of distinct diagonal elements (i.e., ' $K_i$ 's) and loops of off-diagonal elements of different sizes (i.e.,  $K_{ij}K_{ji}$ ,  $K_{ij}K_{jk}K_{ki}$ , etc.). The permanent of the matrix (i.e. equation 3.17) is a mathematical expression in symbolic form. It ensures an estimate of the process performance. Equation (3.18) contains  $M!$  terms. Similarly other terms of the expression are defined. The performance Index function for characterizing modes of vibration considered in machining operation as it contains all possible structural components of the factors and their relative importance.

#### 3.10.4. Quantification of $K_i$ 's and $K_{ij}$ 's:

Quantification of the  $K_i$ 's and  $K_{ij}$ 's (i.e. the diagonal and off-diagonal elements of permanent matrix function) is required for evaluation and comparison of overall performance. The quality measure of the factors (i.e. the  $K_i$ 's) is evaluated considering each  $K_i$ . The performance index is a measure of the ease with which materials can satisfactorily be machined in a given mode of vibration. The performance function defined above i.e., Eq. (3.18) is used for evaluation of the Hybrid EDM performance index as it contains all factors and their relative

importance. The numerical value of the performance function is called the performance index. As the quantitative values are not available, a standard ranked value judgment on a scale, e.g., from 1 to 9, is adopted from Table 3.2. The value of  $K_i$  and  $K_{ij}$  are evaluated with a standard or specified tests and results from literature review which represents the performance attributes on a qualitative scale. The relative importance between two attributes (i.e.,  $K_{ij}$ ) for a Hybrid EDM operation is also assigned a value on the scale 1 to 5 and is arranged into five classes in Table 3.3. The relative importance implies that an attribute 'i' is compared with another attribute 'j' in terms of its relative importance. The relative importance between  $i, j$  and  $j, i$  is distributed on the scale 1 to 5.

It is, however, desirable to choose a lower scale for  $K_i$  and  $K_{ij}$  to obtain a manageable value of the performance index for proposed process. The performance index for each mode of vibration is evaluated using Equation (3.18) substituting the values of  $K_i$  and  $K_{ij}$ . The performance of various mode of vibration in Hybrid EDM process can be arranged in descending or ascending order of performance index to rank them for a mode of vibration. These are called the ranking values of the ultrasonic vibration assisted EDM process for the three modes of vibration. The mode of vibration for which the value of performance index is highest is the best choice for the machining operation.

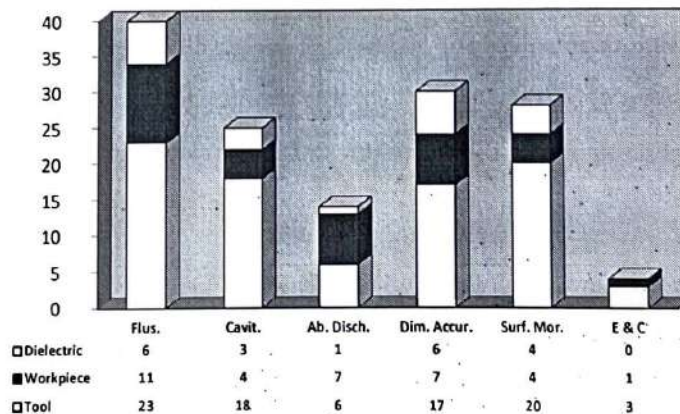


Figure 3.11 Stacked diagram for the frequency of factors considered in literature for mode of vibration 1) Tool; 2) Workpiece; 3) Dielectric medium;

However, the final decision depends on the factors such as design, function, cost, availability, and technical feasibility. A compromise may have to be made to select the mode of vibration having the highest value of performance index. To neglect the biasing in ranking and judging the values of  $K_i$  and  $K_j$ , authors have selected values from the retrospective literature review and as according to Equation (3.19). Authors have drawn the stake frequency diagram in Figure 3.11 for factors under taken in literature.

$$K_{ij} = \left\lfloor \frac{f_i}{f_i + f_j} \times 10 \right\rfloor \{ \text{Nearest integer number to value in Table 3.10} \} \dots (3.19)$$

Where  $f_i$  &  $f_j$  are corresponding values of frequency considered for ( $K_i$ ) & ( $K_j$ ) factors respectively. It has been assumption that the researchers have considered the factors as of their relative importance in proposed process performance.

$$[A] = \begin{matrix} \text{Factors} & & K_1 & K_2 & K_3 & K_4 & K_5 & K_6 \\ \begin{matrix} K_1 \\ K_2 \\ K_3 \\ K_4 \\ K_5 \\ K_6 \end{matrix} & \begin{bmatrix} K_1 & 8 & 8 & 6 & 6 & 9 \\ 2 & K_2 & 5 & 2 & 3 & 7 \\ 2 & 5 & K_3 & 2 & 2 & 6 \\ 4 & 8 & 8 & K_4 & 5 & 9 \\ 4 & 7 & 8 & 5 & K_5 & 9 \\ 1 & 3 & 3 & 1 & 1 & K_6 \end{bmatrix} & \dots \dots \dots \end{matrix} \quad (3.20)$$

The permanent of this matrix  $A$  in Equation (3.20), i.e., per  $[A]$ , is expressed as the HYBRID EDM a performance index function with six factors along relative importance is shown in equation (3.20) used for presented work to compare the performance index of under three modes of vibration assistance i.e. tool, workpiece and the dielectric medium, and their diagonal elements are selected from the Table 3.10 below through literature review.

Table 3.10 Relative importance diagonal value ( $K_i$ ) for tool, workpiece and dielectric

Mode of Vibration	Flushing (K1)	Cavitation (K2)	Abnormal Discharge (K3)	Dimensional Accuracy (K4)	Surface Morphology (K5)	Environment hazard & Chemical effect (K6)
Tool	8	2	2	5	5	1
Workpiece	9	1	4	7	2	1
Dielectric	9	4	1	9	6	1

### 3.10.5. Range of Hybrid EDM performance Index under three mode:

The range of performance index can be evaluated by assuming the hypothetical extreme values of the performance matrix diagonal elements. These are the maximum

and minimum values of performance index. The performance index is maximum or minimum when all the factors are equally important or equally not important, respectively. As the importance of each factor is calculated frequency of consideration of that factor by the researcher as per domain of the experimentation. So it is proposed here the maximum value of proposed process performance index can be obtained by ranking 9 in equation 3.21 i.e. extremely importance of all the factors, and 1 in equation 3.22 to the entire factors extremely unimportant (as per Table 3.10). Hence, the performance function matrix for this category may be rewritten as equation 3.21 & 3.22.

$$\begin{array}{c}
 \text{Factors} \\
 K_1 \\
 K_2 \\
 K_3 \\
 K_4 \\
 K_5 \\
 K_6
 \end{array}
 \begin{array}{cccccc}
 K_1 & K_2 & K_3 & K_4 & K_5 & K_6 \\
 \left[ \begin{array}{cccccc}
 10 & 8 & 8 & 6 & 6 & 9 \\
 2 & 10 & 5 & 2 & 3 & 7 \\
 2 & 5 & 10 & 3 & 3 & 7 \\
 4 & 8 & 7 & 10 & 6 & 9 \\
 4 & 7 & 7 & 4 & 10 & 9 \\
 1 & 3 & 3 & 1 & 1 & 10
 \end{array} \right]
 \end{array}
 \dots(3.21)$$

The maximum performance index value for the given process giving all factors extreme importance that is;  $per [A^{max}] = 1.64901 \times 10^7$ .

$$\begin{array}{c}
 \text{Factors} \\
 K_1 \\
 K_2 \\
 K_3 \\
 K_4 \\
 K_5 \\
 K_6
 \end{array}
 \begin{array}{cccccc}
 K_1 & K_2 & K_3 & K_4 & K_5 & K_6 \\
 \left[ \begin{array}{cccccc}
 1 & 8 & 8 & 6 & 6 & 9 \\
 2 & 1 & 5 & 2 & 3 & 7 \\
 2 & 5 & 1 & 3 & 3 & 6 \\
 4 & 8 & 7 & 1 & 6 & 9 \\
 4 & 7 & 7 & 4 & 1 & 9 \\
 1 & 3 & 3 & 1 & 1 & 1
 \end{array} \right]
 \end{array}
 \dots\dots (3.22)$$

The minimum performance index value for the proposed process giving all factors extreme unimportance that is;  $per [A^{min}] = 0.188535 \times 10^7$ .

The value of permanent function of each mode of vibration is evaluated by a generalized equation (3.18). The performance function matrixes for Tool, Workpiece and Dielectric medium have been provided in equation 3.23, 3.24 and 3.25 respectively, using generalized performance matrix function equation 6. These values of  $K_i$  are selected from Table 3.12.



$$\begin{array}{c}
 \text{Factors} \\
 \begin{array}{c} K_1 \\ K_2 \\ K_3 \\ K_4 \\ K_5 \\ K_6 \end{array}
 \end{array}
 \begin{array}{c}
 K_1 \\ K_2 \\ K_3 \\ K_4 \\ K_5 \\ K_6
 \end{array}
 \begin{array}{c}
 K_2 \\ K_3 \\ K_4 \\ K_5 \\ K_6
 \end{array}
 \begin{array}{c}
 K_3 \\ K_4 \\ K_5 \\ K_6
 \end{array}
 \begin{array}{c}
 K_4 \\ K_5 \\ K_6
 \end{array}
 \begin{array}{c}
 K_5 \\ K_6
 \end{array}
 \begin{array}{c}
 K_6
 \end{array}
 \begin{array}{c}
 9 \\ 8 \\ 8 \\ 6 \\ 6 \\ 9 \\ 2 \\ 4 \\ 5 \\ 2 \\ 3 \\ 7 \\ 2 \\ 5 \\ 4 \\ 3 \\ 3 \\ 6 \\ 4 \\ 8 \\ 7 \\ 6 \\ 6 \\ 9 \\ 4 \\ 7 \\ 7 \\ 4 \\ 6 \\ 9 \\ 1 \\ 3 \\ 3 \\ 1 \\ 1 \\ 2
 \end{array}
 \left. \vphantom{\begin{array}{c} K_1 \\ K_2 \\ K_3 \\ K_4 \\ K_5 \\ K_6 \end{array}} \right\} \dots\dots(3.23)$$

$$\begin{array}{c}
 \text{Factors} \\
 \begin{array}{c} K_1 \\ K_2 \\ K_3 \\ K_4 \\ K_5 \\ K_6 \end{array}
 \end{array}
 \begin{array}{c}
 K_1 \\ K_2 \\ K_3 \\ K_4 \\ K_5 \\ K_6
 \end{array}
 \begin{array}{c}
 K_2 \\ K_3 \\ K_4 \\ K_5 \\ K_6
 \end{array}
 \begin{array}{c}
 K_3 \\ K_4 \\ K_5 \\ K_6
 \end{array}
 \begin{array}{c}
 K_4 \\ K_5 \\ K_6
 \end{array}
 \begin{array}{c}
 K_5 \\ K_6
 \end{array}
 \begin{array}{c}
 K_6
 \end{array}
 \begin{array}{c}
 9 \\ 8 \\ 8 \\ 6 \\ 6 \\ 9 \\ 2 \\ 1 \\ 5 \\ 2 \\ 3 \\ 7 \\ 2 \\ 5 \\ 4 \\ 3 \\ 3 \\ 6 \\ 4 \\ 8 \\ 7 \\ 7 \\ 6 \\ 9 \\ 4 \\ 7 \\ 7 \\ 4 \\ 3 \\ 9 \\ 1 \\ 3 \\ 3 \\ 1 \\ 1 \\ 1
 \end{array}
 \left. \vphantom{\begin{array}{c} K_1 \\ K_2 \\ K_3 \\ K_4 \\ K_5 \\ K_6 \end{array}} \right\} \dots\dots(3.24)$$

$$\begin{array}{c}
 \text{Factors} \\
 \begin{array}{c} K_1 \\ K_2 \\ K_3 \\ K_4 \\ K_5 \\ K_6 \end{array}
 \end{array}
 \begin{array}{c}
 K_1 \\ K_2 \\ K_3 \\ K_4 \\ K_5 \\ K_6
 \end{array}
 \begin{array}{c}
 K_2 \\ K_3 \\ K_4 \\ K_5 \\ K_6
 \end{array}
 \begin{array}{c}
 K_3 \\ K_4 \\ K_5 \\ K_6
 \end{array}
 \begin{array}{c}
 K_4 \\ K_5 \\ K_6
 \end{array}
 \begin{array}{c}
 K_5 \\ K_6
 \end{array}
 \begin{array}{c}
 K_6
 \end{array}
 \begin{array}{c}
 9 \\ 8 \\ 8 \\ 6 \\ 6 \\ 9 \\ 2 \\ 6 \\ 5 \\ 2 \\ 3 \\ 7 \\ 2 \\ 5 \\ 1 \\ 3 \\ 3 \\ 6 \\ 4 \\ 8 \\ 7 \\ 8 \\ 6 \\ 9 \\ 4 \\ 7 \\ 7 \\ 4 \\ 6 \\ 9 \\ 1 \\ 3 \\ 3 \\ 1 \\ 1 \\ 1
 \end{array}
 \left. \vphantom{\begin{array}{c} K_1 \\ K_2 \\ K_3 \\ K_4 \\ K_5 \\ K_6 \end{array}} \right\} \dots\dots(3.25)$$

A computer program in MATLAB has been developed to solve the permanent matrix functions. The performance index values for three mode of vibration can be raked as in Table 3.13. Dielectric medium ultrasonic vibration is ranked as the first, Tool ultrasonic vibration as second and workpiece Vibration as third.

Table 3.11 The performance Index values for three modes of vibrations

Rank	HYBRID EDM mode of vibration	Permanent of performance Index [A]	Maximum performance Index	Minimum performance Index
1	Workpiece	4.64165 X 106		
2	Tool	4.51851 X 106	16.4901 X 106	1.88535 X 106
3	Dielectric	3.75519 X 106		

### 3.11. Interim Conclusion:

The exceptional commitment of the present work is to measure the impacts of different attributes in the execution ultrasonic vibration in traditional EDM process. The interdependency of the component/sub-variables signifies the importance of that specific attribute/sub-attributes with other element/sub-elements under thought. It has been observed in this study that, other than flushing and dimensional accuracy,

cavitation likewise has a critical contribution. As cavitation is being viewed as essentially, one can't disregard the cavitation part of ultrasonic vibration usage and its repercussions.

The scientific model proposed in this paper can be utilized to add to a suitable speculation for the execution of ultrasonic vibration in traditional EDM process in view of the legacy and interdependency of various proposed component/sub-variables. This would help in controlling and upgrading process of customary EDM. Be that as it may, this methodology is to some degree new thinking in the space of Hybrid EDM. Portions of the outcome might significant commitment of this study are;

- The enormous numerical estimation of the performance index is  $3.28647 \times 10^{18}$ . As the coefficient of variable for the Hybrid EDM is high that demonstrates the noteworthiness of the variables considered for performance Index.
- The coefficient of variable for surface morphology and flushing is underneath 20% that show that ultrasonic vibration conferred to this proposed process clearly enhance the flushing, surface morphology and dimensional accuracy.
- Cavitation and Abnormal discharge's coefficient of variable is high and these attributes are less investigated by the researchers in literature, yet influence the performance index fundamentally.
- The digraph representation shows complex interdependency of variables and sub elements, cavitation influences every other component and corresponding coefficient of variable for this is high it deciphers very noteworthy element in this process. In any case, the specialized impediments restrain its appropriateness in this process.
- The major limitation is the big numerical value of the performance index.  $16.4901 \times 10^6$  may appear to be an odd figure for practical purposes, but provide a comparison. This could be used to compare the three modes of vibration.
- This approach can further be utilized to evaluate the performance of various hybrid processes used in Advance manufacturing technology to analyze the effects of various qualitative/quantitative attributes.

---

**ISM ANALYSIS FOR HYBRID EDM**

---

**4.1. Introduction:**

A conventional EDM process would hardly be a complete solution for present industrial metal cutting requirement. Lots of research work is going on throughout the world to ameliorate its productivity and process stability. The stationary machining gap between the tool electrode and the workpiece is usually replaced with reciprocating motion of work pieces to regulate the fresh dielectric circulation in the gap. This perception is still under developing stage. The evaluation and optimization for Hybrid-EDM performance and its parameters is intricate in this perception. There are different technical difficulties associated with execution of this process (Hoang and Yang, 2013). The measures and attributes in Hybrid-EDM, contrast each other, and generate uncertainty conditions and yield loads of space for further growth. Vital conditions for accomplishing productive in Hybrid-EDM comprise in understanding the present and forthcoming objective and attribute of the Hybrid-EDM. There is a requirement for basic, orderly and logical scientific approach for analyzing of different perceptions considering in EDM. To come up to such labyrinthine difficulties of UV implementation in EDM framework, the authors have proposed Interpretive Structural Modeling (ISM) & MICMAC analysis methodologies. ISM approach is necessary for effective and economical execution of such innovative technological reforms. This approach is helpful to understand the highest productivity of diverse perceptions and resources for access to predetermine multiple objectives and attributes problem like Hybrid-EDM: Singh and Khamba, (2011) used ISM approach for modeling the utilization barriers in Advanced Manufacturing Technologies (AMTs). The target of ISM and MICMAC investigation approach was to recognize fitting determination characteristics, and to acquire the most suitable blend of parameters in conjunction with the genuine metal cutting requirement. An undertaking has been fixed through this present study to recognize the nature and thusly surveyed interdependency and heritage of different dependent and driver variables in EDM process. The results of this work are validated further with the execution of continuous ultrasonic vibration in Wire-EDM in phase-II & III.

## **4.2. Application of Interpretive Structural Modelling (ISM):**

ISM strategy is an intuitive learning process and assist in ameliorate order and direction of miscellaneous correlation among the parameters a framework. Most often, the capability of a manufacturing process is analyzed considering a selected driver controllable variable with the objective of optimizing dependent variables. Contingent upon the technical and financial needs of a perception and the manufacturing requirement, a few criteria may have essential or optional parts of the general machining capability assessment. Nonetheless, appropriate and exhaustive judgment for a manufacturing perception can be carried out simply by looking at all of diver and dependent parameters concurrently. In this proposed study, an arrangement of indirectly and straightforwardly parameters influencing comprehensively the Hybrid-EDM process is organized through a fundamental digraph model. This is a unique approach in this direction, i.e., simultaneous consideration of all the driver and dependent variables in manufacturing technology. The ISM and MICMAC analysis facilitate in formalizing a generalized digraph structure of complex properties. According to Attri and Grover, (2015), this methodology is a convincing conditional approach which has already been applied successfully in various decision making areas. This approach provides better logical and diagrammatic visualization into the system as a whole. The mathematical foundations of the ISM methodology can be found in various reference works. Govindan et al., (2010) applied ISM approach for auto industry supplier development and found that, the ISM methodology's major limitation, prejudices of the individual who is deciding upon the parameters. This limitation is removed by exhaustive literature review and confirmation experimental investigation for familiarity and understudies the relations among the variables.

Moreover, in ISM methodology, no weights are associated with the parameters correlation with respect to their relative influence. A generalized systematic streamline flow chart for the ISM strategy is depicted in Figure 4.1.

### **4.2.1. Identification of the various drivers:**

It has been acknowledged that the performance of ultrasonic vibration to EDM framework is an intricate endeavor. On that point are certain factors which impede the performance of ultrasonic vibration in Hybrid-EDM process. The sixteen fundamental

parameters for execution of perceptions of ultrasonic vibration in Hybrid-EDM have been perceived in Table 4.1 as taking over;

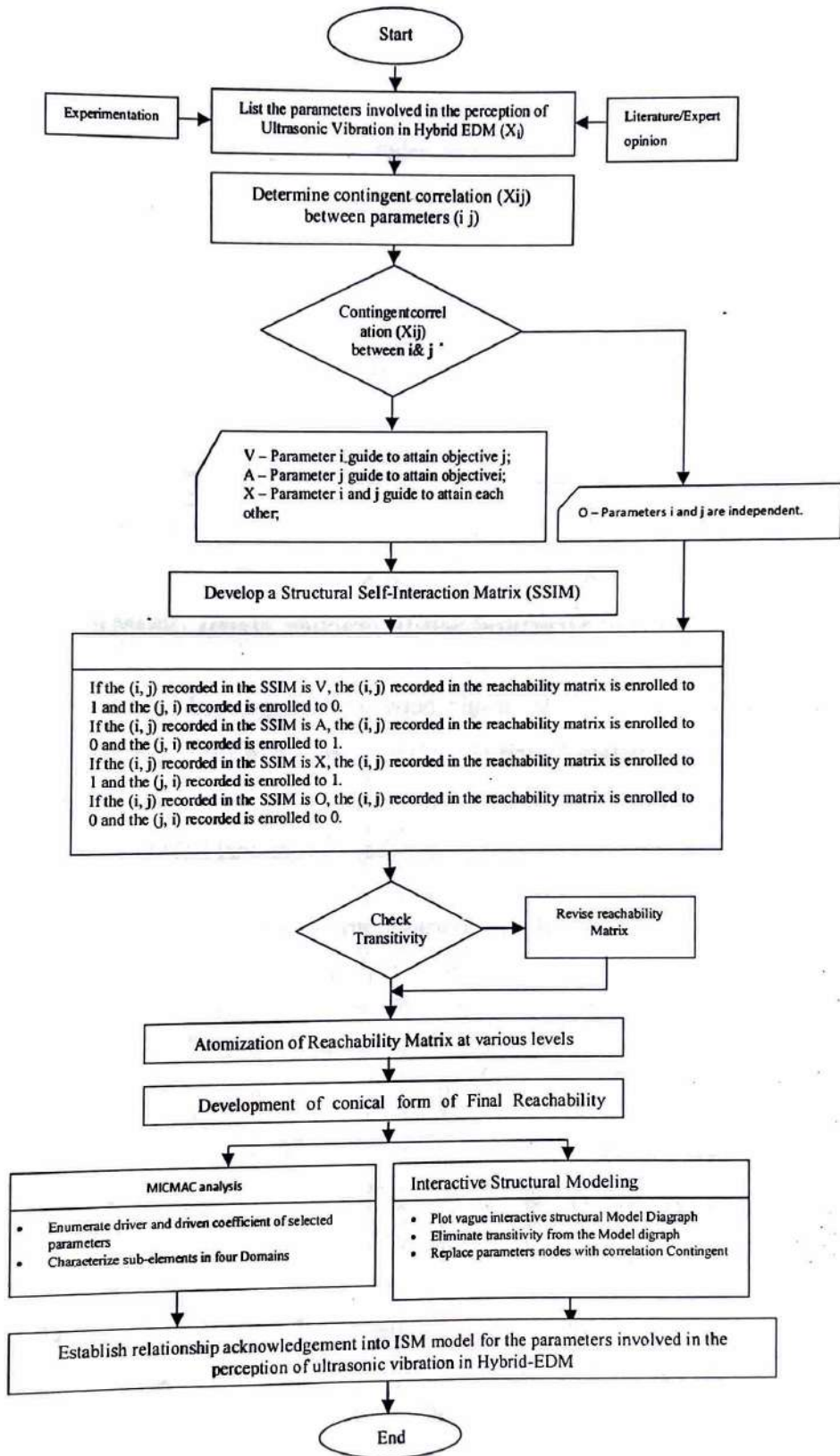


Figure 4.1. The flow chart for the ISM & MICMAC methodology

Table 4.1. Drivers of Ultrasonic vibration assisted Hybrid-EDM.

Parameters	Reference
Metal Removal Rate	(Chen and Lin, 2009) (Masuzawa and Heuvelman, 1983) (Prihandana et al., 2009) (Nani, 2017) (Gao and Liu, 2003) (Egashira and Masuzawa, 1999) (Shabgard and Alenabi, 2015)
Tool Wear Rate	(Prihandana et al., 2011) (Egashira & Masuzawa, 1999) (Shabgard and Alenabi, 2015)
Surface Roughness	(Chen and Lin, 2009) (Masuzawa and Heuvelman, 1983) (Abdullah et al., 2009)
Thickness heat effect layer	(Kremer et al., 1991) (Abdullah and Shabgard, 2008) (Meseet et al., 2014)
Ultrasonic field forces	(Kremer et al., 1989) (Liew et al., 2014) (Gao and Liu, 2003)
Suction & Exhaust of action for fresh dielectric	(Jujhar Singh et al., 2011) (Ogawa et al., 2012) (Gao and Liu, 2003)
Evacuation of gas bubble debris	(Zhixin et al., 1995a) (Zhixin et al., 1995b) (Guo et al., 1997)
Stirring effect	(Hoang and Yang, 2013) (Liew et al., 2014)
Amplitude of vibration	(Kremer et al., 1989) (Murthi and Philip, 1987)
Acoustic Pressure	(Kremer et al., 1989) (Gao and Liu, 2003) (Ogawa et al., 2012)
Arcing & short circuit	(Ghoreishi and Atkinson, 2002) (Lin et al., 2001) (Shabgard et al., 2011)
Debris concentration	(Nishiwaki et al., 2008) (Yu, et al., 2009)
Discharge wave distribution	(Iwai et al., 2013) (Lin et al., 2000) (Guo et al., 1995)
Micro-cracks and pin-holes	(Khosrozadeh and Shabgard, 2017) (Jujhar Singh et al., 2011)
Residual compressive stress	(Kremer et al., 1989) (Guo et al., 1997) (Khosrozadeh and Shabgard, 2017)
Micro-Hardness	(Shabgard et al., 2011) (Jujhar Singh et al., 2011)

#### 4.2.2. Development of Structural Self-Interaction Matrix (SSIM):

In view of the relevant relationship between distinguished affecting parameters, a Structural Self-Interaction Matrix (SSIM) was created in Table 4.2. This matrix shows the combine shrewd connections among the driver parameters influencing the implementation of ultrasonic vibration for the conventional EDM under thought.

Table 4.2. Structural self-interaction matrix for the Hybrid-EDM drivers.

Variables	16	15	14	13	12	11	10	9	8	7	6	5	4	3	2	1
Metal Removal Rate(MRR)	V	V	V	A	V	X	A	A	A	A	A	A	V	X	X	-
Tool Wear Rate(TWR)	O	O	O	X	X	X	X	O	O	O	O	X	V	V	-	-
Surface Roughness(Ra)	O	O	A	A	A	A	A	A	A	A	A	A	A	-	-	-
Thickness of heat effected Zone	X	X	O	A	O	A	A	O	A	A	A	O	-	-	-	-
Ultrasonic filed forces	O	O	O	O	V	O	V	O	V	V	V	-	-	-	-	-
Suction & Exhaust of action of fresh dielectric	V	V	V	V	V	V	A	A	V	V	-	-	-	-	-	-
Evacuation of gas bubble debris	V	V	V	V	V	V	A	A	A	-	-	-	-	-	-	-
Stirring effect	V	V	V	V	V	V	A	A	-	-	-	-	-	-	-	-
Amplitude of vibration	O	O	O	V	O	O	V	-	-	-	-	-	-	-	-	-
Acoustic pressure	O	O	O	V	V	O	-	-	-	-	-	-	-	-	-	-
Arcing & short circuit	V	V	V	A	X	-	-	-	-	-	-	-	-	-	-	-
Debris concentration	O	O	V	V	-	-	-	-	-	-	-	-	-	-	-	-
Discharge wave Distribution	V	V	V	-	-	-	-	-	-	-	-	-	-	-	-	-
Micro-cracks&pin-holes	A	O	-	-	-	-	-	-	-	-	-	-	-	-	-	-
Residual compressive stress	V	-	-	-	-	-	-	-	-	-	-	-	-	-	-	-
16. Micro-Hardness	-	-	-	-	-	-	-	-	-	-	-	-	-	-	-	-

### 4.2.3. Reachability Matrix:

The rudimentary reachability matrix is produced from the structural self-communication framework (SSIM) produced in the preceding paragraph utilizing to generalize systematic streamline flow chart for the ISM strategy from Figure 4.1. The ultimate reachability matrix in Table 4.4 is driven from the rudimentary reachability grid from Table 4.3 considering the transitivity control, which expresses that if a variable 'A' is correlated with 'B' and 'B' is correlated with 'C', at that point 'A' is surly correlated with 'C'

Table 4.3. Rudimentary reachability matrix for the variables.

S. No	Variables	1	2	3	4	5	6	7	8	9	10	11	12	13	14	15	16	
1.	Metal Removal Rate	1	1	1	1	0	0	0	0	0	0	1	1	0	1	1	1	
2.	Tool Wear Rate	1	1	1	1	1	0	0	0	0	1	1	1	1	0	0	0	
3.	Surface Roughness	1	0	1	0	0	0	0	0	0	0	0	0	0	0	0	0	
4.	Thickness of heat effected Zone	0	0	1	1	0	0	0	0	0	0	0	0	0	0	1	1	
5.	Ultrasonic Field forces	1	1	1	0	1	1	1	1	0	1	0	1	0	0	0	0	
6.	Suction & Exhaust action of fresh dielectric	1	0	1	1	0	1	1	1	0	0	1	1	1	1	1	1	
7.	Evacuation of gas bubble debris	1	0	1	1	0	0	1	0	0	0	1	1	1	1	1	1	
8.	Stirring affect	1	0	1	1	0	0	1	1	0	0	1	1	1	1	1	1	
9.	Amplitude of Vibration	1	0	1	0	0	1	1	1	1	1	0	0	1	0	0	0	
10.	Acoustic pressure	1	1	1	1	0	1	1	1	0	1	0	1	1	0	0	0	
11.	Arcing & short circuit	1	1	1	1	0	0	0	0	0	0	1	1	0	1	1	1	
12.	Debris concentration	0	1	1	0	0	0	0	0	0	0	1	1	1	1	0	0	
13.	Discharge wave Distribution	1	1	1	1	0	0	0	0	0	0	1	0	1	1	1	1	
14.	Micro-cracks & Pin-holes	0	0	1	0	0	0	0	0	0	0	0	0	0	0	1	0	0
15.	Residual compressive stress	0	0	0	1	0	0	0	0	0	0	0	0	0	0	0	1	1
16.	Micro-Hardness	0	0	0	1	0	0	0	0	0	0	0	0	0	0	1	0	1

Table 4.4 Ultimate reachability matrix for the variables.

Variables	1	2	3	4	5	6	7	8	9	10	11	12	13	14	15	16	Driver power
1	1	1	1	1	1	0	0	0	0	1	1	1	1	1	1	1	12
2	1	1	1	1	1	1	1	1	0	1	1	1	1	1	1	1	15
3	1	0	1	1	1	0	0	0	0	1	1	1	1	1	1	1	11
4	1	0	1	1	0	0	0	0	0	0	0	0	0	1	1	1	6
5	1	1	1	1	1	1	1	1	0	1	1	1	1	1	1	1	15
6	1	1	1	1	0	1	1	1	0	0	1	1	1	1	1	1	13
7	1	1	1	1	0	0	1	0	0	0	1	1	1	1	1	1	11
8	1	1	1	1	0	0	1	1	0	0	1	1	1	1	1	1	12
9	1	1	1	1	0	1	1	1	1	1	1	1	1	1	1	1	15
10	1	1	1	1	1	1	1	1	0	1	1	1	1	1	1	1	15
11	1	1	1	1	1	0	0	0	0	1	1	1	1	1	1	1	12

12	1	1	1	1	1	0	0	0	0	1	1	1	1	1	1	12
13	1	1	1	1	1	0	0	0	0	1	1	1	1	1	1	12
14	1	0	1	0	0	0	0	0	0	0	0	0	1	0	0	3
15	0	0	1	1	0	0	0	0	0	0	0	0	1	1	1	5
16	0	0	1	1	0	0	0	0	0	0	0	0	1	1	1	5
Dependence power	14	11	16	15	8	5	7	7	1	9	12	12	12	16	15	15

#### 4.2.4. Atomization of Level:

The ultimate reachability matrix acquired in paragraph 4.2.3 was atomized into various stratum. The reachability and precursor group of all driver were established from the ultimate reachability matrix of Table 4.4. The reachability group formation for a distinctive driver comprises of self and other equivalent drivers which it might assist to fulfill. The Precursor group formation comprises of usual drivers and other equivalent drivers which it's supposed to accomplish. The convergence of both these groups was additionally inferred for all drivers is thought to be in level I and is given the best placement in the ISM chain of importance. With this atomization, cycle Repetition 1 in Table 4.5 is accomplished.

Table 4.5 Cycle Repetition -1; atomization of level for drivers

	Reach ability group	Precursor group	Intersection	Level
1.	1,2,3,4,5,10,11,12,13,14,15,16	1,2,3,4,5,6,7,8,9,10,11,12,13,14	1,2,4,5,10,11,12,13,14	
2.	1,2,3,4,5,6,7,8,10,11,12,13,14,15,16	1,2,5,6,7,8,9,10,11,12,13	1,2,5,6,7,8,10,11,12,13	
3.	1,3,4,5,10,11,12,13,14,15,16	1,2,3,4,5,6,7,8,9,10,11,12,13,14,15,16	1,3,4,5,10,11,12,13,14,15,16	I
4.	1,3,4,14,15,16	1,2,3,4,5,6,7,8,9,10,11,12,13,15,16	1,3,4,15,16	
5.	1,2,3,4,5,6,7,8,10,11,12,13,14,15,16	1,2,3,5,10,11,12,13	1,2,3,5,10,11,12,13	
6.	1,2,3,4,6,7,8,11,12,13,14,15,16	2,5,6,9,10	2,6	
7.	1,2,3,4,7,11,12,13,14,15,16	2,5,6,7,8,9,10	2,7	
8.	1,2,3,4,7,8,11,12,13,14,15,16	2,5,6,8,9,10	2,8	
9.	1,2,3,4,6,7,8,9,10,11,12,13,14,15,16	9	9	
10.	1,2,3,4,5,6,7,8,10,11,12,13,14,15,16	1,2,3,5,9,10,11,12,13	1,2,3,5,10,11,12,13	
11.	1,2,3,4,5,10,11,12,13,14,15,16	1,2,3,5,6,7,8,9,10,11,12,13	1,2,3,5,10,11,12,13	
12.	1,2,3,4,5,10,11,12,13,14,15,16	1,2,3,5,6,7,8,9,10,11,12,13	1,2,3,5,10,11,12,13	
13.	1,2,3,4,5,10,11,12,13,14,15,16	1,2,3,5,6,7,8,9,10,11,12,13	1,2,3,5,10,11,12,13	
14.	1,3,14	1,2,3,4,5,6,7,8,9,10,11,12,13,14,15,16	1,3,14	I
15.	3,4,14,15,16	1,2,3,4,5,6,7,8,9,10,11,12,13,15,16	3,4,15,16	
16.	3,4,14,15,16	1,2,3,4,5,6,7,8,9,10,11,12,13,15,16	3,4,15,16	

Table 4.6 CycleRepetition-2; atomization of level for drivers



	Reach ability group	Precursor group	Intersection	Level
1.	1,2,4,5,10,11,12,13,15,16	1,2,4,5,6,7,8,9,10,11,12,13	1,2,4,5,10,11,12,13	
2.	1,2,4,5,6,7,8,10,11,12,13,14,15,16	1,2,5,6,7,8,9,10,11,12,13	1,2,5,6,7,8,10,11,12,13	
4.	1,4,15,16	1,2,4,5,6,7,8,9,10,11,12,13,15,16	1,4,15,16	II
5.	1,2,4,5,6,7,8,10,11,12,13,15,16	1,2,5,10,11,12,13	1,2,5,10,11,12,13	
6.	1,2,4,6,7,8,11,12,13,15,16	2,5,6,9,10	2,6	
7.	1,2,4,7,11,12,13,15,16	2,5,6,7,8,9,10	2,7	
8.	1,2,4,7,8,11,12,13,15,16	2,5,6,8,9,10	2,8	
9.	1,2,4,6,7,8,9,10,11,12,13,15,16	9	9	
10.	1,2,4,5,6,7,8,10,11,12,13,15,16	1,2,5,9,10,11,12,13	1,2,5,10,11,12,13	
11.	1,2,4,5,10,11,12,13,15,16	1,2,3,5,6,7,8,9,10,11,12,13	1,2,5,10,11,12,13	
12.	1,2,4,5,10,11,12,13,15,16	1,2,3,5,6,7,8,9,10,11,12,13	1,2,5,10,11,12,13	
13.	1,2,4,5,10,11,12,13,15,16	1,2,3,5,6,7,8,9,10,11,12,13	1,2,5,10,11,12,13	
15.	4,15,16	1,2,4,5,6,7,8,9,10,11,12,13,15,16	4,15,16	II
16.	4,15,16	1,2,4,5,6,7,8,9,10,11,12,13,15,16	4,15,16	II

Table 4.7 CycleRepetition-3; atomization of level for drivers

	Reach ability group	Precursor group	Intersection	Level
1.	1,2,5,10,11,12,13	1,2,5,6,7,8,9,10,11,12,13	1,2,5,10,11,12,13	III
2.	1,2,5,6,7,8,10,11,12,13	1,2,5,6,7,8,9,10,11,12,13	1,2,5,6,7,8,10,11,12,13	III
5.	1,2,5,6,7,8,10,11,12,13	1,2,5,10,11,12,13	1,2,5,10,11,12,13	
6.	1,2,6,7,8,11,12,13	2,5,6,9,10	2,6	
7.	1,2,7,11,12,13	2,5,6,7,8,9,10	2,7	
8.	1,2,7,8,11,12,13	2,5,6,8,9,10	2,8	
9.	1,2,6,7,8,9,10,11,12,13	9	9	
10.	1,2,5,6,7,8,10,11,12,13	1,2,5,9,10,11,12,13	1,2,5,10,11,12,13	
11.	1,2,5,10,11,12,13	1,2,3,5,6,7,8,9,10,11,12,13	1,2,5,10,11,12,13	III
12.	1,2,5,10,11,12,13	1,2,3,5,6,7,8,9,10,11,12,13	1,2,5,10,11,12,13	III
13.	1,2,5,10,11,12,13	1,2,3,5,6,7,8,9,10,11,12,13	1,2,5,10,11,12,13	III

Table 4.8 CycleRepetition-4; atomization of level for drivers.

	Reach ability group	Precursor group	Intersection	Level
5.	5,6,7,8,10	5,10	5,10	
6.	6,7,8	5,6,9,10	6	
7.	7	2,5,6,7,8,9,10	7	IV
8.	7,8	5,6,8,9,10	8	
9.	6,7,8,9,10	9	9	
10.	5,6,7,8,10	5,9,10	5,10	

Table 4.9 CycleRepetition-5; atomization of level for drivers.

	Reach ability group	Precursor group	Intersection	Level
5.	5,6,8,10	5,10	5,10	
6.	6,8	5,6,9,10	6	
8.	8	5,6,8,9,10	8	V
9.	6,8,9,10	9	9	
10.	5,6,8,10	5,9,10	5,10	

Table 4.10 CycleRepetition-6; atomization of level for drivers.

	Reach ability group	Precursor group	Intersection	Level
5.	5,6,10	5,10	5,10	<b>VI</b>
6.	6	5,6,9,10	6	
9.	6,9,10	9	9	
10.	5,6,10	5,9,10	5,10	

Table 4.11 CycleRepetition-7; atomization of level for drivers.

	Reach ability group	Precursor group	Intersection	Level
5.	5,10	5,10	5,10	<b>VII</b>
9.	9,10	9	9	<b>VII</b>
10.	5,10	5,9,10	5,10	

Table 4.12 CycleRepetition-8; atomization of level for drivers.

	Reach ability group	Precursor group	Intersection	Level
9.	9	9	9	<b>VIII</b>

Later on the primary cyclic redundancy, the drivers incorporated into layer-I are deserted from whatever is entrusted of the drivers, this method is proceeded in Table (4.5-4.12). These cyclic redundancies are preceded until the period of every attribute is a established in the hierarchy.

#### 4.3. Formation of ISM model:

Table 4.5 infers that the surface roughness and micro-cracks & pinholes drivers are situated at level I and frame the topmost stratum in the ISM progression of Hybrid-EDM performance. With the assistance of the level atomization appeared in Tables 4.5-4.12, an ISM model of the different drivers critical for perceptions in ultrasonic vibration assisted Hybrid-EDM was produced, and appeared in Figure 4.2. The thickness of heat affected zone, residual stresses and Micro-hardness drivers are situated at stratum II; the discharge wave distribution, Debris concentration, arcing and short circuit, MRR and TWR five perceptions are put at stratum III; the evacuation of gas bubble debris, Stirring effect and suction and exhaust action of fresh dielectric medium perceptions are grouped at level IV, V and VI exclusively; and the ultrasonic field force and acoustic pressure parameters fall in at stratum VI; and amplitude of vibration compel in bottom stratum VIII.

The cycle reiteration is finished in eight stages, Tables 4.5-4.12 represents all the repetitions starting form elementary to final stratum of each parameter perceptions. This model indicates the dependency of various parameters selected for the implementation of ultrasonic vibration perception in traditional EDM. Kumar et al., (2016) proposed a Graph theory model to explain the perception of UV in EDM. They classified the parameters affecting the performance of Hybrid-EDM in five groups. These were flushing, cavitation, abnormal discharge, dimensional accuracy and surface morphology. In this study to gain the confidence in proposed ISM Model, all parameters could further be grouped in four major perceptions.

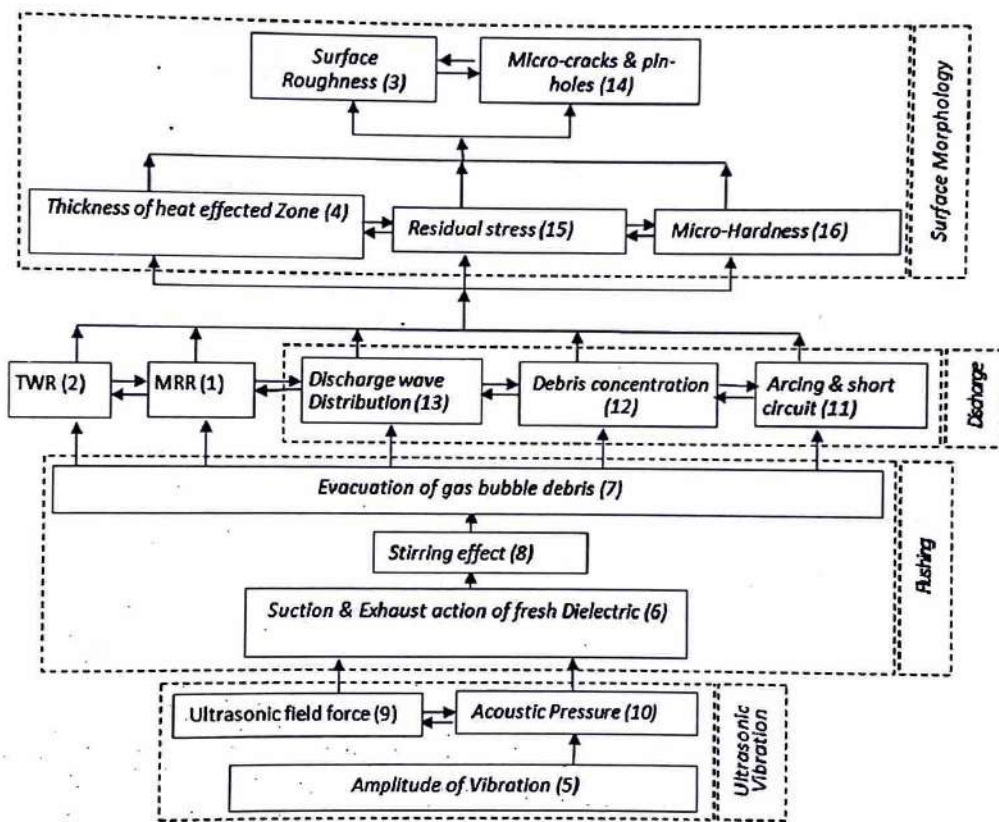


Figure 4.2 ISM hierarchy model for the perceptual drivers affecting the Hybrid EDM

These four groups are related to Flushing, Discharge, Ultrasonic vibration and surface Morphology. In other words, Ultrasonic vibration improves flushing, Flushing cause enhancement of in normal discharge, and normal results in better surface morphology of machined surface.

#### **4.4. MICMAC analysis for affecting and reliance coefficient:**

The MICMAC analysis is also known as Cross-Impact Matrix Multiplication method. The objective of this analysis is to identify relevance of the objective and parameters selected in perception of UV that are obtained from literature review.

A causal relationship is built among these objective and parameters, and then finding of key parameters affecting the whole system. This approach is quite useful to execute a particular perception in manufacturing system like EDM, where a complex relationship exists between objective and the parameters. An Applied cross impact matrix multiplication is generated to assign sector, and the base is multiplication properties of matrices. The outcome of MICMAC analysis is the quantitative value assigned to parameters in term of affecting coefficient and reliance coefficient of (Attari & Grover, 2015). The parameters consider in this study is categorized into four sectors in as Figure 4.3. The sector-I contain autonomous variables that have low affecting coefficient and low reliance coefficient of parameters. These variables are relatively inert in nature from a system and having only little inter-relationship that could be strong enough. Sector-II accommodates dependent variables that have low affecting coefficient and high reliance coefficient of parameters. Sector-III includes the parameters that have high affecting coefficient and low reliance which are unequal and any activity on these parameters will have an effect to others. Sector IV includes the independent parameters and having high affecting coefficient and high reliance coefficient of parameters.



- **Group-III:** Normal Discharge (Discharge wave Distribution, Debris concentration and Arching & short circuit)
- **Group IV:** Surface Morphology (surface Roughness, Thickness of recast layer & heat effected zone, Micro-hardness, Size of Micro- cracks & holes and Residual stresses)

In Figure 4.2, it is evident that ultrasonic field force and acoustic pressure are significant drivers to achieve the flushing of contaminated dielectric medium by pumping and stirring action which ultimately enhance evacuation of debris and gas bubbles form due to erosion, which is in tern critical to achieving the Ultrasonic vibration in conventional EDM.

From the MICMAC analysis, there is no such driver that has weak dependence and weak driving power as no drivers is mapped in sector I. Next, the Group IV variables (Surface Morphology) i.e. surface Roughness, Thickness of recast layer & heat affected zone, Micro-hardness, Size of Micro- cracks & holes and Residual stresses drivers are found to have weak driving power and strong dependence power so it maps to sector II of Figure 4.3. The drivers such as discharge wave distribution, Debris concentration, Arching & short circuit MRR, TWR and acoustic pressure are found to have strong driving power and strong dependence power so they map to sector III of Figure 4.3.

These drivers are unstable due to the fact that any change occurring to them will affect other drivers and may themselves be affected through a feedback mechanism. Lastly, Pumping action, Stirring effect and Debris, Gas bubble debris evacuation and Ultrasonic field force drivers posses strong driving power and weak dependence power so they map to sector IV of Figure 4.3. The scientific model proposed in this paper can be utilized to add to a suitable speculation for the execution of ultrasonic vibration in conventional EDM process in view of the legacy and interdependency of various proposed variables. This would control of process gather and the upgrades required in customary Hybrid-EDM process.

The majority of the scientists in literature affirm this through their experimentation as 84% analyst considered flushing of sullied dielectric liquid and 40% surface morphology to improve the execution of convention EDM process. Normal

discharges condition (23%) driver variables are less investigated by the scientist in literature likewise, yet influence the Hybrid-EDM execution fundamentally. The ISM model representation shows complex interdependency of variables. Flushing influences every other component and it is the major criteria for implementing ultrasonic vibration in conventional EDM, very noteworthy element in Hybrid-EDM system. This approach is new thinking in the domain of Hybrid-EDM. As no new work is perfect, the present work is also associated with some limitations.

## DESIGN AND FABRICATION OF EXPERIMENTAL SETUP

Ultrasonic vibration assisted Hybrid Wire-EDM (Hybrid-WEDM) system is used as hybrid machining process in this study for better circulation of dielectric and the removal of machine debris. Therefore, an appropriate frame and housing was designed that were necessary to accommodate the system and proper functioning of the experimental setup.

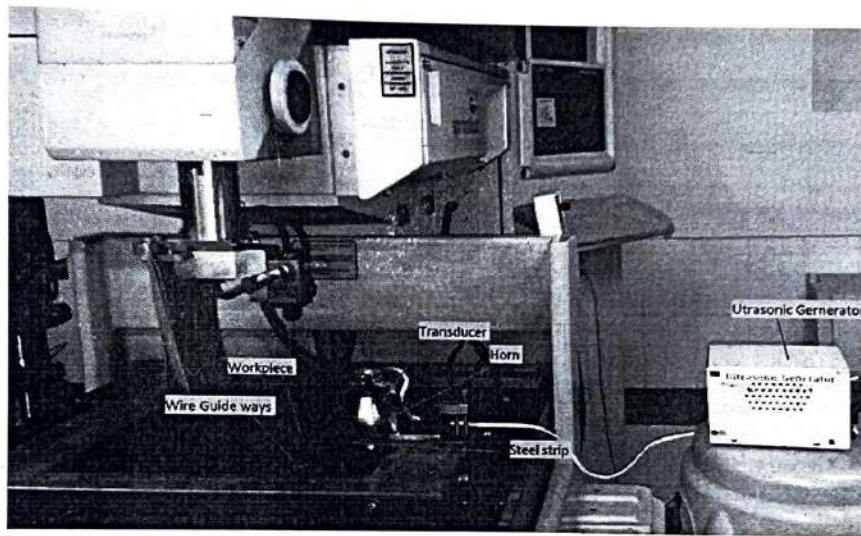


Figure 6.1. Developed set up design for Ultrasonic vibration assisted Hybrid-WEDM (Kumar et al., 2018)

The experimental set up and its important element for this study developed for this research work has been described in Figure 6.1.

### 6.1. Basic Principle:

In this experimental set-up, Ultrasonic waves were transferred Indirect to the workpiece instead of wire. The high amplitude vibration is necessary to develop a large pressure gradient to obtain the maximum flushing effect. Ultrasonic wave applied to the workpiece through the proposed cantilever arrangement caused a strong drift to gas bubbles and debris by a spatial gradient as shown in Figure 6.2. (a-b). This mechanism not only charged the gap with a fresh dielectric with but also allowed cooling of the machined surface. This cantilever arrangement provided comparatively high acceleration to debris and gas bubble to evacuate than that of the ultrasonic wave



transferred perpendicular to the machined surface due to a cyclic spatial variation and pressure gradient in upper and lower half of the workpiece.

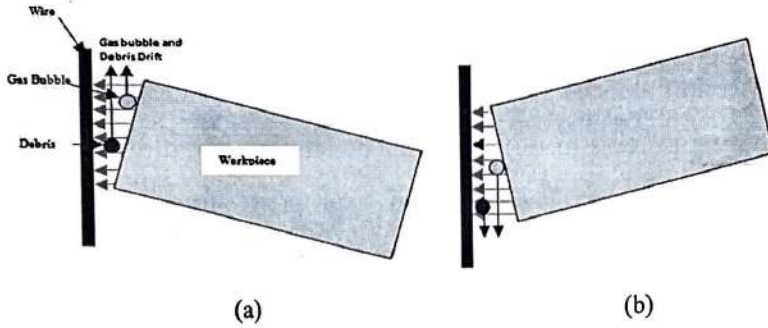


Figure 6.2. Model for debris and cavitation bubbles removal through gap for Hybrid-WEDM :(a) workpiece upward motion due to cantilever motion and (b) workpiece downward motion due to cantilever motion

## 6.2. Ultrasonic System:

The proposed ultrasonic system incorporates a ultrasonic generator, piezo-electric transducer and horn to operate at a design frequency of 21.5 kHz. In previous studies, the pumping and hammering action of ultrasonic wire vibration facilitate the debris and the gaseous particles to expel from machining zone (Guo et al., 1997).

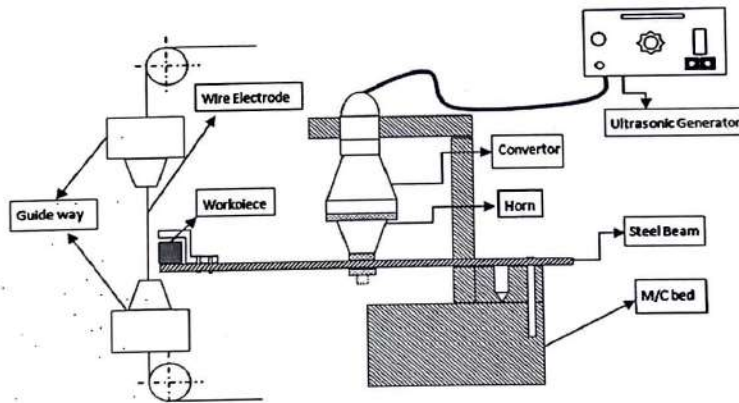


Figure 6.3. Schematic diagram of experimental setup for ultrasonic vibration of work piece in Wire-EDM.

The reciprocating movement of wire electrode creates acoustic pressure difference. This pressure gradient generates a shock wave propagates throughout the discharge gap. This same effect may be obtained if the ultrasonic vibration introduced to the work piece in place of the wire electrode. Ultrasonic work piece vibration will help in

expelling debris and molten metal from the machined surface and machining corridor due to the inertial forces set. The Schematic diagram of experimental setup for ultrasonic vibration of work piece in Wire-EDM is shown in Figure 6.3.

Ultrasonic pulse generator with the piezoelectric transducers assembly is used to create vibration. A suitable frame and housing were designed, which were important to oblige the framework and appropriate working of the setup to stay away from the resonance. The following are the major components of the ultrasonic system.

- Ultrasonic Generator & Piezo-electric transducer
- Continuous and discontinuous Control system.
- Cantilever plate with holding fixture.

#### **6.2.1. Ultrasonic Generator and Piezo-electric transducer:**

High performance ultrasonic transducer with 21.5 kHz settled frequency and 120W Ultrasonic PCB was utilized to develop an ultrasonic mechanical vibration generator. A suitable horn was designed, which were important to oblige the resonance. The resonance with the ultrasonic vibration device was the basic issue; it turned out to be more urgent when bestowed to workpiece in the traditional EDM system (Kumar et al., 2017a). These resonances developed clamors and oppose the fruitful execution of ultrasonic vibration in ultrasonic vibration assisted EDM system. Piezoelectric transducer is made of both positive and negative components that adjust themselves within the sight of an electric field. This property makes them really change measurements. At the point when a substituting electric field is connected to the transducer, the material vibrates forward and backward and produces a ultrasonic vibration. Piezoelectric materials are the establishment of ultrasonic sensors. Piezoelectric transducers were earlier made of piezoelectric gems, however are now a day made of ceramic. They deliver a wavelength that is double the measure of the component's thickness.

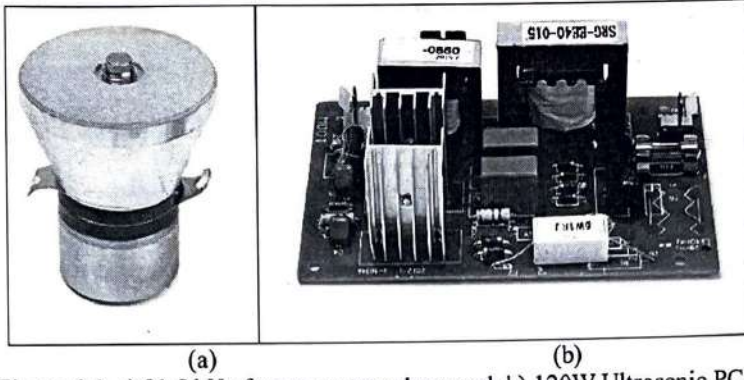


Figure 6.4. a) 21.5 kHz frequency transducer and; b) 120W Ultrasonic PCB

Because of this, elements are cut to be  $\frac{1}{2}$  the size of the desired wavelength. This also means that thinner elements produce higher frequencies. The piezoelectric transducer is chosen which can operate at 21.5 kHz. Fig. 6.4 shows the (a) piezoelectric transducer and (b) circuit plate which are parts of ultrasonic system.

### 6.2.2. Continuous and discontinuous Control system:

A self designed ultrasonic control system is used to control the type of ultrasonic vibration (i.e. continuous and discontinuous) as shown in Figure 6.5.



Figure 6.5. Continuous and discontinuous vibration mode On/Off

Further Figure 6.6 shows the principle of ultrasonic piezo-electric transducer in which continuous and discontinuous ultrasonic vibrations are provided through the control of oscillator. The “Knob” is provided to change the mode of vibration.

The continuous vibrations are attained in default case, as and when discontinuous vibration is needed the selector will control the same through relay. In case of discontinuous vibrations, the high frequency electrical impulse from the generator to the transducer is discontinuous. Interval times are adjusted in terms of make and break frequency of the relay which is adjustable by electronic circuit with the gap of micro

half second. However the frequency of energizing the ultrasonic transducer has to be maintained at 21.5 kHz, being the resonant frequency of the transducer.

This frequency remains same in both the modes. The frequency of discontinuity was achieved with customizable by an electronic circuit after trials.

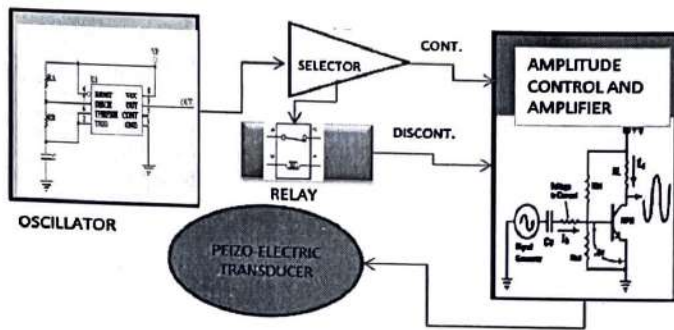


Figure 6.6 Circuit diagram for Continuous and discontinuous vibration mode

However the frequency of the ultrasonic transducer must be kept up at 21.5 KHz, remained same in both of the modes.

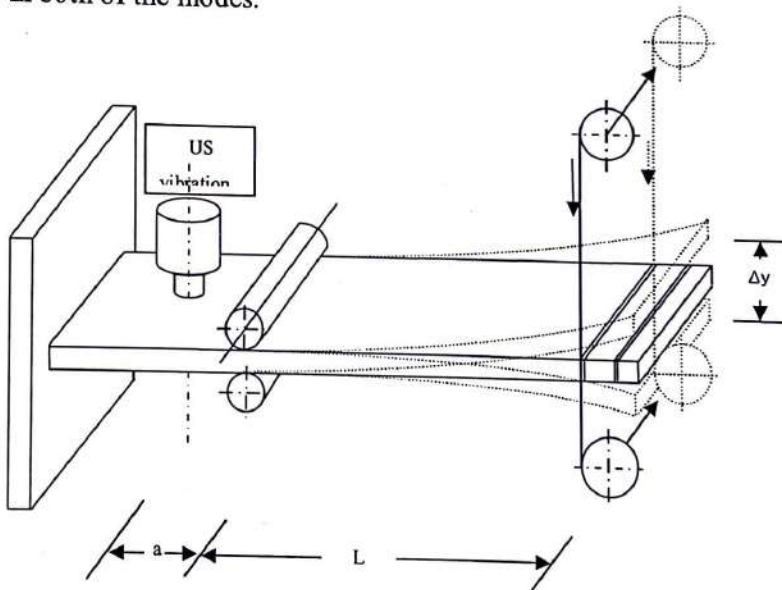


Figure.6.7 Cutting edge of ultrasonic vibration actuator as a cantilever beam.

This frequency is being measure with the help of high frequency oscilloscope.

### 6.2.3. Cantilever plate with holding fixture:

A steel strip was used to transfer the varying amplitude simply by changing the holding position of the work piece. The one end of steel strip was fixed to machine table and the other end was provided with a holding fixture for the work piece. The

programming for machining was done with the reference to the world coordinate system of CNC Wire-EDM machine tool. Also, dielectric fluid was flushed to the machining gap through nozzle jet from top and bottom. Each set of experiments were performed at room temperature in a narrow temperature range ( $32 \pm 2^\circ \text{C}$ ).

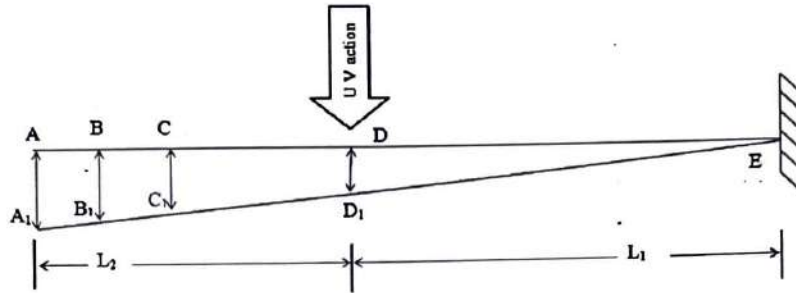


Figure 6.8 Varying amplitude with Cutting Edge Ultrasonic vibration as a cantilever beam

The vibratory horn is placed 31.11mm from the fixed end and cutting tip is 70mm from the fixed end. The output amplitude of Ultrasonic vibration of steel strip beam at point 'D' is  $8\mu\text{m}$  fixed.

Using triangular rule

$$\Delta EDD_1 \cong \Delta EAA_1$$

$$\frac{AA_1}{DD_1} = \frac{EA}{ED} = \frac{L_1 + L_2}{L_1}$$

$$AA_1 = \frac{EA}{ED} DD_1$$

$$AA_1 = 18\mu\text{m}$$

S No.	Amplitude( $\mu\text{m}$ )	Horizontal length(mm)
1	$AA_1=18 \mu\text{m}$	$EA=31.11$
2	$BB_1=14 \mu\text{m}$	$EB=50.00$
3	$CC_1=10 \mu\text{m}$	$EC=56.00$

### 6.3. Wire Electric Discharge Machine Tool :

The experiments were carried out on a wire-cut EDM machine (ELEKTRA SPRINTCUT 734) of Electronica Machine Tools Ltd. installed at CNC Laboratory of

Mechanical Department, J C Bose UST, YMCA Faridabad Haryana. The Wire- EDM machine tool shown in Figure 6.9 has the following specifications. The Figure 6.10 (a) and (b) shows Display Screen and Emergency Power off Button and Wire Feed Spool respectively.

### 1. Pulse on Time:

The pulse on time is eluded as  $T_{on}$  and it speaks to the span of time in miniaturized micro seconds,  $\mu s$ , for which the current is streaming in each cycle. Amid this time the voltage,  $VP$ , is connected over the terminals. The  $T_{on}$  setting time extend accessible on the machine apparatus is 100-131 which is connected in ventures of 1 unit. The single pulse rate release vitality increments with expanding  $T_{on}$  period, bringing about higher cutting rate. With higher estimations of  $T_{on}$ , be that as it may, surface roughness has a tendency to be higher. The higher estimation of release vitality may likewise cause wire breakage.

Table 6.1 Wire- EDM machine tool specifications.

Design	: Fixed Column, Moving Table
Maximum working current	: 50 Ampere
Input Mains Voltage	: 415V $\pm$ 10%, 3 phase, 50 Hz.
Open Gap Voltage	: 1-300 V
Pulse-on Time	: 1 to 2000 $\mu s$
Duty factor	: 1-100
Fluid pressure	: 0.1-2.1 Kg/cm <sup>2</sup>
Pulse frequency	: 0.07 to 300 KHz
Maximum stock removal (Cu-Steel)	: 300 (cu.mm/min.)
Best surface finish	: 0.5 micron CLA
Electrode wear	: 0.3 % to 20%.
Power Factor	: Approx. 0.9 lag
Power Consumption	: Approx. 7.5 KVA
Weight	: Approx. 300 Kg
Pulse Generator	: MOSFET Type
Height	: 1320 mm
Width	: 725mm
Depth	: 450 mm



Figure 6.9 Pictorial Views of Wire Cut EDM used for experimentation.

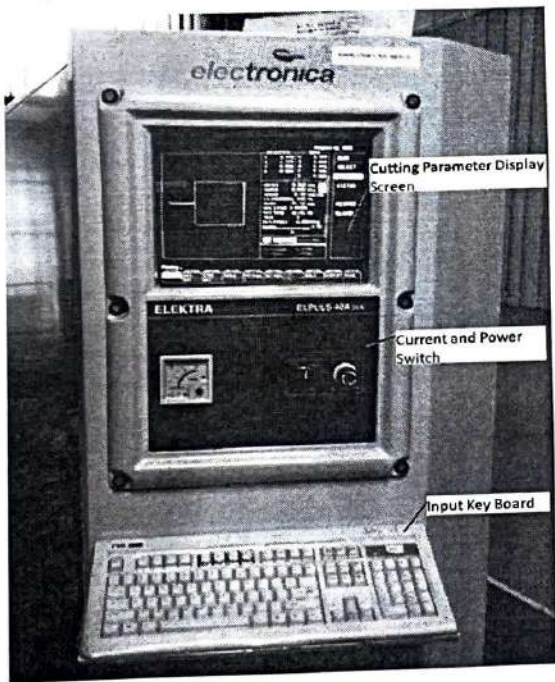


Figure 6.10 (b) Display Screen and Emergency Power off Button.

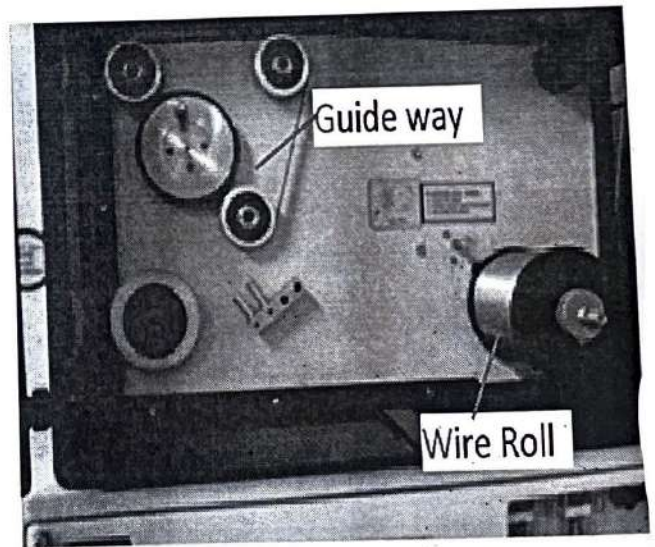


Figure 6.10 (a) Wire Feed Spool

## 2. Pulse off Time:

The pulse off time is eluded as  $T_{off}$  and it speaks to the span of time in micro seconds,  $\mu s$ , between the two concurrent flashes. The voltage is truant amid this piece of the cycle. The  $T_{off}$  setting time run accessible on the machine instrument is 00 - 63 which is connected in ventures of 1 unit. With a lower estimation of  $T_{off}$ , there is more number of releases in a given time, bringing about increment in the discharging efficiency. Therefore, the cutting rate likewise increments. Utilizing low estimations of  $T_{off}$  period, be that as it may, may cause wire breakage which thus decreases the cutting effectiveness. As and when the discharge condition ends up insecure, one can build the  $T_{off}$  time frame. This will permit bring down pulse duty factor and will decrease the average gap current.

## 3. Peak Current:

The peak current is represented by IP and it is the maximum value of the current passing through the electrodes for the given pulse.

## 4. Spark Gap Set Voltage:

The spark gap set voltage is a reference voltage for the actual gap between the work piece and the wire used for cutting. The SV voltage range available on the present machine is 00 - 99 volt and is applied in steps of 1 volt.

## 5. Wire Feed:

Wire feed is the rate at which the wire- electrode goes along the wire direct way and is encouraged persistently to spark. The wire feed go accessible on the present Wire-EDM machine is 1- 15 m/min in ventures of 1m/min. It is constantly attractive to set the wire feed to most extreme. This will bring about less wire breakage, better machining security and marginally all the more cutting rate.

## 6. Wire Tension:

Wire tension decides the extended of wire starched amongst upper and lower wire guides. This is a gram-proportionate load with which the consistently sustained wire



is kept under tension so it stays straight between the wire guides. Progressively the thickness of employment more is the tension required. Uncalled for setting of tension may bring about the activity errors and also wire breakage.

#### **7. Pulse Peak Voltage:**

Pulse-peak voltage setting is for selection of open gap voltage. Increase in the VP value will increase the pulse discharge energy which in turn can improve the cutting rate.

#### **8. Flushing Pressure:**

Flushing Pressure is for selection of flushing input pressure of the dielectric. High input pressure of water dielectric is necessary for cutting with higher values of pulse power and also while cutting the work piece of more thickness. Low input pressure is used for thin work piece and in trim cuts.

#### **9. Servo Feed:**

Servo feed setting decides the servo speed; the servo speed, at the set value of SF, can vary in proportion with the gap voltage (normal feed mode) or can be held constant while machining (with constant feed mode).

The ranges of process parameters for the experiments will be decided on the basis of literature survey and the pilot experiments using one factor at a time approach (OFAT).

# PROCESS PARAMETER SELECTION AND EXPERIMENTATION

---

In order to identify the process parameters that may affect the machining characteristics of Ultrasonic vibration assisted wire-EDM an Ishikawa cause and effect diagram was constructed and shown in Figure 7.1. The input process parameters and output characteristics selected based on this cause and effect diagram for the present work.

### 7.1. Selection of process parameters and their Range:

In order to obtain high material removal rate, low surface roughness and better quality of surface morphology produced by Ultrasonic vibration assisted Hybrid Wire-EDM process; the working range of the various parameters was determined.

Based on the critical review of literature, process variables of the Hybrid Wire-EDM were grouped in the following eight categories:

- Machining Condition
- Electrical Parameters
- Material parameters
- Wire Electrode Parameters
- Ultrasonic vibration parameters
- Mode of Vibration
- Additional Assistance
- Dielectric Parameters

All the above processes parameters affect material removal and surface integrity produced by normal EDM process. The cause and effect diagram so developed illustrated the possible effect of the various process parameters on the material removal and surface integrity.

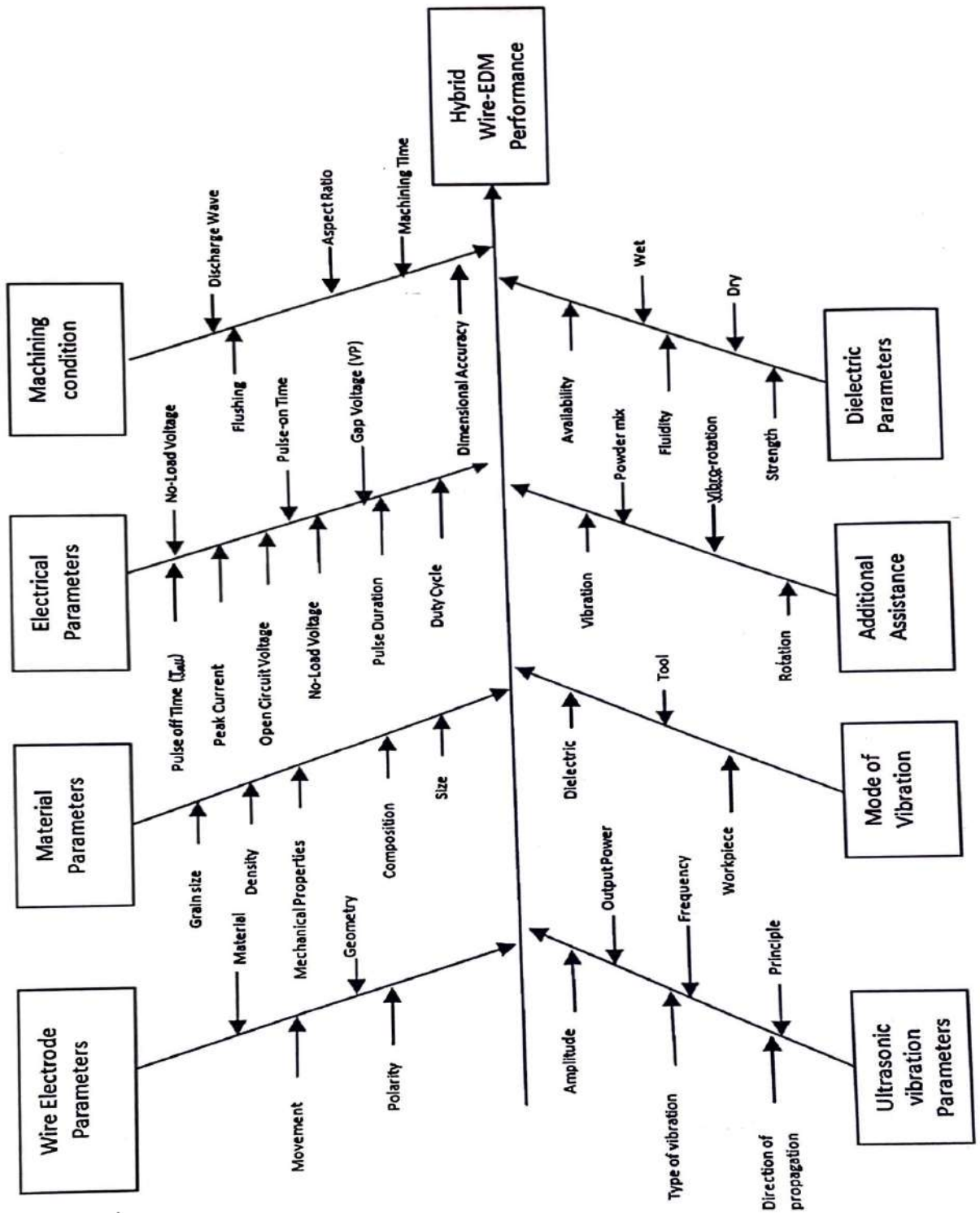


Figure 7.1 Ishikawa cause and effect diagram for Hybrid Wire-EDM

Out of these four parameters selected for this study. Those were ultrasonic vibration, Electrical, wire electrode and workpiece parameters considered for this study.

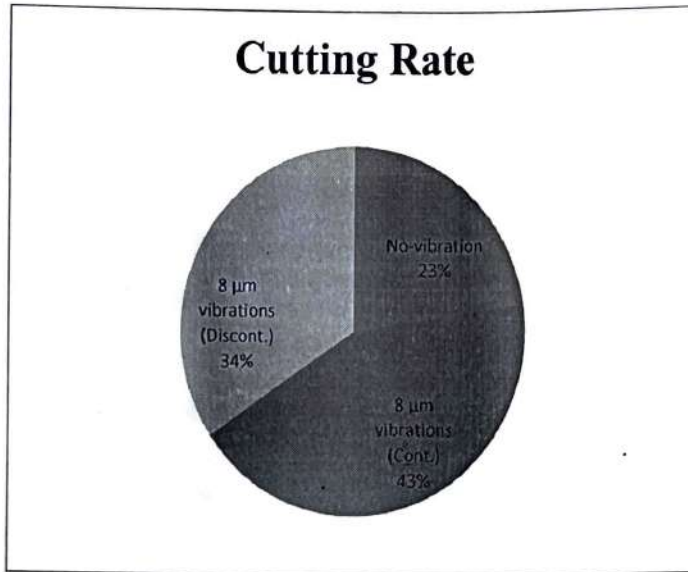


Figure 7.2: Comparison of cutting rate (mm/min) in Normal Wire-EDM, continuous and discontinuous vibration assisted EDM for high Carbon high Chromium Steel (Peak current 120A, Servo voltage 1150, pulse-on time 120 $\mu\text{s}$  and duty cycle 62 %)

#### 7.1.1. Type of Vibration:

The ultrasonic vibration assisted Wire-EDM has high cutting rate when it was compared with conventional Wire-EDM (having no vibration); this was proven by the pilot study of high Carbon high Chromium steel as shown in Figure 7.2.

Further pilot study showed that discontinuous vibration had significant effect as compared to continuous vibrations. The effect of type of vibration on high Carbon high Chromium Steel for MRR is shown in Fig. 7.3. A possible explanation for the differences in the Wire-EDM and vibration assisted Wire-EDM was that mechanical ultrasonic vibration. If work piece made the gap vary very rapidly, a high frequency alternate pressure variation is generated [Guo et al. (1997)]. Guo et al. (1997) endeavoured the wire vibration along and normal to the cutting direction and vindicated 30% increment in cutting rate as well as diminishment in surface roughness. Hoang and Yang, (2013) transferred ultrasonic vibration to work piece. They recognized that the ultrasonic vibration of workpiece brought some 1.5 times higher machining rate compared to that of wire vibration in Wire-EDM. They acquired cutting rate 2.5 times to that of the normal wire-EDM process and at the same time increase the wire cutting accuracy with minimum kerf width.

### 7.1.2. Amplitude of vibration and Peak current for cutting rate:

The cutting rate of Hybrid wire-EDM is proportional to the discharge frequency during machining. The amplitude of vibration increases the acoustic pressure and that results in high ultrasonic field force.

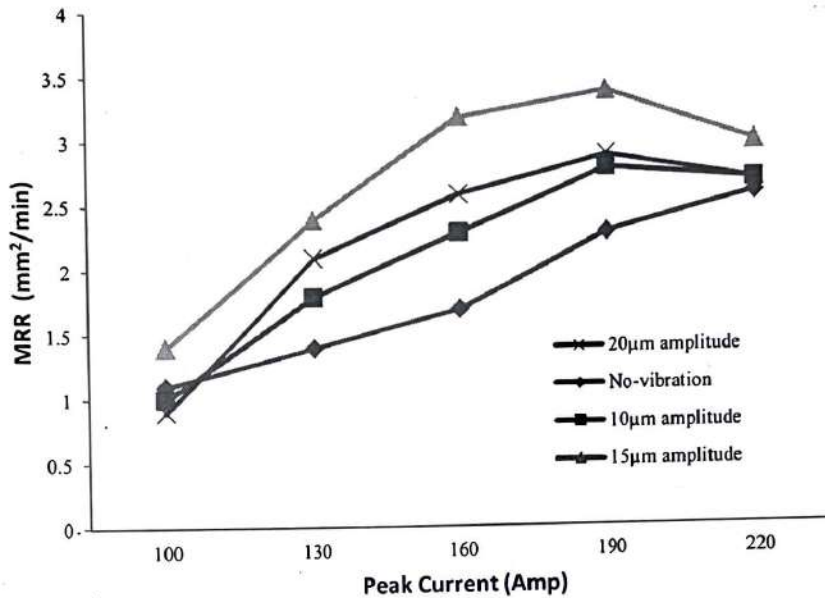


Figure 7.3 Graphical presentation of Cutting rate variation vs. peak current

The acoustic pressure developed due to the acoustic discharge gap between the wire and workpiece caused by vibration of workpiece. The ultrasonic field force imparted the acceleration to the debris and gas bubbles, the intensity of acceleration proportional to the ultrasonic field force. This ultrasonic field force guides the debris and gas bubble exhaust and suction of the fresh dielectric medium. This proposed experiment set-up ensured the alternating gap variation that forced the debris and guided to mixing properly, which enhanced the evacuation of debris and gas bubble. This same sequence has been proposed in the ISM hierarchical model in Figure 4.3 (Chapter 4). The ultrasonic vibration of work piece increased the number of effective discharge. The graphical representation of results for cutting rate vs. peak current at different amplitude is shown in Figure 7.3 along the No-vibration. Peak current value varies in the range of 100-220 ampere in a regular interval of 30 ampere. Under No-vibration condition the pattern of the curve is linear profile. It was observed that, a high value of peak current resulted in frequent wire breakage, although high cutting

rate was obtained. That was due to the high peak current produced larger discharge energy. But high cutting rate stimulation the debris concentration within the discharge gap, and resulted in secondary discharges. The secondary discharge did not allow the cutting speed to increase further with peak current, in fact, that reduced the cutting speed as shown Figure 7.3. The amplitude of vibration increased the cutting rate of Wire-EDM. The profile of the cutting rate curve at various amplitudes of vibration is bell shaped, but the peak of curve varies with amplitude of vibration. The amplitude of vibration provided the flexibility to widen the range of peak current to work with. Higher cutting speed rate was obtained range of 14-16  $\mu\text{m}$  amplitude of vibration. The acoustic pressure increased with the amplitude of vibration. Large amplitude of vibration and low suction lead to cavitation bubbles, and a small amplitude and high suction lead to fragmentation of large pieces debris. This phenomenon increased the gas bubble and debris concentration in gap and reduced the cutting rate at high amplitude of vibration. High amplitude of vibration also provoked the arcing and short circuit, it was observed that due to the increase in frequency of wire breakage.

Han et al. (2013) studied the effect of workpiece as a horn ultrasonic vibration in wire EDM, and discussed the effect of workpiece vibration on kerf width, machining rate and surface finish. They observed 10% improvement in machining rate, but ironically surface roughness also increased with that. In an exclusive work carried out by Nani V. M., (2017), concluded that wire vibration increase the intensity of dielectric liquid breakdown. The hammering action caused by an ultrasonic field to that debris helped in improving the surface finish. The outcomes built up in this pilot run that better machining yield for ultrasonic vibration could be obtained in traditional Wire-EDM by work piece as compare to wire.

### **7.1.3. Amplitude of vibration and Peak current for Surface morphology:**

The surface roughness, Micro-hole & micro crack variables have the highest dependent coefficient. The residual stresses, heat affected zone and the micro-hardness developed for surface come in second level. In this study, residual stress measured to confirm the proposed ISM model. The High amplitude of vibration caused vast pressure difference between the wire anode and the work piece. This pressure gradient prompts a pumping and mixing of dielectric in discharge gap. Although amplitude of vibration improved the flushing of debris and gas bubbles but

at higher amplitude of this vibration decline surface morphology as; the pace of debris evacuation lingers behind the debris aggregation. It could be observed from an ISM model that there existed a significant connection between surface morphology, amplitude of vibration and peak current. The discharge wave distribution and arcing and short circuits were the element of discharge energy, increase with the amplitude of vibration. The compressive residual stresses were the warm generation of the temperature gradient of re-solidified metal on the machined surface.

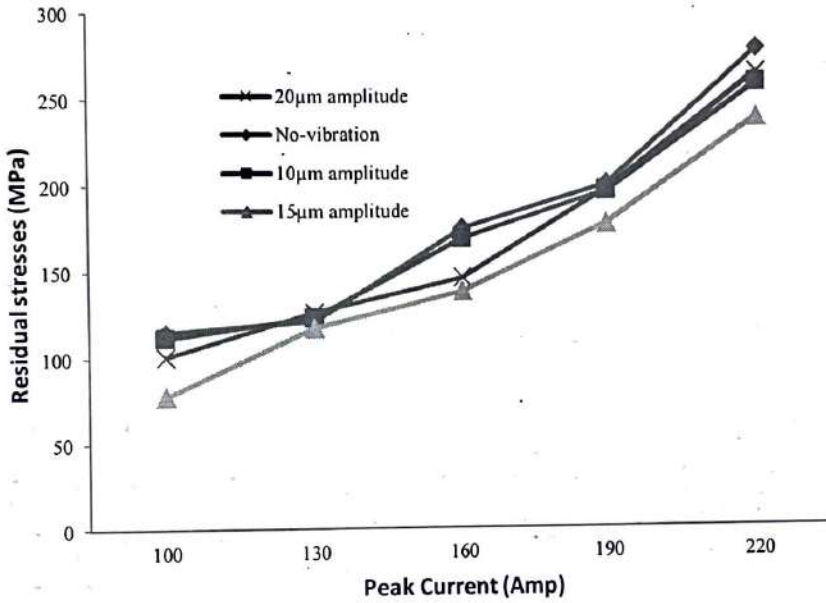


Figure 7.4. Graphical presentation of residual stresses variation vs peak current

These residual stresses produced in the EDMed surface because of metallurgical changes and non-homogeneity of the heat stream. The strong flushing impact ascribed to higher amplitude of vibration to lessen the heat concentration and re-solidification. Khosrozadeh & Shabgard (2017) determined the pattern of residual stresses of ultrasonic vibration assisted Die-sink EDM and conclude that the stresses decreased with the amplitude; however when increment pasted certain limit the impact was inverted. The compressive residual stresses were measured during the experimentation, these compressive residual stresses increased with the peak current. Figure 7.4 shows graphical variation of residual stresses variation vs. peak current, with increases in amplitude of vibration the residual stress decreased. The maximum deviation in residual stresses is obtained at 15µm and minimum at 20µm. Figure 7.5 to 7.8 represent the 2D, 3D, distortion ring and peak strength of experimental results

at No-vibration, 10 $\mu$ m amplitude of vibration, 15 $\mu$ m amplitude of vibration and 20 $\mu$ m amplitude of vibration respectively. The results confirm that the residual stresses developed in the wire - EDMed surface area of compressive nature. The magnitude of stresses decreased with the application of ultrasonic vibration. The variance of stresses decreased with the application of ultrasonic vibration. The variance of residual stresses with the amplitude of vibration is non-uniform. The maximum reduction in residual stresses was observed at 15 $\mu$ m amplitude of vibration. At low amplitude of vibration the variation in residual stress was marginal. The amplitude of vibration helped in uniformizing the discharge wave distribution in the discharge gap and reduced the arcing and short circuit. This phenomenon reduced the discharge energies and resulted less residual stress, micro-pin holes and micro-cracks.

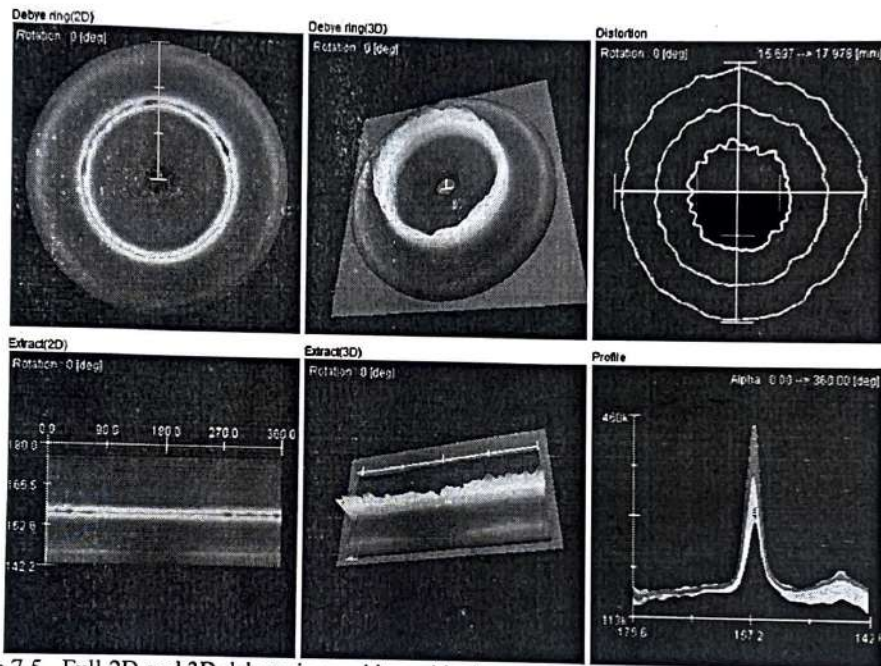


Figure 7.5. Full 2D and 3D debye ring and its residual stresses profile with peak current 160 amp and pulse on time 100, Pulse off time 50, Servo Voltage 1150 units at No-Vibration; Residual stress= 176MPa



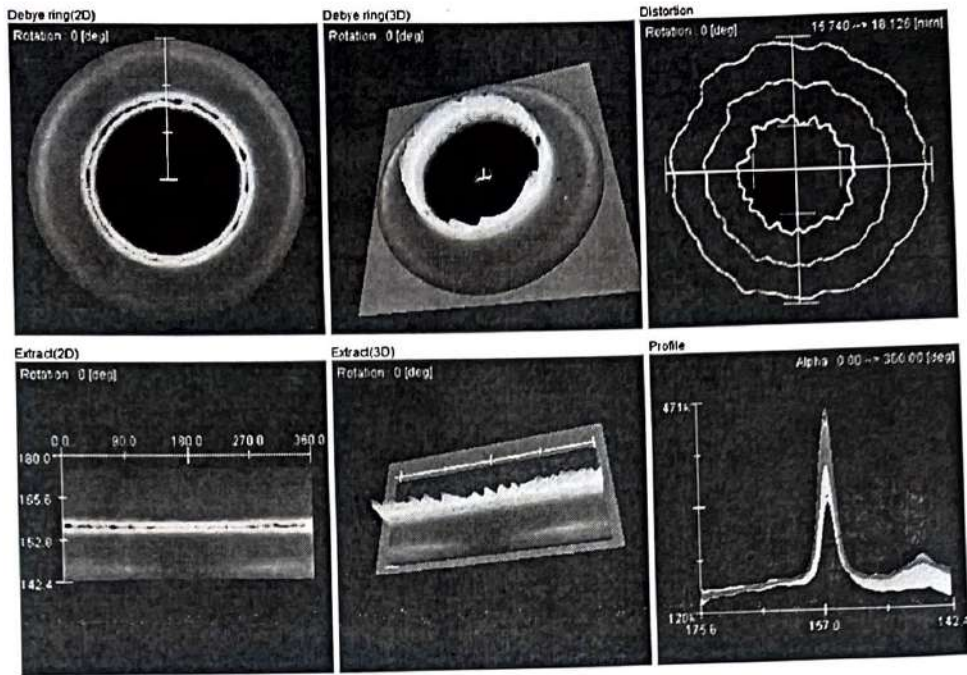


Figure 7.6 Full 2D and 3D debye ring and its residual stresses profile with peak current 160 amp and pulse on time 100, Pulse off time 50, Servo Voltage 1150 units at 10 $\mu$ m amplitude of vibration; Residual stress= 170MPa

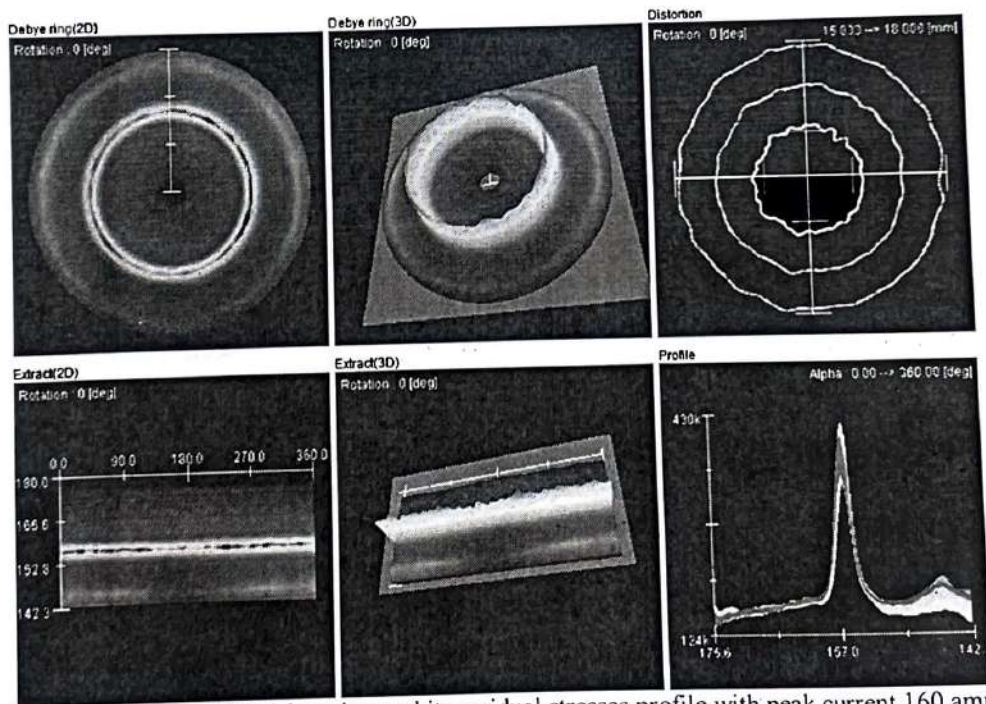


Figure 7.7 Full 2D and 3D debye ring and its residual stresses profile with peak current 160 amp and pulse on time 100, Pulse off time 50, Servo Voltage 1150 units at 15 $\mu$ m amplitude of vibration; Residual stress=139MPa

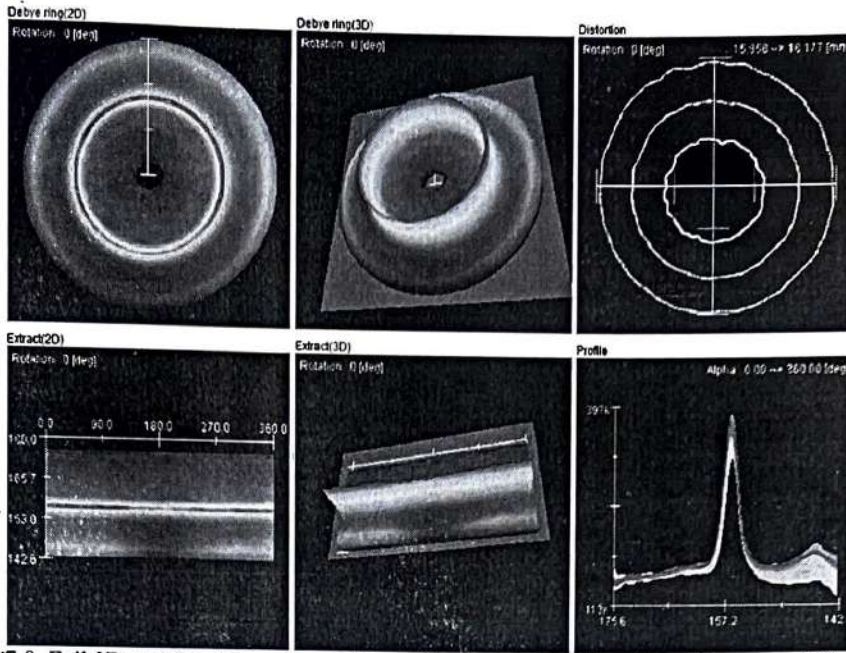


Figure 7.8 Full 2D and 3D debye ring and its residual stresses profile with peak current 160 amp and pulse on time 100, Pulse off time 50, Servo Voltage 1150 units at 20 $\mu$ m amplitude of vibration; Residual stress=149MPa

Distorted 3D Debye-Scherrer ring profile portrayed the damaged workpiece surface and high compressive residual stresses. With the amplitude of ultrasonic vibration, the uniformity of the 3D Debye ring was comparatively high. The uniformity in distortion ring was an indication of smooth crater size, and healthy surface morphology of machined surface with less residual stresses.

## 7.2. Work-piece Material:

**For Phase-II:** The workpiece material AISI D3 steel a high carbon-high chromium die steel extensively used in dies and mold industry was used for the experimentations.

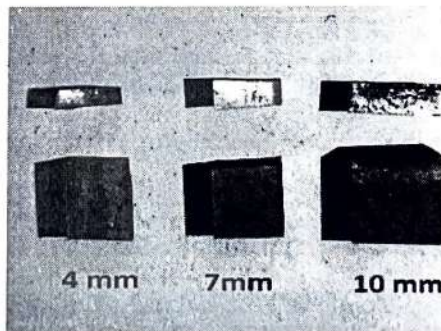


Figure 7.9 AISI D3 steel Materials Cut for Phase-II experimentation

The 18 examples were cut to cuboids shape with 4X10X20, 7X10X20, 10X10X20 mm<sup>3</sup> six each on Wire-EDM shown in Figure 7.9, and after that confronted and ground with diamond grinding wheel. Chemical composition of workpiece material and main mechanical properties has been listed in Tables 7.1. The mechanical properties at room temperature for AISI D3 are given in Table 7.2.

Table 7.1. Chemical composition of workpiece material phase-II (AISI D3 steel).

% weight composition of Components									
C	Si	Mn	Mo	P	S	V	W	Cr	Ni
1.55	0.30	0.35	0.75	0.03	0.03	0.90	-	10.41	0.30

AISI D3 is a high carbon-high chromium steel produced for applications requiring high protection from wear or to scraped spot and for protection from overwhelming pressure as compare to sudden stun.

Table 7.2. Properties at room Temperature for AISI D3

Young's Modulus, E(GPa)	210
Ultimate Tensile strength(N/mm2)	2010
Yield Strength(N/mm2)	2150
Poisson's Ratio	0.27-0.30
Rockwell Hardness	62
Density Kg/m <sup>3</sup>	7700
Thermal Expansion (10 <sup>6</sup> /°C)	12

As a result of these characteristics and its non-disfiguring properties, D3 is top notch for die work on long creation runs. It is basically oil- hardening steel, and it solidifies to an awesome depth.

The production from a die after each grind is consistently uniform. While the impact strength is comparatively low, by proper adjustment of tool design and heat treatment, this steel has been used successfully for punches and dies on quite heavy material (up to ¼ inch thick).

**For Phase-III:** In this phase, the AISI D2 high carbon high chromium Cold Work Tool steel workpiece material was chosen. The 32 specimens were cut to cuboids shape with 10X10X24 mm<sup>3</sup> on Wire-EDM as shown in Figure 7.10 and then faced and ground with grinding wheel. Chemical composition of workpiece material and principle mechanical properties has been recorded in Tables 7.3 and 7.4, separately.

Table 7.3 Chemical composition of workpiece material (AISI D2).

% weight composition of Components									
C	Si	Mn	Mo	P	S	V	W	Cr	Ni
2.01	0.67	0.34	2.0	0.03	0.03	1.00	1.00	12.00	0.30

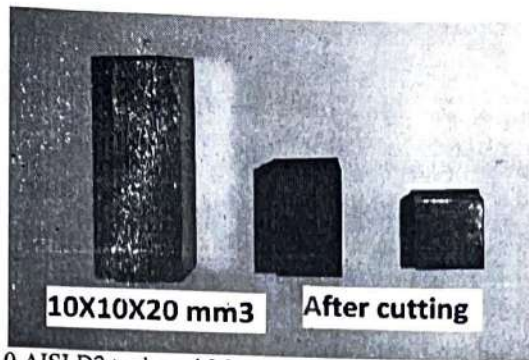


Figure 7.10 AISI D2 tool steel Materials Cut for Phase-III experimentation

AISI D2 Cold Work Tool Steel is air or oil hardened, with maximum dimensional stability during heat treatment, offering very high hardness and abrasion resistance. Generally supplied annealed to HB 250 max.

Table 7.4 Properties at room Temperature for AISI D2

Young's Modulus, E(GPa)	210
Ultimate Tensile strength(N/mm <sup>2</sup> )	1900
Yield Strength(N/mm <sup>2</sup> )	2150
Poisson's Ratio	0.27-0.30
Rockwell Hardness	64
Density Kg/m <sup>3</sup>	7700
Thermal Expansion (106/0C)	10.7

Typical applications of AISI D2 are Deep drawing and forming dies, cold drawing punches, hobbing, blanking, lamination and stamping dies, shear blades, burnishing rolls, master tools and gauges, slitting cutters, thread rolling & wire dies, extrusion dies etc.

### 7.3. Response Characteristics:

The effect of selected process parameters was studied on the following response characteristics of Hybrid Wire-EDM process:

- Cutting Rate (CR) / Material Removal Rate (MRR)
- Surface Roughness (SR)
- Residual Stresses

#### 7.3.1. Cutting Speed (CS)/ Material Removal Rate (MRR):

For Wire-EDM, cutting rate is a desirable characteristic and it should be as high as possible to give least machine cycle time leading to increased productivity. In the

present study cutting rate is a measure of job cutting which is digitally displayed on the screen of the machine and is given quantitatively in mm/min (Figure 6.10). Material removal rate was calculated by measuring the cutting rate and then multiplying it with the length of the cut.

For Wire-EDM, cutting rate is an alluring trademark and it ought to be as high as conceivable to give slightest machine process duration prompting expanded efficiency. In the present investigation cutting rate is a measure of occupation cutting which is carefully shown on the screen of the machine and is given quantitatively in mm/min (Figure 6.10). Material evacuation rate was figured by estimating the cutting rate and afterward increasing it with the length of the cut.

### **7.3.2. Surface Roughness (SR):**

Surface roughness is the measure of the fine surface anomalies in the surface. These are the aftereffects of the EDM procedure utilized to make the surface. Surface irregularities are connected as the arithmetic average deviation of the surface valleys and pinnacles communicated in micro-meters. The parameter for the most part utilized for general surface roughness is Ra. It gauges normal surface texture irregularities by contrasting every one of the pinnacles and valleys with the mean line, and after that averaging them everywhere throughout the whole cut-off length. Cut-off length is the length that the stylus was hauled over the surface; a more drawn out cut-off length will give a more normal esteem, and a shorter cut-off length may give a less exact outcome over a shorter stretch of surface. In this work the surface roughness is estimated by Taylor Hobson Surtronic 3+ profilometer. Before taking estimations for surface roughness, the work piece was cleaned with acetone ( $C_3H_6O$ ) solution. The surface analyzer is a shop- floor composes compact surface-roughness estimating instrument, which follows the surface of different machine parts and computes the surface roughness in light of roughness gauges, and shows the outcomes in  $\mu m$ . The work piece is appended to the finder unit of the Surtronic 3+ profilometer which follows the moment abnormalities of the work piece surface. The horizontal stylus dislodging amid the follow is prepared and digitally displayed on the display of the instrument.

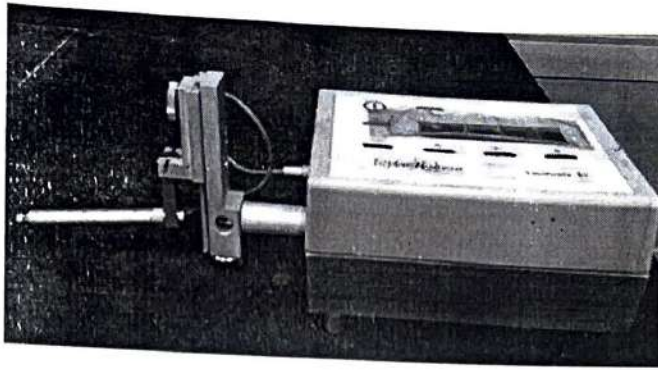


Figure 7.11 Surface Roughness Tester (Taylor Hobson Surtronic 3+ profilometer)

The surf test has a determination differing from  $0.01 \mu\text{m}$  to  $0.4 \mu\text{m}$  relying upon the estimation go. The roughness esteems are taken by averaging no less than three estimations for each specimen at various areas of specimen. Figure 7.11 demonstrates the surface roughness analyzer utilized for the measure of surface unpleasantness.

### 7.3.3. Residual stresses:

In this work the portable X-ray Residual Stress Analyzer  $\mu\text{-X360}$ , a non-destructive X-ray analyzer of Pulstec Industrial Corporation Limited shown in Figure 7.12 is used for measuring the residual stress in Wire-EDMed machined surfaces.

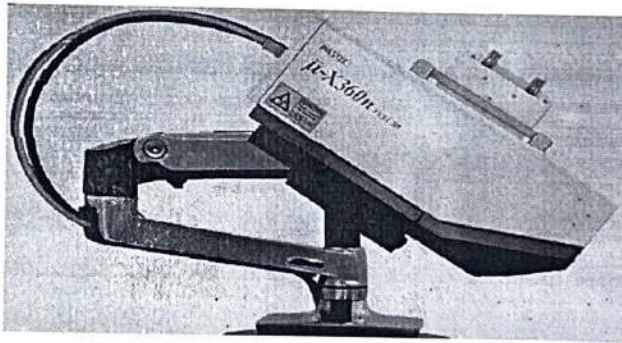


Figure 7.12 Portable X-ray Residual Stress Analyzer ( $\mu\text{-X360}$ FULL 2D X-ray detection)

This analyzer can measure the stress efficiently by detecting the full Debye ring data from a single incident X-ray angle and Non goniometer stage influence on the measurement result. Measurement conditions for residual stresses in present experiment are demonstrated in the Table 7.5.

Measurement	Units
Measurement area	All (3.000 - 30.000)
Pitch	50 [ $\mu\text{m}$ ]

X-ray irradiation time(Setup)	30 [sec]
X-ray irradiation time(Meas.)	30 [sec]
X-ray irradiation time(Max)	120 [sec]
X-ray tube current	1.00 [mA]
X-ray tube voltage	30.00 [kV]
Sample distance(Monitor)	39.000 [mm]
Sample distance(Analysis)	39.263 [mm]
X-ray incidence angle	35.0 [deg]
Offset of alpha angle	0 [deg]
X-ray wavelength (K-Alpha)	2.29093 [Å]
X-ray wavelength (K-Beta)	2.08480 [Å]
X-ray tube total use time	106.83 [h] (384601)
Detection sensitivity	20.3 [%] (174204)
Level of ambient light	0.2 [%]
Correction coefficient	0.00xx + 1.00x + 0.00
Valid range of alpha angle	18.00 <---> 90.
Peak analysis method	Fitting Lorentz

Compact, light-weight and portable for non-destructive measurements-designed for stress analysis, whether on-site measurement including large structures such as pressure vessels, or work-shop and laboratory based analysis. Low operational power and air cooled X-ray source. It is safe to operate and environmentally friendly.

These residual stresses developed during Hybrid-WEDM play a vital role in surface morphology of workpiece. These stresses are the major factors for the failure of any component. The extensive empirical testing and analysis of these stresses is the key for the success of any product. In this study, the residual stresses developed on the machined surface were measured using advanced X-ray Cos  $\alpha$  Method. In comparison to  $\text{Sin}^2\psi$  residual stress measurement method, the Cos  $\alpha$  method requires only a single angular measurement for complete analysis. This advanced method is based on the calculation of stain within crystal structure in certain plane. There exist a clear relationship between diffracted X-Ray and the inter-plane spacing of crystal lattices in a particular atomic plane. A stressed crystalline structure material surface results in change in wave length of the diffracted X-ray beam because of elongations and contractions within the crystal lattice. The inter-planer spacing (d) of certain crystal utilizes as the gauge length for measuring strain. When particular wavelength X-ray

incident on crystalline grain that satisfies Bragg's law gets diffracted and form as a cone around the axis of incident ray. This is because of the varying orientation of crystalline grain. According to the Bragg's law, a numerical relationship between incident X-ray and the inter-planer spacing of a crystal could be expressed as equation (7.1);

$$n\lambda = 2d \sin\theta \quad \dots\dots(7.1)$$

Where 'n' = An integer represents "order" of reflection,

$\lambda$ = The X-rays wavelength,

$d$  = The inter-planar spacing of the crystal,

$\theta$  = The incidence angle/diffraction angle

When a crystalline structure is under the stress, X-ray incident angle  $\psi_i$  is smaller and therefore the magnitude of Strain ( $\epsilon_i$ ) developed can be expressed as equation (7.2);

$$\text{Strain } (\epsilon_i) = \frac{d_f - d_i}{d_i} \quad \dots (7.2)$$

Where  $d_i$ = Initial inter=planar spacing of the crystal, and  $d_f$ = Final inter-planar spacing of the crystal after machining. The magnitude of strain developed is calculated using formula in equation (7.3 & 7.4) by acquiring the full Debye-Sherrer ring with a position detector sensor (Ashyralyev, 2010). The strain increases as a result of increase in ( $d_f$ ) and there by decrease ( $\theta$ ) in equation (7.22). The residual stresses are calculated from the change of diffraction normal angle ( $\psi$ ) as shown in Figure 7.13.

$$\epsilon_{\alpha 1} = \frac{1}{2} \{ (\epsilon_{\alpha} - \epsilon_{\pi+\alpha}) + (\epsilon_{-\alpha} - \epsilon_{\pi-\alpha}) \} \quad \dots\dots$$

(7.3)

$$\epsilon_{\alpha 2} = \frac{1}{2} \{ (\epsilon_{\alpha} - \epsilon_{\pi+\alpha}) + (\epsilon_{-\alpha} - \epsilon_{\pi-\alpha}) \} \quad \dots\dots$$

(7.4)



$$\epsilon_{\alpha 1} = \frac{1+\nu}{E} \sigma_x \cdot \sin 2\eta \cdot \sin 2\psi_i \cdot \cos \alpha \quad \dots\dots$$

(7.5)

$$\epsilon_{\alpha 2} = \frac{1+\nu}{E} \tau_{xy} \cdot \sin 2\eta \cdot \sin \psi_i \cdot \sin \alpha \quad \dots\dots\dots$$

(7.6)

$$\sigma_x = \frac{E}{(1+\nu) \sin 2\eta \cdot \sin 2\psi_i} \cdot \frac{\epsilon_{\alpha 1}}{\cos \alpha} \quad \dots\dots\dots$$

(7.7)

Where;  $\epsilon_{\alpha}$  = Strain measured in the direction of  $\alpha$ ,

$\epsilon_{\pi+\alpha}$  = Strain measured in the direction of  $\pi+\alpha$ ,

$\epsilon_{\alpha 1}$  = Strain measured in the vertical direction,

$\epsilon_{\alpha 2}$  = Strain measured in the horizontal direction,

$\sigma_x$  = Residual axial stress,

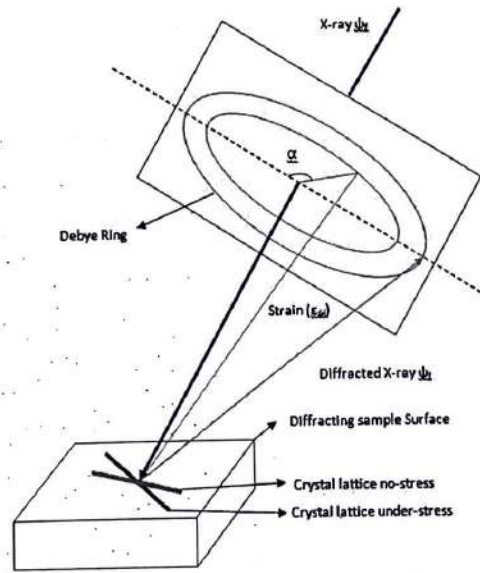


Figure 7.13. Geometric representation of the  $\cos(\alpha)$  geometry using a 2D Single position of detector.

$\tau_{xy}$  = Residual shear stress,

$\nu$  = Poisson's ratio,

$E$  = Young's Modulus of Elasticity,

$\Psi_i$  = Diffraction normal angle,

$\alpha$  = Azimuth angle of Debye-Scherrer ring,

$\eta$  = Angle between Debye-Scherrer ring axis and the sample diffraction detector of X-ray,

This diffracted cone shape around the axis is the Debye-Scherrer ring. The full Debye-Scherrer ring is procured by a single short duration X-Ray presentation. The residual stresses are determined by precisely estimating the position of the Debye-Scherrer rings; their positions are an immediate measure of strains  $\epsilon_{a1}$  and  $\epsilon_{a2}$ . The residual stresses can be calculated with the formula expressed in equation (7.6 and 7.7) (Peterson et al., 2017).

#### 7.4. Scheme of Experiments:

The entire experimental investigation is divided into two phases. The choice and selection of the parameters in each phase is decided by considering the objective of that particular phase.

##### 7.4.1. Scheme of Experiments (Phase-II):

The experiments in this phase are designed to study the effect of some of the Hybrid Wire-EDM parameters on response characteristics. Taguchi parametric design methodology was adopted in this phase. Table 7.6 shows the process parameters selected and their range available and their values at different levels.

Table 7.6 The controlled parameters and their Levels of experimental design (Phase-II)

Factors	Parameters	Levels		
		Level 1	Level 2	Level 3
A	Type of Vibration	Continuous	Discontinues	-
B	Amplitude of Work piece Vibration	10	14	18
C	Peak Current	100	140	180
D	Duty Cycle(Pulse off Time)	66%	72%	78%
E	Thickness of wok piece	10	7	4
F	Wire Feed Rate	5	8	11

**7.4.1.1. Selection of Orthogonal Array (OA) and Parameter Assignment:**

Before selection a particular OA to be used as a matrix for conducting the experiments, the following two points were considered as suggested by Ross (1996) and Roy (1990):

- The number of parameters and interactions of interest
- The number of levels for the parameters of interest

The non-linear behavior, if exist, among the process parameters can only be studied if more than two levels of the parameters are used. Therefore, each parameter was analyzed at three levels. In this phase Taguchi's mixed level design is selected as it is decided to keep two levels of type of vibration. The rest five parameters are studied at three levels. Two level parameters has 1 DOF, and five three level parameters have 10 DOF, i.e., the total DOF required will be 11 [= (1\*1+ (5\*2)]. The most appropriate orthogonal array in this case is  $L_{18}(2^1 * 3^7)$  OA with 17 [=18-1] DOF. Standard  $L_{18}$  OA with the parameters assigned by using linear graphs is given in Table 7.7. The unassigned columns were treated as error. For each trial, experiments were replicated three times.

Table 7.7 The  $L_{18}(2^1 * 3^7)$  OA (Parameters assigned) with Response (Phase I)

Ex p. No.	Run order	Parameters Trail Conditions								Responses (Raw Data)			S/N ratio (db)
		A	B	C	D	E	F	G	H	R1	R2	R3	
		1	2	3	4	5	6	-	-				
1	15	1	1	1	1	1	1	1	1	Y1 1	Y12	Y13	S/N (1)
2	8	1	1	2	2	2	2	2	2	Y2 1	Y22	Y23	S/N (2)
3	3	1	1	3	3	3	3	3	3	-	-	-	-
4	9	1	2	1	1	2	2	3	3	-	-	-	-
5	1	1	2	2	2	3	3	1	1	-	-	-	-
6	7	1	2	3	3	1	1	2	2	-	-	-	-
7	16	1	3	1	2	1	3	2	3	-	-	-	-
8	12	1	3	2	3	2	1	3	1	-	-	-	-
9	5	1	3	3	1	3	2	1	2	-	-	-	-
10	11	2	1	1	3	3	2	2	1	-	-	-	-
11	14	2	1	2	1	1	3	3	2	-	-	-	-
12	18	2	1	3	2	2	1	1	3	-	-	-	-
13	2	2	2	1	2	3	1	3	3	-	-	-	-
14	17	2	2	2	3	1	2	1	1	-	-	-	-
15	13	2	2	3	1	2	3	2	2	-	-	-	-
16	4	2	3	1	3	2	3	1	1	-	-	-	-

17	10	2	3	2	1	3	1	2	2	-	-	-	-
18	6	2	3	3	2	1	2	3	3	Y1	Y18	Y18	S/N(18)
Total										81	2	3	
										Σ	Σ	Σ	

R1, R2, R3 represent response value for three repetitions of each trail. The 1's, 2's and 3's represent levels 1, 2, 3 of the parameters, which appear at the top of the column. (--) represents no assignment in the column. Yij are the measured values of the quality characteristics (response).

**7.4.1.2. Experimentation (Phase-II):**

In phase-II, six process parameters viz. type of vibration, amplitude of vibration, workpiece thickness, peak current, duty cycle and wire feed rate were selected which are shown in Table 7.6 and the other parameters were kept constant. Experiments were conducted according to the test conditions specified by the L<sub>18</sub> OA (Table 7.7). Taguchi recommends the use of S/N ratio to measure the quality characteristics deviating from the desired values. The quality characteristic for cutting rate is taken “higher the better” and for surface roughness and residual stresses, it is taken as “lower-the better”. The S/N ratio for the “higher-the-better” equation (7.2) and “lower-the-better” equation (7.3) of response can be computed (Ross, 1996; Roy, 1990) as:

$$(S / N)_{HB} = -10 \log \left[ \frac{1}{R} \sum_{j=1}^R (Y_j^{-2}) \right] \quad \dots 7.2$$

$$(S / N)_{LB} = -10 \log \left[ \frac{1}{R} \sum_{j=1}^R (Y_j^2) \right] \quad \dots 7.3$$

Where, Y<sub>j</sub> (j= 1, 2, 3.....n) is the response value under the trail condition repeated R times.

Analysis of Variance (ANOVA) was performed to identify the process parameters that were statistically significant. With the S/N and ANOVA analyses, the optimal combination of the process parameters was predicted. Each experiment was repeated three times in each of the trail conditions. In each of the trial conditions and for every replication, the MRR, SR and residual stresses are measured. The cutting rate, surface roughness and residual stresses response characteristics are given in Table 7.8.

Table 7.8 – Experimental plan and Results of performance characteristics

Ex No	Type of Vibration	Amplitude of Vibration	Peak Current	Duty Cycle	Workpiece Thickness	Wire Feed Rate	Response for Erosion Rate (mm/min)			Response for Residual Stress (MPa)			Response for SR (µm)		
							R1	R2	R3	R1	R2	R3	R1	R2	R3
1	A	B	C	D	E	F	0.43	0.45	0.46	198	185	198	1.22	1.32	1.38
2	C	10	100	66	10	5	2.9	2.82	2.98	252	260	266	3.02	3	2.98
3	C	10	180	78	4	11	5.22	5.32	5.26	292	295	287	3.22	3.86	3.76
4	C	14	100	66	7	8	2.39	2.41	2.45	134	136	142	1.62	1.84	1.76
5	C	14	140	72	4	11	4.63	4.65	4.54	225	256	265	3.1	3.02	3.11
6	C	14	180	78	10	5	3.52	3.51	3.47	302	310	305	3.18	3.53	3.43
7	C	18	100	72	10	11	1.45	1.47	1.43	235	234	220	1.68	1.36	1.47
8	C	18	140	78	7	5	2.76	2.78	2.66	226	227	216	2.36	2.96	2.52
9	C	18	180	66	4	8	4.16	4.18	4.08	284	298	286	3.5	3.06	3.42
10	D	10	100	78	4	8	3.51	3.58	3.45	291	287	268	3.32	3.08	2.98
11	D	10	140	66	10	11	1.92	1.88	1.92	193	218	265	1.56	1.62	1.58
12	D	10	180	72	7	5	3.75	3.83	3.77	268	243	243	2.96	2.64	2.84
13	D	14	100	72	4	5	3.63	3.75	3.65	175	183	234	1.6	1.52	1.57
14	D	14	140	78	10	8	4.45	4.57	4.73	221	226	231	2.06	1.86	1.97
15	D	14	180	66	7	11	3.53	3.75	3.79	126	134	136	1.58	1.6	1.59
16	D	18	100	78	7	11	2.76	2.88	2.78	170	167	174	2.06	1.66	1.87
17	D	18	140	66	4	5	3.37	3.49	3.36	231	154	167	1.9	1.72	1.83
18	D	18	180	72	10	8	4.23	4.35	4.24	267	265	284	1.65	2.06	2.04

7.4.2. Scheme of Experiments (Phase-III):

In this phase, five process parameters viz. amplitude of vibration, peak current, pulse-on time, Pulse of Time, wire feed rate were selected for the purpose of investigating their effect on the response parameters of Hybrid Wire-EDM process. Thirty two pieces were processed according to the central composite design for five variables. In each of the trial conditions for every replication, the MRR and SR were measured. The MRR and surface roughness response characteristics were given in Table 7.12. For the proposed experimental work, RSM approach has been adapted for developing the numerical equation of correlation for quality characteristics of Hybrid Wire-EDM process. High carbon, high chromium D3 tool steel was selected for conducting experiments, as this was used extensively in blanking and forming dies industry. In applying RSM, the indigent variable has been seen as a surface to which a numerical model was fitted (Myers, R. H., & Montgomery, 1995). For the expansion of regression equations or correlation related to SR and MRR has been considered as the second order response surface as in equation (7.4):

$$U = b_0 + \sum_{i=1}^k b_i v_i + \sum_{i=1}^k b_{ii} v_i^2 + \sum_{i < j=2}^2 b_{ij} v_i v_j \pm e_r \quad \dots (7.4)$$

Quantitative response surface equation [U] for Hybrid Wire-EDM was obtained by substituting numerical values of the ' $v_i$ 's and ' $v_{ij}$ 's which were obtained analytically. Equation (7.4) for surface response [U] contains linear, squared and cross product terms of variables  $v_i$ 's. The choice and advancement of fitting response surface models were accomplished with the help of software programming in Design Expert (DX-11). The detailed design summary of statistical software used for this study is given in Table 7.9.

Table 7.9 Design Summary for statistical software used

Response	Units	Obs	Analysis	Min	Max	Mean	Std. Dev.	Ratio	Trans	Model
Metal removal rate (MRR)	mm <sup>2</sup> /min	32	Polynomial	1.89	26.39	14.55	7.33	13.96	None	Reduced Quadratic
Surface Roughness (Ra)	μm	32	Polynomial	1.02	2.64	1.52	0.4979	2.59	None	Reduced Quadratic
File Version	11.0.3.0									
Study Type	Response Surface	Subtype								
Design Type	Central Composite	Runs								

The parameter ranges and their corresponding levels with coded values that are used in present RSM approach given in Table 7.10. The coded values of variables were decided in experimental design matrix by the extreme values of variables using Equation (7.5).

Table 7.10 Process Parameters range and their Levels

S.No	Symbol	Parameters	Levels					Coded values
			(-2)	(-1)	(0)	(+1)	(+2)	
1	B	Peak Current	100	105	110	115	120	Real Values
2	C	Pulse On Time	70	90	110	130	150	
3	D	Pulse off Time	52	49	46	43	40	
4	A	Amplitude of Vibration	0	6	12	18	24	
5	E	Wire Feed Rate	0	6	12	18	24	

Type of Vibration: Ultrasonic vibration 21.5 KHz; Work Material: High-carbon High-chromium D3 steel; Polarity: Positive; Dielectric Fluid: Distilled water;

#### 7.4.2.1. Coding of Variables:

The coded values of variables as required in experimental design matrix (Table 7.11) can be found, once, the extreme values of variables are decided. The coded values have been found out using the following transformation equation (7.5):

$$Z_i = p_i + q_i X_i \quad \text{for } i = 1, 2, 3, \dots, k$$

.....(7.5)

Where

$Z_i$  = coded values of variables

$X_i$  = real values of variables

$P_i$  and  $q_i$  = Values of coefficient determined to satisfy the extreme values of real variables at the extreme ends of scale of coded variables i.e. -2 and 2 for five variables. The values of the process parameters at the desired levels have been given in Table 7.10, the experiment conditions are specified in Table 7.12.

Table 7.11 Coded Values and Real Values of the Variables (Phase III)

Ex No.	A Code d	B Coded	C Coded	D Coded	E Coded
1	-1	-1	-1	-1	1
2	1	-1	-1	-1	-1
3	-1	1	-1	-1	1
4	1	1	-1	-1	-1
5	-1	-1	1	-1	1
6	1	-1	1	-1	-1
7	-1	1	1	-1	1
8	1	1	1	-1	-1
9	-1	-1	-1	1	1
10	1	-1	-1	1	-1
11	-1	1	-1	1	1
12	1	1	-1	1	-1
13	-1	-1	1	1	1
14	1	-1	1	1	-1
15	-1	1	1	1	1
16	1	1	1	1	-1
17	-2	0	0	0	0
18	2	0	0	0	0
19	0	-2	0	0	0
20	0	2	0	0	0
21	0	0	-2	0	0
22	0	0	2	0	0
23	0	0	0	-2	0
24	0	0	0	2	0
25	0	0	0	0	-2
26	0	0	0	0	2
27	0	0	0	0	0
28	0	0	0	0	0
29	0	0	0	0	0
30	0	0	0	0	0
31	0	0	0	0	0
32	0	0	0	0	0

#### 7.4.2.2. Experimentation precaution:

While performing various experiments, the following precautionary measures were taken.

1. To reduce the error due to experimental setup, each experiment was repeated three times in each of the trail conditions.

2. The order and replication of experiment was randomized to avoid bias, if any, in the results.
3. Each set of experiments was performed at room temperature in a narrow range ( $32\pm 2^{\circ}\text{C}$ ).
4. The workpiece was cleaned with acetone before taking any measurement.

The experimental data of 32 runs at random were collected for a standard second-order experimental design called face-centered central composite design (CCD).

Table 7.12 Experimental trail conditions and results of response characteristics (MRR and SR)

Std. Order	Run order	Factor A	Factor C	Factor D	Factor E	Factor B	Response R1	Response R2
		Peak Current (Amp)	Pulse on Time ( $\mu\text{s}$ )	Pulse off Time ( $\mu\text{s}$ )	Amplitude of Vibration ( $\mu\text{m}$ )	Wire Feed Rate (mm/min)	MRR ( $\text{mm}^3/\text{min}$ )	SR ( $\mu\text{m}$ )
10	1	150	100	40	24	12	12.29	1.21
13	2	70	100	52	24	12	8.96	1.11
19	3	110	90	46	12	8	5.17	1.14
4	4	150	120	40	0	12	21.91	2.64
5	5	70	100	52	0	4	1.89	1.13
3	6	70	120	40	0	4	8.12	1.51
8	7	150	120	52	0	4	11.84	1.45
20	8	110	130	46	12	8	24.67	2.31
26	9	110	110	46	12	16	11.61	1.39
16	10	150	120	52	24	12	19.82	2.25
27	11	110	110	46	12	8	22.23	1.34
11	12	70	120	40	24	12	9.56	1.16
6	13	150	100	52	0	12	9.53	1.54
9	14	70	100	40	24	4	11.21	1.25
1	15	70	100	40	0	12	4.83	1.34
18	16	150	110	46	12	8	26.39	2.55
32	17	110	110	46	12	8	23.89	1.26
15	18	70	120	52	24	4	10.36	1.25
17	19	30	110	46	12	8	7.38	1.14
21	20	110	110	34	12	8	19.59	2.18
25	21	110	110	46	12	0	13.89	1.43
30	22	110	110	46	12	8	20.12	1.23
31	23	110	110	46	12	8	23.28	1.39
12	24	150	120	40	24	4	23.52	2.43
28	25	110	110	46	12	8	21.28	1.27
14	26	150	100	52	24	4	6.87	1.02
23	27	110	110	46	-12	8	12.12	1.59
2	28	150	100	40	0	4	18.38	2.49
7	29	70	120	52	0	12	5.89	1.25
29	30	110	110	46	12	8	23.93	1.22
24	31	110	110	46	36	8	20.34	1.17
22	32	110	110	58	12	8	4.88	1.12



### ANALYSIS AND DISCUSSION OF RESULTS

---

This chapter contains the analysis and discussion of the results of experiments conducted for phase-II and phase-III.

#### 8.1. Analysis and discussion of results of Phase-II:

In phase-II, the experiments were planned by using the parametric approach of the Taguchi's L18 Orthogonal Array (OA) method. The response characteristics data are provided in chapter 7 (Table 7.8). The standard procedure to analyze the data, as suggested by Taguchi, is employed. The average values and S/N ratio of the response characteristics for each parameter at different levels were calculated from experimental data. The main effects of process parameters both for raw data and S/N data were plotted. The response curves (main effects) were used for examining the parametric effects on the response characteristics. The analysis of variance (ANOVA) of raw data and S/N data was performed to identify the significant parameters to quantify their effect on the response characteristics. The most favorable conditions (optimal settings) of process parameters in terms of mean response characteristic were established by analyzing response curves and the ANOVA Tables.

Further, the effect of independent process parameters for Hybrid WEDM like type of vibration, amplitude of vibration, peak current, wire feed rate and duty cycle on the selected response characteristics (cutting rate, surface roughness and residual stresses) has been discussed. The interaction effect of type of vibration and amplitude were also discussed. The average value of response characteristics and S/N ratio (dB) for each parameter at level one, level two and level three (L1, L2 and L3) were calculated.

Each trial was rehashed three times in each of the trail conditions. In each run conditions and for each replication, the cutting rate (CR), residual stresses (RS) and surface roughness (SR) were measured. The S/N ratio and ANOVA investigation for cutting rate, residual stress were obtained by utilizing excel sheet in Microsoft office and the values acquired are given in respective tables.

### 8.1.1. Effect of type of vibration(Ultrasonic vibration Parameter):

The effect of continuous/Discontinues vibration on cutting rate (CR) in Hybrid-WEDM has been perceived for quite a while. It was presumed that ultrasonic vibration prompt increment in cutting rates.

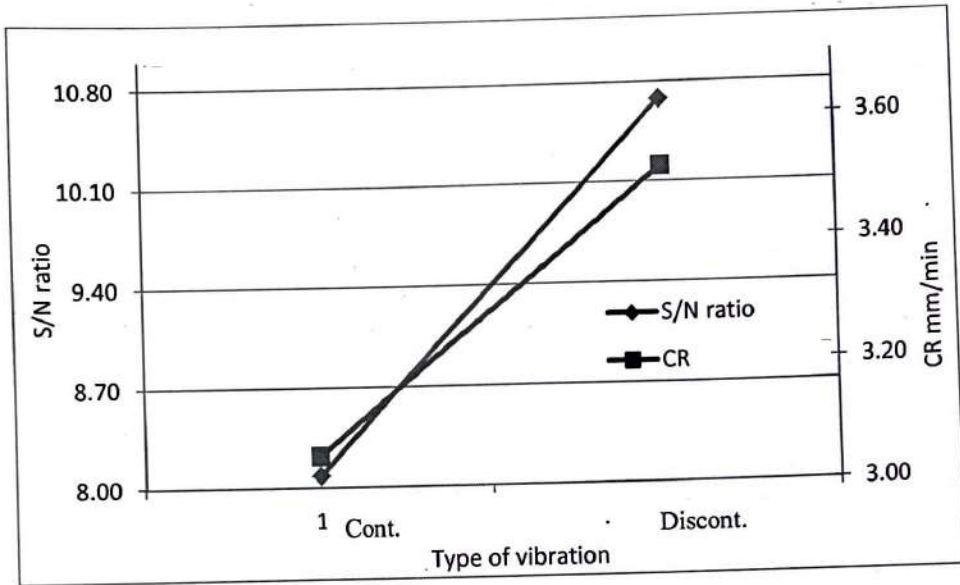


Figure 8.1 Main Effect and S/N ratio of type of Vibration on cutting rate

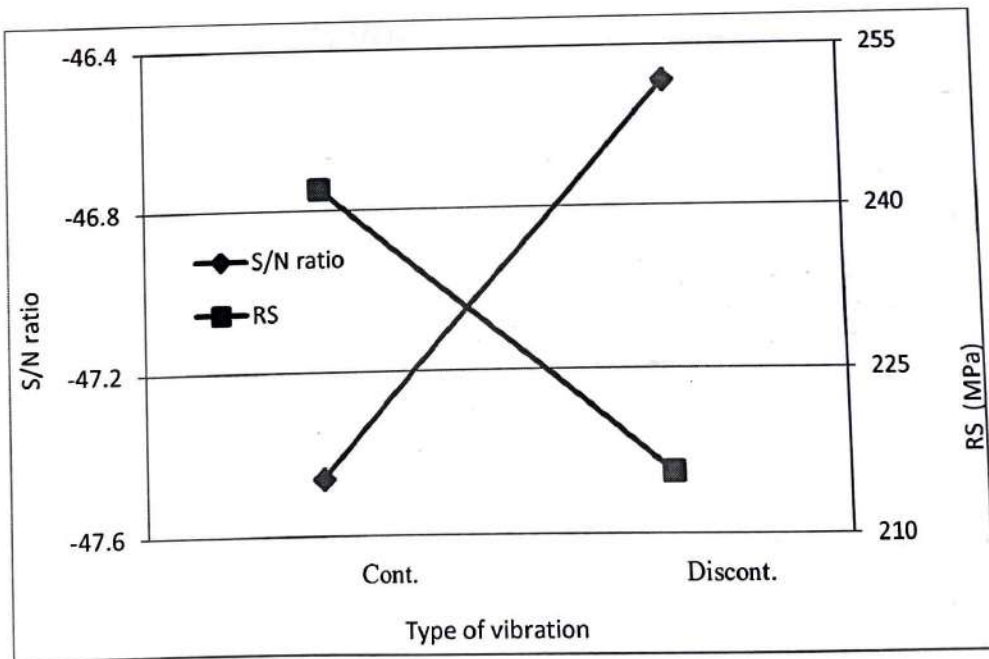


Figure 8.2 Main Effect and S/N ratio of type of Vibration on residual stress

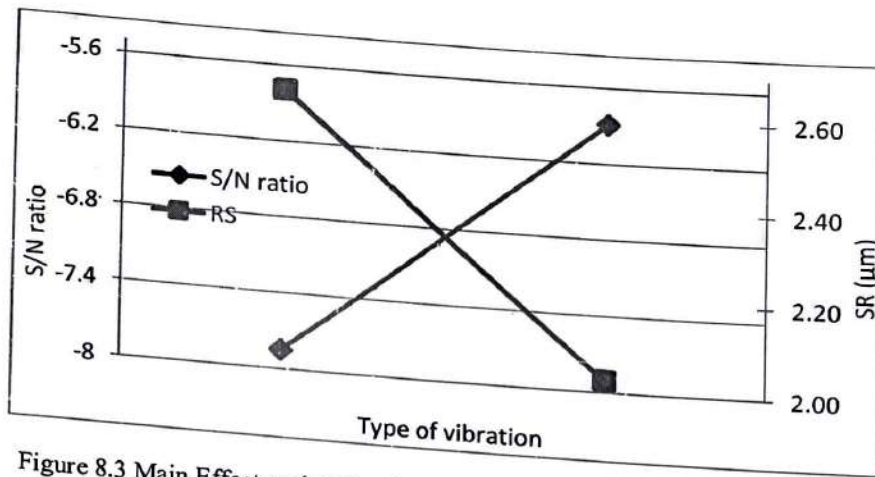


Figure 8.3 Main Effect and S/N ratio of type of Vibration on surface roughness

The ultrasonic vibration helped in enhancing 30 % MRR for wire EDM when it was contrasted and traditional u Cont. DM (Guo et al., 19 Discont.

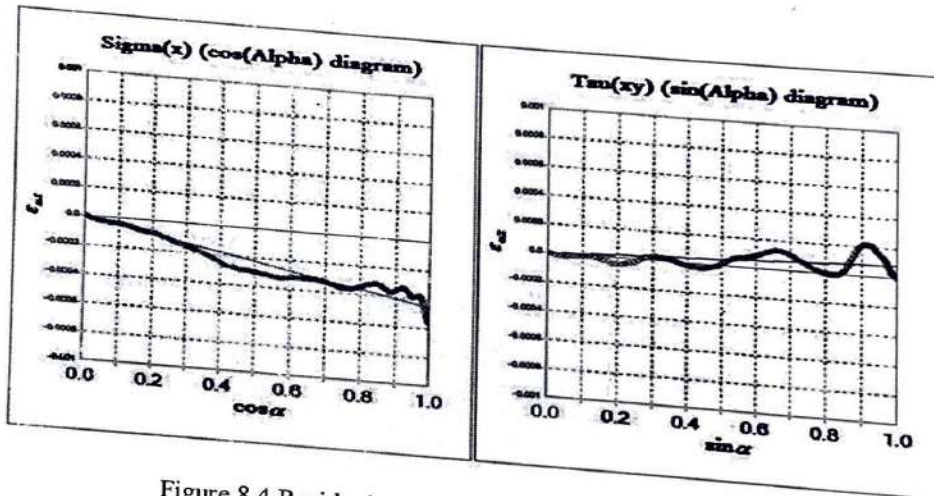


Figure 8.4 Residual stress graphs for continuous vibration

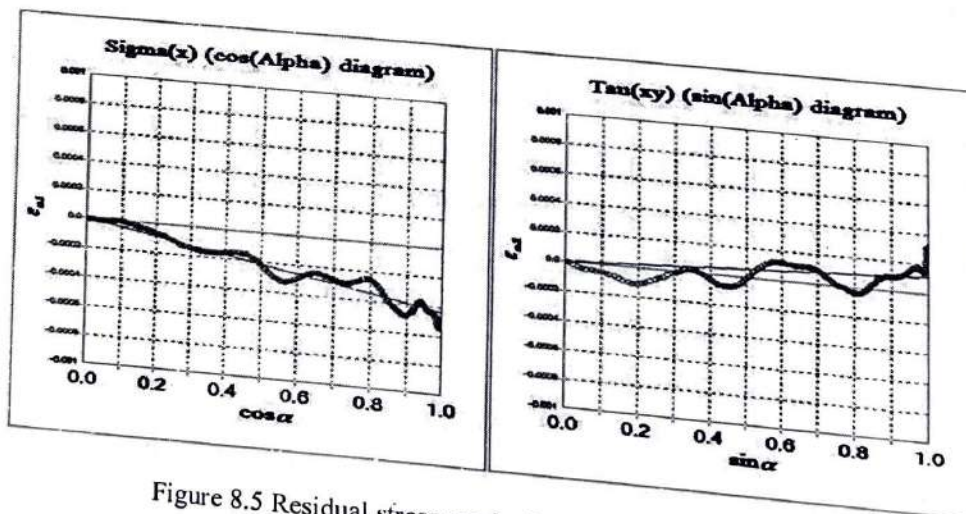


Figure 8.5 Residual stress graphs for discontinuous vibration

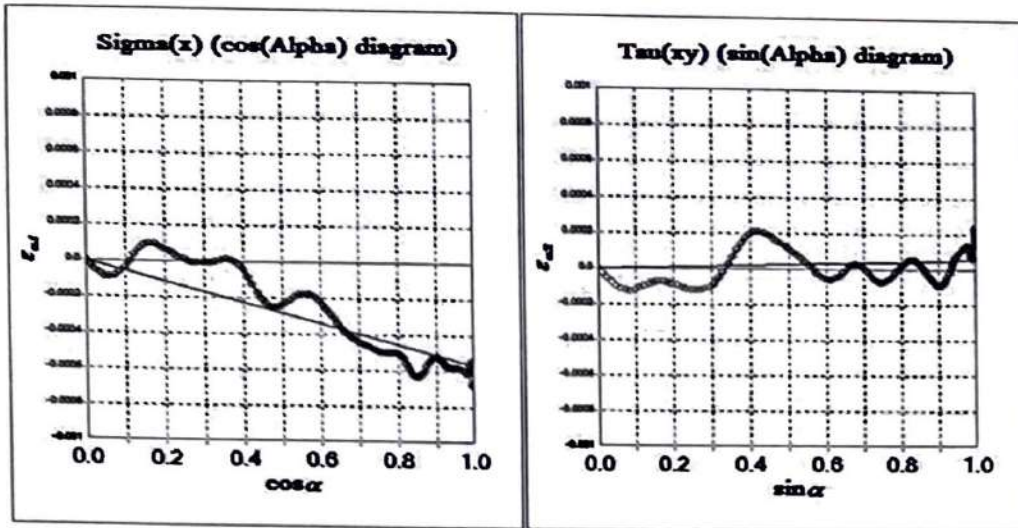


Figure 8.6 Residual stress graphs for No-vibration

This was affirmed in the pilot trails in present experimental study. Further experiments were conducted with discontinuous vibration in wire EDM with Taguchi experimental design. Figures 8.1-8.3 demonstrated the graphical variation of cutting rate, residual stresses and surface roughness, which upgraded with discontinuous vibration. The principle impact of vertical discontinuous vibration was multiple discharge point with enough time ranges to empty the debris and gas bubble. In the meantime the extra inertial forces setup in the work piece helped the clearing of debris. The upside of giving vibration to the workpiece is the opportunity from the wire resonance as if there should arise an occurrence of ultrasonic vibration bestowed to the wire. With discontinuous vibration, it was clearly observed that residual stresses diminish as vibration on the workpiece provided more change than continuous vibration of workpiece. At the point when vibration was connected to the workpiece, last recorded residual stress was around 20% than without vibration. Whereas, when discontinuous vibration was connected to the workpiece the change was roughly 27%. This was because the peak discharge density was much smaller in periodic vibration than created by the continuous workpiece vibration. The dielectric circulation and the flushing of debris were more uniformed in this case. The material under investigation was a  $\alpha$  Fe(211) with Lattice constant(a) 2.8664 Å. The X-Ray wave with Wavelength K-Alpha Diffraction angle ( $2\theta$ ) 156.396 deg, Diffraction lattice angle ( $2\theta$ ) 23.604 deg was used for measurement. The workpiece specification obtained during measurements were Inter-planar spacing (d) 1.170, Diffraction plane(h,k,l) 2, 1, 1 and B.C.C Crystal structure, Young's modulus(E) 224.000 GPa, Poisson's ratio( $\nu$ ) 0.280.

The values of the constants were  $\sigma_x$  stresses constant (K) -465.097 GPa,  $\tau_{xy}$  stress constant (K) 380.985 GPa and  $\sigma_y$  stress constant (K) -2091.661 GPa.

As appeared in Figures 8.4-8.6, horizontal axes  $\cos(\alpha)$  are the COS of Azimuth angle of Debye-Sherrer ring and the vertical axis is a strain ( $\epsilon_{\alpha 1}$ ). This incline of the bend so acquired was the measure of residual stresses. In Figure 8.4 for continuous vibration the incline is higher as contrast with the slope in Figure 8.5 for discontinuous vibration. Though, in case of no-vibration the slope was comparatively very high as shown in Figure 8.6.

**8.1.2. Effect amplitude of vibration (Ultrasonic vibration Parameter):**

As appeared in Figure 8.7 the cutting rate increments from 10 to 14  $\mu\text{m}$  amplitudes of vibration, however past that it diminishes. This was on account of the higher amplitude of vibration disturbance to the essential discharge condition for the wire EDM process. The secondary discharge occurred between the debris and wire electrode and develop an abnormal discharge condition and short circuit.

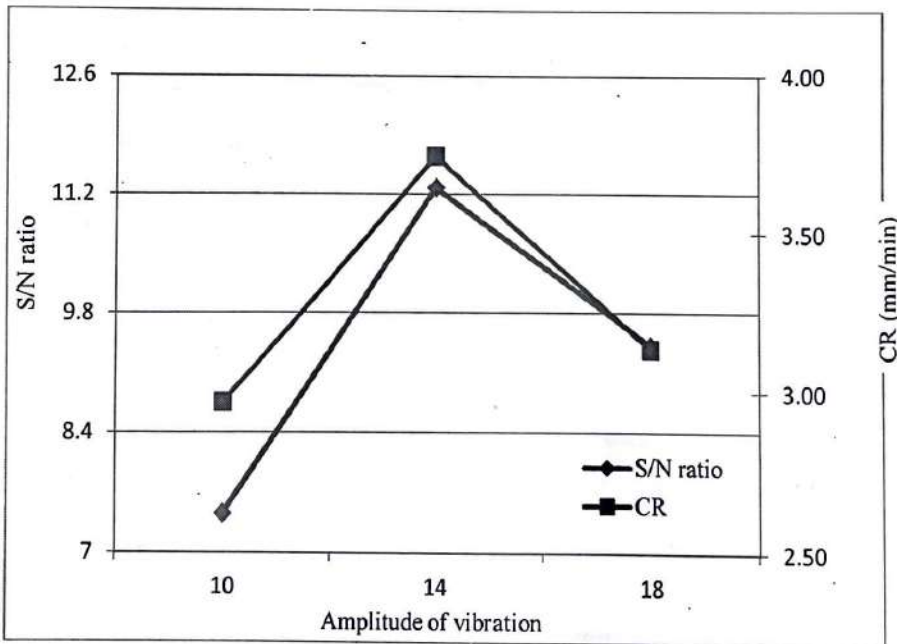


Figure 8.7 Main Effect and S/N ratio of amplitude of vibration on cutting rate

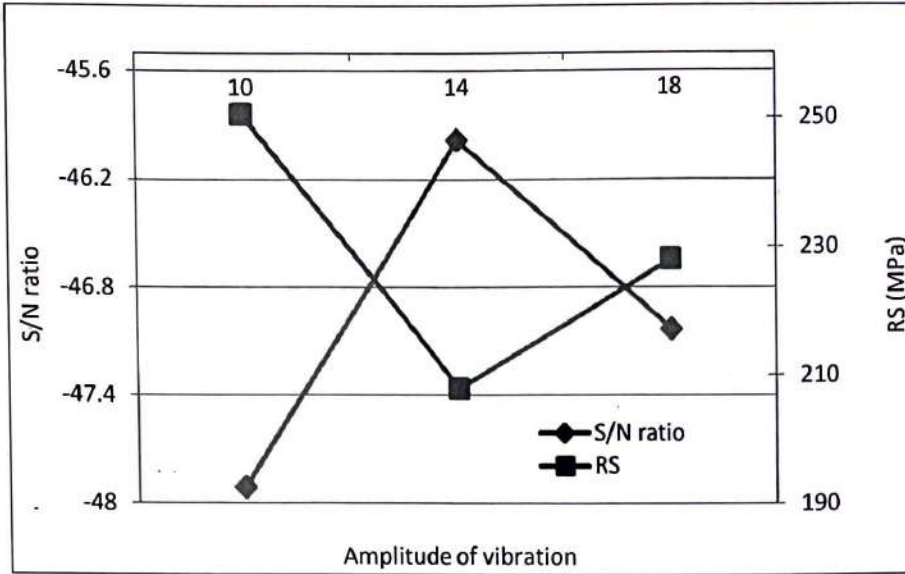


Figure 8.8 Main Effect and S/N ratio of amplitude of Vibration on residual stress

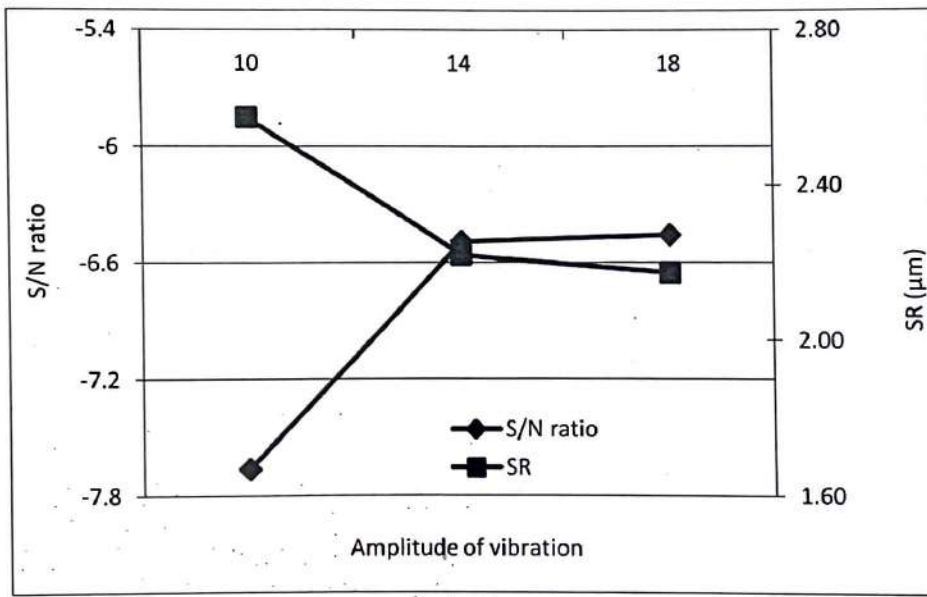


Figure 8.9 Main Effect and S/N ratio of amplitude of Vibration on surface roughness

However, at this higher amplitude of vibration could be clarified as; the pace of debris evacuation lingers behind the debris aggregation. It was watched that there exist a cozy connection between cutting rate and surface roughness. The cutting rate was an element of discharge energy, increment with the amplitude of vibration up to 14  $\mu\text{m}$  than additionally diminish at 18  $\mu\text{m}$ . The compressive residual stresses were the resultant of the temperature gradient of re-solidified metal on the machined surface.

These residual stresses were produced in the EDMed surface because of metallurgical changes and non-homogeneity of the heat stream. The strong flushing impact ascribed to higher amplitude of vibration to lessen the heat concentration and re-solidification. Scientist demonstrated that the stresses decrease with the amplitude. However, when amplitude limit crossed a certain limit, the impact was found inverted (Khosrozadeh & Shabgard, 2017). Figures 8.10-8.12 show comparative full width at half maximum (FWHM) distribution of entire Debye-Scherrer ring at different amplitude of vibration.

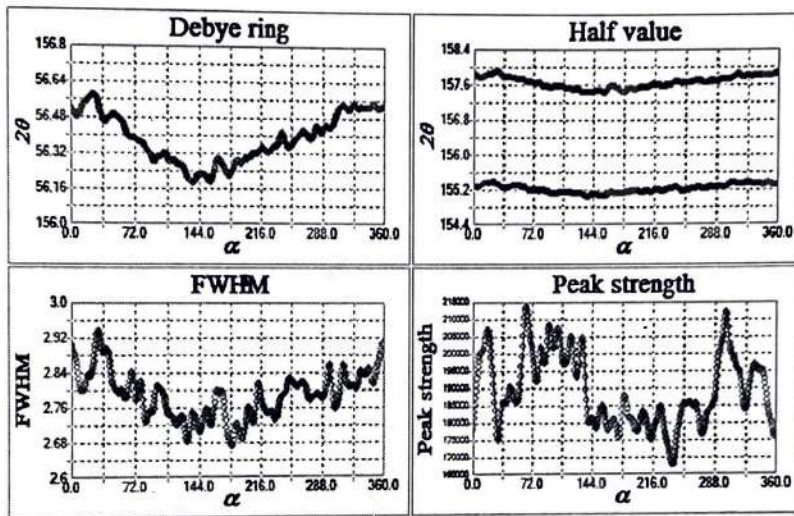


Figure 8.10 FWHM graph at 10µm amplitude of vibration

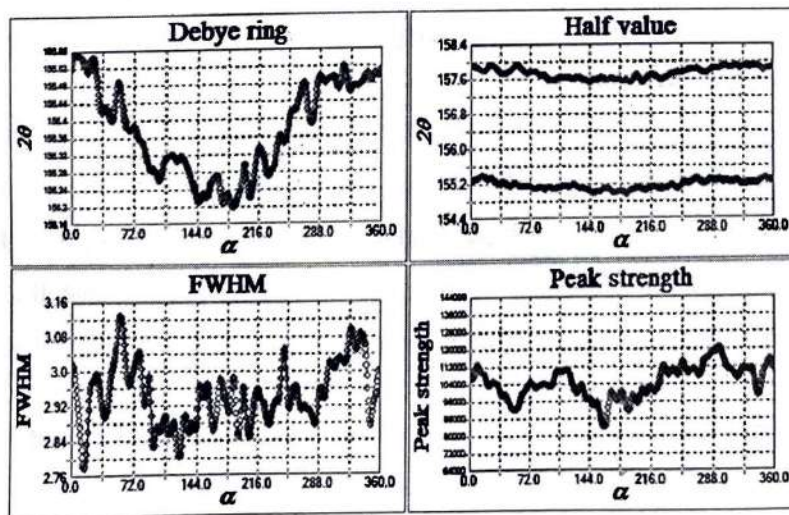


Figure 8.11 FWHM graph at 14µm amplitude of vibration

At 10 $\mu\text{m}$  the FWHM 2.79 $^\circ$  the variation lies between (2.68 - 2.93 deg) and  $\alpha_{\text{Max}}$  30.96 $^\circ$  and  $\alpha_{\text{Min}}$  131.04 $^\circ$ . with Peak strength (Ave) 189k. Considering other parameters constant the value of FWHM 2.95 $^\circ$  lied between (2.80 - 3.13 $^\circ$ )  $\alpha_{\text{Max}}$  57.60 $^\circ$  to  $\alpha_{\text{Min}}$  125.28 $^\circ$  at 14 $\mu\text{m}$  amplitude of vibration with and Peak strength (Ave) 104k. At 18 $\mu\text{m}$  the FWHM 2.75 deg the variation lie between (2.64 - 2.86 $^\circ$ )  $\alpha_{\text{Max}}$  301.68 $^\circ$   $\alpha_{\text{Min}}$  144.72 $^\circ$  Peak strength (Ave) 143k. The Peak strength is maximum at 10 $\mu\text{m}$  and minimum at 14 $\mu\text{m}$  that indicated the intensity of residual stresses as shown in Figure 8.8.

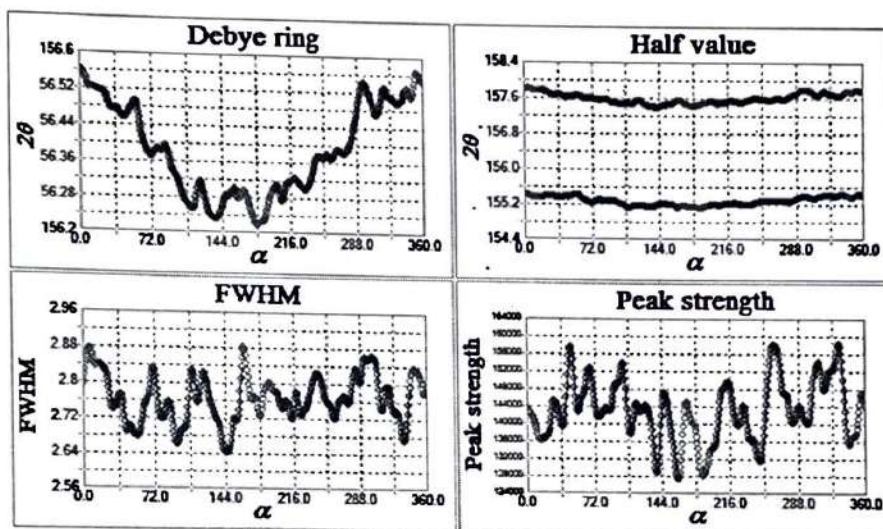


Figure 8.12 FWHM graph at 18 $\mu\text{m}$  amplitude of vibration

Peak broadening could be used to quantify the average crater size; micro strain might also create peak broadening (Sasaki et al., 2014). But by analyzing the peak widths over a long range of  $2\theta$  one could differentiate micro strain and crater size.

Disordering of full width at half maximum (FWHM) distribution of entire Debye-Scherrer ring at 18 $\mu\text{m}$  in minimum and at 14 $\mu\text{m}$  was maximum, which represents the poor surface integrity at that amplitude. Surface texture appeared decreased from 10 to 14 $\mu\text{m}$ , but after that it appears improving. Figure 8.9 indicate that the surface roughness follow the same pattern as that of the residual stresses.

### 8.1.3. Effect of workpiece thickness parameters(Material Parameter):

Although the cutting rate increased and residual stresses decreased with discontinuous vibration, when comparing with the continuous vibration, but the effect was more prominent for the thinner workpiece, whereas surface roughness improved with increase in the workpiece thickness as shown in Figures 8.13-8.15.



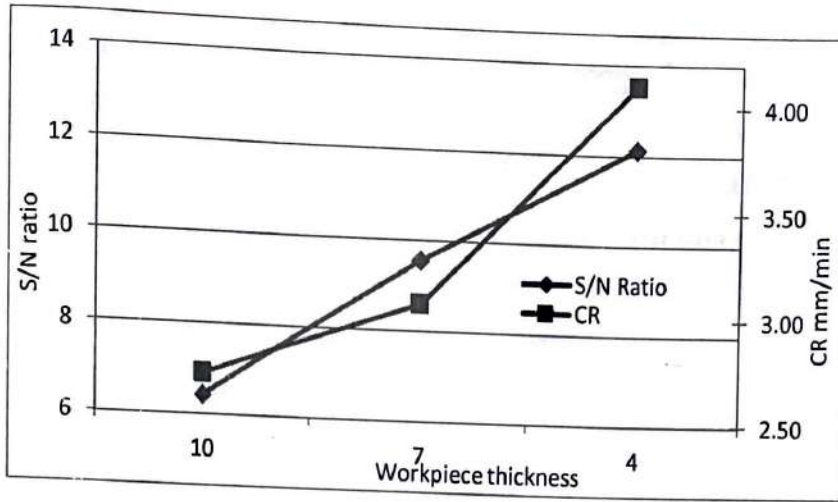


Figure 8.13 Main Effect and S/N ratio of workpiece thickness on cutting rate

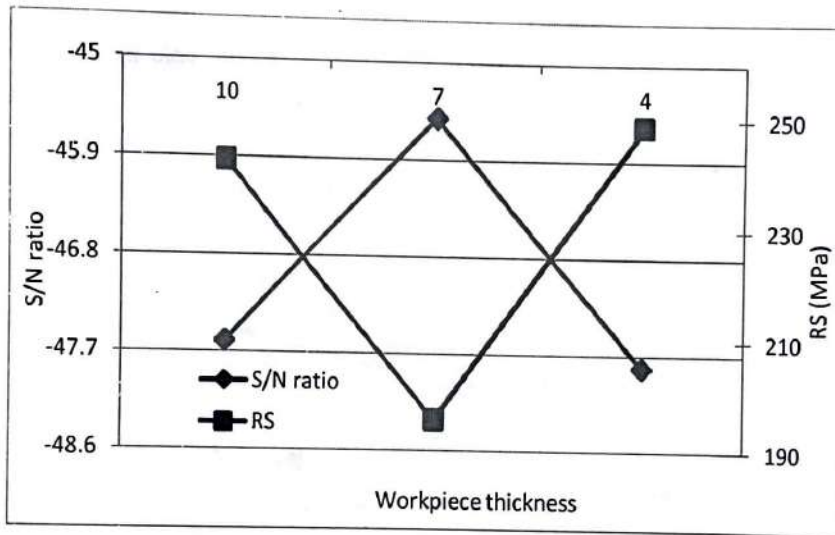


Figure 8.14 Main Effect and S/N ratio of workpiece thickness on residual stress

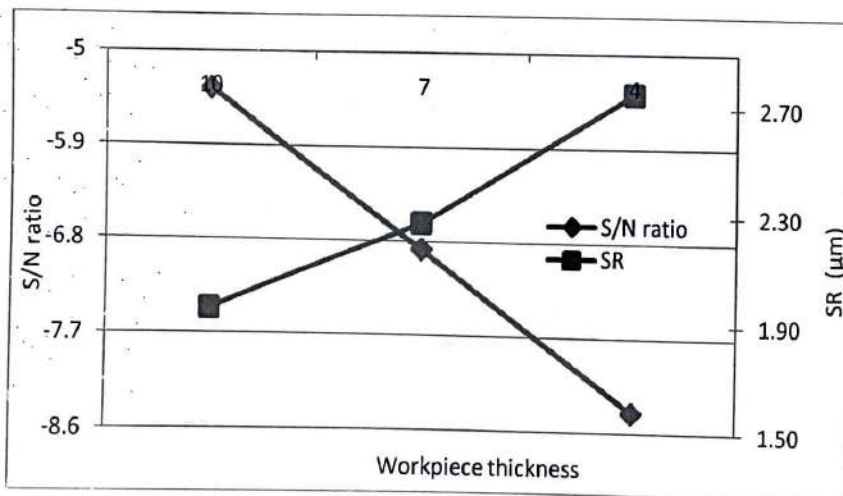


Figure 8.15 Main Effect and S/N ratio of workpiece thickness on surface roughness

However, it was further noticed in Figure 8.15 that residual stresses decreases with the decrease of workpiece sizes up to 7mm, after that it further increases. This was because of the high string effect obtained at 7mm thickness. The vibration of workpiece was less effective at higher thickness of workpiece. Although high flushing effect could be attained at high amplitude of vibration, but also the resonance of workpiece vibration restricts improvement of debris. The workpiece thickness significant play a role in residual stresses improvement. The cutting rate linearly decreases with thickness.

**8.1.4. Effect of Duty cycle and Peak Current (Electrical parameters):**

After carrying out the pilot experiments run the peak current range was selected from 100-180 ampere in the increment of 40 ampere and duty cycle from 66-78% in the increment of 8 for the selected performance characteristics.

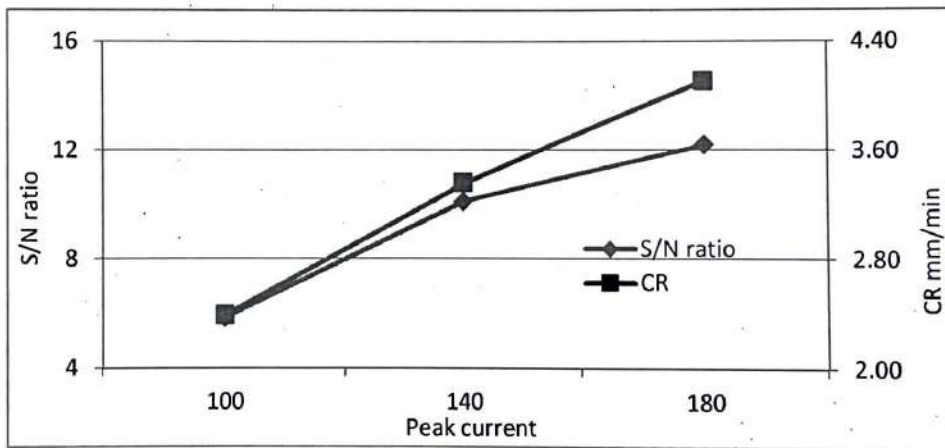


Figure 8.16 Main effect and S/N peak current of vibration on cutting rate

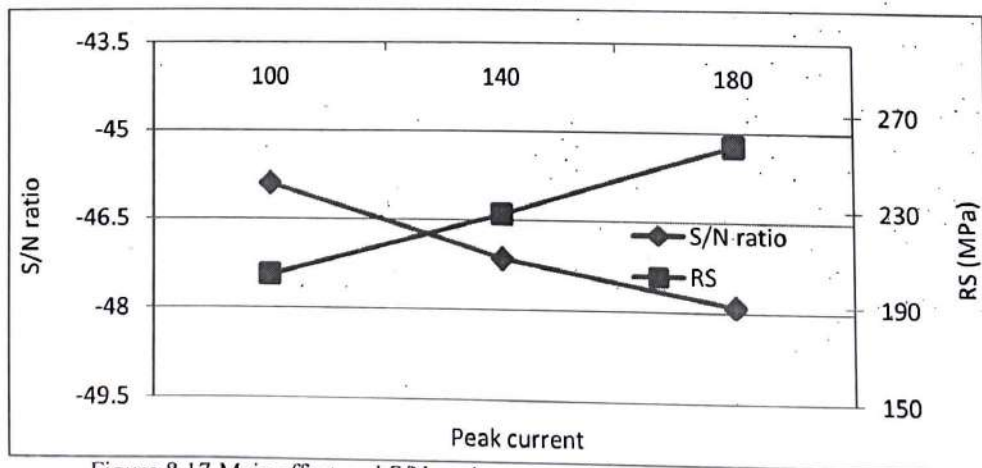


Figure 8.17 Main effect and S/N peak current of vibration on residual stresses

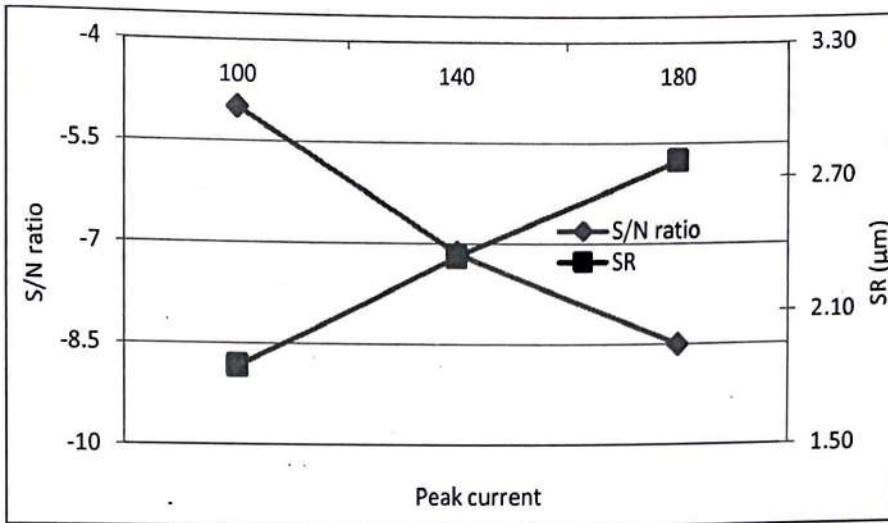


Figure 8.18 Main effect and S/N peak current of vibration on surface roughness

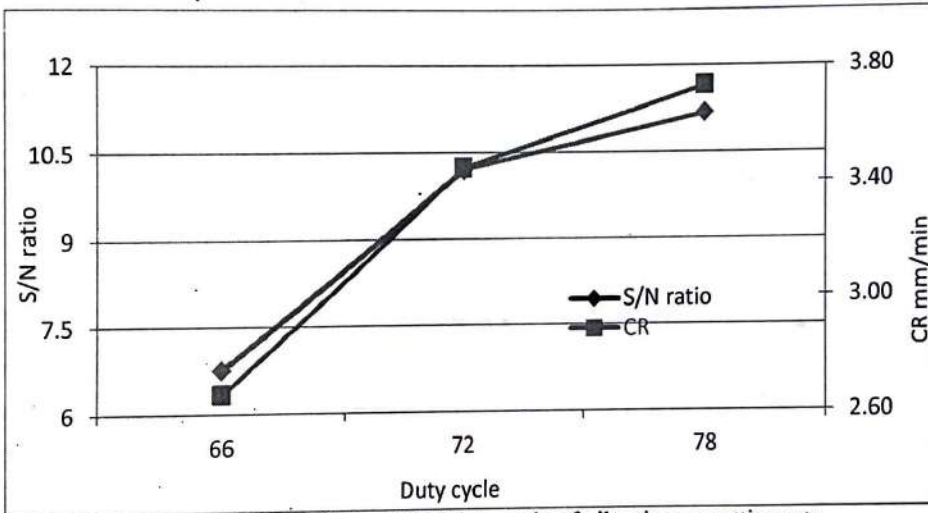


Figure 8.19 Main effect and S/N duty cycle of vibration on cutting rate

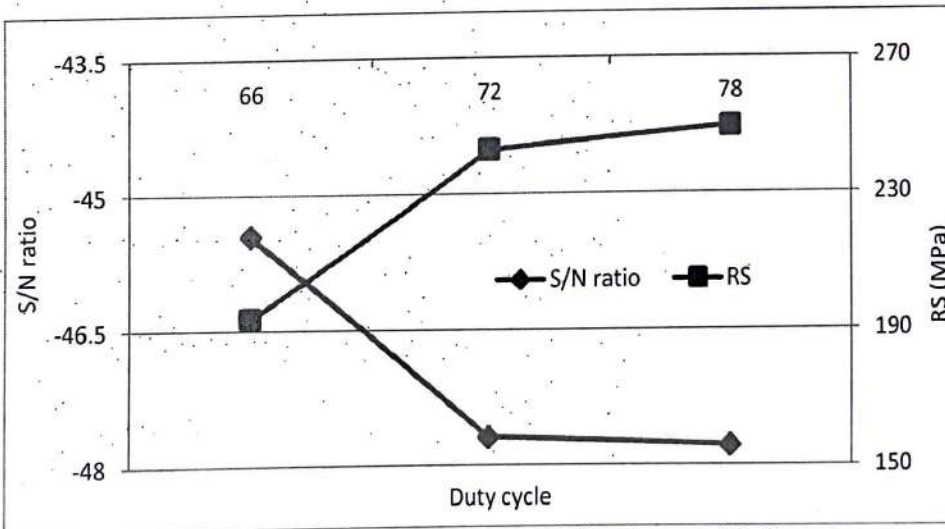


Figure 8.20 Main effect and S/N duty cycle of vibration on residual stresses

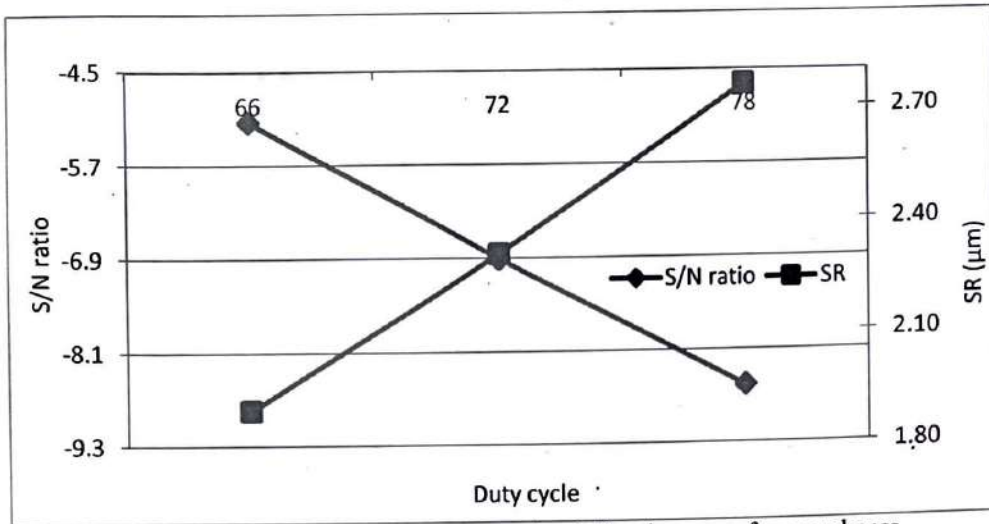


Figure 8.21 Main effect and S/N duty cycle of vibration on surface roughness

The duty cycle selected for experiments was the percentage pulse-on-time with respect to the total of the pulse on and off time setting for a particular cutting condition. The duty cycle basically represents the utilization of discharge energy in a given pulse-on-time interval. It was observed that combination of high peak current and high duty cycle increase the wire breakage frequency. So, the values of parameters SV = 20 volt; WT = 8 unit; SF = 1150 unit were kept low. For continuous/discontinuous vibration at higher value of peak current, discharge became unstable with an improper combination of spark voltage and duty cycle settings. That developed high discharge energy of wire, so machining performance was affected negatively (Han et al., 2013). In this experiment study, it was observed that the cutting rate, residual stresses and surface roughness were vitally affected by peak current and duty cycle. These were the sure factor; peak current and duty showed linear effect to all the three performance characteristics as shown in Figure 8.16-8.21. Table 8.1 provides the corresponding residual stresses results of map of 3D debye ring profile with peak current varies from 100-180 Amp, other parameters kept constant under three different modes No, Continuous and Discontinuous vibration. As shown, the 3D Debye-Scherrer rings at 100 Amp peak current were uniform and clear with small residual stresses compare to 140 and 180 amp peak current. With an increase in peak current the shape of 3D Debye-Scherrer ring became more distorted. Surface residual stresses were the resultant of molten melt the layer of workpiece surface, expelled away by the fresher dielectric medium, while the workpiece underneath remains solid.

That temperature difference also created poor surface texture (Guu, Y. H., Hocheng, 2001).

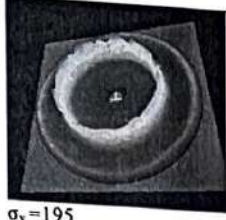
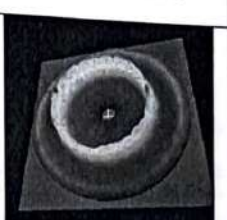
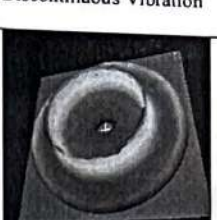
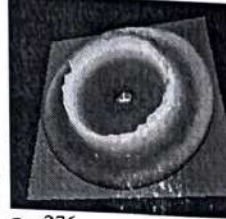
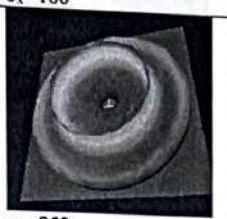
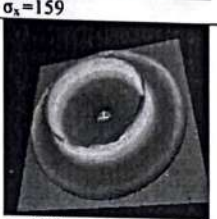
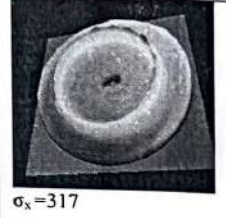
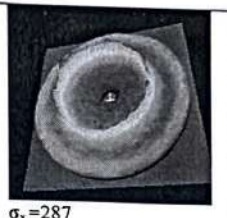

Peak Current	No Vibration	Continuous Vibration	Discontinuous Vibration
100Amp	 $\sigma_x = 195$	 $\sigma_x = 186$	 $\sigma_x = 159$
140Amp	 $\sigma_x = 276$	 $\sigma_x = 253$	 $\sigma_x = 203$
180Amp	 $\sigma_x = 317$	 $\sigma_x = 287$	 $\sigma_x = 257$

Table 8.1 Experimental results of Map of 3D debye ring and its residual stresses profile with peak current varies from 100-180 Amp: i) No vibration; ii) Continuous vibrations; iii) Discontinuous vibration; other parameters constant.

At higher values of peak current the discharge energies were high that resulted higher residual stress, micro-pin holes and micro-cracks. The Distorted 3D Debye-Scherrer ring was an indication of damaged workpiece surface and high residual stresses. With discontinues vibration, the uniformity of 3D Debye ring comparatively was high. The proposed model can further being up-date by utilizing interactive simulation with the application the finite element model. A user interactive simulation for the residual stresses would help to predict the life of the machined surface at different levels of design parameters such as fatigue, heat affected zone and crater size. This would facilitate in further development of Hybrid Wire-EDM process performance.

Table 8.2 represents the residual stress profile by controlling XY stage with duty cycle varies from 66-78 %. The duty cycle is percentage utilization of length of pulse on time. Peak strength increases with the duty cycle, whereas peak width decreases from continuous vibration to discontinuous vibration. The increase in duty cycle

results in increase in residual stresses. The results confirmed with those of Guo et al. (1997). The reason for high cutting rate was more electrical discharge energy was conducted into the machining gap within single pulse interval and more work-piece material cutting.

Duty Cycle	No Vibration	Continuous Vibration	Discontinuous Vibration
66	<p><math>\sigma_x=220</math></p>	<p><math>\sigma_x=203</math></p>	<p><math>\sigma_x=186</math></p>
72	<p><math>\sigma_x=262</math></p>	<p><math>\sigma_x=246</math></p>	<p><math>\sigma_x=233</math></p>
78	<p><math>\sigma_x=312</math></p>	<p><math>\sigma_x=276</math></p>	<p><math>\sigma_x=256</math></p>

Table 8.2. Experimental results of residual Stress profile by controlling XY axis stage with duty cycle varies from 66-78 % using; i) No vibration; ii) Continuous vibrations; iii) Discontinuous vibration; other parameters constant.

That spark discharge energy was a function of peak current and the length of the pulse on-time (Kansal, 2005).

### 8.1.5. Effect of wire feed rate (Non electrical parameter):

The wire was passed at a particular speed through a wire guided path for continuous sparking within discharge gap. It was preferred to set the wire feed rate to its

maximum to reduce wire breakage. Figure 8.22-8.24 show the graph of wire feed rate versus response characteristics.

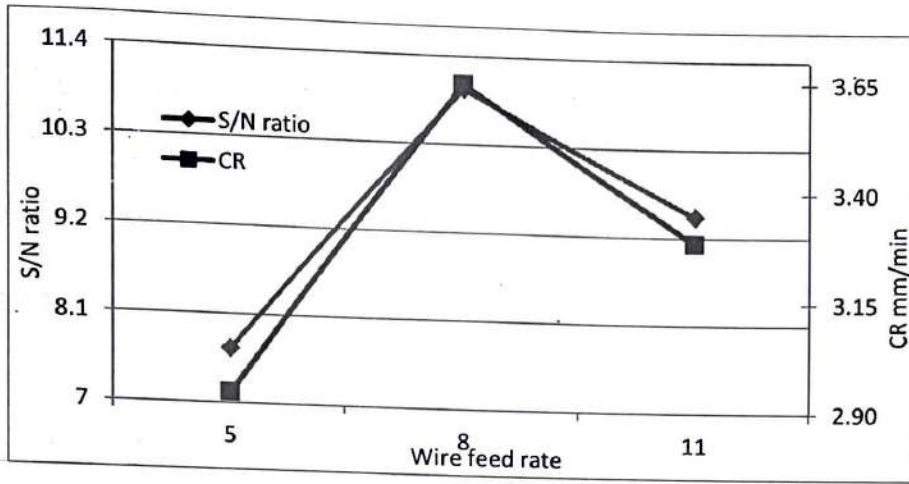


Figure 8.22 Main effect and S/N wire feed rate on cutting rate

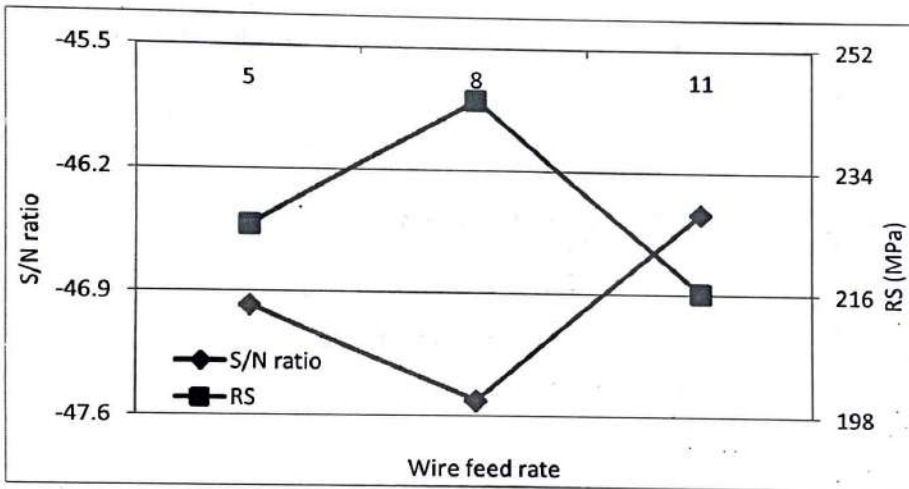


Figure 8.23 Main effect and S/N wire feed rate on residual stresses

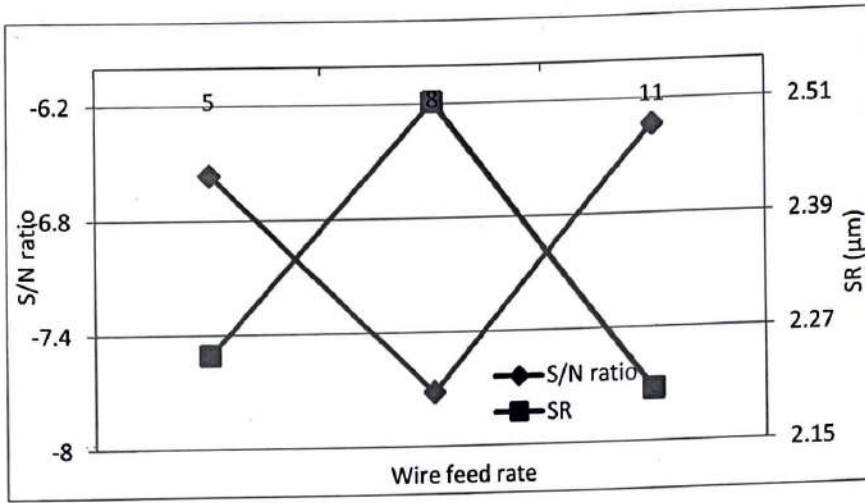


Figure 8.24 Main effect and S/N wire feed rate on surface roughness

It was observed that the effect of wire feed rate was wavy in nature. There was insignificant affect observed for cutting rate and remained almost constant between 5-11 mm/min and with slight increase at 8 mm/min. Although, the residual stress and surface roughness curves were also wavy in nature as it first increased with increase in the wire feed rate and then decreased. So it is always preferred to have a high wire feed rate. The higher wire feed rate reduced the wire breakage frequency.

#### 8.1.6. Selection of optimal levels for cutting rate:

To determine which factors significantly affects the response characteristics, ANOVA has been performed. The main effect of cutting rate at various levels larger-is-better for raw data as well as S/N data is given in Table 8.5 & 8.6 respectively. In this table the delta is the average main effect when the corresponding parameter changes from level 1 to level 2. The results of main effects for cutting rate form Table (8.3 and 8.4) reveal that the optimum levels of cutting rate(CR) for the Hybrid WEDM were obtained: Discontinuous type of vibration (level 2), 14μm amplitude (level 2), 180 A peak current (level 3), 78% duty cycle (level 3), 7mm workpiece thickness (level 2), and 8 mm/min wire feed rate (level 2), which provide maximum CR for proposed Hybrid Wire-EDM process.



Table 8.3 Main effects of Cutting rate (mm/min) (Raw Data) at various levels Larger is better

Level	Type of vibration	Amplitude	Peak Current	Duty cycle	Workpiece thickness	Wire feed rate
L1	3.05	2.97	2.39	2.67	3.06	2.92
L2	3.52	3.75	3.36	3.45	4.10	3.64
L3	*	3.14	4.11	3.73	0.36	3.29
Delta	0.46	0.78	0.97	0.78	2.69	0.71
Rank	6	3	2	4	1	5

L1, L2 and L3 represent level of parameters 1, 2 and 3; Delta is the average main effect when the corresponding parameter changes from level 1 to level 2.

Table 8.4 Main effects of Cutting rate (S/N Ratio) at various levels Larger is better

Level	Type of vibration	Amplitude	Peak Current	Duty cycle	Workpiece thickness	Wire feed rate
L1	8.08	7.46	5.84	6.76	6.42	7.68
L2	10.68	11.28	10.12	10.20	9.58	11.00
L3	*	9.42	12.19	11.19	12.15	9.47
Delta	2.60	3.82	4.27	3.44	3.16	3.31
Rank	6	2	1	3	5	4

L1, L2 and L3 represent level of parameters 1, 2 and 3; Delta is the average main effect when the corresponding parameter changes from level 1 to level 2.

Table 8.5 Analysis of variance of Raw data for Cutting rate

SOURCE	SS	DOF	V	P	F-Ratio
Type of Vibration	2.91	1.00	2.91	3.95	6.93
Amplitude of Vibration	6.02	2.00	3.01	8.16	7.16
Peak current	26.89	2.00	13.44	36.49	6.94
Duty Cycle	10.96	2.00	5.48	14.88	13.04
Workpiece Thickness	4.67	2.00	2.34	6.34	5.56
Wire Feed Rate	4.58	2.00	2.29	6.22	5.45
ERROR	17.65	42.00	0.42	23.96	
T	73.68	53.00		100.00	

Significant at 95% confidence level, SS: Sum of Squares; DOF: Degree of Freedom; V: Variance; F-Fisher test factor tabulated for Type of vibration: 4.07, F-Fisher test factor tabulated for other parameters: 3.22.

Table 8.6 Analysis of variance of S/N ratio for Cutting rate

SOURCE	SS	DOF	V	P	F-Ratio
Type of Vibration	30.35	1.00	30.35	7.27	8.75
Amplitude of Vibration	43.82	2.00	21.91	10.50	6.31
Peak current	125.75	2.00	62.88	30.13	18.12
Duty Cycle	64.81	2.00	32.41	15.53	9.34
Workpiece Thickness	98.77	2.00	49.38	23.67	14.23
Wire Feed Rate	32.99	2.00	16.50	7.91	4.75
ERROR	20.82	6.00	3.47	4.99	
Total	417.31	17.00	*	100.00	

Significant at 95% confidence level, SS: Sum of Squares; DOF: Degree of Freedom; V: Variance; F-Fisher test factor tabulated for Type of vibration: 5.99, F-Fisher test factor tabulated for other parameters: 5.14.

Table 8.5 & 8.6 represent the analysis of variance (ANOVA) for raw data and the S/N ratio for the cutting rate respectively. The results reveal all the factors significantly affected the cutting rate for Hybrid WEDM process for both the raw data and S/N ratio. The column "P" represents the % contribution of the particular factor to the response characteristic. Table 8.5 indicate that the peak current (36.49%), duty cycle (14.88%), amplitude of vibration (8.16%), and workpiece thickness (6.34%) and Type of vibration (3.95%) are the highest contributors to cutting rate and S/N Table 8.6 confirm the same. Whereas in S/N ratios Table 8.3 indicate that wire feed rate (6.22%) is a contributor for raw data but did not have significant S/N ratio. The graph has been discussed in previous sections.

### 8.1.6.1. Estimation of optimum cutting rate response:

The optimum value of cutting rate (CR) (mm/min) was predicted at the selected levels of significant parameters  $A_2 B_2 C_3 D_3 E_2 F_2$ . The estimated mean ( $\mu_{CR}$ ) of the response characteristic CR was determined as in equation (8.1). Where T: Overall mean of CR = 3.28,  $A_2$ : Average CR at the second level of type of vibration = 3.52,  $B_2$ : Average CR at the second level of amplitude of vibration = 3.75,  $C_3$ : Average CR at the third level of peak current = 4.11,  $D_3$ : Average CR at the third level of duty cycle = 3.73,  $E_3$ : Average CR at the third level of workpiece thickness = 4.10;  $F_2$ : Average CR at the second level of workpiece thickness = 3.64; reference from Table 8.3 and 8.4. By substituting the values of various terms in the equation (8.1) estimated mean ( $\mu_{CR}$ ) can be calculated.

$$\mu_{CR} = \bar{A}_2 + \bar{B}_2 + \bar{C}_3 + \bar{D}_3 + \bar{E}_2 + \bar{F}_2 - 5 \times T \quad \dots \quad (8.1)$$

$$\mu_{CR} = 3.52 + 3.75 + 4.11 + 3.73 + 4.10 + 3.64 - 5 \times 3.28 = 6.45$$

The 95% confidence interval of confirmation experiments ( $CI_{CE}$ ) and of population ( $CI_{POP}$ ) was calculated by using the following equations (8.2) and (8.3).

$$CI_{CE} = \sqrt{F_{\alpha}(1, f_e) V_e \left[ \frac{1}{n_{eff}} + \frac{1}{R} \right]} \quad \dots \quad (8.2)$$

$$CI_{POP} = \sqrt{\frac{F_{\alpha}(1, f_e) V_e}{n_{eff}}} \quad \dots \quad (8.3)$$

Where  $F_{\alpha}(1, f_e)$ : The F ratio at the confidence level of  $(1-\alpha)$  against DOF 53 and error DOF  $f_e=42$ , N: Total number of results = 54 (Treatment=18, Repetition=3), R : Sample size for confirmation experiments =3  $V_e$ : Error variance = 3.47 (Ref. Table 8.5),  $f_e$  error DOF = 42. The value of  $n_{eff}$  is calculated with the equation (8.4).

$$n_{eff} = \frac{N}{1 + [\text{DOF associated in the estimate of mean response}]} = 4.5 \quad \dots(8.4)$$

$F_{0.05}(1, 42) = 4.076$  (tabulated F value) , So  $CI_{CE} = \pm 2.81$ ,  $CI_{POP} = \pm 1.77$

The predicted optimal range ( for a confirmation runs of three experiments) is :

$$\mu_{CR} - CI_{CE} < \mu_{CR} < \mu_{CR} + CI_{CE} ; 3.64 < \mu_{CR} < 9.26$$

The 95% conformation interval of the predicted mean is as follows:

$$\mu_{CR} - CI_{POP} < \mu_{CR} < \mu_{CR} + CI_{POP}; 4.68 < \mu_{CR} < 8.22$$

### 8.1.6.2. Confirmation experiment:

The purpose of confirmation experiment is to validate the conclusions drawn during the analysis phase. The three confirmation experiments for CR were conducted at the optimum setting of the process parameters. The type of vibration is set at 2<sup>nd</sup> level, amplitude of vibration at 2<sup>nd</sup> level, peak current at 3<sup>rd</sup> level, Duty cycle at 2<sup>nd</sup> level, workpiece thickness at 2<sup>nd</sup> level and wire feed rate at 2<sup>nd</sup> level. The Confirmation experimental value of average CR is found to be 5.09 mm/min, which fall within the 95% confidence interval of the predicted optimum parameters. The conformation run were repeated thrice to ensure the main effect on CR at  $A_2 B_2 C_3 D_3 E_2 F_2$  levels as shown in Table 8.7.

Table 8.7 Confirmation experiments results values observed for quality characteristics

Exp. No	Cutting Rate(CR) mm/min	Residual Stress (RS) MPa	Surface Roughness (SR) $\mu\text{m}$
	$A_2 B_2 C_3 D_3 E_2 F_2$	$A_2 B_2 C_1 D_1 E_2 F_3$	$A_2 B_3 C_1 D_1 E_1 F_3$
R1	5.11	105	0.62
R2	5.09	103	0.72
R3	5.07	98	0.63
Average	5.09	102	0.66

### 8.1.7. Selection of optimal levels for Residual stresses (RS):

Table 8.8 and 8.9 represent the Main Effects of Residual stresses (MPa) (Raw Data) and S/N ratio at various levels smaller-is-better for raw data and the S/N ratio for the residual stress respectively. The results of Main effects of residual stresses from Table 8.8 reveal that the optimum levels of residual stresses for the Hybrid Wire-EDM are: Discontinuous vibration (level 2), 14 $\mu$ m amplitude (level 2), 100A peak current (level 1), 66% duty cycle (level 1), 7mm workpiece thickness (level 2), and 11 mm/min wire feed rate (level 3), which provided minimum residual stresses.

Table: 8.8 Main Effects of Residual stresses (MPa) (Raw Data) at various levels smaller is better

Level	Type of vibration	Amplitude	Peak Current	Duty cycle	Workpiece thickness	Wire feed rate
L1	242.00	250.50	201.72	193.61	242.06	225.83
L2	215.59	207.83	227.72	243.06	195.56	244.33
L3	*	228.06	256.94	249.72	248.78	216.22
Delta	-26.41	-42.67	26.00	49.44	-46.50	18.50
Rank	5	3	5	1	2	6

L1, L2 and L3 represent level of parameters 1, 2 and 3; Delta is the average main effect when the corresponding parameter changes from level 1 to level 2.

Table 8.9 Main Effects of Residual stresses (MPa) (S/N Ratio) at various levels smaller is better

Level	Type of vibration	Amplitude	Peak Current	Duty cycle	Workpiece thickness	Wire feed rate
L1	-47.46	-47.91	-45.89	-45.45	-47.60	-46.98
L2	-46.49	-45.98	-47.14	-47.69	-45.51	-47.51
L3	*	-47.03	-47.89	-47.78	-47.81	-46.44
Delta	0.97	1.93	-1.25	-2.23	2.09	-0.53
Rank	5	3	4	1	2	6

L1, L2 and L3 represent level of parameters 1, 2 and 3; Delta is the average main effect when the corresponding parameter changes from level 1 to level 2.

Table 8.10 Analysis of variance of Raw data for Residual stresses(MPa)

SOURCE	SS	DOF	V	P	F-Ratio
Type of Vibration	9414.24	1.00	9414.24	6.40	9.27
Amplitude of Vibration	16398.81	2.00	8199.41	11.15	8.07
Peak current	27476.59	2.00	13738.30	18.68	13.52
Duty Cycle	33825.93	2.00	16912.96	23.00	16.65
Workpiece Thickness	9933.87	2.00	4966.94	6.75	4.89
Wire Feed Rate	7349.15	2.00	3674.57	5.00	3.62
ERROR	42674.17	42.00	1016.05	29.02	
T	147072.76	53.00		100.00	

Significant at 95% confidence level, SS: Sum of Squares; DOF: Degree of Freedom; V: Variance; F-Fisher test factor tabulated for Type of vibration: 4.07, F-Fisher test factor tabulated for other parameters: 3.22.

Table 8.11 Analysis of variance of S/N ratio for Residual stresses (MPa)

SOURCE	SS	DOF	V	P	F-Ratio
Type of Vibration	4.24	1.00	4.24	5.45	4.03
Amplitude of Vibration	11.23	2.00	5.62	14.45	5.34
Peak current	12.25	2.00	6.13	15.76	5.82
Duty Cycle	20.83	2.00	10.42	26.80	9.90
Workpiece Thickness	19.41	2.00	9.71	24.97	9.23
Wire Feed Rate	3.45	2.00	1.73	4.44	1.64
ERROR	6.31	6.00	1.05	8.12	
Total	77.73	17.00	*	100.00	

Significant at 95% confidence level, SS: Sum of Squares; DOF: Degree of Freedom; V: Variance; F-Fisher test factor tabulated for Type of vibration: 5.99, F-Fisher test factor tabulated for other parameters: 5.14.

It could be further noticed that in case of all the parameters, the higher values of average response characteristics correspond to higher values of S/N ratio. It is clear that parameter peak current, duty cycle, workpiece thickness and amplitude of vibration significantly affect on residual stresses. Table 8.10 and 8.11 represent the analysis of variance for raw data and the S/N ratio for the residual stress respectively. From Table 8.10, it can be observed that the percentage contribution of duty cycle (23.00%) was highest and for type of vibration (6.40%), workpiece thickness (6.75%), peak current (18.68%), the amplitude of vibration (11.15%) and wire feed rate (5.00%). The principle controllable factors were discontinuous vibration, amplitude of vibration, workpiece thickness, peak current and duty cycle from S/N ratio Table 8.11 that affected the Hybrid Wire-EDM response characteristics. Whereas wire feed rate is not significant factor. It was being demonstrated greatest S/N ratio for each factor in Table 8.11.

#### 8.1.7.1. Estimation of optimum residual stress response:

The optimum value of Residual stresses (RS) (MPa) was predicted at the selected levels of significant parameters  $A_2B_2C_1D_1E_2F_3$ . The estimated mean ( $\mu_{RS}$ ) of the response characteristic RS was determined as in equation (8.5) (Ross, 1988) and (Roy, 1990);

$$\mu_{RS} = \bar{A}_2 + \bar{B}_2 + \bar{C}_1 + \bar{D}_1 + \bar{E}_2 + \bar{F}_3 - 5\bar{T} \quad \dots (8.5)$$

Where T: Overall mean of RS = 228.80,  $A_2$ : Average RS at the second level of type of vibration = 215.59,  $B_2$ : Average RS at the second level of amplitude of vibration = 207.83,  $C_1$ : Average RS at the first level of peak current = 201.72,  $D_1$ : Average RS at

the first level of duty cycle = 193.61, E<sub>2</sub>: Average RS at the second level of workpiece thickness= 195.56, F<sub>3</sub>: Average RS at the third level of wire feed rate = 216.22, reference from Table (8.8 and 8.9). Substitute the values of various terms in the equation (8.5)

$$\mu_{RS} = 215.59 + 207.8333 + 201.72 + 193.61 + 195.56 + 216.22 - 5 \times 228.80 = 86.53$$

The 95% confidence interval of confirmation experiments (CI<sub>CE</sub>) and of population (CI<sub>POP</sub>) was calculated by using the following equations (8.2) and (8.3):

Where  $F_{\alpha}(1, f_e)$ : The F ratio at the confidence level of  $(1-\alpha)$  against DOF 53 and error DOF  $f_e=42$ , N: Total number of results = 54 (Treatment=18, Repetition=3), R : Sample size for confirmation experiments =3  $V_e$ : Error variance = 657.24 (Ref. Table 11),  $f_e$  error DOF = 42. The value of  $n_{eff}$  is calculated with the equation (8.6).

$$F_{0.05}(1, 42) = 4.076 \text{ (tabulated F value) , So } CI_{CE} = \pm 48.16, CI_{POP} = \pm 24.40$$

The predicted optimal range ( for a confirmation runs of three experiments) was :

$$\mu_{RS} - CI_{CE} < \mu_{RS} < \mu_{RS} + CI_{CE} ; 38.37 < \mu_{RS} < 134.69$$

The 95% conformation interval of the predicted mean was as follows:

$$\mu_{RS} - CI_{POP} < \mu_{RS} < \mu_{RS} + CI_{POP}; 62.13 < \mu_{RS} < 110.93$$

### 8.1.7.2. Confirmation experiment for residual stress:

The three confirmation experiments for RS were conducted at the optimum setting of the process parameters. The type of vibration is set at 2<sup>nd</sup> level, amplitude of vibration at 2<sup>nd</sup> level, peak current at 1<sup>st</sup> level, Duty cycle at 1<sup>st</sup> level, workpiece thickness at 2<sup>nd</sup> level, wire feed rate at 3<sup>rd</sup> level. From the confirmation experiments the average RS is found to be 102 MPa, which falls within the 95% confidence interval of the predicted optimum parameter. The conformation run were repeated thrice to ensure the main effect on RS at A<sub>2</sub>B<sub>2</sub>C<sub>1</sub>D<sub>1</sub>E<sub>2</sub>F<sub>3</sub> levels as shown in Table 8.7.

### 8.1.8. Selection of optimal levels for surface roughness:

Table 8.12 and 8.13 show that the optimum levels of machining parameters for surface roughness are: discontinuous vibration (level 2), 18 $\mu$ m amplitude (level 3), 100A peak current (level 1), 66% duty cycle (level 1), 10mm workpiece thickness (level 1), 11 mm/min wire feed rate (level 3). Table 8.14 and 8.15 show that A, B, C, D and E significantly affect both the mean and the variation in the SR values.

Table 8.12 Main Effects of surface roughness ( $\mu$ m) (Raw Data) at various levels smaller is better

Level	Type of vibration	Amplitude	Peak Current	Duty cycle	Workpiece thickness	Wire feed rate
L1	2.62	2.57	1.85	1.89	1.94	2.25
L2	2.03	2.22	2.34	2.31	2.27	2.51
L3	*	2.17	2.77	2.76	2.75	2.21
Delta	-0.59	-0.36	0.49	0.42	0.33	0.26
Rank	1	4	2	3	5	6

L1, L2 and L3 represent level of parameters 1, 2 and 3; Delta is the average main effect when the corresponding parameter changes from level 1 to level 2.

Table 8.13 Main Effects of surface roughness ( $\mu$ m) (S/N Ratio) at various levels smaller is better

Level	Type of vibration	Amplitude	Peak Current	Duty cycle	Workpiece thickness	Wire feed rate
L1	-7.85	-7.66	-4.99	-5.14	-5.34	-6.56
L2	-5.89	-6.49	-7.13	-6.91	-6.87	-7.72
L3	*	-6.46	-8.49	-8.56	-8.40	-6.33
Delta	1.96	1.17	-2.13	-1.77	-1.52	-1.15
Rank	2	5	1	3	4	6

L1, L2 and L3 represent level of parameters 1, 2 and 3; Delta is the average main effect when the corresponding parameter changes from level 1 to level 2.

Table 8.14 Analysis of variance of Raw data for surface roughness ( $\mu$ m)

SOURCE	SS	DOF	V	P	F-Ratio	Rank
Type of Vibration	4.72	1.00	4.72	14.84	62.68	4
Amplitude of Vibration	1.74	2.00	0.87	5.46	11.54	5
Peak current	7.68	2.00	3.84	24.14	50.99	1
Duty Cycle	6.75	2.00	3.37	21.22	44.82	3
Workpiece Thickness	6.77	2.00	3.38	21.28	44.96	2
Wire Feed Rate	0.99	2.00	0.50	3.12	6.59	6
ERROR	3.16	42.0	0.08	9.94		
T	31.79	53.0		100.0		
		0		0		

Significant at 95% confidence level, SS: Sum of Squares; DOF: Degree of Freedom; V: Variance; F-Fisher test factor tabulated for Type of vibration: 4.07, F-Fisher test factor tabulated for other parameters: 3.22.

Table 8.15 Analysis of variance of S/N ratio for surface roughness ( $\mu\text{m}$ )

SOURCE	SS	DOF	V	P	F-Ratio	Rank
Type of Vibration	17.26	1.00	17.26	11.92	6.90	4
Amplitude of Vibration	5.66	2.00	2.83	3.90	1.13	6
Peak current	37.26	2.00	18.63	25.72	7.44	1
Duty Cycle	35.13	2.00	17.57	24.25	7.02	2
Workpiece Thickness	27.97	2.00	13.99	19.31	5.59	3
Wire Feed Rate	6.58	2.00	3.29	4.54	1.31	5
ERROR	15.02	6.00	2.50	10.37		
Total	144.88	17.00	*	100.00		

Significant at 95% confidence level, SS: Sum of Squares; DOF: Degree of Freedom; V: Variance; F-Fisher test factor tabulated for Type of vibration: 5.99, F-Fisher test factor tabulated for other parameters: 5.14.

The percentage contribution of peak current is high (24.14%) and for workpiece thickness (21.28%), duty cycle (21.22%) type of vibration (14.84%), amplitude of vibration (5.46%). The wire feed rate (3.12%) did not significantly contribute to the surface roughness. The interdependency of process quantitative controllable parameters in Hybrid-WEDM is complex due to other qualitative parameter such as cavitation, abnormal discharge and flushing of contaminated dielectric medium. Taguchi's DOE interactive manufacturing approach helped in ranking and selecting the corresponding optimum level the process parameters under study.

### 8.1.8.1. Estimation of optimum performance Characteristics:

The optimum value of SR is predicted at the selected levels of significant parameters  $A_2B_3C_1D_1E_1F_3$ . The estimated mean of the response characteristic SR is determined (Ross 1996; Roy 1990) as

$$\mu_{SR} = \bar{A}_2 + \bar{B}_3 + \bar{C}_1 + \bar{D}_1 + \bar{E}_1 + \bar{F}_3 - 5 \times \bar{T}$$

.....8.6

Where  $T$ : Overall mean of SR = 2.32,  $A_2$ : Average SR at the second level of type of vibration = 2.03,  $B_3$ : Average SR at the third level of amplitude of vibration = 2.17,  $C_1$ : Average SR at the first level of peak current = 1.85,  $D_3$ : Average SR at the first level of duty cycle = 1.89,  $E_1$ : Average SR at the first level of workpiece thickness =



1.94, F<sub>3</sub>: Average SR at the third level of wire feed rate = 2.21 (Ref. to Table 8.12 and 8.13). Substituting the values of various terms in the above equation (8.6)

$$\mu_{SR} = 2.03 + 2.17 + 1.85 + 1.89 + 1.94 + 2.21 - 5 \times 2.32 = 0.49$$

The 95% confidence interval of confirmation experiments (CI<sub>CE</sub>) and population (CI<sub>POP</sub>) is calculated by using the equation (8.2) and (8.3):

Where,

F<sub>α</sub>(1, f<sub>e</sub>): The F ratio at the confidence level of (1-α) against DOF 53 and error DOF f<sub>e</sub> = 42

N: Total number of results = 54 (Treatment=18, Repetition=3) R : Sample size for confirmation experiments = 3

V<sub>e</sub>: Error variance = 0.075, f<sub>e</sub> error DOF = 42 (Table 8.14)

$$n_{eff} = \frac{N}{1 + [\text{DOF associated in the estimate of mean response}]} = 4.5 \quad \dots\dots 8.7$$

where

F<sub>0.05</sub>(1, 42) = 4.07 (tabulated F value), So CI<sub>CE</sub> = ±0.41 and CI<sub>POP</sub> = ±0.26

The predicted optimal range ( for a confirmation runs of three experiments) is :

$$\mu_{SR} - CI_{CE} < \mu_{SR} < \mu_{SR} + CI_{CE} \quad ; \quad 0.08 < \mu_{SR} < 0.90$$

The 95% conformation interval of the predicted mean is as follows:

$$\mu_{SR} - CI_{POP} < \mu_{SR} < \mu_{SR} + CI_{POP} \quad ; \quad 0.23 < \mu_{SR} < 0.75$$

### 8.1.8.2. Confirmation experiments:

The three confirmation experiments for SR were conducted at the optimum setting of the process parameters. The type of vibration is set at 2<sup>nd</sup> level, amplitude of vibration at 3<sup>rd</sup> level, peak current at 1<sup>st</sup> level, Duty cycle at 1<sup>st</sup> level, workpiece thickness at 1<sup>st</sup> level and wire feed rate at 3<sup>rd</sup> level. The Confirmation experimental value of average SR is found to be 0.66 μm, which fall within the 95% confidence interval of the predicted optimum parameters. The conformation run were repeated thrice to ensure the main effect on surface roughness at A<sub>2</sub>B<sub>3</sub>C<sub>1</sub>D<sub>1</sub>E<sub>1</sub>F<sub>3</sub> levels as shown in Table 8.7.

## 8.2. Analysis and discussion of results Phase-III:

A total number of 32 experimental runs data were collected for a standard second-order experimental design called face-centered central composite design (CCD). Table 7.12 (Chapter 7) shows experimental trail conditions and results of response characteristics for material removal rate (MRR) and SR performance characteristics. The 3-D graphs results, based on RSM provide better visualization of the responses. From the experimental data of RSM, empirical models were developed and the confirmation experiments were performed.

### 8.2.1. ANOVA for Material Removal Rate of Hybrid-WEDM:

The F-value of 19.60 for the present Response surface Model for MRR demonstrated the importance of model for Hybrid Wire-EDM. There was only 0.01% chance that the large F - value occurred due to uncontrollable parameters. The P-values under 0.0500 indicated that the model terms are huge. For this study the terms like peak current (A), pulse on time (B), pulse of time (C) and amplitude of vibration (D), AB, AC, CE, A<sup>2</sup>, B<sup>2</sup>, C<sup>2</sup>, D<sup>2</sup>, E<sup>2</sup> were significatory model terms. The other noteworthy model terms were removed as having P-value more than 0.1000. The Lack of Fit F-value 3.01 was an index of insignificance to pure error. There was 11.58 % probability that a "Lack of Fit F-value" vast could happen because of the commotion. The "Predicted R<sup>2</sup>" (0.7300) was insensible concurrently with the "Adjusted R<sup>2</sup>" (0.8936). This model was utilized to explore the plan space. The peak current, pulse on time and pulse off time have the overwhelming impact on the MRR. The MRR straightforwardly built from peak current and pulse on time; however, at the same crumble the surface morphology. The outcomes showed the significant impact of the amplitude of vibration in execution of Hybrid-WEDM performance. The mechanical vibration of work piece conferred inertial energy and grants the kinetic vitality to the bubbles and debris to empty discharge gap. The effortlessly expel of debris and gas bubbles come about fewer shot circuits and resulted in efficient discharge. The ANOVA Table 8.16 was a portrayal of complex interdependency of all the factors selected for experimentation. That was on the grounds that amplitude of vibration in Hybrid WEDM impacted extremely to each segment of ultrasonic vibration assisted Wire-EDM process. The amplitude of vibration developed acoustic pressure, which resulted in suction of fresh dielectric and

exhaust of contaminated one. In this proposed experimental set-up, the ultrasonic vibration developed alternative compression and expansion of discharge gap in the upper and lower half of the workpiece.

Table 8.15 Pooled analysis of variance for MRR

Source	Sum of Squares	Df	Mean Square	F-value	P-value	
Model	1568.59	14	112.04	19.60	< 0.0001	Significant
A-Peak current	428.03	1	428.03	74.89	< 0.0001	Significant
B-Pulse on Time	241.02	1	241.02	42.17	< 0.0001	Significant
C-Pulse off Time	171.17	1	171.17	29.95	< 0.0001	Significant
D-Amplitude of Vibration	55.95	1	55.95	9.79	0.0061	Significant
E-Wire Feed Rate	0.6419	1	0.6419	0.1123	0.7416	Not significant
AB	33.05	1	33.05	5.78	0.0279	Significant
AC	28.69	1	28.69	5.02	0.0387	Significant
CE	41.91	1	41.91	7.33	0.0149	Significant
A <sup>2</sup>	74.01	1	74.01	12.95	0.0022	Significant
B <sup>2</sup>	126.87	1	126.87	22.20	0.0002	Significant
C <sup>2</sup>	222.09	1	222.09	38.86	< 0.0001	Significant
D <sup>2</sup>	90.13	1	90.13	15.77	0.0010	Significant
E <sup>2</sup>	201.70	1	201.70	35.29	< 0.0001	Significant
Residual	97.17	17	5.72			
Lack of Fit	85.37	12	7.11	3.01	0.1158	Not significant
Pure Error	11.80	5	2.36			
Cor Total	1665.76	31				
Std. Dev.	2.39	R <sup>2</sup>	0.9417			
Mean	14.55	Adjusted R <sup>2</sup>	0.8936			
C.V. %	16.43	Predicted R <sup>2</sup>	0.7300			
		Adeq Precision	16.1383			

The 3-D response surface graphs in Figures (8.25-8.27) were plotted to ponder the combined effect of two process factors on MRR. It was observed that the MRR had an increasing trend with the peak current and pulse on time. Nani, (2017) explained that ultrasonic vibration encouraged the fundamental discharge condition to enhanced MRR and thereby process stability.

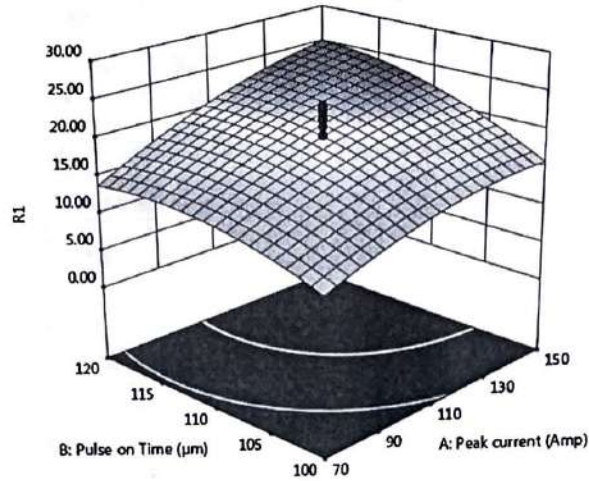


Figure 8.25 Effect of peak current and pulse on time on MRR

This phenomenon resulted in efficient flushing mechanism for debris. This improved flushing mechanism, prepared a ground for the recurrence of normal discharge and hence increased the MRR.

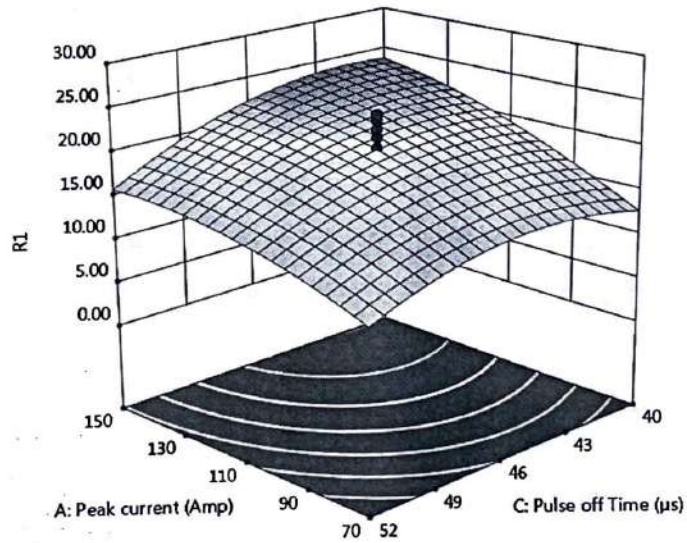


Figure 8.26 Effect of peak current and pulse off time on MRR

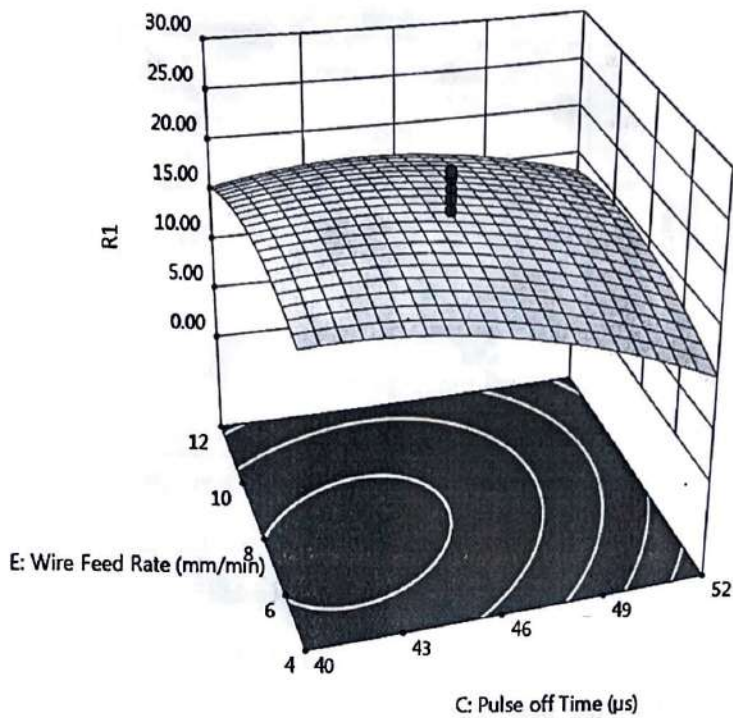


Figure 8.27 Effect of wire feed rate and pulse off time on MRR

The MRR for the proposed Hybrid-WEDM is proportional to the discharge frequency during machining. The Ultrasonic vibration of work piece increased the frequency of effective discharge. The peak current value above 150 ampere and pulse on time above 130 not only increased MRR but also resulted in high wire breakage. The high peak current at high pulse on time led to high discharge energy.

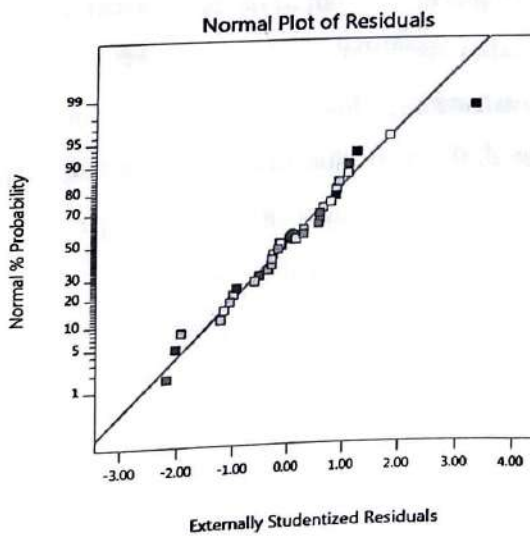


Figure 8.28 Normal Plot of Residuals for MRR

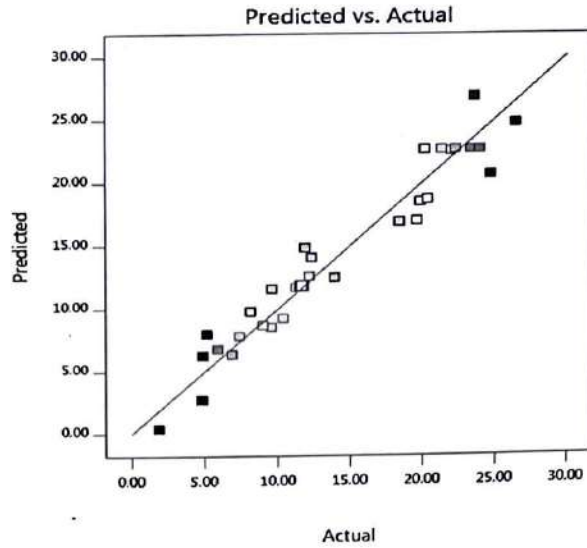


Figure 8.29 Predicted vs. Actual for MRR

Although, the effect of amplitude of vibration on the MRR in Hybrid-WEDM was much less than that of the peak current and pulse on time but the amplitude of vibration provided the flexibility to widen the range of peak current and pulse of time to work with. Higher MRR was obtained at 14  $\mu\text{m}$  amplitude of vibration. It was also observed that MRR remains almost constant with the wire feed rate. The effect of wire feed rate was not significant compared to other parameters selected in this study. Though, the wire feed rate increased the process stability and decreased frequency of wire breakage.

The residual analyses plotted in Figure (8.28-8.29) for the model were a main diagnostic tool for normal probability plot of the residuals. That plot was to check for normality of residuals and to check for constant error. Most of the experimental data points were normally distributed and following the straight line as in Figure 8.28. The Figure 8.29 showed that all the real values were following the anticipated values and along these lines proclaiming model suppositions were right. The condition of MRR as far as components under thought could be utilized to make forecasts about the MRR execution normal for Hybrid-WEDM for given levels of each factor. The high levels of the elements were coded as +1 and the low levels of the components are coded as -1.

$$\begin{aligned}
 \text{MRR} &= \\
 &-405.30016 \\
 &+0.214333 \text{ Peak current} \\
 &+4.49704 \text{ Pulse on Time} \\
 &+6.66100 \text{ Pulse off Time} \\
 &+0.684425 \text{ Amplitude of Vibration}
 \end{aligned}$$

-0.520675	Wire Feed Rate
+0.003593	Peak current * Pulse on Time
-0.005579	Peak current * Pulse off Time
+0.067435	Pulse off Time * Wire Feed Rate
-0.000993	Peak current <sup>2</sup>
-0.020797	Pulse on Time <sup>2</sup>
-0.076433	Pulse off Time <sup>2</sup>
-0.012173	Amplitude of Vibration <sup>2</sup>
-0.163888	Wire Feed Rate <sup>2</sup>

..... (8.8)

The coded condition is important for recognizing the relative effect of each variable by contrasting the factor coefficients. The pulse on time and pulse off time along the peak current factors have a most astounding coefficient assessed in the given condition of the MRR for Hybrid-WEDM process. The effect of amplitude of vibration could not be overlooked and had significant effect on MRR. The final equation in terms of code factors is given in equation (8.8).

### 8.2.2. ANOVA for Surface Roughness of Hybrid-WEDM:

The model F-value (35.16) for the proposed Hybrid-WEDM process suggests essentialness of the model. The ANOVA sum of squares for surface roughness was Type III – Partial. The critical interdependency of choosing factors for proposed Hybrid Wire-EDM performance has been illustrated in Table 8.16. For this situation A, B, C, D, AB, AC, BD, BE, CD, CE, A<sup>2</sup>, B<sup>2</sup>, C<sup>2</sup> are the convincing model terms. The Lack of Fit F-value (4.41) inferred that there was a 5.63% shot that a Lack of Fit F-value could happen because of unpredictable factors. The Predicted R<sup>2</sup> (0.8234) was insensible concurrence with the Adjusted R<sup>2</sup> (0.9391); i.e. the distinction is under 0.2. Adeq Precision measures the signal to commotion proportion. A proportion more prominent than 4 was alluring. The proportion of 18.806 demonstrated a sufficient signal.

Table 8.16 Pooled analysis of variance for Surface roughness

Source	Sum of Squares	Df	Mean Square	F-value	P-value	
Model	7.43	14	0.5305	35.16	< 0.0001	Significant
A-Peak current	2.57	1	2.57	170.16	< 0.0001	Significant
B-Pulse on Time	1.12	1	1.12	74.38	< 0.0001	Significant
C-Pulse off Time	1.11	1	1.11	73.24	< 0.0001	Significant

D-Amplitude of Vibration	0.2625	1	0.2625	17.40	0.0006	Significant
E-Wire Feed Rate	0.0005	1	0.0005	0.0334	0.8571	Not significant
AB	0.2943	1	0.2943	19.50	0.0004	Significant
AC	0.2475	1	0.2475	16.40	0.0008	Significant
BD	0.2889	1	0.2889	19.15	0.0004	Significant
BE	0.1139	1	0.1139	7.55	0.0137	Significant
CD	0.2998	1	0.2998	19.87	0.0003	Significant
CE	0.4323	1	0.4323	28.65	<	Significant
A <sup>2</sup>	0.4123	1	0.4123	27.32	<	Significant
B <sup>2</sup>	0.2290	1	0.2290	15.18	0.0012	Significant
C <sup>2</sup>	0.1416	1	0.1416	9.39	0.0070	Significant
Residual	0.2565	17	0.0151			
Lack of Fit	0.2344	12	0.0195	4.41	0.0563	Not significant
Pure Error	0.0221	5	0.0044			
Cor Total	7.68	31				
Std. Dev.	0.1228	R <sup>2</sup>	0.9666			
Mean	1.52	Adjusted R <sup>2</sup>	0.9391			
C.V. %	8.06	Predicted R <sup>2</sup>	0.8234			
		Adeq	18.8064			
		Precision				

The 3-D response surface graphs for Hybrid-WEDM process variables for the surface roughness were illustrated in Figures (8.29 - 8.32). It was clear in Figure (8.29-8.32), that the peak current and pulse on time deteriorated the surface integrity.

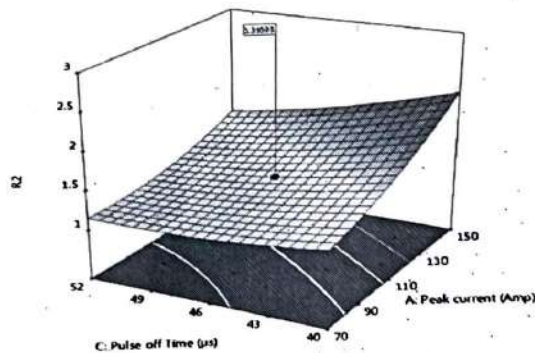


Figure 8.30 Effect of peak current and pulse off time on SR



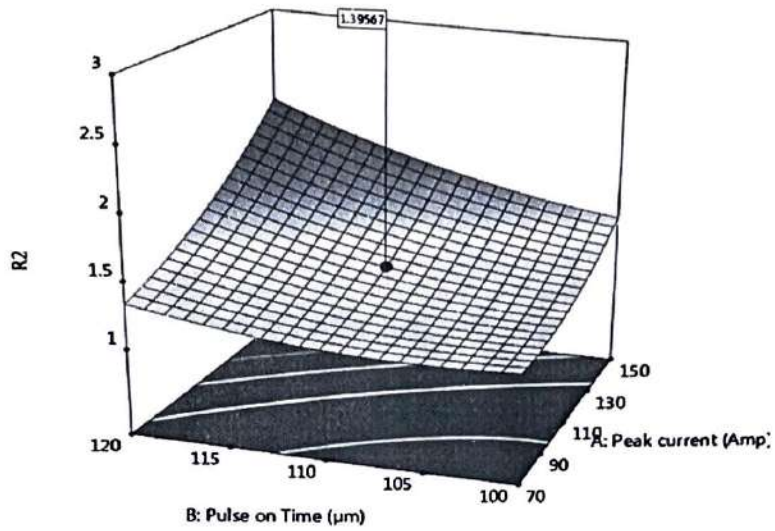


Figure 8.31 Effect of pulse on time and peak current on SR

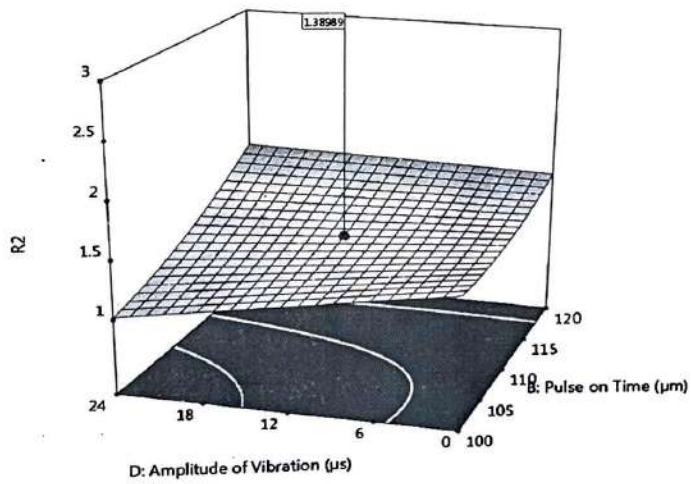


Figure 8.32 Effect of pulse on time and amplitude of vibration

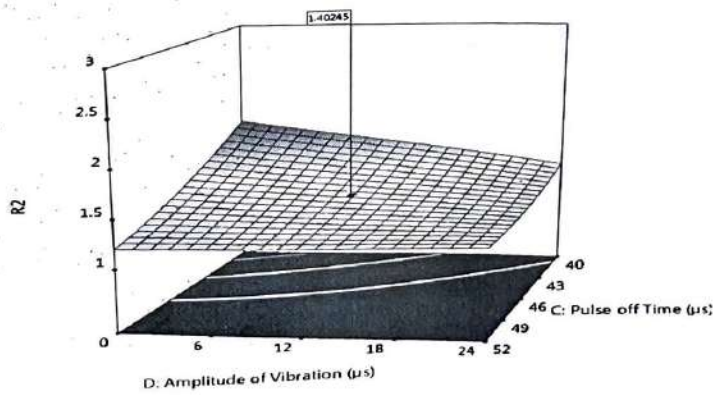


Figure 8.33 Effect of pulse off time and amplitude of vibration

The high peak current for each spark, produced high discharge energy per pulse for more time interval. That caused the large crater size and high residual stresses on the surface. The Figure 8.32 demonstrated that, the surface rough declined with increment in pulse off time. High peak current generated high discharge energy that led to higher temperature gradient and that creates crater of large size.

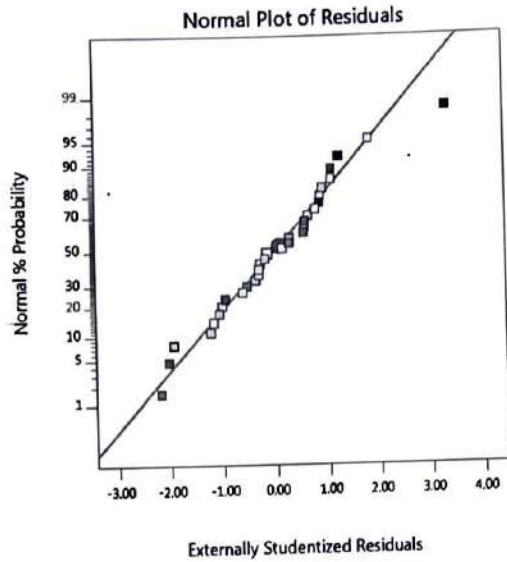


Figure 8.34 Normal Plots of Residuals for SR

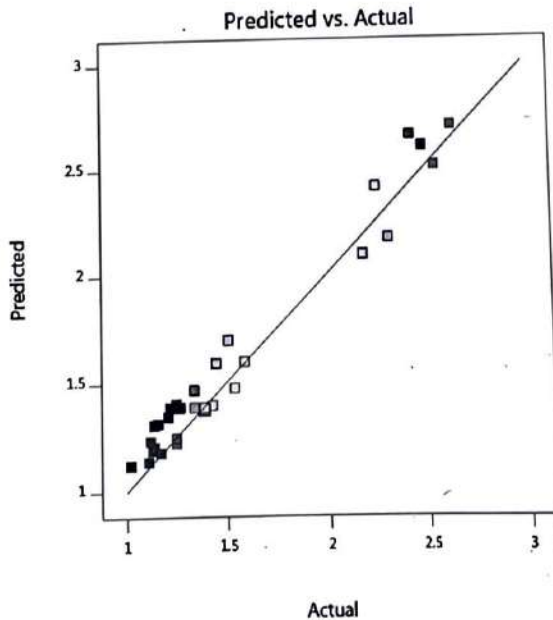


Figure 8.35 Predicted vs. Actual for SR

That caused a bigger surface harshness on the workpiece surface. It was seen from Figure (8.34- 8.35) that the optimum surface roughness could be accomplished

with an amplitude of vibration extend between 12-14 $\mu\text{m}$ , and beyond that the surface roughness increased.

Normal probability plot has been drawn for externally studentized residuals in Figure (8.34) to check the typicality of residual. Linearity of this normal plot affirmed the typical distribution of the experimentally obtained data.

The Figure (8.34) displayed that all the actual and predicted values were following the normal distribution linearity with least steady error.

$$\begin{aligned}
 \text{SR} &= \\
 +23.75414 & \\
 -0.021477 & \text{ Peak current} \\
 -0.239119 & \text{ Pulse on Time} \\
 -0.232794 & \text{ Pulse off Time} \\
 -0.219340 & \text{ Amplitude of Vibration} \\
 -0.548229 & \text{ Wire Feed Rate} \\
 +0.000339 & \text{ Peak current * Pulse on Time} \\
 -0.000518 & \text{ Peak current * Pulse off Time} \\
 +0.001120 & \text{ Pulse on Time * Amplitude of Vibration} \\
 +0.002109 & \text{ Pulse on Time * Wire Feed Rate} \\
 +0.001901 & \text{ Pulse off Time * Amplitude of Vibration} \\
 +0.006849 & \text{ Pulse off Time * Wire Feed Rate} \\
 +0.000074 & \text{ Peak current}^2 \\
 +0.000878 & \text{ Pulse on Time}^2 \\
 +0.001918 & \text{ Pulse off Time}^2
 \end{aligned}
 \tag{8.9}$$

The equation (8.9) is contemplated for surface roughness execution of Hybrid-WEDM regarding coded factors. This condition can be utilized to make better forecasts about the Surface roughness for a given range of each factor. As a matter of course, larger amounts of the variables are coded as +1 and the low levels of the components are coded as - 1. The proposed actual variable equation is helpful in distinguishing the relative effect of the parameters by looking at the factor coefficients.

### 8.3. Multi Response optimization using desirability function (Phase-IV):

It is recognized that Hybrid-WEDM performance qualities characteristics MRR and SR are separating in nature. The maximum value of MRR could be accomplished for 12-16 $\mu\text{m}$  amplitude of vibration. At the point when high amplitude vertical ultrasonic vibration is connected to work piece through a cantilever course of action, caused solid mixing impact and caused higher MRR and on the other side high heat energy caused poor surface morphology.

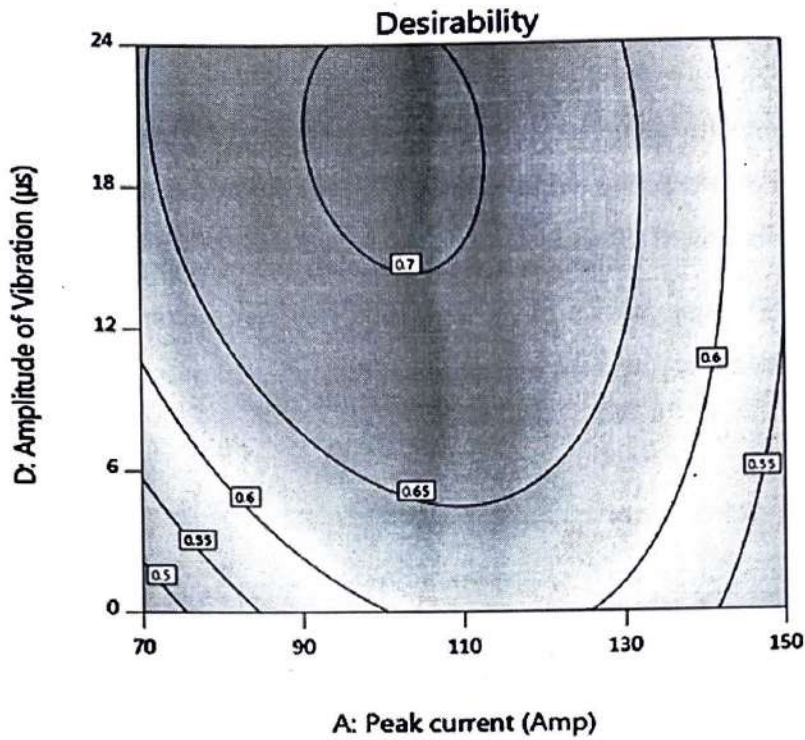


Figure 8.36 Overall desirability variations with Amplitude of vibration vs. pulse on time

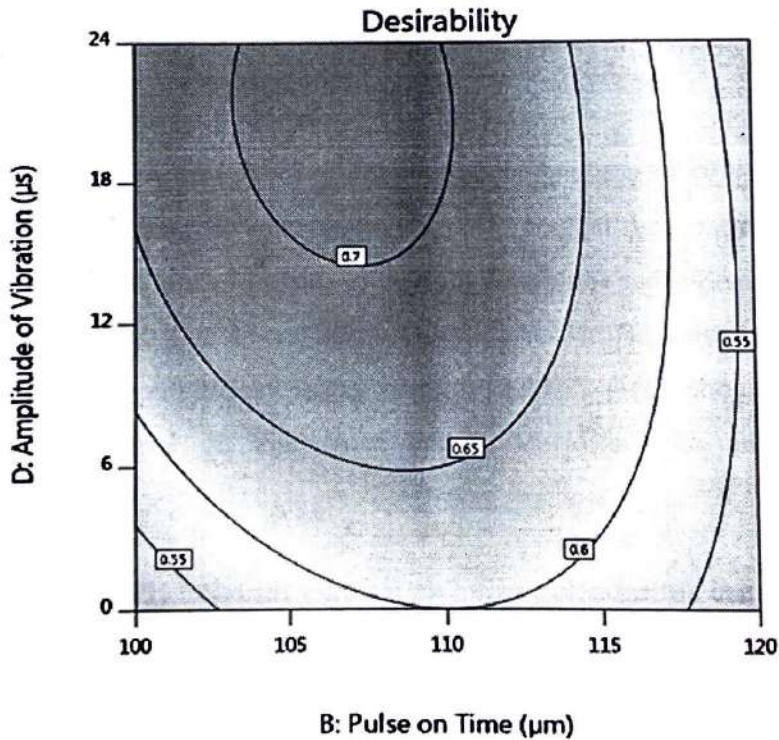


Figure 8.37 Overall desirability variations with Amplitude of vibration vs. peak current

Desirability function has been utilized to decide the ideal parameters for Hybrid-WEDM process to streamlining of MRR and SR for Hybrid-WEDM process. The single response and multi response optimizations were accomplished through

desirability function. Utilizing Design expert software, ideal arrangements are inferred for determining outline space imperatives for multi performance characteristics. The overall desirability variation contour for amplitude of vibration (A), Peak current (B) and pulse on time (C) are demonstrated in Figure (8.36- 8.37). The value of the amplitude of vibration range between 12-16 $\mu$ m is desirable to obtain maximum performance of Hybrid-WEDM for both performance characteristics. The Figure (8.38) demonstrates the desirability numerical value of Hybrid-WEDM process parameters for the solution of 1 out of 16 confirmation runs. Equal importance is assigned to all the process variables.

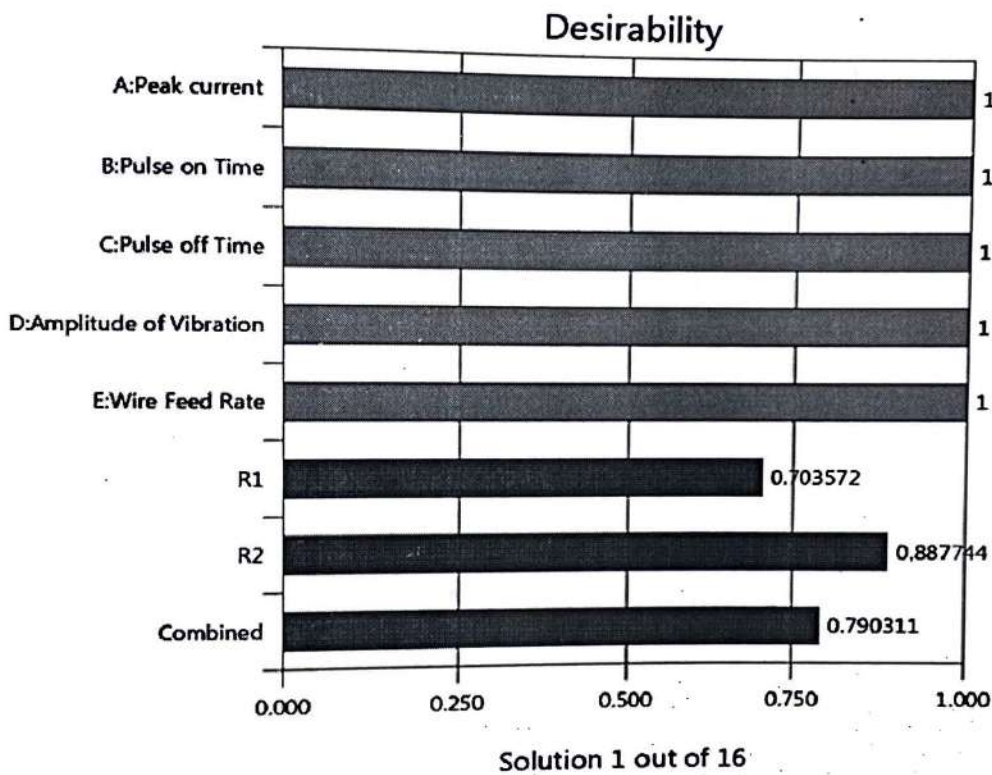


Figure 8.38 Bar Graph of combined Desirability for MRR and SR

The individual desirability value for MRR and SR is 0.703572 and 0.887744 respectively. The desirability function is the index of most desirable to the least desirable. The desirable value an objective to be achieved lies between 0 to 1 scales. SR is more desirable than MRR. The overall combined desirability for Hybrid-WEDM performance characteristics is 0.790311.

## MULTI CHARACTERISTICS OPTIMIZATION USING UTILITY FUNCTION

---

### 9.1. Introduction:

In recent years, ultrasonic vibration assisted Hybrid-WEDM have been developed to curve the limitations of normal Wire-EDM process. But the complex interdependency and interrelationship of performance restrain the best factors setting for which multiple responses could be optimized simultaneously. Although many mathematical techniques have been available in literature to solve such types of engineering optimization problems. The use of multiple criteria decision making methodology helped in reducing the computational effort involved (Rao, 2009). But some of these methods further complicate the optimization of the multi response problems of Hybrid-WEDM, as it required complicated mathematical models. Shiau, (1990) proposed a combined neuro-fuzzy model and Taguchi approach to resolve a complex parameter design problem with multiple responses. Rao and Gandhi (2002) applied graph theoretic approach to analysis the universal machinability of work material. They convert the quantitative variables affecting the machinability criteria into qualitative scale. Dubey, (2008) utilized the Taguchi loss function and utility function approach to optimize the multi-response electro-chemical honing machining (ECH). They confirmed the feasibility of this approach over wide range of parameters of ECH and also evaluated that this approach provide flexibility to the user for the selection of desirable quality attribute. Jangra et al., (2010) presented gray relationship analysis of multi-response optimization methodology to analysis machining of punching die D3 tool steel using wire-EDM process. Tripathy and Tripathy, (2016) proved the feasibility of TOPSIS and grey relational analysis for optimization of multi-response performance variable of powder-mixed EDM process. Kumar et al., (2012) analyzed the turning of uni-directional glass fiber-reinforced plastics utilizing Taguchi experimental design and utility concept. A utility model was developed by them to evaluate the utility of surface rough and metal removal rate for various input parameters and found that this approach provide appropriate solution for multi-response optimization problem. Kumar et al., (2017) proposed graph theoretic

approach for analysis and modeling of Ultrasonic vibration assisted EDM process. They considered the qualitative as well as quantitative attribute on the same platform. An undertaking has been made through this investigation to check general Hybrid-WEDM execution, by considering the relative commitment of all the quality attributes at the same time. A strategy in light of utility capacity and Taguchi technique has been proposed for deciding the ideal settings of process or parameters for multi-reaction. The weighted-utility function for Hybrid -WEDM quality characteristics optimization is the novelty of the proposed study to identify the most appropriate combination of variable in conjunction with optimum utility of the process.

## 9.2. Multi-response optimization through utility concept (Phase-V):

A product or a procedure is regularly assessed based on certain number of value qualities, sometimes clashing in nature. Accordingly, a joined measure is important to check its overall performance, which must consider the relative commitment of all the quality attributes. In the accompanying, a system in light of utility idea and Taguchi strategy a philosophy has been advanced for deciding the ideal settings of process or parameters for multi-reaction/multi-qualities process or product. The multi- response streamlining of value attributes of Hybrid-WEDM has been completed in the accompanying areas.

### 9.2.1. The Concept of Utility:

Utility can be characterized as the convenience of an item or a procedure in reference to the desires for the clients. The general helpfulness of a procedure/item can be spoken to by a bound together record named as Utility which is the aggregate of the individual utilities of different quality attributes of the procedure/item. The methodological reason for Utility approach is to change the evaluated response of every quality characteristics into a typical index. In the event that  $X_i$  is the measure of adequacy of a trait (or quality characteristics)  $i$  and there are  $n$  properties assessing the result space, than the joint Utility capacity can be communicated as in Equation (9.1):

$$U(X_1, X_2, \dots, X_n) = f(U_1(X_1), U_2(X_2), \dots, U_n(X_n)) \dots(9.1)$$

Where  $U_i(X_i)$  is the utility of the  $i^{\text{th}}$  characteristic.

The general Utility function equation (9.2) is the whole of individual utilities if the attributes are independent, and is given as follows:

$$U(X_1, X_2, \dots, X_n) = \sum_{i=1}^n U_i(X_i) \quad \dots$$

(9.2)

The attribute might be doled out weights relying on the relative significance or needs of the qualities. The general utility function in the wake of appointing weights to the qualities can be communicated as Equation (9.3):

$$U(X_1, X_2, \dots, X_n) = \sum_{i=1}^n W_i U_i(X_i) \quad \dots$$

(9.3)

Where  $W_i$  is the weight doled out to the property 'i'. The total of the weights for every one of the factor must be equivalent to 1.

**9.2.2. The Utility Value determination:**

An inclination scale for every quality characteristic is developed for deciding its utility esteem. Two self-assertive numerical qualities (inclination number) 0 and 9 are allocated to the simply adequate and the best estimation of the quality characteristic individually. The inclination number ( $P_i$ ) can be communicated as Equation (9.4) on a logarithmic scale as takes after, (Gupta and Murthy, 1980):

$$P_i = A \times \log \left( \frac{X_i}{X'_i} \right) \quad \dots \text{Eq}$$

(9.4)

Where  $X_i$  = estimation of any quality value or characteristic  $i$

$X'_i$  = simply acceptable estimation of value or characteristic  $i$

A = constant

The estimation of A can be found by the condition that if  $X_i = X^*$  (where  $X^*$  is the ideal or best esteem), at that point  $P_i = 9$

In this manner, 
$$A = \frac{9}{\log \frac{X^*}{X'_i}} \quad \dots \dots (9.4)a$$



The general utility can be computed by Equation (9.5) as takes after:

$$U = \sum_{i=1}^n W_i P_i \quad \dots(9.5)$$

Subject to the condition:  $\sum_{i=1}^n W_i = 1$

Among different quality attributes compose viz. smaller the better, higher the better, and ostensible the better proposed by Taguchi, the Utility concept would be higher the better sort. In this manner, if the Utility concept is augmented, the quality attributes considered for its assessment will naturally be improved (amplified or limited by and large).

Table 9.1: Experimental results of various response characteristics

Ex p. No.	Cutting Rate (mm/min)			S/N Ratio (dB)	Residual stresses (MPa)			S/N Ratio (dB)	Surface Roughness(μm)			S/N Ratio (dB)
	R1	R2	R3		R1	R2	R3		R1	R2	R3	
1	0.43	0.45	0.46	-7.01	198	185	198	45.75	1.22	1.32	1.38	-2.33
2	2.9	2.82	2.98	9.24	252	260	266	48.28	3.02	3.00	2.98	-9.54
3	5.22	5.32	5.26	14.43	292	295	287	49.29	3.22	3.86	3.76	11.18
4	2.39	2.41	2.45	7.66	134	136	142	42.76	1.62	1.84	1.76	-4.82
5	4.63	4.65	4.54	13.27	225	256	265	47.93	3.10	3.02	3.11	-9.76
6	3.52	3.51	3.47	10.88	302	310	305	49.71	3.18	3.53	3.43	10.59
7	1.45	1.47	1.43	3.23	235	234	220	47.23	1.68	1.36	1.47	-3.57
8	2.76	2.78	2.66	8.73	226	227	216	46.97	2.36	2.96	2.52	-8.38
9	4.16	4.18	4.08	12.34	284	298	286	49.23	3.5	3.06	3.42	10.45
10	3.51	3.58	3.45	10.91	291	287	268	49.01	3.32	3.08	2.98	-9.91
11	1.92	1.88	1.92	5.60	193	218	265	47.13	1.56	1.62	1.58	-4.01
12	3.75	3.83	3.77	11.56	268	243	243	48.01	2.96	2.64	2.84	-8.99
13	3.63	3.75	3.65	11.31	175	183	234	45.98	1.60	1.52	1.57	-3.88
14	4.45	4.57	4.73	13.22	221	226	231	47.08	2.06	1.86	1.97	-5.87
15	3.53	3.75	3.79	11.33	126	134	136	42.42	1.58	1.60	1.59	-4.03
16	2.76	2.88	2.78	8.96	170	167	174	44.63	2.06	1.66	1.87	-5.44
17	3.37	3.49	3.36	10.64	231	154	167	45.44	1.90	1.72	1.83	-5.19
18	4.23	4.35	4.24	12.61	267	265	284	48.70	1.65	2.06	2.04	-5.69
	58.61	59.67	59.02		4090	4078	4187		41.59	41.71	42.1	
	$\bar{T}_{CR}$ = Overall mean of CR= 3.28				$\bar{T}_{RS}$ = Overall mean of RS= 228.80				$\bar{T}_{SR}$ = Overall mean of SR=2.32			

### 9.2.3. The Algorithm:

The stepwise system for completing multi-response improvement with Utility concept and Taguchi strategy is shown as:

1. Use the Taguchi framework trial plan and examination to discover the ideal estimation of every one of the chosen process response.
2. Construct an inclination scale for every response in view of their ideal esteem and least worthy level (Eq. 9.4).
3. Assign weights ( $W_i$ ) in light of the experience and client preference, keeping in see that the aggregate entirety of weights is equivalent to 1.
4. Find general utility qualities for various test preliminary conditions considering every one of the response associated with multi- response enhancement (Eq. 9.5).
5. Use the qualities decided in stage 4 as crude response of various preliminary states of the test framework. On the off chance that preliminaries are rehashed, discover S/N ratio (HB compose), as the utility is a higher-the-better write trademark [Roy (1990)]
6. Analyze the outcomes according to the standard technique recommended by Taguchi [Roy (1990)].
7. Find the ideal settings of process parameters for mean and S/N utility in view of the investigation performed in stage 6.
8. Predict ideal estimations of various response qualities for the ideal parametric setting that augments the general utility as decided in stage 7.
9. Conduct affirmation tests to check the ideal outcomes.

### 9.2.4. Utility for the Model of CR, RS and SR (Phase-V):

In view of the system created in the past section, following case have been considered to get the ideal settings of the procedure parameters of Hybrid-WEDM for foreseeing the ideal estimations of joined responses. All the three quality attributes (CR, RS and SR) have been incorporated into utility response. Taguchi L18 symmetrical exhibit (OA) [Roy (1990)] has been adopted for directing the investigations. Type of vibration, amplitude of vibration (B), peak current (C), duty cycle (D), workpiece thickness (E) and wire feed rate (F) are chosen as information

parameters. The watched estimations of response parameters are given in Table 9.1 Response parameters (quality attributes) were Cutting rate (CR), residual stresses (RS) and surface roughness (SR), when these were advanced independently; the outcomes of results was delivered in Table 9.2.

Table 9.2: Optimal setting and values of process parameters (individual quality characteristics optimization)

Response Characteristics	Optimal level of process parameters	Significant process parameters	Predicted optimal value of quality characteristics
CR	A2B2C3D3E3F2	A, B, C, D, E, F	6.45 mm/min
RS	A2B2C1D1E2F3	A, B, C, D, E, F	86.53 MPa
SR	A2B3C1D1E1F3	A, B, C, D, E, F	0.49 $\mu\text{m}$

Following is the stepwise procedure for transforming experimental data into utility data.

#### 9.2.4.1. Construction of preference scales:

a) Preference scale for Cutting Rate ( $P_{CR}$ ):

$X^*$  = Optimal value of Cutting Rate = 6.45 (refer Table 9.2)

$X_i'$  = Just acceptable value of CR = 0.42 (All the observed values of CR are greater than 0.42)

Using equation (9.4a) for calculating  $A_{CR}$

$$A_{CR} = \frac{9}{\log \frac{X^*}{X_i'}} = 7.59$$

Following equation is obtained from equation 9.4:

$$P_{CR} = 7.59 \times \log \left( \frac{X_{CR}}{0.42} \right)$$

.....(9.6)

b) Preference scale for Residual stresses ( $P_{RS}$ ):

$X^*$  = Optimal value of RS = 86.53 (refer Table 9.2)

$X'_i$  = Just acceptable value of RS = 315 (All the observed values of RS are lesser than 315)

Using equation (9.4a) for calculating  $A_{RS}$

$$A_{RS} = \frac{9}{\log \frac{X^*}{X'_i}} = -16.36$$

Following equation is obtained from equation 9.4:

$$P_{RS} = -16.36 \times \log \left( \frac{X_{RS}}{315} \right)$$

.....(9.7)

c) Preference scale for SR ( $P_{SR}$ ):

$X^*$  = Optimal value of SR = 0.49 (refer Table 9.2)

$X'_i$  = Just acceptable value of SR = 3.9 (All the observed values of SR are lesser than 3.9)

Using equation (9.4a) for calculating  $A_{SR}$

$$A_{SR} = \frac{9}{\log \frac{X^*}{X'_i}} = -10.05$$

Following equation is obtained from equation 9.4:

$$P_{SR} = -10.05 \times \log \left( \frac{X_{SR}}{3.9} \right) \quad \text{.....(9.8)}$$

#### 9.2.4.2. Calculation of Utility Value:

Meet weights (1/3 each) have been allocated to the chosen quality attributes expecting every one of the qualities is similarly imperative. Be that as it may, these weights can be differed relying on the case or client prerequisites, assuming any.

The accompanying connection was utilized to compute the utility function in view of the exploratory preliminaries:

$$U(n, r) = P_{CR}(n, r) \times W_{CR} + P_{RS}(n, r) \times W_{RS} + P_{SR}(n, r) \times W_{SR} \quad \dots (9.9)$$

Where  $W_{CR} = 0.33$ ;  $W_{RS} = 0.33$ ;  $W_{SR} = 0.33$

$n$  is the trial number ( $n = 1, 2, 3, \dots, 18$ ) and  $r$  is the repetition number ( $r = 1, 2, 3$ ). The calculated Utility values are shown in Table 9.3.

Table 9.3: Calculated Utility data based on responses

Trail No.	Utility values			S/N ratio (dB)
	R1	R2	R3	
1	2.79	2.88	2.71	8.92
2	2.99	2.90	2.92	9.35
3	3.19	2.93	3.02	9.67
4	5.16	4.95	4.93	14.00
5	3.73	3.47	3.32	10.87
6	2.71	2.49	2.56	8.23
7	3.25	3.58	3.58	10.77
8	3.55	3.22	3.52	10.68
9	2.89	2.98	2.89	9.31
10	2.73	2.89	3.06	9.19
11	4.12	3.76	3.36	11.38
12	3.16	3.57	3.45	10.58
13	5.01	5.01	4.36	13.56
14	4.32	4.44	4.34	12.80
15	5.77	5.67	5.65	15.11
16	4.41	4.81	4.51	13.19
17	4.03	5.16	4.84	13.25
18	4.14	3.87	3.69	11.79

R1, R2, R3 = repetitions of experiments against each of the trial conditions.

#### 9.2.4.3. Analysis of Utility data for optimal setting of process parameters:

The average and main response in terms of Utility values and S/N ratio (Tables 9.4 and 9.5) are plotted in Fig. 9.1 to 9.6. It can be observed from Fig. 9.1 to 9.6 that the 2<sup>nd</sup> level of type of vibration ( $A_2$ ), 2<sup>nd</sup> level of amplitude of vibration ( $B_2$ ), 3<sup>rd</sup> level of peak current ( $C_3$ ), 3<sup>rd</sup> level of duty cycle ( $D_3$ ), 2<sup>nd</sup> level of workpiece thickness ( $E_2$ ), and 2<sup>nd</sup> level of wire feed rate ( $F_2$ ) are expected to yield a maximum values of the utility and S/N ratio within the experimental range.

It can be seen from Table 9.6 that all the parameters did huge impact (at 95% confidence level) on the utility function. Then again, from Table 9.7 indicates that the types of vibration, amplitude of vibration are the most astounding donors of general utility of Hybrid-WEDM process. In this way, other immaterial parameters for S/N ratio can be taken as economy factor. The ideal estimations of utility and hence the

ideal estimations of response attributes in thought are anticipated at the above levels of significant parameters.

Table 9.4: Main Effects of Utility Raw Data (: CR, RS and SR)

Level	Type of vibration	Amplitude of vibration	Peak current	Duty cycle	Workpiece thickness	Wire feed rate
L1	3.30	3.14	3.92	4.14	3.48	3.61
L2	4.23	4.33	3.78	3.67	4.18	3.67
L3	*	3.83	3.59	3.48	3.64	4.01
L2-L1	0.93	1.19	-0.15	-0.48	0.70	0.06
L3-L2		-0.50	-0.19	-0.18	-0.54	0.34

Table 9.5: Main Effects of Utility S/N Data (: CR, RS and SR)

Level	Type of vibration	Amplitude of vibration	Peak current	Duty cycle	Workpiece thickness	Wire feed rate
L1	10.20	9.85	11.61	12.00	10.65	10.87
L2	12.32	12.43	11.40	11.15	12.15	11.07
L3	*	11.50	10.78	10.63	10.97	11.83
L2-L1	2.12	2.58	-0.22	-0.84	1.50	0.20
L3-L2	*	-0.93	-0.61	-0.52	-1.180	0.76

Table 9.6: ANOVA for Utility raw data (CR, RS and SR)

SOURCE	SS	DOF	V	P	F-Ratio
Type of Vibration	11.59	1	11.59	27.04	54.51
Amplitude of Vibration	12.90	2	6.45	30.10	30.35
Peak current	1.009	2	0.50	2.33	54.51
Duty Cycle	4.159	2	2.08	9.69	9.77
Workpiece Thickness	2.66	2	1.33	6.20	6.25
Wire Feed Rate	1.63	2	0.82	3.81	3.84
ERROR	8.93	42	0.21	20.83	
T	42.86	53		100	

Significant at 95% confidence level, SS: Sum of Squares; DOF: Degree of Freedom; V: Variance; F-Fisher test factor tabulated for Type of vibration: 4.07, F-Fisher test factor tabulated for other parameters: 3.22.

Table 9.7 ANOVA Utility S/N Data: (CR, RS and SR)

SOURCE	SS	DOF	V	P	F-Ratio
Type of Vibration	20.19	1	20.19	29.65	13.57
Amplitude of Vibration	20.49	2	10.25	30.09	6.89
Peak current	2.20	2	1.10	3.22	0.74
Duty Cycle	5.70	2	2.85	8.36	1.91
Workpiece Thickness	7.52	2	3.76	11.03	2.53
Wire Feed Rate	3.09	2	1.54	4.53	1.04
ERROR	8.93	6	1.49	13.11	
T	68.11	17	*	100	

Significant at 95% confidence level, SS: Sum of Squares; DOF: Degree of Freedom; V: Variance; F-Fisher test factor tabulated for Type of vibration: 5.99, F-Fisher test factor tabulated for other parameters: 5.14.

#### 9.2.4.4. Optimal values of quality characteristics (predicted means):

The average values of all the response characteristics at the optimum levels of significant parameters with respect to utility function are recorded in Table 9.1. The optimal values of the predicted means ( $\mu$ ) of different response characteristics can be obtained from the following equation (9.10):

The normal estimations of all the response characteristics at the ideal levels of noteworthy parameters concerning utility function are recorded in Table 9.3. The ideal estimations of the anticipated means ( $\mu$ ) of various response attributes can be obtained from the accompanying condition (9.10):

$$\mu_{Utility} = A_2 + B_2 - 3\bar{T}$$

.....(9.10)

Where,  $A_2$ -Second level of type of vibration,  $B_2$ -Second level of amplitude of vibration and

$\bar{T}$  = Overall mean. The 95% confidence interval of confirmation experiments ( $CI_{CE}$ ) can be computed [Roy (1990)] by using the following equation (9.11):

$$CI_{CE} = \sqrt{F_{\alpha}(1, f_e) V_e \left[ \frac{1}{n_{eff}} + \frac{1}{R} \right]}$$

(9.11)

Where,  $F_{\alpha}(1, f_e)$  = The F-ratio at the confidence level of  $(1-\alpha)$  against DOF 1 and error degree of freedom  $f_e$ ,  $R$  = Sample size for conformation experiments,  $V_e$  = Error variance,  $n_{eff} = \frac{N}{1+DOF}$ ,  $N$  = total number of trials, and DOF = Total degrees of freedom associated in the estimate of mean response.

a) Cutting Rate:

$$\mu_{CR} = A_2 + B_2 - \bar{T} = 3.99$$

Where  $A_2 = 3.52$ ,  $B_2 = 3.75$  (Table 9.5) and  $T_{CR} = 3.28$  (Table 9.2)

The following values have been obtained by the ANOVA:

$$N = 54, f_e = 42; v_e = 0.42, n_{eff} = 4.5, R = 3, F_{0.05}(1, 42) = 4.0764$$

From equation 9.11,  $CI_{CE} = \pm 0.98$

The predicted optimal range (for conformation runs of three experiments) for CR is given by  $CI_{CE}: 3.01 < \mu_{CR} < 4.97$

b) Residual Stresses:

$$\mu_{RS} = A2 + B2 - \bar{T} = 194.62$$

Where  $A2 = 215.59$ ,  $B2 = 207.83$  from (Table 9.5):  $T_{RS} = 228.80$  (Table 9.2)

The following values have been obtained by the ANOVA:

$$N = 54, f_e = 42; v_e = 1016.052, n_{eff} = 4.5, R = 3, F_{0.05}(1, 42) = 4.0764$$

From equation 9.11,  $CI_{CE} = \pm 48.16$

The predicted optimal range (for conformation runs of three experiments) for Residual stresses is given by  $CI_{CE}: 146.46 < \mu_{RS} < 242.78$

c) Surface Roughness:

$$\mu_{SR} = A2 + B2 - \bar{T} = 1.93$$

Where  $A2 = 2.03$ ,  $B2 = 2.22$  (Table 9.5):  $T_{SR} = 2.32$  (Table 9.2)

The following values have been obtained by the ANOVA:

$$N = 54, f_e = 42; v_e = 0.08, n_{eff} = 4.5, R = 3, F_{0.05}(1, 42) = 4.0764$$

From equation 9.11,  $CI_{CE} = \pm 0.43$

The predicted optimal range (for conformation runs of three experiments) for SR is given by  $CI_{CE}: 1.50 < \mu_{SR} < 2.36$



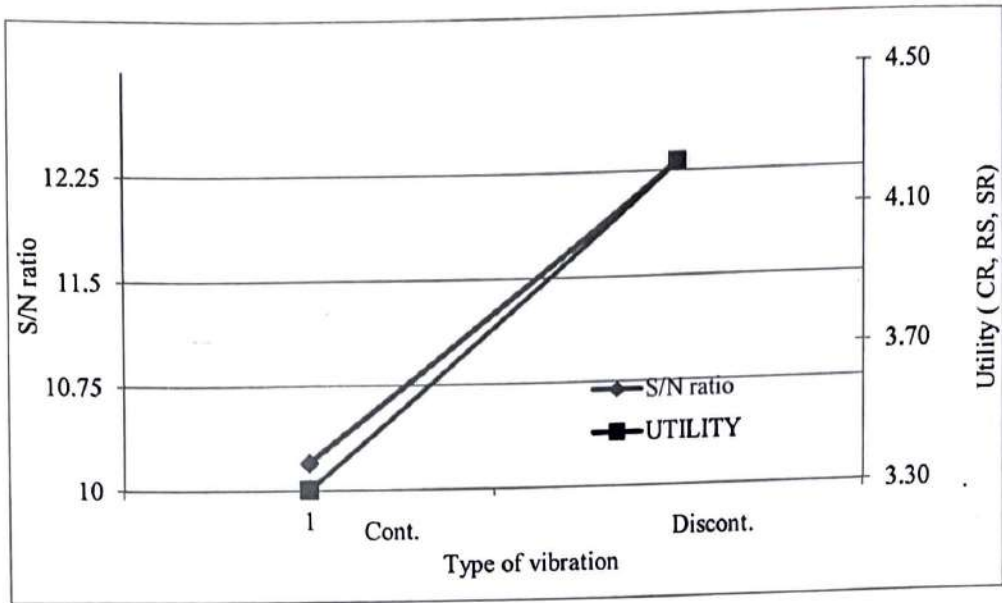


Figure. 9.1 Effect of Type of Vibration on S/N ratio and Utility

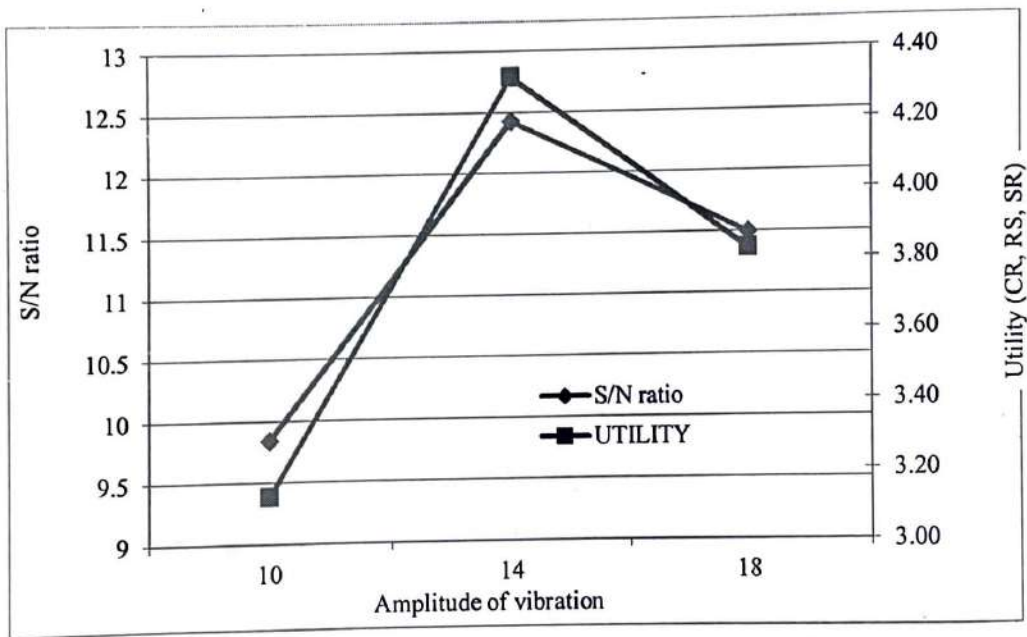


Fig. 9.2 Effect of Amplitude of Vibration on S/N ratio and Utility

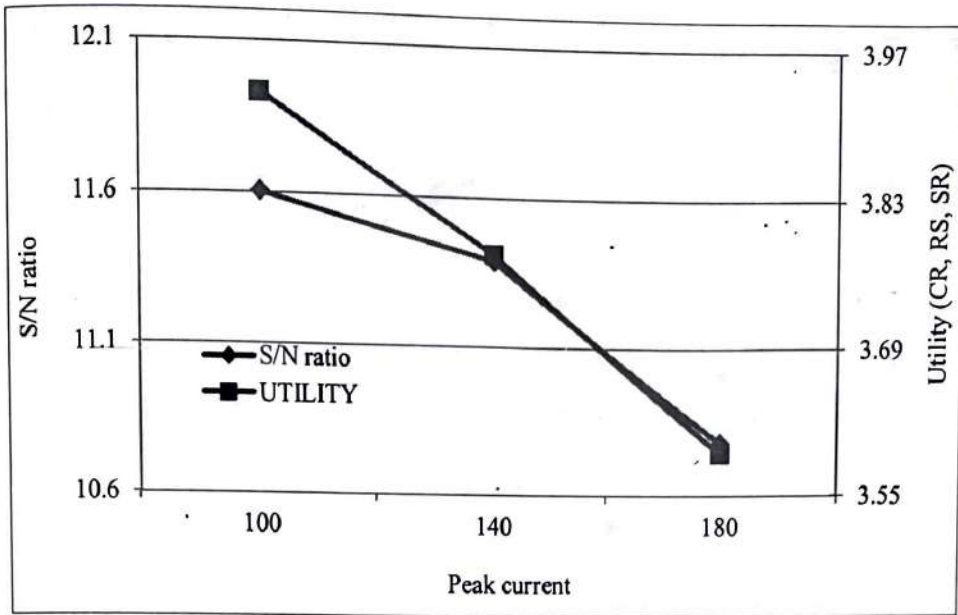


Fig. 9.3 Effect of Peak current on S/N ratio and Utility

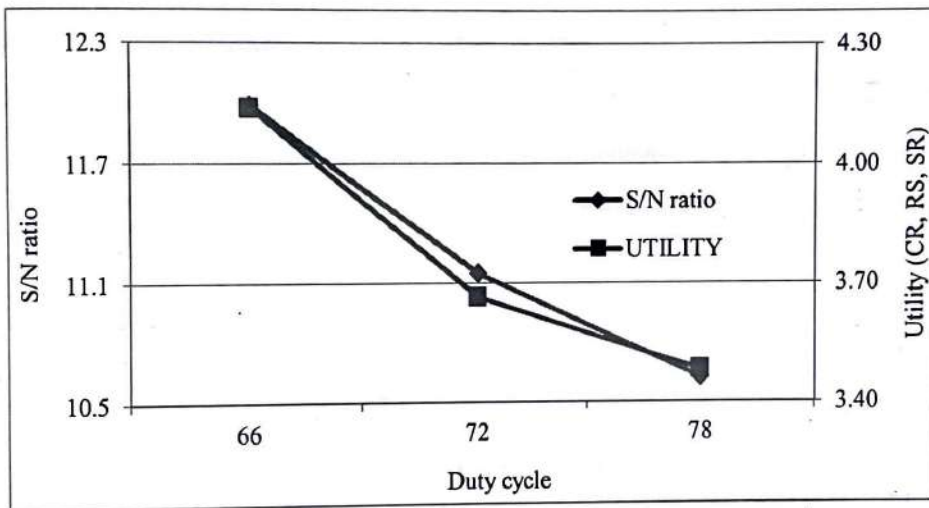


Fig. 9.4 Effect of Duty cycle on S/N ratio and Utility

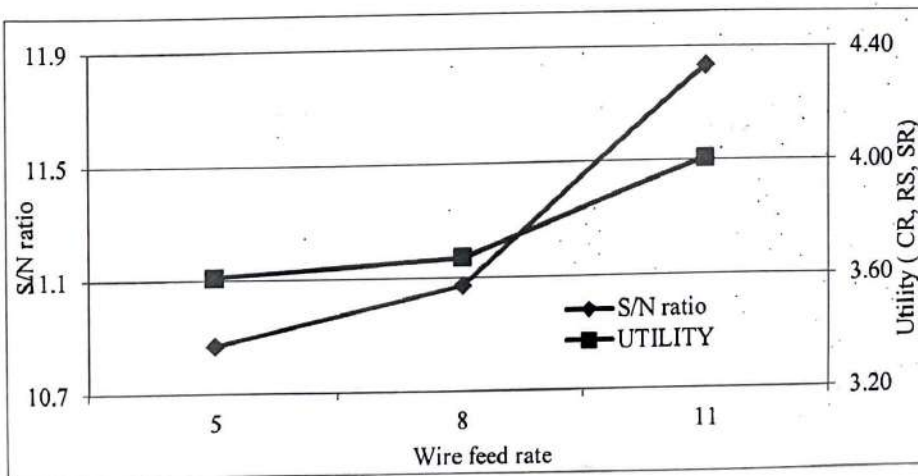


Fig. 9.5 Effect of Wire feed rate on S/N ratio and Utility

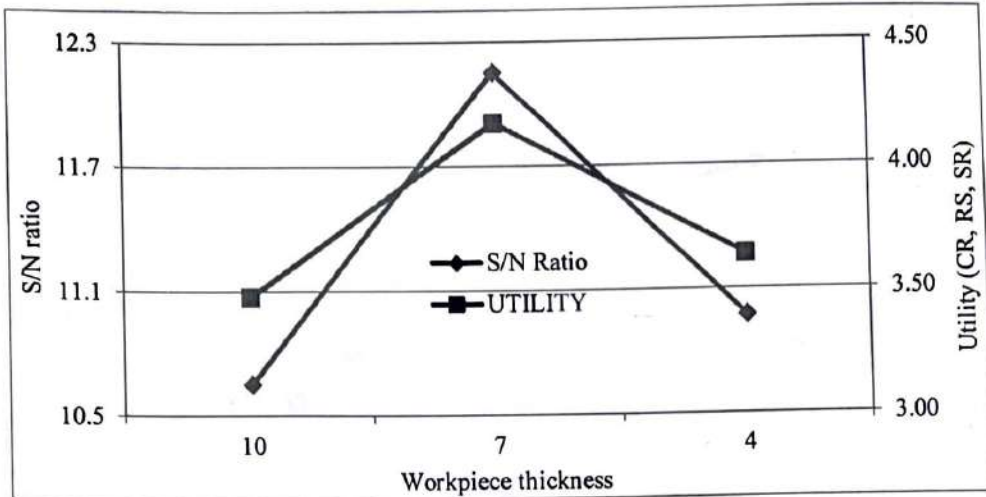


Fig. 9.6 Effect of Workpiece thickness on S/N ratio and Utility

The data from Table 9.4 and 9.5 were plotted in Figures 9.1-9.6. It is clear from the Figure 9.1 that discontinuous vibration increase the overall utility of Hybrid-WEDM process. Whereas, the utility fo the proposed process is maximum for second level of amplitude of vibration as indicated in Figure 9.2. The peak current and duty cycle increase the cutting rate but decrease the utility function. It is clear for Figure 9.3 and 9.4 that the best utility was obtained at first level of peak current and duty cycle. Although the involvement of wire feed rate for the performance of Hybrid-WEDM was negligible but the higher level of wire feed rate desired to obtain maximum utility as shown in Figure 9.5. The utility function is uncertain under workpiece thickness. In Figure 9.6 the maximum utility is attained at second level of workpiece thickness.

## CONCLUSION AND SCOPE OF FUTURE WORK

The investigation into Hybrid-EDM process for exploring the opportunity of enhancement in normal Wire-EDM process usefulness by applying continuous and discontinuous vibrations have lead to useful results. This Hybrid-WEDM process suggested in this research effort can be measured as one of the significant processes in the field of machining of tools and dies with precision and finishing of components. The experimental details are discussed in section 10.1; the significant conclusions from this research work are programmed in section 10.2. Section 10.3 presents the scope for further work that may be supportive to the manufactures, customer and the researchers occupied in this expertise.

### 10.1. Experimental Details:

Experiments have been conducted to investigate cutting rate(CR), Residual Stress (RS) and Surface roughness (SR) under a wide range (Table 10.1) of machining parameters such as type of vibration (continuous and discontinuous), amplitude of vibration, peak current, duty cycle, wire feed rate and workpiece thickness. The effects of continuous and discontinuous vibration assisted Wire-EDM were explored for high Carbon high Chromium D2 steel as workpiece.

Table 10.1 Taguchi Methodology (Phase-II)

Factors	Parameters	Unit	Levels		
			Level 1	Level 2	Level 3
A	Type of Vibration	-	Continuous	Discontinues	-
B	Amplitude of Work piece Vibration	$\mu\text{m}$	10	14	18
C	Peak Current	Amp	100	140	180
D	Duty Cycle(Pulse off Time)	%	66%	72%	78%
E	Thickness of wok piece	mm	10	7	4
F	Wire Feed Rate	mm/min	5	8	11

The L18 orthogonal array depended on Taguchi design was used to perform a succession of experiments and the investigational data was statistically evaluated by Analysis of Variance (ANOVA). The confirmation experiments were performed

which were found within 95% confidence interval. Finally, the process parameters were optimized for maximum CR, minimum RS and minimum SR in addition to utility factor and investigation of surface morphology.

Response surface methodology (RSM) was functional for developing the mathematical models in the outward appearance of multiple regression equations correlating the dependent parameters with the autonomous parameters. Metal removal rate (MRR) and Surface roughness (SR) were investigated under a wide range (Table 10.2) of machining parameters such as pulse-on time, pulse off time, amplitude of vibration and Wire feed rate of and high Carbon high Chromium D3 steel. Utilizing the proposed model equations, the response surfaces have been designed to study the possessions of process parameters on the concert characteristics such as MRR and SR. From the experimental data of RSM, experimental models were developed and the authentication experiments were performed, which were found within 95% confidence interval.

Table 10.2 Response Surface Methodology (Phase-III)

S.N	Symbol	Parameters	Units	Levels					Code d values
				(-2)	(-1)	(0)	(+1)	(+2)	
1	B	Peak Current	A	100	105	110	115	120	Real Value s
2	C	Pulse on Time	μs	70	90	110	130	150	
3	D	Pulse off Time	μs	52	49	46	43	40	
4	A	Amplitude of Vibration	μm	0	6	12	18	24	
5	E	Wire Feed Rate	mm/min	0	6	12	18	24	

The outcomes in light of RSM were discovered like that of Taguchi's strategy and were more enlightening and wide range of spectrum. There was better perception of the performance characteristics because of 3-D graphs visualization in RSM, where as there was no such portrayal of the performance characteristics through Taguchi's approach. Besides, it is conceivable to get relapse conditions connecting the regression equations with the autonomous factors through RSM which was impractical through Taguchi's method.

From equation 9.11,  $CI_{CE} = \pm 0.98$

The predicted optimal range (for conformation runs of three experiments) for CR is given by  $CI_{CE}: 3.01 < \mu_{CR} < 4.97$

b) Residual Stresses:

$$\mu_{RS} = A2 + B2 - \bar{T} = 194.62$$

Where  $A2 = 215.59$ ,  $B2 = 207.83$  from (Table 9.5):  $T_{RS} = 228.80$  (Table 9.2)

The following values have been obtained by the ANOVA:

$N = 54$ ,  $f_e = 42$ ;  $v_e = 1016.052$ ,  $n_{eff} = 4.5$ ,  $R = 3$ ,  $F_{0.05}(1, 42) = 4.0764$

From equation 9.11,  $CI_{CE} = \pm 48.16$

The predicted optimal range (for conformation runs of three experiments) for Residual stresses is given by  $CI_{CE}: 146.46 < \mu_{RS} < 242.78$

c) Surface Roughness:

$$\mu_{SR} = A2 + B2 - \bar{T} = 1.93$$

Where  $A2 = 2.03$ ,  $B2 = 2.22$  (Table 9.5):  $T_{SR} = 2.32$  (Table 9.2)

The following values have been obtained by the ANOVA:

$N = 54$ ,  $f_e = 42$ ;  $v_e = 0.08$ ,  $n_{eff} = 4.5$ ,  $R = 3$ ,  $F_{0.05}(1, 42) = 4.0764$

From equation 9.11,  $CI_{CE} = \pm 0.43$

The predicted optimal range (for conformation runs of three experiments) for SR is given by  $CI_{CE}: 1.50 < \mu_{SR} < 2.36$

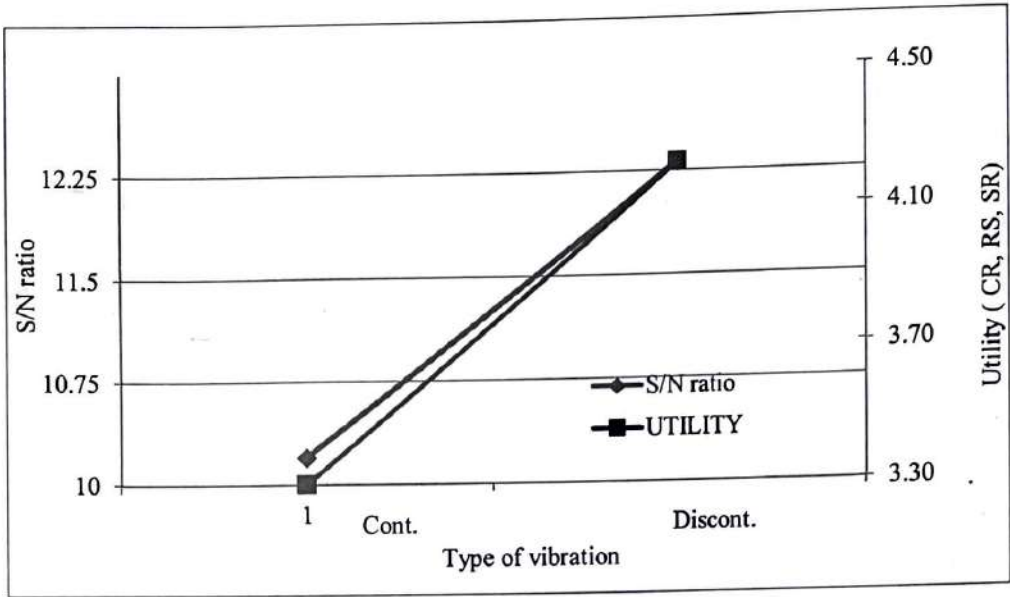


Figure. 9.1 Effect of Type of Vibration on S/N ratio and Utility

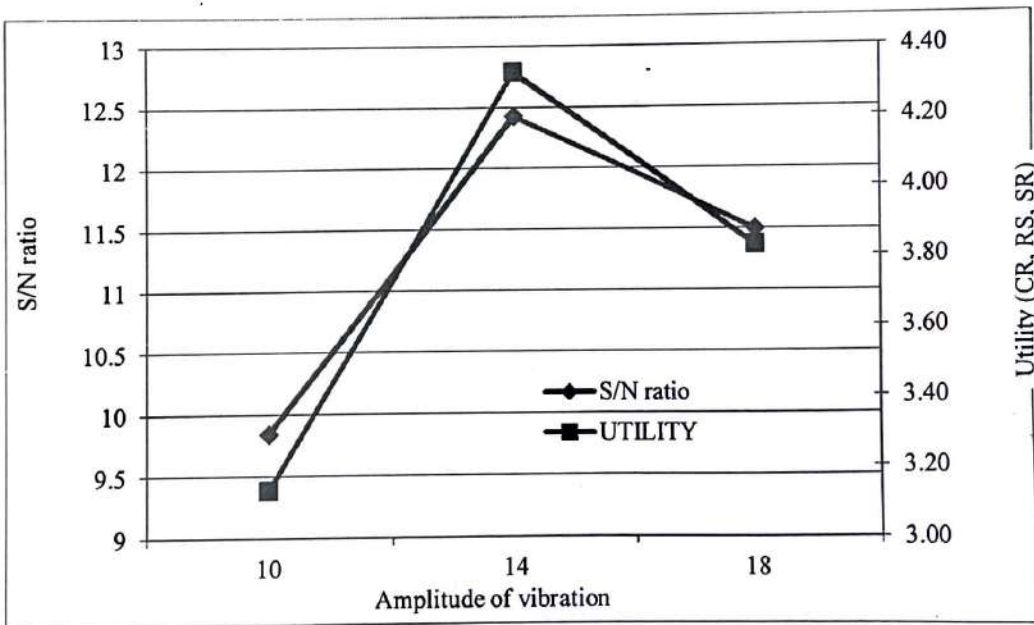


Fig. 9.2 Effect of Amplitude of Vibration on S/N ratio and Utility

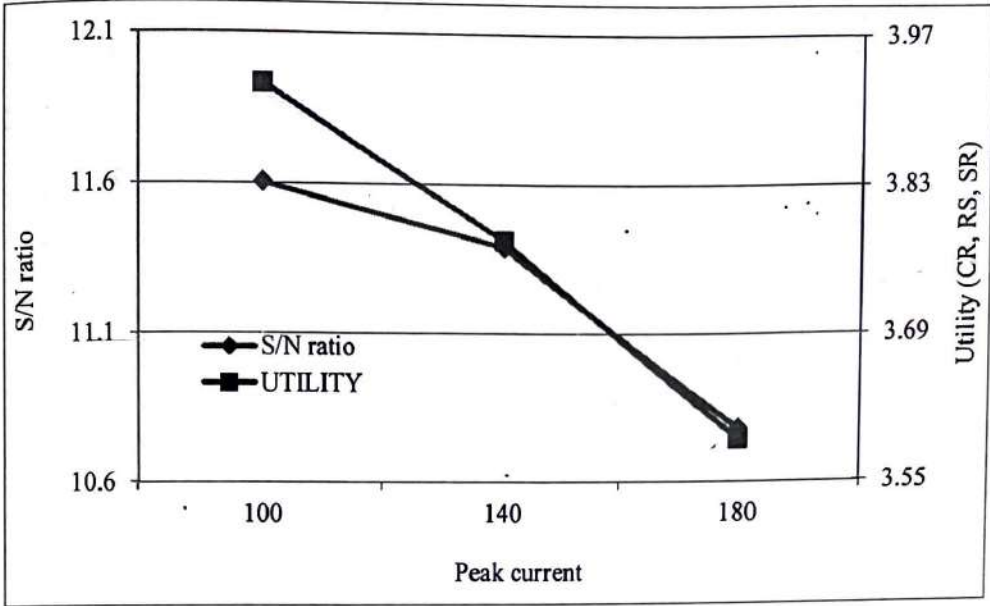


Fig. 9.3 Effect of Peak current on S/N ratio and Utility

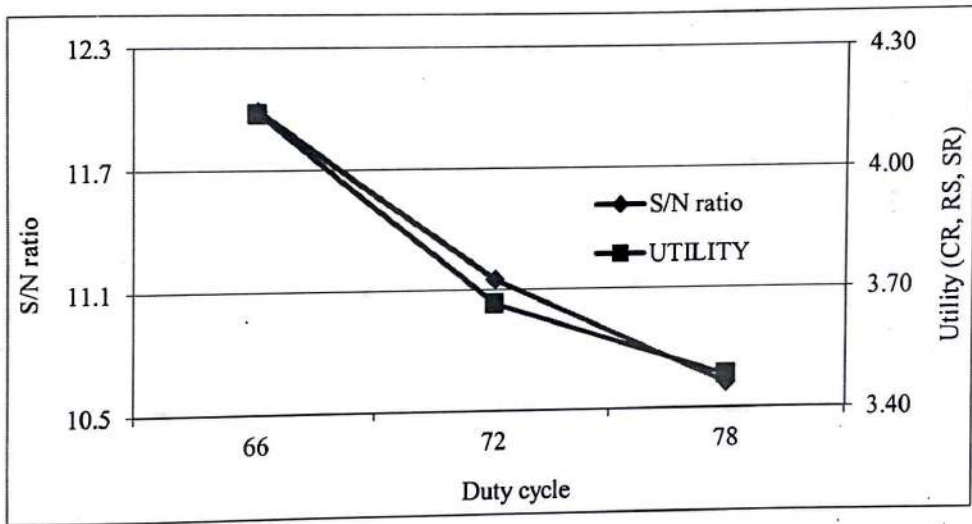


Fig. 9.4 Effect of Duty cycle on S/N ratio and Utility

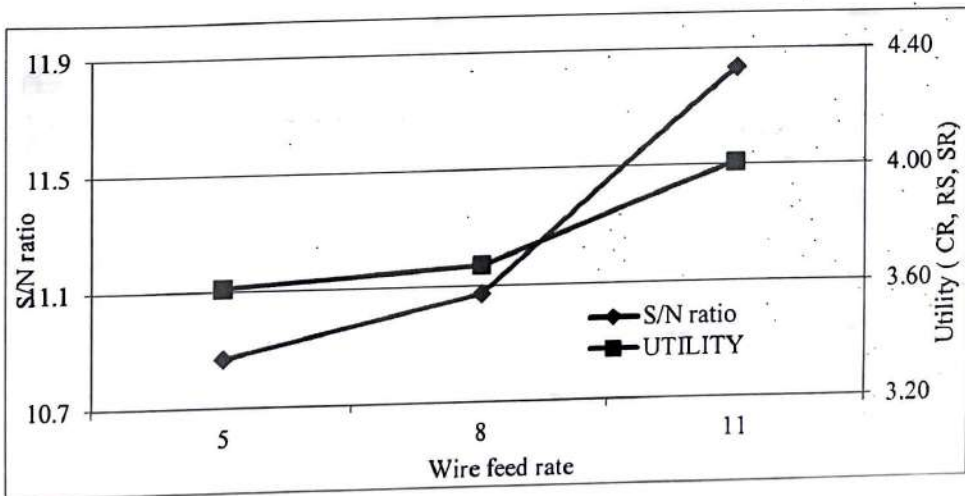


Fig. 9.5 Effect of Wire feed rate on S/N ratio and Utility



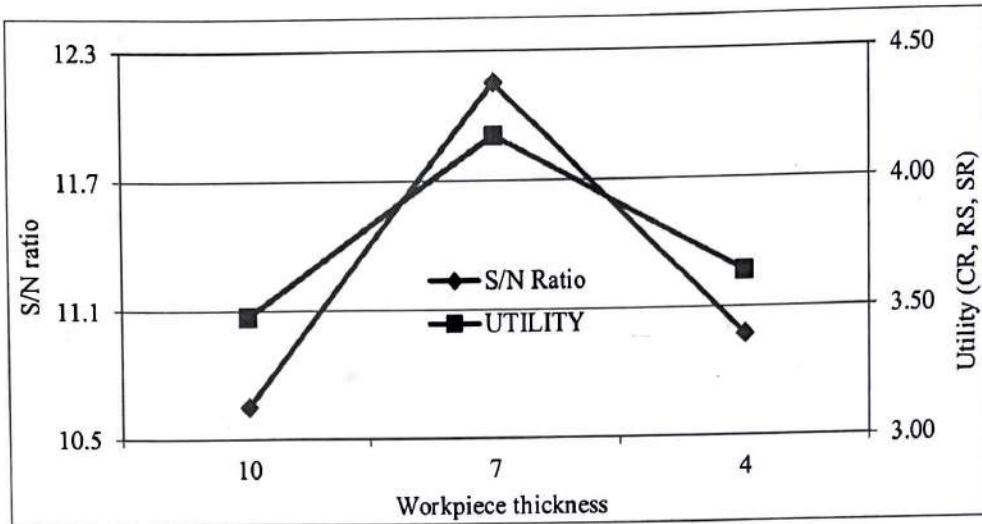


Fig. 9.6 Effect of Workpiece thickness on S/N ratio and Utility

The data from Table 9.4 and 9.5 were plotted in Figures 9.1-9.6. It is clear from the Figure 9.1 that discontinuous vibration increase the overall utility of Hybrid-WEDM process. Whereas, the utility fo the proposed process is maximum for second level of amplitude of vibration as indicated in Figure 9.2. The peak current and duty cycle increase the cutting rate but decrease the utility function. It is clear for Figure 9.3 and 9.4 that the best utility was obtained at first level of peak current and duty cycle. Although the involvement of wire feed rate for the performance of Hybrid-WEDM was negligible but the higher level of wire feed rate desired to obtain maximum utility as shown in Figure 9.5. The utility function is uncertain under workpiece thickness. In Figure 9.6 the maximum utility is attained at second level of workpiece thickness.

## CONCLUSION AND SCOPE OF FUTURE WORK

The investigation into Hybrid-EDM process for exploring the opportunity of enhancement in normal Wire-EDM process usefulness by applying continuous and discontinuous vibrations have lead to useful results. This Hybrid-WEDM process suggested in this research effort can be measured as one of the significant processes in the field of machining of tools and dies with precision and finishing of components. The experimental details are discussed in section 10.1; the significant conclusions from this research work are programmed in section 10.2. Section 10.3 presents the scope for further work that may be supportive to the manufactures, customer and the researchers occupied in this expertise.

### 10.1. Experimental Details:

Experiments have been conducted to investigate cutting rate(CR), Residual Stress (RS) and Surface roughness (SR) under a wide range (Table 10.1) of machining parameters such as type of vibration (continuous and discontinuous), amplitude of vibration, peak current, duty cycle, wire feed rate and workpiece thickness. The effects of continuous and discontinuous vibration assisted Wire-EDM were explored for high Carbon high Chromium D2 steel as workpiece.

Table 10.1 Taguchi Methodology (Phase-II)

Factors	Parameters	Unit	Levels		
			Level 1	Level 2	Level 3
A	Type of Vibration	-	Continuous	Discontinues	-
B	Amplitude of Work piece Vibration	$\mu\text{m}$	10	14	18
C	Peak Current	Amp	100	140	180
D	Duty Cycle(Pulse off Time)	%	66%	72%	78%
E	Thickness of wok piece	mm	10	7	4
F	Wire Feed Rate	mm/min	5	8	11

The L18 orthogonal array depended on Taguchi design was used to perform a succession of experiments and the investigational data was statistically evaluated by Analysis of Variance (ANOVA). The confirmation experiments were performed

which were found within 95% confidence interval. Finally, the process parameters were optimized for maximum CR, minimum RS and minimum SR in addition to utility factor and investigation of surface morphology.

Response surface methodology (RSM) was functional for developing the mathematical models in the outward appearance of multiple regression equations correlating the dependent parameters with the autonomous parameters. Metal removal rate (MRR) and Surface roughness (SR) were investigated under a wide range (Table 10.2) of machining parameters such as pulse-on time, pulse off time, amplitude of vibration and Wire feed rate of and high Carbon high Chromium D3 steel. Utilizing the proposed model equations, the response surfaces have been designed to study the possessions of process parameters on the concert characteristics such as MRR and SR. From the experimental data of RSM, experimental models were developed and the authentication experiments were performed, which were found within 95% confidence interval.

Table 10.2 Response Surface Methodology (Phase-III)

S.N	Symbol	Parameters	Units	Levels					Code d value s
				(-2)	(-1)	(0)	(+1)	(+2)	
1	B	Peak Current	A	100	105	110	115	120	Real Value s
2	C	Pulse on Time	μs	70	90	110	130	150	
3	D	Pulse off Time	μs	52	49	46	43	40	
4	A	Amplitude of Vibration	μm	0	6	12	18	24	
5	E	Wire Feed Rate	mm/min	0	6	12	18	24	

The outcomes in light of RSM were discovered like that of Taguchi's strategy and were more enlightening and wide range of spectrum. There was better perception of the performance characteristics because of 3-D graphs visualization in RSM, where as there was no such portrayal of the performance characteristics through Taguchi's approach. Besides, it is conceivable to get relapse conditions connecting the regression equations with the autonomous factors through RSM which was impractical through Taguchi's method.

## 10.2. Conclusion:

Some of the major contributions of this research work are as follows:

- It was evident that the amplitude of vibration is significant parameters to achieve the flushing of contaminated dielectric by pumping and stirring action which ultimately enhances evacuation of debris and gas bubbles from gap.
- The enormous numerical estimation of the performance index for Hybrid-EDM process is  $3.28647 \times 10^{18}$ . As the coefficient of variable for this process is high that demonstrates the noteworthiness of the variables considered for performance Index.
- The coefficient of variable for surface morphology and flushing is underneath 20% that show that ultrasonic vibration conferred to this proposed process clearly enhance the flushing, surface morphology and dimensional accuracy.
- Cavitation and Abnormal discharge's coefficient of variable is high and these attributes were less investigated by the researchers in literature, yet influence the performance index fundamentally.
- The digraph representation shows complex interdependency of variables and sub elements, cavitation influences every other component and corresponding coefficient of variable for this is high it deciphers very noteworthy element in this process. In any case, the specialized impediments restrain its appropriateness in this process.
- The major limitation is the big numerical value of the performance index.  $16.4901 \times 10^6$  may appear to be an odd figure for practical purposes, but provide a comparison. This could be used to compare the three modes of vibration.
- ISM model developed here in this study highlight the 16 types of drivers and the interactions between these drivers. These variables can further be grouped into four categories using MICMAC analysis
  - Group-I: Ultrasonic Vibration (Ultrasonic field force and Acoustic Pressure)
  - Group-II: Flushing (Pumping action, Stirring effect and Debris and gas bubble debris evacuation)

- Group-III: Normal Discharge (Discharge wave Distribution, Debris concentration and Arching & short circuit)
  - Group IV: Surface Morphology (surface Roughness, Thickness of recast layer & heat)
- From the MICMAC analysis, there is no such driver that has weak dependence and weak driving power as no drivers is mapped in sector I. Next, the Group IV variables (Surface Morphology) i.e. surface Roughness, Thickness of recast layer & heat affected zone, Micro-hardness, Size of Micro- cracks & holes and Residual stresses drivers are found to have weak driving power and strong dependence power so it maps to sector II. The drivers such as discharge wave distribution, Debris concentration, Arching & short circuit MRR, TWR and acoustic pressure are found to have strong driving power and strong dependence power so they map to sector III.
  - These drivers are unstable due to the fact that any change occurring to them will affect other drivers. Pumping action, Stirring effect and Debris, Gas bubble debris evacuation and Ultrasonic field force drivers posses strong driving power and weak dependence power so they map to sector IV. The scientific model proposed in this study can be utilized to add to a suitable speculation for the execution of ultrasonic vibration in Hybrid-WEDM process in view of the legacy and interdependency of various proposed variables.
  - Mathematical regression equation obtained for surface roughness for Hybrid-WEDM is:  

$$\text{Surface Roughness} = 23.75414 - 0.021477 \text{ Peak current} - 0.239119 \text{ Pulse on Time} - 0.232794 \text{ Pulse off Time} - 0.219340 \text{ Amplitude of Vibration} - 0.548229 \text{ Wire Feed Rate} + 0.000339 \text{ Peak current} * \text{ Pulse on Time} - 0.000518 \text{ Peak current} * \text{ Pulse off Time} + 0.001120 \text{ Pulse on Time} * \text{ Amplitude of Vibration} + 0.002109 \text{ Pulse on Time} * \text{ Wire Feed Rate} + 0.001901 \text{ Pulse off Time} * \text{ Amplitude of Vibration} + 0.006849 \text{ Pulse off Time} * \text{ Wire Feed Rate} + 0.000074 \text{ Peak current}^2 + 0.000878 \text{ Pulse on Time}^2 + 0.001918 \text{ Pulse off Time}^2$$
  - Mathematical regression equation obtained for material removal rate for Hybrid-WEDM is:

$$\text{Material Removal Rate} = - 405.30016 + 0.214333 \text{ Peak current} + 4.49704 \text{ Pulse on Time} + 6.66100 \text{ Pulse off Time} + 0.684425 \text{ Amplitude of vibration} - 0.520675 \text{ Wire Feed Rate} + 0.003593 \text{ Peak current} * \text{ Pulse on Time} - 0.005579 \text{ Peak current} * \text{ Pulse off Time} + 0.067435 \text{ Pulse off Time} * \text{ Wire Feed Rate} - 0.000993 \text{ Peak current}^2 - 0.020797 \text{ Pulse on Time}^2 - 0.076433 \text{ Pulse off Time}^2 - 0.012173 \text{ Amplitude of Vibration}^2 - 0.163888 \text{ Wire Feed Rate}^2$$

- The individual desirability value for MRR and SR is 0.703572 and 0.887744 respectively. SR is more desirable than MRR. The overall combined desirability for Hybrid-WEDM performance characteristics is 0.790311.
- The residual stresses estimations were made on high carbon, high chromium D2 and D3 steel and all the residual stresses readings were observed tensile in nature. The higher erosion rate attained by the workpiece ultrasonic vibration was attributed to enchantment in dielectric dissemination.
- The residual stresses were lower in discontinuous vibration as a contrast with continuous vibration. Discontinuous vibration gave adequate time traverse to attain normal steady state discharge condition, and furthermore enabled additional inertial forces to evacuate the debris and gas bubbles from the wire electrode and the work piece discharge gap. The efficient ejection of molten metal developed from the machined surface likewise brought about lesser remaining residual stresses.
- When high amplitude vertical ultrasonic vibration is applied to work piece through the proposed cantilever arrangement, causes strong scavenging effect of contaminated dielectric fluid rather than simple oscillation. That not only charges the gap with fresh dielectric but also allows cooling of machined surface.
- This cantilever arrangement provides comparatively high acceleration to debris and gas bubble to evacuate than that of the ultrasonic wave transferred perpendicular to the machined surface due to cyclic spatial variation and pressure gradient.
- Although, higher amplitude is desired to create a strong string effect in the discharge gap by producing large pressure gradient to enhance flushing. When amplitude of vibration increased beyond 14 $\mu$ m has negative effects on response. This is caused by the insufficient time interval to clear the gap from

contaminated. A noteworthy contrast is seen in the surface integrity while machining with continuous and discontinuous ultrasonic vibration helped Wire EDM.

- The most favourable significance of process parameters for the envisaged range of optimal Residual stress were like so: Type of Vibration (A, 2<sup>nd</sup> level), Amplitude of Vibration (B, 2<sup>nd</sup> level) = 14 $\mu$ m, Peak Current (E, 1<sup>st</sup> level) = 100 Amp., Duty cycle (F, 1<sup>st</sup> level) = 66%, Workpiece Thickness (C, 2<sup>nd</sup> level) = 7mm and Wire feed rate (D, 3<sup>rd</sup> level) = 11 mm/min.
- The most favourable significance of process parameters for the envisaged range of optimal material erosion rate were as follows: Type of Vibration (A, 2<sup>nd</sup> level) = discontinuous, Amplitude of Vibration (B, 2<sup>nd</sup> level) = 14 $\mu$ m, Peak Current (E, 3<sup>rd</sup> level) = 180 Amp., Duty cycle (F, 3<sup>rd</sup> level) = 78%, Workpiece Thickness (E, 3<sup>rd</sup> level) = 4 mm and Wire feed rate (D, 2<sup>nd</sup> level) = 8 mm/min.

### 10.3. Limitation and scope for future work :

- The resonance is a crucial problem in ultrasonic vibration actuators. It produces huge noise that hinders in the successful implementation of UV action.
- At exorbitantly high amplitude, the expansion in various cavitation air bubbles may hinder the dielectric liquid from streaming into the discharge region. This wonder influences the machining to process unstable, prompting the decrease of material erosion rate.
- Ultrasonic vibration reduced the ignition delay which generated a coarser surface and increase in electrode wear rate. Also, acoustic cavitations lead to larger over cut.
- Ultrasonic vibration has been applied for quantitative analysis with quantitatively controllable parameters, not for qualitative parameters.
- The performance of Hybrid-WEDM is difficult to evaluate because of the complex inter-relationships among quantitative and qualitative factors.

## REFERENCES

- Abdullah, A., Shabgard, M.R., 2008. Effect of ultrasonic vibration of tool on electrical discharge machining of cemented tungsten carbide (WC-Co). *Int. J. Adv. Manuf. Technol.* 38, 1137–1147. <https://doi.org/10.1007/s00170-007-1168-8>
- Abdullah, A., Shabgard, M.R., Ivanov, A., Shervanyi-Tabar, M.T., 2009. Effect of ultrasonic-assisted EDM on the surface integrity of cemented tungsten carbide (WC-Co). *Int. J. Adv. Manuf. Technol.* 41, 268–280. <https://doi.org/10.1007/s00170-008-1476-7>
- Agrawal, S., Singh, R.K., Murtaza, Q., 2016. Outsourcing decisions in reverse logistics: sustainable balanced scorecard and graph theoretic approach. *Resour. Conserv. Recycl.* 108, 41–53.
- Akhazarova, S., Kafarov, V., 1982. In: *Experiment optimization in chemistry and chemical engineering*. Moscow: Mir Publishers. Mir Publishers, Moscow in Russian.
- Attri, R., Grover, S., 2015. Contextual relationship among the quality enabled factors of inventory control system stage. *Int. J. Recent Adv. Mech. Eng.* 4, 45–57.
- B. Bhattacharyya, B.N. Doloi, S.K.S., 1999. Study of electrochemical discharge machining technology for slicing non-conductive brittle materials. *J. Mater. Process. Technol.* 50, 338–343. <https://doi.org/10.1016/j.jmachtools.2009.09.004>
- Barker, T.B., 1990. *Engineering quality by design: interpreting the Taguchi approach*. CRC Press.
- Basak, I., Ghosh, A., 1997. Mechanism of material removal in electrochemical discharge machining: a theoretical model and experimental verification. *J. Mater. Process. Technol.* 71, 350–359. [https://doi.org/10.1016/S0924-0136\(97\)00097-6](https://doi.org/10.1016/S0924-0136(97)00097-6)
- Box, G.E.P., Hunter, J.S., 1957. Multi-Factor Experimental Designs for Exploring Response Surfaces. *Ann. Math. Stat.* 28, 195–241. <https://doi.org/10.1214/aoms/1177707047>
- Bunday, B.D., Hines, W.W., Montgomery, D.C., 1981. *Probability and Statistics in Engineering and Management Science*. 2nd Edition. *Appl. Stat.* <https://doi.org/10.2307/2346359>
- Byrne, D.M., Taguchi, S., 1986. The Taguchi Approach to Parameter Design. *Asqc* 20, 168–177.
- Cao, M.R., Wang, Y.Q., Yang, S.Q., Li, W.H., 2009. Experimental and Mechanism Research on EDM Combined with Magnetic Field. *Key Eng. Mater.* 416, 337–341. <https://doi.org/10.4028/www.scientific.net/KEM.416.337>
- Chen, Y.F., Lin, Y.C., 2009. Surface modifications of Al-Zn-Mg alloy using combined EDM with ultrasonic machining and addition of TiC particles into the dielectric. *J. Mater. Process. Technol.* 209, 4343–4350. <https://doi.org/10.1016/j.jmatprotec.2008.11.013>
- Chugh, S., Goyal, S., Kumar, S., 2015. Parameter Optimization of Wire EDM using Low Frequency Vibrations. *Invertis J. Sci. Technol.* 1, 119–124.
- Corporation, A.E., n.d. Precision fasthole and micohole EDM drilling [WWW Document]. URL <http://aaedmcorp.com/applications.html>
- Deo, N., 2017. *Graph theory with applications to engineering and computer science*. Courier Dover Publications.
- Dubey, A.K., 2008. Multi-response optimization of electro-chemical honing process using utility-based Taguchi approach. *Int. J. Adv. Manuf. Technol.*



- Egashira, K., Masuzawa, T., 1999. Microultrasonic machining by the application of workpiece vibration. *CIRP Ann. - Manuf. Technol.* 48, 131–134. [https://doi.org/10.1016/S0007-8506\(07\)63148-5](https://doi.org/10.1016/S0007-8506(07)63148-5)
- Gandhi, O.P., Agrawal, V.P., 1994. A digraph approach to system wear evaluation and analysis. *J. Tribol.* 116, 268–274.
- Gao, C., Liu, Z., 2003. A study of ultrasonically aided micro-electrical-discharge machining by the application of workpiece vibration. *J. Mater. Process. Technol.* 139, 226–228. [https://doi.org/10.1016/S0924-0136\(03\)00224-3](https://doi.org/10.1016/S0924-0136(03)00224-3)
- Garn, R., Schubert, A., Zeidler, H., 2011. Analysis of the effect of vibrations on the micro-EDM process at the workpiece surface. *Precis. Eng.* 35, 364–368. <https://doi.org/10.1016/j.precisioneng.2010.09.015>
- Ghiculescu, D., Marinescu, N., Nanu, S., 2014. Innovative Solutions for Performances Increase At Micro-.
- Ghiculescu, D., Marinescu, N.I., Nanu, S., Ghiculescu, D., 2012. Multiphysics 3D Finite Element Modelling of Micro- Electrodischarge Machining Aided by Ultrasonics 72–77.
- Ghoreishi, M., Atkinson, J., 2002. A comparative experimental study of machining characteristics in vibratory, rotary and vibro-rotary electro-discharge machining. *J. Mater. Process. Technol.* 120, 374–384. [https://doi.org/10.1016/S0924-0136\(01\)01160-8](https://doi.org/10.1016/S0924-0136(01)01160-8)
- Govindan, K., Kannan, D., Haq, A.N., 2010. Analysing supplier development criteria for an automobile industry. *Ind. Manag. Data Syst.* 110, 43–62.
- Grover, S., Agrawal, V.P., Khan, I.A., 2006. Role of human factors in TQM: a graph theoretic approach. *Benchmarking An Int. J.* 13, 447–468. <https://doi.org/10.1108/14635770610676290>
- Grover, S., Agrawal, V.P., Khan, I.A., 2004. A digraph approach to TQM evaluation of an industry. *Int. J. Prod. Res.* 42, 4031–4053. <https://doi.org/10.1080/00207540410001704032>
- Guo, Z.N., Lee, T.C., Yue, T.M., Lau, W.S., 1997. Study on the machining mechanism of WEDM with ultrasonic Vibration of the Wire. *J. Mater. Process. Technol.* 69, 212–221.
- Guo, Z.N., Lee, T.C., Yue, T.M., Lau, W.S., 1995. A Study of Ultrasonic-aided Wire Electrical Discharge Machining. *Jornal Mater. Process. Tech.* 63, 823–828.
- Gupta, V., Murthy, P., 1980. *An Introduction to Engineering Design Method*. Tata McGraw-Hill, New Delhi.
- Guu, Y. H., Hocheng, H., 2001. Effect of workpiece rotation on Machinability during electric discharge machining. *Mater. Manuf. Process.* 16, 91–101.
- Han, G.C., Soo, S.L., Aspinwall, D.K., Bhaduri, D., 2013. Research on the Ultrasonic Assisted WEDM of Ti-6Al-4V. *Adv. Mater. Res.* 797, 315–319. <https://doi.org/10.4028/www.scientific.net/AMR.797.315>
- Hassan Abdel Gawad El-Hofy, 2005. *Advanced Machining Processes; Non Traditional and Hybrid Machining Processes*, McGraw-Hill, Mechanical Engineering Series. <https://doi.org/10.1088/1751-8113/44/8/085201>
- Ho, K.H., Newman, S.T., Rahimifard, S., Allen, R.D., 2004. State of the art in wire electrical discharge machining {(WEDM)}. *Int. J. Mach. Tool. Manufact.* 44, 1247–1259.

<https://doi.org/10.1016/j.ijmachtools.2004.04.017>

- Hoang, K.T., Yang, S.H., 2013. A study on the effect of different vibration-assisted methods in micro-WEDM. *J. Mater. Process. Technol.* 213, 1616–1622. <https://doi.org/10.1016/j.jmatprotec.2013.03.025>
- Huang, H., Zhang, H., Zhou, L., Zheng, H.Y., 2003. Ultrasonic vibration assisted electro-discharge machining of microholes in Nitinol. *J. Micromechanics Microengineering* 13, 693.
- Ichikawa, T., Natsu, W., 2013. Realization of micro-EDM under ultra-small discharge energy by applying ultrasonic vibration to machining fluid. *Procedia CIRP* 6, 326–331. <https://doi.org/10.1016/j.procir.2013.03.094>
- Iwai, M., Ninomiya, S., Suzuki, K., 2013. Improvement of EDM properties of PCD with electrode vibrated by ultrasonic transducer. *Procedia CIRP* 6, 146–150. <https://doi.org/10.1016/j.procir.2013.03.070>
- Jameson, E.C., 2001. Electrical Discharge Machining. <https://doi.org/10.2493/jjspe.75.68>
- Jangra, K., Jain, A., Grover, S., 2010. Optimization of multiple-machining characteristics in wire electrical discharge machining of punching die using Grey relational analysis. *J. Sci. Ind. Res. (India)*. 69, 606–612.
- Jawalkar, C.S., Sharma, A.K., Kumar, P., Variable, D.C., 2012. Micromachining with ECDM: Research Potentials and Experimental Investigations. *World Acad. Sci. Eng. Technol.* 61, 90–95.
- Ji, R., Liu, Y., Zhang, Y., Cai, B., Li, X., Zheng, C., 2013. Effect of machining parameters on surface integrity of silicon carbide ceramic using end electric discharge milling and mechanical grinding hybrid machining. *J. Mech. Sci. Technol.* 27, 177–183. <https://doi.org/10.1007/s12206-012-1215-8>
- Jurkat, W.B., Ryser, H.J., 1966. Matrix factorizations of determinants and permanents. *J. Algebr.* 3, 1–27.
- Kansal, H.K., Singh, S., Kumar, P., 2007. Technology and research developments in powder mixed electric discharge machining (PMEDM). *J. Mater. Process. Technol.* 184, 32–41. <https://doi.org/10.1016/j.jmatprotec.2006.10.046>
- Kavtaradze, O. N., Lipchanskii, A. B., & Nechaev, G.G., 1989. ibration of wire electrode during electro erosion machining with the superposition of ultrasonic vibrations. *Sov Surf Eng Appl Electrochem* 4, 13–17.
- Kei-Lin, K.U.O., 2009. Ultrasonic vibrating system design and tool analysis. *Trans. Nonferrous Met. Soc. China* 19, s225--s231.
- Khosrozadeh, B., Shabgard, M., 2017. Effects of hybrid electrical discharge machining processes on surface integrity and residual stresses of Ti-6Al-4V titanium alloy. *Int. J. Adv. Manuf. Technol.* 93, 1999–2011. <https://doi.org/10.1007/s00170-017-0601-x>
- Kim, D.J., Yi, S.M., Lee, Y.S., Chu, C.N., 2006. Straight hole micro EDM with a cylindrical tool using a variable capacitance method accompanied by ultrasonic vibration. *J. OF Micro Mechanics and Micro Engineering* 16, 1092–1097. <https://doi.org/10.1088/0960-1317/16/5/031>
- Kozak, J., Rajurkar, K.P., 2001. Hybrid machining process evaluation and development, in: *Proceedings of the 2nd International Conference on Machining and Measurement of Sculptured*

- Surfaces. Krakow, pp. 501–536.
- Kremer, D., Lebrun, J.L., Hosari, B., Moisan, A., Paris, E.N.S.A.M., 1989. Effects of Ultrasonic Vibrations on the Performances in EDM. *Ann. CIRP* 38, 199–202.
- Kremer, D., Lhiaubet, C., Moisan, A., 1991. A Study of the Effect of Synchronizing Ultrasonic Vibrations with Pulses in EDM. *CIRP Ann. - Manuf. Technol.* 40, 211–214. [https://doi.org/10.1016/S0007-8506\(07\)61970-2](https://doi.org/10.1016/S0007-8506(07)61970-2)
- Kulkarni, A., Sharan, R., Lal, G.K., 2002. An experimental study of discharge mechanism in electrochemical discharge machining. *Int. J. Mach. Tools Manuf.* 42, 1121–1127. [https://doi.org/10.1016/S0890-6955\(02\)00058-5](https://doi.org/10.1016/S0890-6955(02)00058-5)
- Kulkarni, A. V., 2007. Electrochemical Discharge Machining Process. *Def. Sci. J.* 57, 765–770. <https://doi.org/10.14429/dsj.64.1812>
- Kumar, A., Kumar, V., Kumar, J., 2016. Surface crack density and recast layer thickness analysis in WEDM process through response surface methodology. *Mach. Sci. Technol.* 20, 201–230. <https://doi.org/10.1080/10910344.2016.1165835>
- Kumar, S., Grover, S., Walia, R.S., 2018. Effect of hybrid wire EDM conditions on generation of residual stresses in machining of HCHCr D2 tool steel under ultrasonic vibration. *Int. J. Interact. Des. Manuf.* 1–19. <https://doi.org/10.1007/s12008-018-0474-8>
- Kumar, S., Grover, S., Walia, R.S., 2017a. Analyzing and modeling the performance index of ultrasonic vibration assisted EDM using graph theory and matrix approach. *Int. J. Interact. Des. Manuf.* 12, 225–242. <https://doi.org/10.1007/s12008-016-0355-y>
- Kumar, S., Grover, S., Walia, R.S., 2017b. Analyzing and modeling the performance index of ultrasonic vibration assisted EDM using graph theory and matrix approach. *Int. J. Interact. Des. Manuf.* 12, 225–242. <https://doi.org/10.1007/s12008-016-0355-y>
- Kumar, S., Grover, S., Walia, R.S., 2016. Optimisation strategies in ultrasonic vibration assisted electrical discharge machining: a review. *Int. J. Precis. Technol.* 7, 51–83. <https://doi.org/10.1504/IJPTECH.2017.084557>
- Kumar, S., Meenu, Satsangi, P.S., Sardana, H.K., 2012. Optimization of surface roughness in turning unidirectional glass fiber reinforced plastics (UD-GFRP) composites using polycrystalline diamond (PCD) cutting tool. *Indian J. Eng. Mater. Sci.* 19, 163–174.
- Kuo, C., Huang, J., 2003. Fabrication of 3D Metal Microstructures Using a Hybrid Process of Micro-EDM and Laser Assembly. *Int. Journ. Adv. Manufac. Tech.* 21, 796–800.
- Kuo, K.L., 2009. Ultrasonic vibrating system design and tool analysis. *Trans. Nonferrous Met. Soc. China (English Ed.)* 19. [https://doi.org/10.1016/S1003-6326\(10\)60275-0](https://doi.org/10.1016/S1003-6326(10)60275-0)
- Kwan, K. M., Benatar, A., 2001. Modeling of Ultrasonic Forced Wetting Process by Dimensional Analysis, in: *Annual Technical Conference - ANTEC: Society of Plastics Engineers Annual Technical Papers*. pp. 1239–1243.
- Lazarenko B.R., 1943. *About the Inversion of Metal Erosion and Methods to Fight Ravage of Electric Contacts*. WEI-Institut.
- Lee, T.C.C., Zhang, J.H.H., Lau, W.S.S., 1998. Machining of Engineering Ceramics by Ultrasonic Vibration Assisted EDM Method. *Mater. Manuf. Process.* 13, 133–146.

<https://doi.org/10.1080/10426919808935224>

- Li, L., Diver, C., Atkinson, J., Giedl-Wagner, R., Helml, H.J., 2006. Sequential laser and EDM micro-drilling for next generation fuel injection nozzle manufacture. *CIRP Ann. - Manuf. Technol.* 55, 179–182. [https://doi.org/10.1016/S0007-8506\(07\)60393-X](https://doi.org/10.1016/S0007-8506(07)60393-X)
- Liew, P.J., Yan, J., Kuriyagawa, T., 2014. Fabrication of deep micro-holes in reaction-bonded SiC by ultrasonic cavitation assisted micro-EDM. *Int. J. Mach. Tools Manuf.* 76, 13–20.
- Lin, Y.C., Chen, Y.F., Wang, A.C., Sei, W.L., 2012. Machining performance on hybrid process of abrasive jet machining and electrical discharge machining. *Trans. Nonferrous Met. Soc. China (English Ed.)* 22, s775–s780. [https://doi.org/10.1016/S1003-6326\(12\)61803-2](https://doi.org/10.1016/S1003-6326(12)61803-2)
- Lin, Y.C., Chen, Y.F., Wang, D.A., Lee, H.S., 2009. Optimization of machining parameters in magnetic force assisted EDM based on Taguchi method. *J. Mater. Process. Technol.* 209, 3374–3383. <https://doi.org/10.1016/j.jmatprotec.2008.07.052>
- Lin, Y.C., Yan, B.H., Huang, F.Y., 2001. Surface modification of Al - Zn - Mg aluminum alloy using the combined process of EDM with USM. *Journal Mater. Process. Tech.* 115.
- Lin, Y.C.C., Yan, B.H., Chang, Y.S., 2000. Machining Characteristics of titanium alloy (Ti-6Al-4V) using a combination process of EDM with USM. *J. Mater. Process. Technol.* 104, 171–177. [https://doi.org/10.1016/S0924-0136\(00\)00539-2](https://doi.org/10.1016/S0924-0136(00)00539-2)
- Lipchanskii, A.B., 1991. Experimental investigation of wire electrical discharge machining assisted with ultrasonic vibration. *Sov Surf Eng Appl Electrochem* 1, 5–9.
- Liu, Y., Chang, H., Zhang, W., Sha, Z., Zhang, S., 2018. A Simulation Study of Debris Removal Process in Ultrasonic Vibration Assisted Electrical Discharge Machining ( EDM ) of Deep Holes †. *Micromachines* 9. <https://doi.org/10.3390/mi9080378>
- Lok, Y.K., Lee, T.C., 1997. Materials Processing Technology Processing of Advanced Ceramics Using the Wire-Cut EDM Process. *J Mater Process Technol* 63, 839–843.
- Mahardika, M., Prihandana, G.S., Endo, T., Tsujimoto, T., Matsumoto, N., Arifvianto, B., Mitsui, K., 2012. The parameters evaluation and optimization of polycrystalline diamond micro-electrodischarge machining assisted by electrode tool vibration. *Int. J. Adv. Manuf. Technol.* 60, 985–993. <https://doi.org/10.1007/s00170-011-3674-y>
- Marinescu, N.I., Ghiculescu, D., Jitianu, G., 2009. Solution for Technological performances increasing at ultrasonic aided electrodischarge Machining. *Int. J. Mater. Form.* 2, 681–684. <https://doi.org/10.1007/s12289-009-0585-7>
- Masuzawa, T., Heuvelman, C.J., 1983. A Self-Flushing Method with Spark-Erosion Machining. *Ann. CIRP* 32, 109–111.
- Mediliyegedara, T.K.K.R., De Silva, A.K.M., Harrison, D.K., McGeough, J.A., 2005. New developments in the process control of the hybrid electro chemical discharge machining (ECDM) process. *J. Mater. Process. Technol.* 167, 338–343. <https://doi.org/10.1016/j.jmatprotec.2005.05.043>
- Iseee, J., Fukuzawa, Y., Shigeru, N., Daiki, H., Muttamara, A., 2014. Surface Modification Using EDM Combined Ultrasonic Vibration P32, 1213–1214.
- hri, N., Saito, N., Higashi, M., Kinoshita, N., 1991. A New Process of Finish Machining on Free

- Surface by EDM Methods. *CIRP Ann. - Manuf. Technol.* 40, 207–210.  
[https://doi.org/10.1016/S0007-8506\(07\)61969-6](https://doi.org/10.1016/S0007-8506(07)61969-6)
- Murti, V.S., Philip, P.K., 1987. A comparative analysis of machining characteristics in ultrasonic assisted edm by the response surface methodology. *Int. J. Prod. Res.* 25, 259–272.  
<https://doi.org/10.1080/00207548708919838>
- Muttamara, A., Nakwonga, P., Thongruang, R., 2018. Investigations on Ultrasonic vibration Assisted EDM in Tin Powder Mixed Dielectric 11, 75–79.
- Myers, R. H., & Montgomery, D.H., 1995. *Response surface methodology*. Wiley, New York.
- Nani, V.M., 2017. The ultrasound effect on technological parameters for increase in performances of W-EDM machines. *Int. J. Adv. Manuf. Technol.* 88, 519–528. <https://doi.org/10.1007/s00170-016-8783-1>
- Nanu, A.S., Marinescu, N.I., Ghiculescu, D., 2011. Study on ultrasonic stepped horn geometry design and FEM simulation. *Nonconv. Technol. Rev.* 4, 25–30.
- Narasimhan, J., Yu, Z., Rajurkar, K.P., 2005. Tool wear compensation and path generation in micro and macro EDM. *J. Manuf. Process.* 7, 75–82. [https://doi.org/10.1016/S1526-6125\(05\)70084-0](https://doi.org/10.1016/S1526-6125(05)70084-0)
- Nishiwaki, N., Hori, S., Natsu, W., 2008. Detection of Electric Discharge Machining State By Using Ultrasonic Technique. 17th World Conf. Nondestruct. Test. 25–28.
- Ogawa, H., Hamada, S., Aoyama, T., 2012. Ultrasonic cavitation assisted EDM of CFRP. *Electr. Mach. Technol.* 36, 21–26.
- Pandey, A., Singh, S., 2010. Current research trends in variants of Electrical Discharge Machining: A review *Int. J. Eng. Sci. Technol.* 2, 2172–2191.
- Pandey, Shan, 1983. *Modern Machining Processes*, Journal of Chemical Information and Modeling. Tata McGraw-Hill, New Delhi.
- Pang, Y.L., Abdullah, A.Z., Bhatia, S., 2011. Review on sonochemical methods in the presence of catalysts and chemical additives for treatment of organic pollutants in wastewater. *Desalination* 277, 1–14. <https://doi.org/10.1016/j.desal.2011.04.049>
- Peace, G.S., 1993. *Taguchi methods: a hands-on approach*. Addison-Wesley Reading, MA.
- Peng, W.Y., Liao, Y.S., 2004. Study of electrochemical discharge machining technology for slicing non-conductive brittle materials. *J. Mater. Process. Technol.* 149, 363–369.  
<https://doi.org/10.1016/j.jmatprotec.2003.11.054>
- Peterson, N., Kobayashi, Y., Sanders, P., 2017. Assessment and Validation of Cos $\alpha$  Method for Residual Stress Measurement, in: 13th International Conference on Shot Peening.
- Praneetpong, C., Fukuzawa, Y., Nagasawa, S., Yamashita, K., 2010. Effects of the Edm Combined Ultrasonic Vibration on the Machining Properties of Si<sub>3</sub>N<sub>4</sub>. *Mater. Trans.* 51, 2113–2120.  
<https://doi.org/10.2320/matertrans.M2010194>
- Prihandana, G.S., Mahardika, M., Hamdi, M., Wong, Y.S., Mitsui, K., 2011. Accuracy improvement in nanographite powder-suspended dielectric fluid for micro-electrical discharge machining processes. *Int. J. Adv. Manuf. Technol.* 56, 143–149. <https://doi.org/10.1007/s00170-011-3152-6>
- Prihandana, G.S., Mahardika, M., Hamdi, M., Wong, Y.S., Mitsui, K., 2009. Effect of micro-powder suspension and ultrasonic vibration of dielectric fluid in micro-EDM processes-Taguchi

- approach. *Int. J. Mach. Tools Manuf.* 49, 1035–1041. <https://doi.org/10.1016/j.ijmachtools.2009.06.014>
- Rao, R.V., Gandhi, O.P., 2002. Failure cause analysis of machine tools using digraph and matrix methods. *Int. J. Mach. Tools Manuf.* 42, 521–528.
- Rao, S.S., 2009. Engineering Optimization. <https://doi.org/10.1002/9780470549124>
- Rasheed, M.S., 2013. Comparison of Micro-Holes Produced By Micro-EDM with Laser Machining. *Int. J. Sci. Mod. Eng.* 1, 14–18.
- Ross, P.J., 1996. Taguchi Techniques for Quality Engineering: Loss Function, Orthogonal Experiments, Parameter and Tolerance Design. McGraw-Hill New York. <https://doi.org/ISBN-13:978-0070539587> ISBN-10: 0070539588
- Roy, R., 1990. A primer on the Taguchi method. *Comput. Integr. Manuf. Syst.* 5, 246. [https://doi.org/10.1016/0951-5240\(92\)90037-D](https://doi.org/10.1016/0951-5240(92)90037-D)
- Sanchez, J.A., Rodil, J.L., Herrero, A., Lacalle, L.N.L. De, Lamikiz, A., 2007. On the influence of cutting speed limitation on the accuracy of wire-EDM corner-cutting 182, 574–579. <https://doi.org/10.1016/j.jmatprotec.2006.09.030>
- Sasaki, T., Miyazaki, T., Ito, H., Furukawa, T., Mihara, T., 2014. X-ray Residual Stress Analysis of Nickel Base Alloys, in: *Advanced Materials Research*. pp. 274–279.
- Schubert, A., Zeidler, H., Oschätzchen, M.H., Schneider, J., Hahn, M., 2013. Enhancing Micro-EDM using Ultrasonic Vibration and Approaches for Machining of Nonconducting Ceramics. *Strojniški Vestn. – J. Mech. Eng.* 59, 156–164. <https://doi.org/10.5545/sv-jme.2012.442>
- Shabgard, M., Kakolvand, H., Seyedzavvar, M., Shotorbani, R.M., 2011. Ultrasonic assisted EDM: Effect of the workpiece vibration in the machining characteristics of FW4 Welded Metal. *Front. Mech. Eng.* 6, 419–428. <https://doi.org/10.1007/s11465-011-0246-7>
- Shabgard, M.R., Alenabi, H., 2015. Ultrasonic assisted electrical discharge machining of Ti-6Al-4V alloy. *Mater. Manuf. Process.* 30, 991–1000. <https://doi.org/10.1080/10426914.2015.1004686>
- Shabgard, M.R.R., Badamchizadeh, M. a. A., Ranjbar, G., Amini, K., 2013. Fuzzy approach to select machining parameters in electrical discharge machining (EDM) and ultrasonic-assisted EDM processes. *J. Manuf. Syst.* 32, 32–39. <https://doi.org/10.1016/j.jmsy.2012.09.002>
- Shiau, G.H., 1990. A study of the sintering properties of iron ores using the Taguchi's parameter design. *J. Chinese Stat. Assoc.* 28, 253–275.
- Singh, H., Khamba, J.S., 2011. An interpretive structural modelling (ISM) approach for advanced manufacturing technologies (AMTs) utilisation barriers. *Int. J. Mechatronics Manuf. Syst.* 4, 35–48.
- Singh, J., Walia, R., Satsangi, P., Singh, V., 2011. FEM Modeling of Ultrasonic Vibration Assisted work-piece in EDM Process. *Int. J. Mech. Syst. Eng.* 1, 8–16.
- Singh, J., Walia, R.S., Satsangi, P.S., Singh, V.P., 2011. Parametric Optimization of Hybrid Electric Discharge Machining Process With Continuous and Discontinuous. *Int. J. Mech. Syst. Eng.* 2, 1–7.
- Srivastava, V., Pandey, P.M., 2012. Effect of process parameters on the performance of EDM process with ultrasonic assisted cryogenically cooled electrode. *J. Manuf. Process.* 14, 393–402.

<https://doi.org/10.1016/j.jmapro.2012.05.001>

- Taguchi, G., Wu, Y., 1993. Introduction to Off-Line Quality Control, Journal of Quality Technology. Addison-Wesley Reading, MA.
- Teimouri, R., Baseri, H., 2013. Experimental study of rotary magnetic field-assisted dry EDM with ultrasonic vibration of workpiece. *Int. J. Adv. Manuf. Technol.* 67, 1371–1384. <https://doi.org/10.1007/s00170-012-4573-6>
- Tripathy, S., Tripathy, D.K., 2016. Multi-attribute optimization of machining process parameters in powder mixed electro-discharge machining using TOPSIS and grey relational analysis. *Eng. Sci. Technol. an Int. J.* 19, 62–70. <https://doi.org/10.1016/j.jestch.2015.07.010>
- Venkata Rao, R., Gandhi, O.P., 2002. Digraph and matrix methods for the machinability evaluation of work materials. *Int. J. Mach. Tools Manuf.* 42, 321–330. [https://doi.org/10.1016/S0890-6955\(01\)00133-X](https://doi.org/10.1016/S0890-6955(01)00133-X)
- Wani, M.F., Gandhi, O.P., 1999. Development of maintainability index for mechanical systems. *Reliab Eng Syst Saf*, 65, 259–270.
- Wansheng, Z., Zhenlong, W., Shichun, D., Guanxin, C., Hongyu, W., 2002. Ultrasonic and discharge machining to deep and small hole on titanium alloy. *Jorurnal Mater. Process. Tech.* 120, 101–106.
- Yan, B.H., Tsai, F.C., Sun, L.W., Hsu, R.T., Kern, R., Menzies, I., Koshy, P., Lin, Y.C., Chen, Y.F., Wang, A.C., Sei, W.L., 2012. Machining performance on hybrid process of abrasive jet machining and electrical discharge machining. *Trans. Nonferrous Met. Soc. China (English Ed.* 22, s775–s780. [https://doi.org/10.1016/S1003-6326\(12\)61803-2](https://doi.org/10.1016/S1003-6326(12)61803-2)
- Yu, Z.Y., Zhang, Y., Li, J., Luan, J., Zhao, F., Guo, D., 2009. High aspect ratio micro-hole drilling aided with ultrasonic vibration and planetary movement of electrode by micro-EDM. *CIRP Ann. - Manuf. Technol.* 58, 213–216. <https://doi.org/10.1016/j.cirp.2009.03.111>
- Zhixin, J., Jianhua, Z., Xing, A., 1995a. Ultrasonic vibration pulse electro-discharge machining of holes in engineering ceramics. *J. Mater. Process. Tech.* 53, 811–816. [https://doi.org/10.1016/0924-0136\(94\)01749-Q](https://doi.org/10.1016/0924-0136(94)01749-Q)
- Zhixin, J., Xing, A., Jianhua, Z., 1995b. Study on mechanical pulse electric discharge machining. *Precis. Eng.* 17, 89–93. [https://doi.org/10.1016/0141-6359\(94\)00007-M](https://doi.org/10.1016/0141-6359(94)00007-M)

## List of Publications:

### 1. List of Published Papers in International Journals (03):

S.No.	Title of the paper along with volume, Issue No, year of Publication	Publisher	Impact factor	Refereed or Non-Refereed	Indexing
1.	Optimisation strategies in ultrasonic vibration assisted electrical discharge machining: a review. Kumar, S, Grover and Walia, R S. 1, 2017, Int. J. Precision Technology, Vol. 7, pp. 51-84.	IJPT, Inderscience Publication, India	Not Mentioned	Refereed	Expanded Academic ASAP (Gale) Google Scholar
2.	Analyzing and modeling the performance index of ultrasonic vibration assisted EDM using graph theory and matrix approach. Kumar, S, Grover and Walia, R S. 2016, Int. J. Interact. Des. Manuf., Vol. 12, pp. 225-242	IJIDeM, Springer-Verlag France	Not Mentioned	Refereed	SCImago, SCOPUS
3.	Effect of Hybrid wire EDM conditions on generation of residual stresses in machining of HCHCr D2 Tool steel under ultrasonic vibration, Kumar, S, Grover and Walia, R S. 2016, Int. J. Interact. Des. Manuf.	IJIDeM, Springer-Verlag France	Not Mentioned	Refereed	SCImago SCOPUS,

### 2. List of Published Papers in International/National Conferences (03):

S.No.	Title of the paper along with volume, Issue No, year of Publication	Publisher	Paid any money or not for publication
1.	A Vibrating System Design and Analysis in Hybrid Electrical Discharge Machining	National Conference RSTTMI - 2016 YMCAUST Faridabad	Conference Fee
2.	A comparative study of optimization strategies Implemented in Ultrasonic Vibration Assisted Wire Electrical Discharge Machining.	National Conference on TAME-2017 YMCAUST Faridabad	Conference Fee
3	A Review on Recent Innovations in Electrical Discharge Machining Process	International Conference ICRIEAT-2016 Aurora's Scientific, Technological and Research Academy Chandrayangutta, Hyderabad	Conference Fee



## 2. List of communicated Papers in International Journals (04):

S.No.	Title of the paper along with volume, Issue No, year of Publication	Publisher	Impact factor	Refereed or Non-Refereed	Indexing	Remarks
1.	A Comparative Study on Performance for Ultrasonic Vibration Assisted using ANP, GTA and MOORA	Journal of The Institution of Engineers (India): Series C Springe, India	Not Mentioned	Refereed	SCOPUS	Revision
2.	A systematic framework for the analysis of ultrasonic vibration perception in Hybrid EDM utilizing ISM and MICMAC approach	IJAMT Springer-Verlag London	2.209	Refereed	SCI-E, SCImago, SCOPUS,	Communicated
3.	Effect of workpiece ultrasonic vibration in Wire Electrical Discharge Machining for AISI D3 tool steel	IJAMT Springer-Verlag London	2.209	Refereed	SCI-E, SCImago, SCOPUS,	Communicated
4.	Evaluation of Cutting Rate for Ultrasonic work piece vibration Assisted Wire-EDM under varying Amplitude of Vibration	Engineering Solid Mechanics (ESM) Growing Science	Not Mentioned	Refereed	SCImago SCOPUS,	Communicated